Fakultät für Medizin

Institut für Experimentelle Hämatologie

Elucidating the timing of NKT cell development and subset differentiation

Sabrina Bortoluzzi

Vollständiger Abdruck der von der Fakultät für Medizin der Technischen Universität München zur Erlangung des akademischen Grades eines

Doctor of Philosophy (Ph.D.)

genehmigten Dissertation.

Vorsitzende/r: Prof. Dr. Agnes Görlach

Betreuer/in: Prof. Dr. Marc Schmidt-Supprian

Prüfer der Dissertation:

1. Prof. Dr. Ludger Klein

2. Prof. Dr. Thomas Korn

Die Dissertation wurde am 16.12.2019 bei der Fakultät für Medizin der Technischen Universität München eingereicht und durch die Fakultät für Medizin am 03.03.2020 angenommen.

ABSTRACT

Natural killer T (NKT) cells are rare glycolipid-recognizing T cells that incorporate features of both adaptive and innate cells. NKT cells provide anti-microbial defence and immune surveillance of malignancies; however, they are also involved in the pathogenesis of allergies, autoimmune and inflammatory diseases as well as certain types of cancer. One of the most striking hallmarks of NKT cells is the acquisition of unconventional memory-like cellular states during their development in the thymus.

In spite of seminal progress in the understanding of NKT cell biology in recent years, the molecular mechanisms that drive the developmental acquisition of their peculiar phenotypes are only incompletely understood. This applies especially to the earliest developmental timepoints, which are hard to characterize due to the rarity of the cells.

Therefore, I established a genetic model to induce a timed wave of synchronous NKT cell generation in order to elucidate early developmental phases and functional differentiation of NKT cell subsets in the mouse. The analysis of several known markers revealed that the NKT cells generated in my system undergo developmental processes which closely resemble physiological NKT cell development. I therefore extensively monitored the expression dynamic of the transcription factors RORγt and PLZF during NKT cell development and defined their relation with other transcription factors and additional critical proteins as well as processes. I characterised the exact timing of cellular proliferation as well as the acquisition of the ability to produce various cytokines. Moreover, by means of Nur77eGFP and *Nr4a3*-Tocky mouse models I monitored the TCR signal strength dynamics during the early developmental phases. Furthermore, I performed a detailed kinetic transcriptional analysis of early NKT cell development in the thymus.

Through the analysis of this genetic model I was able to uncover novel crucial dynamics occurring in early NKT cell development. The versatility of this model will allow me to further explore the development of NKT cell and ultimately define the central mechanisms that determine their unique functional phenotypes.

1. INTRODUCTION

1.1 The immune system

Every day, numerous pathogens try to break the barriers and invade host organisms with life-threatening consequences. The immune system is a highly sophisticated and coordinated system that evolved in vertebrate organisms to recognise and counteract these threats (Chaplin, 2010).
A crucial feature of the immune system resides in its ability to discriminate between pathogenic and commensal micro-organisms as well as to tolerate self. This distinction is achieved through a series of intricate processes – also called immunological tolerance – which constantly instruct and shape the immune system. Beyond this, the immune system needs to maintain a well-balanced response which allows the eradication of threatening pathogens without generating an excessive immune reaction, which would damage the body and compromise the commensal pathogens survival (Waldmann, 2016).

Conventionally, the immune system is divided into two branches – termed innate and adaptive – with distinct ways of action but constant interplay with each other. The innate immune system consists of defence mechanisms (including mucus, tight junctions, epithelial cilia, soluble proteins, cytokines and chemokines) as well as distinct immune cell types, including monocytes, macrophages, neutrophils, basophils, eosinophils and mast cells. These immune cells possess germline encoded receptors which can recognise common molecular patterns found in pathogens and therefore promptly trigger the initial immune reaction.
On the other hand, the adaptive immune system is composed of T and B lymphocytes, which possess somatically rearranged receptors with an extremely high degree of variability, which permits the specific recognition of defined pathogens. In an infection context, adaptive immune cells require additional time to mount a highly specific response driven by clonal expansion of cells specialised for the recognition of a distinct pathogen.

However, this simplistic classification in adaptive and innate system does not take into consideration the immune cell types which exhibit a hybrid nature and perform an additional layer of regulation between the two sides of the immune system (Chaplin, 2010).

1.1.1 Unconventional T cells

Apart from conventional T cells, which recognise highly diverse peptides presented by polymorphic major histocompatibility complex (MHC) class I or II, a distinct group of T cells is characterised by the recognition of a restricted variety of unusual antigens presented by non-polymorphic protein-complexes. These cells, termed "unconventional" T cells, include CD1d-restricted Vα14 invariant Natural Killer T cells (iNKTs), γδ T cells, MR1-restricted Mucosal-Associated Invariant T cells (MAITs) and MHC class Ib-reactive CD8αα Intraepithelial Lymphocytes (Kjer-Nielsen et al.). Overall, these cell types share the ability to recognise their antigens, including lipids, metabolites and special peptides, with a broader specificity than conventional T cells and display rapid effector functions in different challenging contexts. Additionally, unconventional T cells harbour canonical T cell receptor (TCR) repertoires and show a tendency to localise into non-lymphoid tissues (Godfrey et al., 2015).
iNKT cells and MAIT cells are characterised by the expression of a semi-invariant TCR with the distinct ability of recognising non-peptide antigens and releasing abundant amounts of cytokines upon activation (Kjer-Nielsen et al., 2012; Reilly et al., 2010). In a striking contrast to conventional CD4 and CD8 T cells, both iNKT and MAIT cell lineages are positively selected by other double-positive (DP) thymocytes but not by thymic stromal components from a pool of DP thymocyte precursors. Extracellular markers (such as CD24 and CD44) and localisation are also shared between the two lineages (Bendelac, 1995; Seach et al., 2013). Importantly, both cell types depend on the expression of the transcription factor Promyelocytic Leukaemia Zinc Finger (PLZF), essential for their development and further differentiation into functional subsets (Koay et al., 2016; Kovalovsky et al., 2008; Savage et al., 2008). Transcriptomic analyses revealed a high degree of organ specific similarity between T helper (Th)1-type (interferon-γ (IFN-γ)-producing) MAIT (MAIT1)

and Th17-type (interleukin (IL-)17 producing) MAIT (MAIT17) cells with those of Th1-type NKT (NKT1) and Th17-type NKT (NKT17) cells, respectively (Salou et al., 2019). Additionally, NKT1 were shown to possess similarities with NK cells and other Th1-type cytokine secreting cell types such as Th1-T cells, intraepithelial γδ T cells and type-1 innate lymphoid cells (ILC1). Interestingly, in contrast to the above described similarities, Th2-type (IL-4 producing) (NKT2) and NKT17 cell subsets show major similarities with the corresponding γδ subsets and ILCs, but not with the corresponding T helper subsets (Lee et al., 2016).

γδ T cells express a heterodimeric TCR composed by γ and δ variable segments. Although the TCR repertoire is diverse, oligoclonal subsets with the same TCR are differentially distributed within organs (Gerber et al., 1999; Itohara et al., 1990; Takagaki et al., 1989). Depending on the subsets, γδ T cells can recognise a wide variety of antigens presented by likewise diverse MHC class I–like presenting-molecules (Godfrey et al., 2015). Alike iNKT cells, some TRDV1^{+} γδ T cells recognise lipid antigens presented by CD1d molecules (Luoma et al., 2013).

CD8αα IELs represent a subset of unconventional T cells that express CD8αα but lack expressions of CD4 and CD8αß surface molecules. Similar to iNKT cells, CD8αα IELs develop in the thymus in response to a strong recognition of self-ligands (Mayans et al., 2014; McDonald et al., 2014).

Overall, the functionality of these cells goes beyond the classical TCR-peptide antigen interactions and constitutes a distinct as well as an important role in connecting adaptive and innate immune systems.

1.2 NKT cells

iNKT cells, also called type I NKT cells, represent one of the unconventional T lymphocyte subsets, which show features and phenotypes of both αß T cells and natural killer (NK) cells (Godfrey et al., 2004). It is known that iNKT cells can play diverse and even opposite roles in the immune response; on one side, iNKT cells can protect the organism by participating in viral clearance, provide anti-microbial defence as well as immune surveillance of malignancies (Brigl et al.,

2003; Juno et al., 2012). On the other hand, iNKT cells can be involved in the pathogenesis of autoimmune and inflammatory diseases, allergies and some types of cancer (Subleski et al., 2011; Wingender et al., 2011; Wolf et al., 2014). The TCR of iNKT cells is characterised by a unique single invariant TCR-α chain paired with a restricted range of TCR-ß chains. This evolutionarily conserved semi-invariant TCR receptor is found on both murine and human iNKT cells. In mice, the TCR-alpha chain is encoded by Vα14-Jα18 paired with a defined group of ß chains (mainly Vß2, Vß7 or Vß8.2), while in humans it is encoded by Vα24-Jα18 and paired only with Vß11 (Godfrey et al., 2004).

A striking difference between iNKT cells and αß T cells resides in the antigen recognition ability of the TCR. Conventional αß T cells are characterised by an enormously diverse TCR repertoire that results in the highly specific recognition of peptide antigens presented by MHC molecules (Chaplin, 2010). Conversely, the unique semi-invariant TCR expressed by iNKT cells is monospecific and recognises various endogenous or exogenous glycolipids antigens presented by the MHC I-like molecule CD1d (Godfrey et al., 2004).

As mentioned above, a group of iNKT cells also expresses markers which are commonly present on NK cells, including Ly49, NK1.1, NKG2D and CD122. These molecules diversely affect NKT cells function and differentiation by playing different roles in NKT cell responsiveness to stimulation, TCR-independent cytolysis, CD1d co-stimulation, maturation and their homeostasis in the periphery (Bendelac et al., 1997; Gadue and Stein, 2002; Kuylenstierna et al., 2011; Maeda et al., 2001; Seiler et al., 2012). An additional type of NKT cells, called type II or variable NKT cells (vNKTs), can be found both in human and in mice. These CD1d-restricted cells possess a more diverse αß TCR and mostly recognise different lipids than iNKT cells. Although several studies have highlighted the relevance of vNKT cells in several disease contexts, detailed analysis of these cells is rendered challenging by the lack of direct methods to detect them (Singh et al., 2018). Thus, from now on for the sake of simplicity, in this thesis I will focus on iNKT cells and will refer to them as NKT cells.

1.2.1 Discovery of NKT cells

Three independent lines of experimental evidences contributed to the identification of NKT cells as a novel cell type. Firstly, in 1986, analyses of a suppressor T cell hybridoma revealed presence of an invariant Vα14-Jα18 TCRα-chain gene (Imai et al., 1986), where the sequences derived from hybridomas possessed only 4 types of one nucleotide addition at the N-region that resulted in an invariant TCRα-chain at the amino acid level (Koseki et al., 1990). A second line of evidence, reported in 1987 by three independent studies demonstrated presence of a peculiar subpopulation of thymocytes, which lacked CD4, CD8 and CD24 molecules, expressed intermediate levels of TCR αß protein but with particularly high levels of TCR αß mRNA (Budd et al., 1987; Ceredig et al., 1987; Fowlkes et al., 1987). They were also shown to express CD5 and CD3 and to be capable of producing IL-2 upon stimulation (Ceredig et al., 1987; Fowlkes et al., 1987). Remarkably, these cells had a predominant usage of TCR Vß8 gene segment. The analysis of different mouse strains with diverse haplotypes excluded the possibility that this predominance was a result of self-MHC-mediated positive selection processes (Budd et al., 1987). Due to lack of detection of these cells in the fetal thymus, the authors concluded that these cells were not precursors of αß T cells, and proposed that they rather represent a mature T cell subset with distinct functions. A few years later, the discovery of TCR αß thymocytes expressing NK1.1 – a marker considered to be NK cell exclusive – enhanced further interest in this peculiar type of cells. These studies described a new subpopulation of TCR αß+ cells with a predominant usage of the TCR Vß8 gene segment, either CD4− CD8− double negative (DN) or CD4+ single positive (SP), expressing NK1.1 and localised in the thymus (where they derive from), peripheral immune organs and abundantly in bone marrow (Arase et al., 1992; Levitsky et al., 1991; Sykes, 1990). These cells were also shown to express typical markers associated with memory or activated phenotypes such as CD44, Mel-14 (CD62L) and ICAM-1. These findings had introduced an important new concept, namely the memory phenotype, which is now widely accepted to serve as a distinguishing phenotypic marker of NKT cells (Arase et al., 1992).

Of notable importance, a study from Zlotnik et al. demonstrated that both thymic and splenic DN TCR αß+ cells secrete large amounts of cytokines (IL-4, IFN-γ and TNF-α) upon in vivo anti-CD3 stimulation (Zlotnik et al., 1992). Furthermore, it was revealed later that cells with CD4+ CD24- TCR αß+ NK1.1+ surface phenotype produce extremely high levels of IL-4 but low amounts of IFN-γ, IL-2 and IL-5 upon stimulation (Arase et al., 1993; Bendelac and Schwartz, 1991; Hayakawa et al., 1992; Yoshimoto and Paul, 1994).

The third line of evidence, which provided a link between the above-mentioned studies, was provided by Lantz and Bendelac in 1994 (Lantz and Bendelac, 1994). They established hybridomas from Vß8+ CD44+ thymocytes and found that they all expressed the invariant Vα14 TCRα messenger RNA (mRNA), strongly suggesting that Vα14+ cells, Vß8+ DN thymocytes and Vß8+ CD44+ hybridomas represent the same cell type. Thus, this population was later termed Vα14-invariant NKT cells or iNKT cells.

An additional important finding was the discovery of the MHC-independency of these cells. In fact, it was demonstrated that the activation of these cells depend on the interaction with CD1d (Bendelac et al., 1995), which was previously shown to be capable of activating DN αß T cells through the presentation of lipid antigens (Beckman et al., 1994; Porcelli et al., 1992). Moreover, in marked contrast to conventional T cells, the development of NKT cells was independent of the transporter-associated protein (TAP), which is absolutely required in the development of conventional CD8 T cells by virtue of their role in peptide antigen processing that allows its presentation on MHC class I molecules (Adachi et al., 1995; Brutkiewicz et al., 1995).

Another breakthrough finding that greatly accelerated investigations in the field was the identification of α-galactosylceramide (α-GalCer), a marine sponge-derived glycolipid antigen, as a potent NKT cell ligand in 1997. (Kawano et al., 1997). The biological activity of α-GalCer is strictly dependent on its presentation on MHC class I-like molecule CD1d, which leads to increased proliferation and prompt release of many immunoregulatory cytokines such as IL-4, IFN-γ, IL-12 and IL-17 both in vivo and in vitro (Brigl et al., 2003; Fujii et al., 2002; Michel et al., 2007). This glycolipid ligand was further employed in the invention of CD1d tetramer based technology, termed α-GalCer-loaded CD1d-tetramers, that allowed unprecedented sensitivity and

specificity to detect NKT cells, which paved a way for many following studies on NKT cells (Benlagha et al., 2000).

Ten years after their first description, the knowledge on NKT cells has been drastically improved. By the beginning of the 21st century it was clear that a separate T cell subset was identified, bearing a peculiar phenotype incorporating features of NK and memory cells. These unique cells expressing canonical TCR were restricted to non-polymorphic CD1d, and were capable of reacting to glycolipid ligands specifically presented by CD1d by swift production of copious amounts of various immunoregulatory cytokines.

1.2.2 Classification of NKT cells – "linear differentiation" and "lineage diversification" models

Historically, based on a "linear differentiation" model, NKT cells have been classified into four developmental stages, where most immature NKT cells that have just undergone positive selection on CD1d/endogenous glycolipid ligand complex (termed Stage 0) differentiate into the fully mature NKT cells (termed Stage 3) through the intermediate Stage 1 and Stage 2 differentiation stages. The earliest immature Stage 0 NKT cells are detected in the thymus and are characterised by high levels of CD24 and CD69 expression, and are either DP or CD4+. Upon downregulation of CD24 and CD69, NKT cells enter to the Stage 1. At the Stage 2 NKT cells acquire a memory-like $CD44^{high}$ phenotype and continue their differentiation into Stage 3 that is defined by the expression of NK1.1 and other NK cell-related markers (Benlagha et al., 2005).

This initial concept of NKT cell development, termed "linear differentiation model" with strictly sequential maturation steps through above-described four stages, was challenged when a fully mature NKT cell population was found to lack NK1.1 expression with the surface phenotype resembling the Stage 2 NKT cells (Coquet et al., 2008).

As a consequence, a lineage differentiation model based on transcription factor expression and cytokine production repertoires was introduced. The term NKT1 was attributed to the NKT cells that express low levels of PLZF but high T-bet, produce INF-γ and low amount of IL-4. These cells almost exclusively belong to Stage 3. NKT2 cells have a $PLZF^{high}$ $GATA3^{high}$ phenotype and secrete

IL-4 and IL-13, they do not uniformly express CD44 and therefore are shared between Stage 1 and Stage 2. Lastly, NKT17 cells comprise the only subsets to express RORγt, express intermediate levels of PLZF and secrete IL-17A. A minor fraction of NKT17 express NK1.1 but most of them are negative and can be grouped in Stage 2 (Buechel et al., 2015; Coquet et al., 2008; Lee et al., 2013). Additionally, also immature and progenitor NKT cells were included in the lineage differentiation model. Early immature NKT cells (CD24+ $CD44^{low}$ NK1.1−) were named NKT0 (Engel et al., 2016), while uncommitted NKT cell progenitors were defined as $PLZF^{high}$ CD4+ $CD24^{low}$ CCR7+ IL-17RB− IL-4− and termed NKTp (Kwon and Lee, 2017; Lee et al., 2013; Wang and Hogquist, 2018).

The categorisation of NKT cells subsets based on their function was strongly supported by two independent studies showing that NKT0, NKT1, NKT2 and NKT17 display striking differences in their transcriptome and epigenome, proposing the presence of subsets-specific gene-expression patterns (Engel et al., 2016; Georgiev et al., 2016).

Furthermore, three additional functional subsets were described: NKT follicular helper (NKT_{FH}) cells differentiate from mature NKT cells that interact with B cells during an on-going infection and influence primary and memory B cell responses. Their phenotype closely resembles that of T_{FH}, characterized by high expression of PD-1, CXCR5 and BCL-6 (Chang et al., 2011a). Foxp3+ NKT cells are a group of NKT cells that upon antigen exposure express the transcription factor Foxp3. Mainly found in the liver, they express markers typical of T regulatory (Treg) cells, such as CTLA4, CD25 and GITR (Monteiro et al., 2010). Finally, NKT10 represent a regulatory subset with no or low PLZF expression. NKT10 cells express E4BP4, display elevated levels of CTLA4, Neuropilin-1 and FR4, produce IL-2 and IL-10 and mainly reside in adipose tissue (Lynch et al., 2015; Sag et al., 2014).

1.2.3 Phenotypes of functional NKT cell subsets

As a result of their differentiation journey, three main functionally distinct subsets – NKT1, NKT2 and NKT17 – are generated. In addition to the aforementioned differential release of cytokines and expression of the

transcription factors PLZF, RORγt, T-bet and GATA-3, the three functional subsets differ for the expression of many additional markers. Table 1 aims to summarise the most relevant markers and the corresponding expression in each functional subset.

Table 1. Differential expression of surface markers among NKT1, NKT2 and NKT17

Marker	NKT1	NKT2	NKT17	References
CD122	+	–	–	(9)
CXCR3	+	–	–	(2)
IL-17RB	–	+	+	(2, 3)
ICOS	low	high	high	(2)
PD-1	–	+	+	(1)
CD4	±	+	–	(3)
CD49a+	+	–	–	(2)
IL-23R	–	–	+	(5)
CD103	±	low	high	(7)
Neuropilin-1	low	+	+	(7, 8)
CD138	–	–	+	(6, 7)
CD69	high	–	+	(10)
CCR6	–	–	±	(7)
CD27	+	+	–	(9)
Ly6C	+	–	–	(7)
CD127	low	low	high	(7)

(1) (Wang and Hogquist, 2018), (2) (Engel et al., 2016), (3) (Watarai et al., 2012). (4) (Coquet et al., 2008) (5) (Rachitskaya et al., 2008), (6) (Dai et al., 2015), (7) (Drees et al., 2017), (8) (Milpied et al., 2011) (9) (Lee et al., 2013), (10) (Kimura et al., 2018)

1.2.4 Frequency and distribution

NKT cells represent a small fraction of lymphocytes in both mice and men. Overall, murine NKT cells constitute around 0.2-0.5% of lymphocytes and can be found with the highest frequency in the liver, where they account for 12-39% of lymphocytes. Although with a lower frequency, NKT cells populate lung (5-10%), spleen (1-3%), bone marrow (0.4-8%), thymus (0.5-1%), intestine (0.05-0.6%), lymph nodes (0.2-1%) and blood (0.2%) (Berzins et al., 2011; Hammond et al., 2001; Matsuda et al., 2000; Slauenwhite and Johnston, 2015; Wingender et al., 2012). NKT cells are even less prominent in the human body, with frequencies varying between 0.01% and 1% of peripheral blood mononuclear cells (PBMCs) (Berzins et al., 2005; Chan et al., 2009; Lee et al., 2002). Similar to mice, human NKT cells can be found in different organs including spleen (~0.1% of CD3+ cells), bone marrow (~0.1% of lymphocytes), liver (~1% of lymphocytes) and thymus, were NKT cells are extremely rare (0.001–0.01% of lymphocytes) (Baev et al., 2004; Berzins et al., 2005; Chan et al., 2013; Chan et al., 2010; Kenna et al., 2003).

Besides their variable frequencies, murine NKT cell functional subsets are not equally distributed in the different compartments. The abundance of each subset is organ and strain dependent. In C57BL/6 mice, thymic NKT cells consist of NKT1 (87-93%), NKT2 (4-8%) and NKT17 (1-3%) (Drees et al., 2017). Around 30% of all NKT cells are localised in the cortical zone. NKT1 and NKT17 are distributed in the cortex (30%) and in the medulla (70%). However, the majority of NKT2 cells were found to reside in the medulla (Lee et al., 2015). Splenic NKT1 cells mainly localise in the red pulp, whereas NKT2 are mostly found in the T cell zone of the white pulp. In lymph nodes, NKT17 accumulate under the subcapsular area, while in mesenteric lymph nodes (mLN) NKT2 are prevalently in the T cell zone and NKT1 and NKT17 are distributed in T and B cell areas (Lee et al., 2015).

1.2.5 NKT cell activation

Mature NKT cells reside in different locations of the body in a resting state. Within minutes after stimulation, NKT cells release copious amounts of

cytokines whose identity reflects both the functional polarisation of NKT cells as well as the stimulus that they receive (Reilly et al., 2010). Generally, NKT cell activation can be subdivided into three categories: 1) microbial glycolipid-mediated TCR activation, 2) endogenous antigen TCR stimulation with cytokine support and 3) cytokine mediated TCR-independent activation.

Microbial glycolipid-mediated TCR activation

This form of NKT cell activation comprises the interaction of the NKT cell TCR with a CD1d molecule bearing an exogenous glycolipid. Many microorganisms – including *Sphingomonas* (Kinjo et al., 2005), *Borrelia burgdorferi* (Kinjo et al., 2006), *Streptococcus pneumonia* (Kinjo et al., 2011), *Mycobacterium* bovis (Fischer et al., 2004) and *Helicobacter pylori* (Chang et al., 2011b) – have been reported to produce α-linked glycosphingolipids capable to directly activate NKT cells in a TCR-dependent manner.

Similar to α-GalCer, Sphingomonas glycolipid can induce the production of both IL-4 and IFN-γ cytokines in vitro. However, intravenous injection of α-GalCer-loaded dendritic cells (DCs) preferentially induce an IFN-γ response (Kinjo et al., 2006; Kinjo et al., 2005). This T_H1-skewed response is also seen in other cases, including *Boriella burgdorferi*, *Streptococcus pneumonia* as well as α-GalCer (Fujii et al., 2002; Kinjo et al., 2011; Kinjo et al., 2006). Moreover, the stimulation with *Sphingomonas*, *Boriella burgdorferi* antigens as well as α-GalCer was shown to promote the release of IL-17 by a subset of NK1.1− NKT cells (Michel et al., 2007).

Endogenous antigen TCR stimulation with cytokine support

Several microorganisms – such as *Salmonella typhimurium* and *Staphylococcus aureus* – lack specific CD1d-compatible antigens. However, when cultured with DCs they were shown to stimulate NKT cells to produce IFN-γ through a mechanism that involved both Toll-Like Receptor (TLR) activation and CD1d interactions (Brigl et al., 2003; Mattner et al., 2005). Culture of NKT cells with wildtype DCs, but not TLR-signalling-deficient DCs, resulted in the activation of NKT cells, confirming its dependence on TLR engagement (Mattner et al., 2005). Upon binding of bacteria-derived LPS to TLR4 expressed by APCs, APCs release inflammatory cytokines such as IL-1ß,

IL-6, IL-12 and TNF-α. However, only IL-12 was reported to bind to its receptor on the surface of NKT cells and in turn activate them. Anti-IL-12 treatment largely, but not completely, blocked NKT cell activation in this context. Furthermore, NKT cell activation achieved through incubation with heat-killed bacteria and DCs could be largely blocked by anti-CD1d treatment (Brigl et al., 2003; Mattner et al., 2005). This evidence, together with the inability of CD1d-deficient DC to stimulate NKT cells (Mattner et al., 2005), suggested that CD1d-TCR interactions are also required and that NKT cell activations involves a self-antigen recognition, as previously suggested by Gumperz et al. (Gumperz et al., 2000).

Of particular note is the study from Salio et al., who demonstrated that activation of antigen presenting cells (APCs) through TLRs increased their glycosphingolipid biosynthetic pathway. These endogenous glycosphingolipids could bind to CD1d molecules and in turn enhance NKT cell activation (Salio et al., 2007). In line with this concept, DCs stimulated with CpG oligodeoxynucleotides (CpG ODN) (a TLR9 agonist) showed increased levels of diverse glycosyltransferases implicated in the neo-synthesis of glycosphingolipids (GLSs) (Paget et al., 2007).

Moreover, in the case of *Mycobacterium tuberculosis* infection not only IL-12 but also IL-18 was shown to stimulate IFN-γ production by NKT cells (Sada-Ovalle et al., 2008).

Cytokine mediated TCR-independent NKT cell activation

NKT cell activation can also be solely cytokine driven. Murine cytomegalovirus (MCMV) infection results in NKT cell activation and IFN-γ production, but it is largely independent on CD1d, as confirmed by anti-CD1d treatment and CD1d −/− experiments (Tyznik et al., 2008; Wesley et al., 2008). MCMV was reported to stimulate DCs through TLR9 to produce IL-12 which in turn activates NKT cells to release IFN-γ (Tyznik et al., 2008). DCs derived from either IL-12-deficient or TLR9-mutant mice did not induce IFN-γ production by NKT cells, indicating that both IL-12 and TLR9 are required for their activation (Tyznik et al., 2008). However, another study demonstrated that stimulation of DCs with TLR7 and TLR9 agonists resulted in liver-derived NKT cell activation and IFN-γ production (Paget et al., 2007). DCs were shown

to produce both IL-12 and type I IFN, but only the latter was required for NKT cell activation. Moreover, NKT cell activation was partly dependent on CD1d expression of self-antigens (Paget et al., 2007).
Another example of cytokine dependent activation is seen in the case of *E. Coli* infection. Here, NKT cells are activated by IL-12 and IL-18 produced by APCs in response to LPS. LPS alone does not activate NKT cells, but IL-12 and IL-18 together are sufficient to activate NKT cells in vitro. Additionally, CD1d-blockage did not lead to an impaired IFN-γ production (Nagarajan and Kronenberg, 2007).

1.2.6 Effects of NKT cell activation within immune responses

Upon activation, NKT cells express diverse surface markers and release a wide array of cytokine and chemokines; therefore, it is foreseeable that they play an important role in immune responses. Overall, NKT cells are involved in the direct and indirect activation as well as recruitment of other immune cells including DCs, B cells, T cells, NK cells, granulocytes and macrophages.

As described above, DCs are responsible for NKT cell activation in a CD1d-TCR interaction and cytokine-mediated manner. Likewise, NKT cells dictate DCs maturation and in turn modulate the condition of other immune cells (Fujii et al., 2003).
In case of infections, DCs can be stimulated through their pathogen recognition receptors (PRRs) to release IL-12, present stimulatory lipid antigens bound to CD1d molecules to NKT and activate them to release IFN-γ (Brigl et al., 2003; Brigl et al., 2011; Mattner et al., 2005). The NKT-TCR/DC-CD1d linkage, together with CD40-CD40L co-stimulation, results in the maturation of DCs and subsequent increase of IL-12 and IFN-γ production as well as of costimulatory molecules (CD40, CD80, CD86) and MHC class II expression (Fujii et al., 2004; Fujii et al., 2003; Hermans et al., 2003). The IL-12 (and partially IFN-γ)-rich environment boosts the expression of already existent IL-12R on the surface of NKT cells, supporting their activation and IFN-γ release (Kitamura et al., 1999). Moreover, the IL-12 release by activated DCs together

with IFN-γ produced by NKT cells, initiates the so-called NK cell transactivation, which culminates in IFN-γ release by NK cells (Carnaud et al., 1999; Eberl and MacDonald, 2000; Kawakami et al., 2001).
Additionally, NKT cell-matured DCs display increased antigen cross presentation, prime CD4+ and CD8+ T cells and polarise them towards a Th1 differentiation both in vitro and in vivo (Fujii et al., 2003; Hermans et al., 2003; Lang et al., 2006).

The increased cross presentation and DCs maturation occurring upon interactions with NKT cells also affects B cell-dependent antibody production (Lang et al., 2006). In fact, in the presence of a CD1d-reacting lipid and a peptide antigen, NKT cells drive the maturation of DCs which in turn prime T_H cells to become T_{FH} (Doherty et al., 2018; Lang et al., 2006). Moreover, NKT cells can release B-cell activating factor (BAFF) and a proliferation-inducing ligand (APRIL), crucial factors for the survival of antibody-producing plasma cells (Shah et al., 2013).
Alternatively, a specific subset of NKT cells, namely NKT_{FH}, can provide cognate-help to B cells (Chang et al., 2011a). NKT_{FH} can bind to B cells through the recognition of a BCR-presented antigen linked to an NKT cell-compatible lipid antigen. This stable interaction results in extrafollicular plasma-blasts, germinal centre formation, affinity maturation and enhanced IgG antibody production, dependent on IL-12 released by NKT cells. However, this process does not involve the formation of long-lasting memory cell compartment (Chang et al., 2011a; King et al., 2011).

As part of the antigen presenting cells, macrophages are capable of activating NKT cells through lipid antigen presentation. Upon infection, Kupffer cells and subcapsular sinus macrophages activate NKT cells in liver and in lymph nodes, respectively (Barral et al., 2010; Lee et al., 2010a; Schmieg et al., 2005). Similar to DCs, also macrophages experience NKT cell-mediated differentiation. On one side, IFN-γ release by NKT cells can enhance macrophage phagocytosis in a pulmonary infection context (Nieuwenhuis et al., 2002). On the other side, in a murine model of post-viral chronic lung disease, NKT cells can direct the differentiation of M2 macrophages which drive the chronic inflammation in an

IL-13 dependent fashion (Kim et al., 2008). Moreover, NKT cells can modulate tumour growth by killing tumour associated macrophages (TAMs) (Song et al., 2009).

During pulmonary infections, NKT cells can boost the recruitment of neutrophils at the site of inflammation by enhancing the release of the chemokine CXCL2 (possibly by macrophages) (Kawakami et al., 2003; Nieuwenhuis et al., 2002) or through direct IL-17 secretion (Michel et al., 2007). Moreover, NKT cells can convert the differentiation of neutrophils from an immunosuppressive to an antitumor phenotype. Serum amyloid A1 (SAA-1), an acute response protein released in the course of microbial infections, was shown to promote neutrophil-dependent NKT cell activation, defined by IFN-γ release. Additionally, neutrophil-NKT cell co-culture resulted in decreased IL-10 and increased IL-12 production by neutrophils, in a CD1d-dependent manner (De Santo et al., 2010).
Finally, NKT cells can indirectly guide the differentiation of naïve T cells into regulatory T cells (Tregs) through the generation of tolerogenic APCs. Indeed, in the case of nickel administration, NKT cells dictate the tolerogenic phenotype acquisition of APCs through the secretion of IL-10 and IL-4. Consequently, tolerogenic APCs transfer the tolerance to T cells, converting them into Tregs (Roelofs-Haarhuis et al., 2004). A similar scenario is seen in type 1 diabetes, where upon infection NKT cells induce tolerogenic plasmacytoid-DCs in the pancreas, which in turn convert naïve T cells into Tregs (Diana et al., 2011).

1.3 NKT cell development

A substantial part of NKT cell development closely resembles that of conventional T cells. Circulating progenitors migrate from the bone marrow to the thymus where they undergo further differentiation, culminating in the acquisition of both CD4 and CD8 markers, therefore named double-positive (DP) thymocytes (Sambandam et al., 2008). During V(D)J recombination, the rare Vα14 to Jα18 gene segment rearrangement combined with the expression

of a confined group of ß chains renders a DP thymocyte eligible to enter the NKT cell lineage. These NKT cell progenitors can undergo positive selection mediated by CD1d-TCR-mediated interactions with other DP thymocytes (Egawa et al., 2005). This event induces strong TCR signalling relayed by a specific signalling cascade leading to the activation of transcription factors including Egr2 and subsequently to the induction of the key transcription factor PLZF (Seiler et al., 2012). NKT cell precursors continue their differentiation in the thymus (and partially in the periphery), culminating in the formation of three main fully functional mature NKT cell subsets: NKT1, NKT2 and NKT17 (Bennstein, 2017). Figure 1 summarises the currently proposed model for NKT cell development and differentiation and highlights some unresolved questions.

1.3.1 Pre-thymic development

Hematopoietic stem cells (HSCs) are rare multipotent cells which have the potential to differentiate into all immune cell lineages (Spangrude et al., 1988). These long-term self-renewing cells are located in the bone marrow, where they further differentiate into multipotent progenitors (MPPs) with no or little self-renewing capabilities, with increase expression of FLT3 receptor and only short-time multi-lineage reconstituting potential (Adolfsson et al., 2001). MPPs give rise to lymphoid-primed multipotent progenitors (LMPPs), a distinct population characterised by the ability to generate both lymphoid and myeloid cells and expressing high levels of FLT3 and IL-7R (Adolfsson et al., 2005). A subpopulation, defined by high levels of RAG gene expression, was defined as early lymphoid progenitors (ELPs) (Igarashi et al., 2002). Common lymphoid progenitors (CLPs) derive from ELPs/LMPPs and display almost exclusively lymphoid potential (Kondo et al., 1997) and very little myeloid potential (Balciunaite et al., 2005; Rumfelt et al., 2006). Different bone marrow progenitors can egress the bone marrow through the blood stream with the purpose of colonising other organs. The mobilisation mechanism behind is not completely understood, but it certainly relies on an intricate and extremely well-regulated network of cytokines, chemokines, growth factors, and hormones (Schulz et al., 2009).

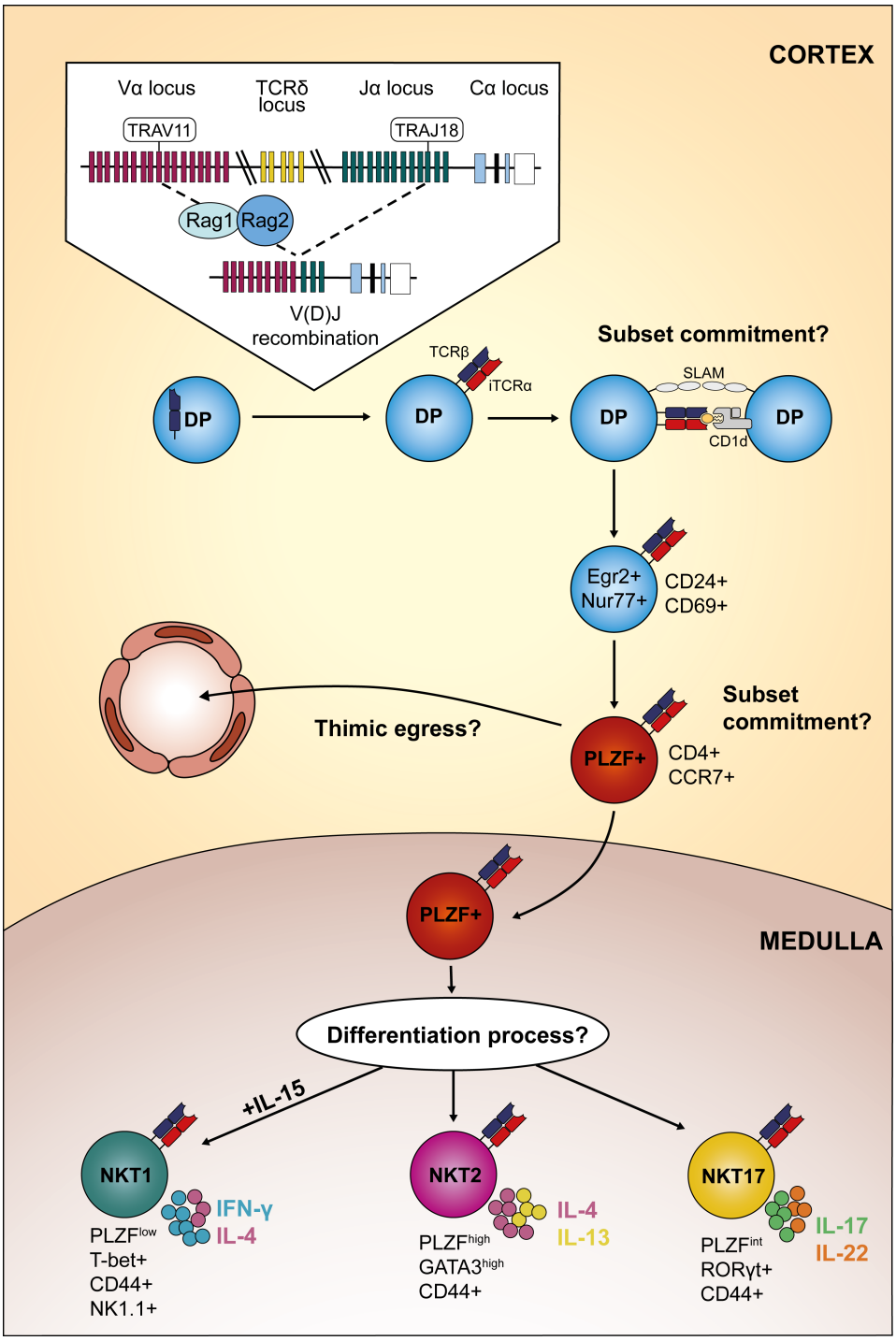

Fig. 1. Schematic representation of NKT cell development and differentiation.

The figure reports the development of NKT cells from the V(D)J recombination to the generation of functional NKT cell subsets. In the thymus, upon V(D)J recombination a Vα14-Jα18 rearrangement can be sporadically generated. The positive selection carried out by DP thymocytes induces a TCR activation, as reported by the expression of CD69 and Nur77 (Gapin, 2016; Moran et al., 2011). Consequently, the expression of the master transcription factor PLZF is induced. These precursors

Fig. 1 **(continued)** cells express CCR7 and can egress the thymus as well as move into the thymic medulla (Wang and Hogquist, 2018). Here, the final differentiation occurs, resulting into three functional subsets termed NKT1, NKT2 and NKT17. These subsets are characterised by differential expression of markers as well as cytokine repertoire. The exact timing of subset commitment as well as differentiation and egress is not completely understood.

1.3.2 Thymic development: from TSPs to DP thymocytes

Thymus-settling progenitors (TSPs) are defined as the progenitors that migrate from the bone marrow through the blood stream, settle in the thymus by entering at the cortico-medullary junction and differentiate into early thymic progenitors (ETPs) (Desanti et al., 2011; Lind et al., 2001; Petrie and Zuniga-Pflucker, 2007; Porritt et al., 2003). Although the identity of TSPs is not completely understood, evidence suggest that they derive from either LMPPs and/or ELPs (Allman et al., 2003; Desanti et al., 2011; Zlotoff and Bhandoola, 2011).

The most immature thymocytes detected in the thymus are called double negative (DN) 1 cells, commonly defined as CD4− CD8− CD44+ CD25− (Porritt et al., 2004). DN1 cells were found to be heterogenous on the base of several markers such as IL-7Rα, CD24, c-Kit and Thy-1. Although all DN1 subpopulations (DN1a-DN1e) could give rise to T cells, injection experiments revealed that c-Kit^{high} IL-7Rα$^{-/low}$ CD24$^{-/low}$ (DN1a and DN1b) represent the true ETPs (Allman et al., 2003; Porritt et al., 2004).

The progression from ETPs to DN3 is a TCR-independent process which implies the migration from the cortico-medullary junction toward the outer cortex (Lind et al., 2001; Porritt et al., 2003). Kinetic analyses revealed that this maturation process is not equally distributed between the different subsets, with ETPs being the longest intermediate (~9-11 days on a total of ~15-16 days) (Porritt et al., 2003). The transition from ETPs to DN2 is outlined by the acquisition of CD25, the outward movement toward deep cortex and consequent increased proliferation (Lind et al., 2001; Porritt et al., 2003; Tourigny et al., 1997). T cell commitment is only completed once the cells reach the DN3 stage (CD44− CD25+ c-Kit−) and simultaneously move to the outer cortex (Lind et al., 2001). Here, DN3 cells undergo extensive recombination

activating gene (RAG)-1 and RAG-2-dependent rearrangement of their TCRß locus in order to generate functional TCR chains (Godfrey et al., 1994; Oettinger et al., 1990; Wilson et al., 1994). Interestingly, the rearrangement of the TCRγ and δ chain gene segments initiates already at the DN2 stage, while the TCRß locus is still largely intact (Livak et al., 1999).

The generation of a pre-TCR complex, composed of freshly rearranged TCRß chain covalently linked to the non-polymorphic pre-Tα chain, coupled with CD3 molecules (one γ, one δ and two ε) and TCR-ζ chain, opens the way for ß-selection (Ardouin et al., 1998; Fehling et al., 1995; Haks et al., 1998; van Oers et al., 1995). In this regard, the expression level of CD27 was shown to reliably discriminate between pre-selection and post-selection cells within DN3, termed DN3a ($CD27^{low}$) and DN3b ($CD27^{high}$), respectively (Taghon et al., 2006).

Failure of generating a functional TCRß and/or TCRγδ culminates in cell death by apoptosis (Falk et al., 2001). Oppositely, successful ß-selection results in inhibition of apoptosis followed by proliferation, prevention of further ß-chain rearrangement of the opposite allele (a.k.a. allelic exclusion) (Borgulya et al., 1992) and down-regulation of CD25, culminating into the entry of the so called DN4 stage (Tourigny et al., 1997). Cells proceed the maturation by upregulating first CD8 to a rapidly cycling stage termed immature single-positive (ISP) (MacDonald et al., 1988) and then CD4, thereby becoming DP thymocytes (Gegonne et al., 2018; Paterson and Williams, 1987). At this stage, the TCRα gene segment somatic rearrangements takes place, resulting in the production of a TCRα chain which can pair with the already rearranged TCRß chain to form a TCR dimer. The fate of cells expressing the newly made TCR is then determined through a process called positive selection where the reactivity of the newly formed TCR is tested, determining its eligibility to continue the differentiation (Huang and Kanagawa, 2001; Jameson et al., 1995).

1.3.3 Somatic V(D)J recombination and rare Vα14-Jα18 rearrangements

Somatic V(D)J recombination is a highly regulated process which is fundamental for the generation of a functional adaptive immune system.

Both B cells and T cells profoundly rely on this mechanism that produces highly antigen-specific immunoglobulins and TCRs, respectively.

TCR structure and genomic landscape

A TCR consist of two chains combined in one heterodimer, either α:ß or γ:δ. Each chain comprises of an antigen-binding variable (V) and a membrane-proximal constant (C) region (Davis and Bjorkman, 1988). These domains adopt an immunoglobulin-like conformation composed by multistrand antiparallel ß-sheet bilayers interposed by loops (Katayama et al., 1995; Novotny et al., 1986). In the variable regions, three of these loops are highly variable and named complementarity-determining regions (CDR) 1, 2 and 3 (Katayama et al., 1995). The variability of these hypervariable regions is either germline determined (in the case of CDR1 and 2) or de novo generated during V(D)J recombination (CDR3) (Davis and Bjorkman, 1988).

At the DNA level, the *Tcr* loci contain numerous V, diversity (D) and joining (J) gene segments; the *Tcrα/δ* loci lack Dα gene segments.

The *Tcrα/δ* locus occupies 1.6 Mb on chromosome 14, and the vast majority of it is occupied by 104 V segment, of which the great majority are Vα. 3' of the Vα gene segments there are two Dδ, two Jδ segments and Cδ, followed by one Vδ segment, 60 Jα segments and the Cα exons (Bosc and Lefranc, 2003; Glusman et al., 2001; Krangel et al., 2004; Thuderoz et al., 2010).

Located on chromosome 6, the *Tcrβ* locus encompasses approximately 0.7 Mb (Rowen et al., 1996) and bears 34 Vß gene segments at the 5' start. Differently from the *Tcrα/δ* locus, the Vß section is followed by two sequentially arranged D-J-C clusters, each of them composed 6 or 7 Jß gene segments bounded by one Dß and one Cß gene segment (Glusman et al., 2001).

V(D)J recombination

Somatic V(D)J recombination consists of systematic double-strand DNA breaks and following re-joining of the gene segments encoding the variable region of the TCR (Hozumi and Tonegawa, 1976). Normally, D-to-J rearrangement occurs first, followed by D-J-to-V joining (Born et al., 1985); as Dα segments are not present, direct Vα-to-Jα rearrangement occurs in the TCRα locus.

Recombination signal sequences (RSSs) are short DNA sequences which flank the coding gene segments and are recognised by RAG-1 and RAG-2 DNA-cutting enzymes during V(D)J recombination (Max et al., 1979; Sakano et al., 1979). The RSS is composed of one heptamer and one nonamer consensus sequence connected by a spacer sequence of either 12 bp or 23 bp (Akira et al., 1987; Early et al., 1980; Max et al., 1979; Sakano et al., 1979). The length of the spacer governs the gene fragment excision choice, as the rearrangement takes place only between RSSs bearing different spacer length (the so-called "12/23 rule") (Steen et al., 1996).

The recombination process can be simplistically described in two steps, namely cleavage and joining (McBlane et al., 1995). During the cleavage phase, RAG proteins (together with the bending factors HMG1A or HMG1B) (van Gent et al., 1997) bind one RSS, nicking the sequence between the RSS and the coding gene segment (Curry et al., 2005; Jones and Gellert, 2002). This single RSS complex (SC) further seeks for a compatible RSS partner to form a paired complex (PC). In this context, RAG proteins nick the partner RSS, driving the formation of a hairpin on the coding end by transesterification through the 3'-OH generated by the nicking, resulting in the cleavage of the RSSs (McBlane et al., 1995).

The joining process is conducted by the classical nonhomologous end joining (cNHEJ) DNA repair pathway (Malu et al., 2012). In the case of coding ends, the hairpins are opened and the two coding ends are ligated introducing minor insertion/deletions. Distinctively, signals ends are joined with almost no variation (Lewis et al., 1985).

Vα14-Jα18 rearrangement: the NKT cell TCR

The TCRα locus retains the exceptional competence to reiteratively rearrange the locus until a productive rearrangement is achieved (Petrie et al., 1993).

The accessibility of Jα gene segments is not equal during the whole V(D)J rearrangement process, and it is controlled by the TCRα enhancer (Eα) (located at the 3' end of the Jα locus) (Sleckman et al., 1997) which in turn regulates the activity of two promoters – namely T early α (TEA) (Mendiratta et al.) and Jα49 (located at the 5' end of the Jα locus). While Eα is essential for all Vα-to-

Jα rearrangements, the two promoters restrict the initial Jα usage to the 5' region of the Jα locus (Hawwari et al., 2005; Villey et al., 1996).
In this regard, TEA and Jα49 promote the transcription of noncoding transcripts spanning over the Jα and Cα gene segments. These transcripts were shown to restrict the initial Jα accessibility by regulating the activity of downstream Jα promoters and remodelling of chromatin structure (Abarrategui and Krangel, 2006; Abarrategui and Krangel, 2007).
Commonly, the initial Vα-to-Jα recombination replaces the TEA (and possibly Jα49) with a Vα promoter, shown to increase the accessibility to a restricted array of downstream Jα gene segments. The V(D)J recombination then proceeds in an outward direction, progressively using more 3' Jα and 5' Vα gene segments, enhancing the exploitation of the full array of Jα gene segments (Hawwari and Krangel, 2007).

The Jα18 gene segment is located in the distal 3' area of the Jα locus in close proximity to Cα; oppositely, the Vα14 gene segment is located in the central region of the Vα locus. Therefore, the Vα14-Jα18 rearrangement probably occurs most often as a secondary rearrangement during relatively later time points (Hawwari and Krangel, 2005). In light of the different Jα segment usage patterns observed during the primary and secondary rearrangements, it is foreseeable that the lifespan of DP thymocytes significantly affects the Vα-to-Jα rearrangement outcome, and in particular the generation of NKT cells (Guo et al., 2002).

Several factors play crucial roles in expanding DP thymocyte lifespan: RORγt (Guo et al., 2002; Sun et al., 2000), T cell factor-1 (TCF-1) (Sharma et al., 2014), Histone Deacetylase 7 (HDAC7) (Kasler et al., 2011), E protein HEB (D'Cruz et al., 2010) and c-Myb (Hu et al., 2010).

RORγt is a transcription factor highly expressed in DP thymocytes that plays a critical role in thymocyte development. Ablation of RORγt results in massive apoptosis of DP thymocytes due to reduced levels of the anti-apoptotic factor Bcl-x_L. Enforced expression of Bcl-x_L supports thymocytes survival, expanding

the window of Vα-to-Jα rearrangements and restoring normal NKT cells development in absence of RORγt (Sun et al., 2000).
Comparable outcomes arise upon ablation of TCF-1 – shown to modulate the expression of RORγt – (Sharma et al., 2014), E protein HEB (D'Cruz et al., 2010), HDAC7 (Kasler et al., 2011) or c-Myb (Hu et al., 2010). However, in the case of c-Myb, the DP survival defect was rescued by Bcl-x_L overexpression, but NKT cell development remained impaired, suggesting its involvement in additional crucial pathways (Hu et al., 2010).

1.3.4 Positive selection

The somatic Vα14-Jα18 rearrangement in the TCRα locus resulting in production of a Vα14i-TCRα-chain, together with the expression of one of a restricted set of TCRß chains (Vß2, Vß7 or Vß8.2) represent a strict requirement for the generation of NKT cells.
Once a double positive thymocyte express these specific α and ß TCR chains it acquires the eligibility to become a NKT cell precursor (termed Vα14i-DP) (Drees et al., 2017).

Similar to T cell precursors, also NKT cell precursors undergo a positive selection process. However, while T cell precursors are positively selected by medullary thymic epithelial cells (mTECs) (Klein et al., 2014), NKT cell precursors undergo positive selection driven by the interaction with other DP thymocytes (Bendelac, 1995; Egawa et al., 2005). This process involves the interaction of the NKT cell TCR with a CD1d molecule, a monomorphic MHC class I-like molecule which presents endogenous glycolipid antigens (Bendelac et al., 1995). A great effort has been invested in the determination of the identity of these endogenous antigens; however, to date there is no clear consensus regarding the identity of the glycolipid antigens responsible for the selection process. (Gadola et al., 2006; Pei et al., 2011; Porubsky et al., 2007; Zhou et al., 2004). Isoglobotrihexosylceramide (iGb3) was one of the first identified endogenous antigens capable of activating NKT cells (Mattner et al., 2005). While a study claimed a role of iGb3 as an essential selective antigen for NKT cells (Zhou et al., 2004), Porubsky et al. showed that mice lacking iGb3

synthase displayed normal NKT cell development (Porubsky et al., 2007), suggesting that other members of this glycolipid family might (also) play a role in the selection process. More recently, a study reported that immune cells produce minute amount of α-linked monoglycosylceramides which could potentially represent the endogenous selecting antigen (Kain et al., 2014). Additionally, endogenous antigens do not strictly need to belong to the glycolipid category but they can be of different nature (Pei et al., 2011).

The CD1d-TCR interaction is combined with a second critical activating signal which is carried out by homotypic interactions between members of the signalling lymphocytic activation molecule (SLAM) family receptor (SFR).
Upon homotypic interaction, the intracellular domains of SFRs can be phosphorylated at the immunoreceptor tyrosine-based switch motifs (ITSM) and therefore recruit the SLAM-adaptor protein SAP and consequently the Fyn kinase. The SLAM-SAP-Fyn complex acts in different ways in the cell; on one side, SLAM-SAP-Fyn can influence the TCR signalling cascade activating NF-κB signalling through PKC-θ and Bcl10. Alternatively, Fyn phosphorylates and recruits the SH2 domain–containing inositol phosphatase (SHIP), Dok1/2 and Ras GTPase-activating protein (RasGAP), ultimately inhibiting the MAPK pathways (Borowski and Bendelac, 2005).

Although the vast majority of NKT cells develop from DP precursors, an alternative pathway for the development of DN NKT cells was recently discovered (Dashtsoodol et al., 2017). In this scenario, DN4 thymocytes which express the NKT cell TCR (Dashtsoodol et al., 2008) can give rise to Th1-type NKT cells with enhanced cytotoxic activity which preferentially home to the liver (Dashtsoodol et al., 2017).

1.3.5 The SLAM-SAP-Fyn signalling pathway

The SFR is composed of 6 receptors: SLAM (SLAMF1), CD48 (SLAMF2), Ly9 (SLAMF3), 2B4 (SLAMF4), CD84 (SLAMF5), Ly108 (SLAMF6) and CRACC (SLAMF7) (Cannons et al., 2011).

Many studies have shown a modest requirement of SLAM and Ly108 for NKT cell development. Overall, deficiency of these two molecules resulted in moderate impairment of NKT cell development and decrease of NKT cell number with the exception of Stage 0 NKT, which did not show major defects (Chen et al., 2017; Griewank et al., 2007; Huang et al., 2016; Jordan et al., 2011; Lu et al., 2019).

However, although the SAP molecule acts downstream of SFRs, the deficiency of this adaptor protein had a more severe impact on NKT cell development, exhibiting a drastic reduction of NKT cell numbers and a substantial developmental block at Stage 0. This effect was at least partially related to Fyn kinase, but it also implied that SAP could display diverse effects on NKT cell development (Kageyama et al., 2012; Nichols et al., 2005; Nunez-Cruz et al., 2008; Pasquier et al., 2005).

Moreover, other phosphatases such as SHIP-1 and SH2 domain phosphatase 1 (SHP-1) were shown to influence NKT cell effector differentiation, function and proliferation (Anderson et al., 2015; Cruz Tleugabulova et al., 2019)

Recent studies shed more light on the role of distinct components of the SLAM-SAP signalling in the positive selection of NKT cells. Chen et al. showed how SAP-dependent SFR signalling signal is essential for the selection of NKT cells through the activation of a CARD9-containing CARMA1–Bcl10–Malt1 (CBM) complex. However, in a SAP-deficiency context, the additional deletion of SFRs minimally affected the phenotype, excluding a strong implication of SFRs in the more severe SAP phenotype and suggesting that SAP-independent SFRs activity does not significantly impact NKT cell development (Chen et al., 2017). Additionally, Ly108 was shown to limit post-selection TCR signalling through the SAP-Fyn pathway. Moreover, Ly108 controls the survival of mature NKT cells (by sustaining Bcl-2 levels) as well as effector functions in a SHP-1-dependent manner (Lu et al., 2019).

Overall, although many aspects remain to be clarified, the SFR-SAP-Fyn pathway plays an important role in the positive selection and subsequent development of NKT cells.

1.3.6 TCR signalling

A peculiarity of NKT cells is the strong TCR signal that they receive upon positive selection. In the case of conventional T cells, a strong TCR signal during positive selection translates into clonal deletion. However, defined T cell subsets are generated upon agonist-selection; these include NKT cells, regulatory T cells (Tregs) and CD8αα intestinal intraepithelial lymphocytes (Leishman et al., 2002; Moran and Hogquist, 2012).

To assess the TCR signal strength in a quantitative manner with single cell resolution, Moran et al. established a murine transgenic model bearing a green fluorescent reporter in a *Nr4a1* transgene (Nur77^{GFP}). *Nr4a1* is an immediate early gene which is rapidly up-regulated upon TCR stimulation (Moran et al., 2011). The analysis of NKT cells revealed that Stage 0 NKT cells expressed high levels of the fluorescent reporter, in a similar range to Treg cells. Both immature Stage 1 and mature Stage 2 NKT cells showed intermediate levels of GFP, while thymic Stage 3 and mature splenic NKT cells expressed very low levels of GFP. This suggests that the time period during which TCR signalling occurs is limited and mainly confined to very early post-selection NKT cells (Moran et al., 2011).

The intricate TCR signalling cascade involves diverse pathways which overall influence the transcriptional landscape. Among these, it determines the release of endoplasmic reticulum (ER)-stored calcium as well as intake of extracellular calcium, leading to the activation of the calcium–NFAT transcriptional signalling (Gaud et al., 2018).
The increased Ca^{2+} concentration leads to the activation of the phosphatase calcineurin, which in turn catalyses the dephosphorylation of transcription factors of the nuclear factor of activated T-cells (NFAT) family, determining its migration to the nucleus and the consequent binding to its target DNA regions.

One of the targets of NFAT factors is the early growth response 2 (Egr2) transcription factor, shown to be absolutely essential for the selection, maturation and survival of NKT cells (Lazarevic et al., 2009).
In line with the previously reported finding of an elevated TCR signal intensity in NKT cells, Egr2 was also shown to display a sustained expression in NKT cells precursors (especially Stage 0) compared to conventional T cells (Seiler et al., 2012).
Importantly, in NKT cells Egr2 was found to directly bind the promoter region of PLZF, mediating its induction and expression. Moreover, Egr2 was shown to control the expression of IL-2Rβ (CD122) and thereby impacting on the maturation of NKT1 cells (Seiler et al., 2012).

1.3.7 PLZF

Particular attention has to be paid to PLZF, the key transcription factor for NKT cell development.
In 2008, two independent studies proposed PLZF as a specific transcription factor required for the development and memory/effector function acquisition of NKT cells (Kovalovsky et al., 2008; Savage et al., 2008). PLZF is expressed in Stage 0 NKT cells at intermediate levels, followed by high levels at Stage 1 and further gradual decrease up to Stage 3, where PLZF reaches low levels (Kovalovsky et al., 2008; Savage et al., 2008). Lethal-7 (let-7) microRNAs, increasingly expressed during NKT cell development, were found to be responsible for the downregulation of PLZF during maturation and the consequent acquisition of a Th1-like phenotype (Pobezinsky et al., 2015).
To assess the impact of PLZF in T cell and NKT cells, PLZF deficient mice were analysed (Kovalovsky et al., 2008; Savage et al., 2008). While conventional T cell did not express PLZF (and therefore where not affected by the deficiency), PLZF-deficient NKT cells presented a dramatic reduction in numbers and an accumulation at Stage 1. Moreover, the few remaining PLZF-deficient NKT cells were mainly located in lymphoid organs at the expense of the liver, showed a naïve phenotype and a decreased ability to produce IL-4 and IFN-γ, strongly resembling conventional CD4+ T cells. Oppositely, overexpression of PLZF in conventional T cells resulted in an impaired distribution of CD4+ T

cells which were highly decreased in lymph nodes and blood. Moreover, they acquired a $CD44^{high}$ $CD62L^{low}$ memory-phenotype and showed an increased frequency of IL-4/IFN-γ double producers, a typical feature of NKT cells (Kovalovsky et al., 2010; Kovalovsky et al., 2008; Savage et al., 2008). Interestingly, overexpression of PLZF did not significantly affect NKT cells (Savage et al., 2008). The acquisition of the typical memory/activated phenotype occurred regardless of antigen stimulation and SAP/Fyn signalling pathway (Kovalovsky et al., 2010) as well as TCR repertoire and selecting cells (Savage et al., 2011), suggesting that PLZF acts independently and downstream of TCR signalling.

Most recently, Park et al. demonstrated that not only the presence of PLZF, but also the quantity produced has an impact on the subset differentiation and effective phenotype acquisition. The employment of an hypomorphic PLZF allele showed that reduced PLZF protein led to decreased NKT cell numbers in thymus and spleen, with a relative increase of NKT1 and a reduction of NKT2 and NKT17 cells (Park et al., 2019).

In addition to NKT cells, PLZF was also detected in human and mouse MAIT cell (Savage et al., 2008) in memory CD4+ T cells (Raberger et al., 2008) as well as in a newly discovered subsets of CD8αα unconventional T cells (Sheng et al., 2019).

Furthermore, a subset of γδ T cells, namely $Vγ1^+$ $Vδ6.3^+/Vδ6.4^+$ cells (also termed γδ NKT cells), showed a PLZF-driven innate-phenotype (Kreslavsky et al., 2009). Similar to NKT cells, this subset of γδ T cells showed impaired functionality (decreased IL-4 and IFN-γ production and absence of double-producers) upon PLZF deficiency. Interestingly, the transgenic expression of the $Vγ1^+$ $Vδ6.3^+/Vδ6.4^+$ TCR as well as strong TCR signalling in polyclonal γδ T cells resulted in PLZF induction.

Overall, these finding presented a new role of PLZF in the regulation of innate-like function and memory/effector acquisition during thymic development.

Given the fact that PLZF is a key transcription factor for NKT cells and directs a memory/effector program, it remains elusive how this transcription factor is only expressed in particular innate cell subsets. Several factors are known to

play a role in PLZF induction: these include Egr2, p21-activated kinase 2 (Pak2), Ly108, Yin Yang 1 (YY1), E proteins, HDAC7 and Jarid2.

As stated above, Egr2 was found to directly bind to the promoter of PLZF inducing its transcription in NKT cells. Egr2 deficiency strongly abrogates NKT cell development but maintains conventional T cells development, suggesting a specific role for Egr2 in NKT cells (Seiler et al., 2012). Interestingly, the Pak2 cytoskeletal remodelling protein was shown to sustain Egr2 and consequently PLZF expression in NKT cells independently of TCR signalling (O'Hagan et al., 2015). Moreover, Pak2 impacted on proper Ly108 expression, supporting the previous hypothesis that Ly108 co-stimulation has a role in PLZF induction (Dutta et al., 2013). Moreover, a recent publication reported the transcription factor YY1 as essential for NKT cell development by sustaining cell survival and directly binding to the PLZF promoter. Mice with YY1-deficiency in T cells displayed a developmental block of NKT cells at Stage 0. The remaining NKT cells did not express PLZF but had normal levels of Egr2, demonstrating that Egr2 alone is not sufficient to induce PLZF (Ou et al., 2019). Moreover, the transcription factor E2A and HEB, part of the E protein family, were shown to directly bind to PLZF and modulate its transcription (D'Cruz et al., 2014)

Importantly, chromatin regulators appear to play a distinct role in the modulation of PLZF induction.

The subcellular localisation of the histone deacetylase 7 (HDAC7) significantly regulates the activity of PLZF. Once in the nucleus, HDAC7 was found to directly bind to PLZF and repress its activity. Contrary, the retention in the cytosol leads to overexpression of PLZF with consequent aberrant effector programs in non-NKT cells (Kasler et al., 2018).

Jarid2, another chromatin regulator component of three lysine methyltransferase complexes, was reported to be upregulated in thymocytes as a result of TCR signalling during positive selection. Jarid2 was found to bind to the PLZF locus and decrease its expression by increasing H3K9me3 (Pereira et al., 2014).

In contrast to other studies proposing that strong TCR signalling induces PLZF expression in thymocytes (Dutta et al., 2013; Kreslavsky et al., 2009; Seiler et al., 2012), Zhang et al. demonstrated that PLZF is stably repressed in non-innate T cells, and that its expression cannot not be induced by TCR activation (Zhang et al., 2015). In line with this notion, the PLZF promoter was found to possess both negative H3K27me3 and positive H3K4me3 modifications in DP thymocytes, while mature NKT cells presented only the positive H3K4me3 mark. The removal of H3K27me3 in CD4-positive thymocytes promoted NKT cell-like differentiation regardless of TCR specificity. Oppositely, the stabilisation of H3K27me3 reduced the NKT cell population (Dobenecker et al., 2015).

Overall, these studies suggested that different levels of epigenetic and transcriptional regulation of the PLZF locus govern its defined expression in innate-like cells, but a complete picture of the molecular mechanisms is still elusive.

PLZF targets

To uncover the transcriptional effects of PLZF in NKT cells, microarrays and ChIP-seq analyses were conducted (Gleimer et al., 2012; Mao et al., 2016). Table 2 reports the most relevant genes shown to be regulated and/or directly bound by PLZF (Table 2). Several genes had a differential expression in the presence or absence of PLZF. Around 7% of these genes belonged to the cytokine/chemokine receptor signalling classification (Gleimer et al., 2012). Some of them where already shown to play a role in NKT cell development, differentiation and function.

The ChIP-seq analysis revealed that PLZF binds to most of the PLZF-regulated genes. PLZF was found to modulate the $CD44^{hi}$ $CD62L^{lo}$ memory/effector phenotype of NKT cells by directly binding to both genes. Additionally, PLZF binds to Klf2, a positive regulator of Sell (encoding CD62L) (Mao et al., 2016). Interestingly, PLZF does not directly bind to cytokine loci (such as *Il4*, *Il13*, *Ifng* and *Il17*); however, it binds cytokine loci regulators and T-helper-specific

Table 2. Relevant genes differentially regulated by PLZF

Gene Name	Protein Name	Category	Effect
*Il12rb1**	IL12RB1	Cytokine receptor	Upregulation
*Il18r1**	IL18R1	Cytokine receptor	Upregulation
*Il21r**	IL21R	Cytokine receptor	Downregulation
*Il4ra**	IL4R	Cytokine receptor	Downregulation
*Il6st**	IL6ST	Cytokine receptor	Downregulation
*Ifngr1**	IFNGR1	Cytokine receptor	Downregulation
Il17rb	IL17R	Cytokine receptor	Upregulation
Ccr10	CCR10	Chemokine receptor	Upregulation
Ccr2	CCR2	Chemokine receptor	Upregulation
*Ccr4**	CCR4	Chemokine receptor	Upregulation
CD40lg	CD40L	Surface molecule	Upregulation
*Icos**	ICOS	Surface molecule	Upregulation
*Slamf6**	Ly108	Surface molecule	Downregulation
*Cd44**	CD44	Surface molecule	Upregulation
*Sell**	CD62L	Surface molecule	Downregulation
*Egr2**	EGR2	Transcription regulator	Downregulation
*Id2**	ID2	Transcription regulator	Upregulation
Tbx21	T-bet	Transcription regulator	Upregulation
Zbtb7b	Th-POK	Transcription regulator	Upregulation
*Gata3**	GATA3	Transcription regulator	Upregulation
*Klf2**	KLF2	Transcription regulator	Downregulation
c-Maf	c-Maf	Transcription regulator	Upregulation
*Runx3**	RUNX3	Transcription regulator	Upregulation
*Rorc**	ROR-γt	Transcription regulator	Upregulation
*Bcl6**	BCL6	Transcription regulator	Downregulation
Bach2	BACH2	Transcription regulator	Downregulation

* genes directly bound by PLZF. (Gleimer et al., 2012; Mao et al., 2016)

transcription factors including *Gata3*, *Maf*, *Rorc* and *Runx3*. Moreover, *Tbx21*, which encodes transcription factor T-bet, is upregulated in the presence of PLZF, despite PLZF does not directly bind the *Tbx21* locus (Gleimer et al., 2012; Mao et al., 2016).

1.3.8 Phenotypic changes during early NKT cell development

The successful positive selection of DP thymocyte precursors expressing an NKT cell TCR defines the beginning of a unique developmental program. After positive selection, early NKT cells undergo a profound reshaping of their phenotypes, which ultimately leads to the emergence of functionally distinct NKT cell subsets.

Post-selection NKT cells retain a phenotype largely similar to their DP thymocyte precursor. In this regard, of great note is the pioneering work of Benlagha et al. who aimed to described the early phases of NKT cell development (Benlagha et al., 2002; Benlagha et al., 2005). In order to detect and analyse extremely rare and early CD24+ NKT cells, NKT cells from 3d, 4d, 5d and 8d old mice were enriched through magnetic cell sorting (MACS) (Benlagha et al., 2005). At 3d, roughly 70% of all Tetramer+-enriched NKT cells were CD24+, and this fraction decreased to 57%, 13% and 2% at days 4, 5 and 8, respectively, suggesting a gradual and relatively fast decrease of CD24 expression upon positive selection. $CD24^{high}$ early NKT cells presented low expression of CD44, lacked NK1.1 and expressed the post-selection activation marker CD69.

At 3d, $CD24^{high}$ cells were mostly CD4+, while the CD24− fraction displayed an equal distribution of CD4+ and DN cells. In older mice, $CD24^{high}$ presented an additional population of DP^{low} cells. Five-to-seven days after intrathymic transfer of CD24− CD4+ NK1.1− NKT cells, two new populations of NK1.1+ CD4+ and NK1.1+ DN cells appeared, demonstrating that CD4+ cells can give rise to more mature DN NKT cells (Benlagha et al., 2005). Although these data suggested a developmental sequence DP → CD4+→ DN, the authors could not

decipher the precise modulation of CD4 and CD8 surface expression during the early phases of development.

Furthermore, the analysis of young mice showed that at 7d old, most of the cells had already downregulated CD24, remained mostly NK1.1− and had a mixed $CD44^{low}$/$CD44^{high}$ expression. The fraction which upregulated NK1.1 was uniformly $CD44^{high}$ (Benlagha et al., 2002). The analysis of 3- and 6-week old mice as well as intrathymic injection experiments revealed a maturational sequence from $CD44^{low}$ NK1.1− to $CD44^{high}$ NK1.1− and further $CD44^{high}$ NK1.1+. Interestingly, the stimulation of these three developmental intermediate states revealed differential cytokine production capabilities (Benlagha et al., 2002). $CD44^{low}$ NK1.1− produced mainly IL-4, $CD44^{high}$ NK1.1− showed a shared IL-4/IFN-γ production profile and $CD44^{high}$ NK1.1+ largely released only IFN-γ (Benlagha et al., 2002; Pellicci et al., 2002).
Differently from $CD24^{high}$ NKT cells, characterised by small size and non-cycling features (Benlagha et al., 2005), CD24− $CD44^{low}$ and CD24− $CD44^{high}$ cells present increased cell size and sustained proliferation (Benlagha et al., 2002). The number of MACS-enriched $CD24^{high}$ and CD24− NKT cells at different age (3d, 4d, 5d and 8d) lead to an estimated expansion of CD24− cells of roughly 8-fold between 4d and 5d of age and 60-fold between 5d and 8d old. Contrarily, the expansion of $CD24^{high}$ cells was almost undetectable between 4d and 5d of age and accounted for less than 6-fold between 5d and 8d, suggesting that the proliferative burst occurs temporally distant from the positive selection (Benlagha et al., 2005).

1.3.9 NKT cell precursor definition

The definition of NKT cell precursors and the separation of immature NKT cells from mature NKT cells has been challenging, especially when relying only on the maturational markers CD44, CD24 and NK1.1.

In addition to the aforementioned markers, early NKT cells display high levels of PLZF (highest at Stage 1) (Kovalovsky et al., 2008; Savage et al., 2008). However, also the NKT2 subset cells express high levels of PLZF, rendering

the separation more difficult. According to the definition of NKT2 cells as IL-4 producers, PLZF^{high} IL-4− NKT cells were analysed. Upon intrathymic injection, PLZF^{high} IL-4− NKT cells could give rise to T-bet+ NKT1 cells, revealing that those cells retain a certain precursor potential (Lee et al., 2013). Moreover, the transcriptome analysis of PLZF^{high} IL-4− NKT reported limited similarity to the functional NKT1, NKT2 and NKT17 (Lee et al., 2016). Altogether, these evidences suggested that the PLZF^{high} population contains a mixture of fully differentiated cells (NKT2) and immature NKT cell precursor.

In this regard, a recent paper evaluated the expression of the chemokine receptor CCR7 on NKT cells and proposed a new definition for a common NKT cell precursor (Wang and Hogquist, 2018).
The majority of CCR7+ NKT cells were CD44$^{-/low}$, CD4+, CD24−. CD69−, T-bet−, RORγt−, IL-4−, PLZF^{high} and expressed high levels of Ki67 and low levels of a Nur77^{GFP} reporter. Upon intrathymic injection, PLZF^{high} CCR7+ NKT cell precursors were able to give rise to all three functional subsets in the thymus as well as migrate to the peripheral organs and continue their maturation.
CCR7 was required for the correct functional differentiation and the localisation in the medulla, where the final maturation takes place (Wang and Hogquist, 2018).
Overall, the aforementioned data clarified a so far controversial definition of NKT cell precursor, confirming the presence of heterogeneity within the PLZF^{high} NKT cell population.

1.3.10 From the thymus to the periphery

Although their development is initiated in the thymus, NKT cells are differentially distributed in many peripheral organs. The first analysis of recent thymic emigrants was performed by two independent groups through in situ labelling of thymocytes of 4- to 6-week old mice (Benlagha et al., 2002; Pellicci et al., 2002). After a labelling period of 24-36h, the RTEs in the spleen and liver were composed of NKT cells with a CD44^{high} phenotype and only minor expression of NK1.1. The percentage of NK1.1+ cells increased to 23% and 55% at 2d and 3d, respectively. A similar pattern was detected in the liver

(Benlagha et al., 2002). These results were additionally confirmed by intrathymic injection of NK1.1− NKT cells or NK1.1− CD4+ NKT cells from 2- to 4-week old mice into NKT cell deficient mice or CD45.1 congenic recipient mice, respectively. After 7d, around 75-85% of injected NKT cells turned on NK1.1 in the thymus, and similar results were seen in spleen and liver (Benlagha et al., 2002; Pellicci et al., 2002). Cell cycle analysis of splenic $CD44^{high}$ NK1.1− NKT cells showed an increased proliferation compared to their NK1.1+ counterpart (Benlagha et al., 2002).
These data, together with the previously mentioned enhanced proliferation of thymic $CD44^{low/high}$ NK1.1− cells, suggested that NKT cells undergo a pre-migratory proliferative burst in the thymus, which continues in the periphery upon arrival. Moreover, NKT cells migrate to the peripheral organs in a partially immature stage and continue their maturation in loco (Benlagha et al., 2002). Along this line, parabiosis experiments revealed that mature NKT cells are largely tissue resident cells, underscoring the concept that NKT cell migration is restricted to a limited period during their development (Wang and Hogquist, 2018).

The mechanism behind the migration of immature NKT cells involves the timed expression of different proteins such as sphingosine-1-phosphate receptor 1 (S1PR1), CD69, Kruppel-like factor 2 (Klf2), CCR7 and CD62-L.
S1PR1 has a well-known role in the modulation of lymphocyte trafficking. It is poorly expressed in thymic NKT cell but highly expressed in hepatic and splenic NKT cells. Independently from the location, NK1.1− NKT cells show higher S1PR1 expression compared to the NK1.1+ counterpart. Knock-out of S1PR1 significantly reduced peripheral but not thymic NKT cells, confirming that S1PR1 is essential for NKT cell thymus egression (Allende et al., 2008).
CD69 is expressed on early CD24+ $PLZF^{high}$ NKT cells and is required for the retention of these precursors in the thymus. Mechanistically, CD69 inhibits the expression of S1PR1. Therefore, absence of CD69 results in premature migration to the peripheral organs (Kimura et al., 2018).
Recently, CCR7 was reported to mark an immature NKT cell population highly prone to migrate to peripheral organs. This population displays high levels of Klf2, a factor essential for the egress of CD4+ and CD8+ T cells from the

thymus and known to regulate the expression of S1PR1 as well as CD62L and CCR7 (Carlson et al., 2006). In the case of naïve T cells, CCR7 and CD62L are necessary for entering the lymph nodes (Girard et al., 2012). Similarly, lymph node NKT cells express high levels of CD62L, while splenic NKT cell are largely negative (Johnston et al., 2003). Therefore, both CCR7 and CD62L play a relevant role in the colonisation of peripheral organs.

1.3.11 Overview of the current understanding of NKT cell fate decisions and functional differentiation

Many studies have expanded our knowledge on the requirements for the generation of NKT cells and the functional differentiation instructed during the development. However, the mechanisms driving NKT cell lineage choices and the subsequent polarisation into functionally distinct subsets remain largely elusive. To date, the current interpretation points towards three critical factors, namely 1) the selecting cell type(s), 2) TCR signalling and 3) microenvironmental factors.

Selecting cell types

Considering that in T cells and NKT cells the positive selection is carried out by two different cell types, it is evident that this can play a role in NKT cell fate decisions.

In a murine model where MHC-II expression is restricted to thymocytes, a particular subset of CD4+ T cells is selected. These cells express low levels of TCR and high levels of CD44, a characteristic feature of NKT cells (Li et al., 2005). Moreover, the development and function of these cells depend on the SAP-Fyn-PKCθ pathway, with SAP being specifically required for IL-4 production (Li et al., 2007b). These innate CD4+ T cells possess effector function and can produce IL-4 and IFN-γ upon TCR stimulation (Li et al., 2007c).

Along this line, the abrogation of CD1d expression on cortical thymocytes and the enforced CD1d expression on epithelial cells resulted in a complete lack of

NKT cells, suggesting that their development requires the direct CD1d-mediated interaction with DP thymocytes (Forestier et al., 2003).
Interestingly, two studies showed that innate thymocyte-selected CD4+ T cells express PLZF both in humans (Lee et al., 2010b) and in mice (Zhu et al., 2013). In the latter study, transgenic mice expressing a TCR originating from thymocyte-selected CD4+ T cells demonstrated that the selection and following development is dependent of SLAM/SAP pathway and part of these cells express IL-4 and PLZF (Zhu et al., 2013). Considering that in a previous study, the forced expression of mTEC-selected CD4+ T cell TCRs (Li et al., 2005) did not lead to the thymocyte-driven selection of innate-like CD4+ T cells, the possibility that the TCR specificity plays a role in the innate-like feature acquisition is still open.

To summarise, in light of the afore-mentioned evidences, it is possible that the selecting cell type, namely DP thymocytes, plays a critical role in the acquisition of an innate-like phenotype and therefore has a crucial role in the NKT cell lineage decision.

TCR signalling

To date, there are controversial hypotheses on how TCR signalling influences the differentiation of NKT cells into defined functional subsets.
Graded reductions in TCR signal strength due to ZAP70 mutations impairs NKT2 and differentially affects NKT17 subset cells. Recently, two studies independently proposed a role for TCR signalling in the functional maturation of NKT cells. To dissect the impact of TCR signalling on NKT cell fate decisions, Tuttle at al. employed two transgenic mouse models hyporesponsive to TCR stimulation, namely SKG (on BALC/c background) and YYAA (on C57BL/6 background) (Hsu et al., 2009; Sakaguchi et al., 2003; Tuttle et al., 2018). SKG mice contain decreased TCR signalling strength due to a hypomorphic mutation in the ZAP70 allele. In these mice, the decreased T cell signal strength resulted in a perturbation of the NKT cell subset distribution, with a predominance of NKT1 and reduction of NKT2 and NKT17. As perceivable, the impaired TCR signal strength in SKG mice resulted in reduced levels of Egr2,

which in turn affected the expression of PLZF (Tuttle et al., 2018). These results were independently confirmed by another study (Zhao et al., 2018).
YYAA mice bear a targeted ZAP70 mutation of two tyrosines into alanines, which reduces TCR-induced ERK phosphorylation in thymocytes, but to a lesser extent compared to the SKG mutation (Hsu, 2009). YYAA mice showed a decrease of NKT2 and increase of NKT17, while NKT1 remained unperturbed (Tuttle et al., 2018). Ly108 was recently reported to decrease the TCR signal upon positive selection (starting from Stage 1). While the study was carried out in SFR KO mice, the effect on TCR signal modulation was reconducted to Ly108 only (Lu et al., 2019). Given the fact the SFR KO mice presented reduced NKT1 and increased NKT17 and NKT2 frequency, it would suggest that persistent/increased TCR signal would skew the NKT cell distribution towards the NKT2 and NKT17 subset (Chen et al., 2017; Lu et al., 2019).

Reduced TCR signal strength due to mutations in CD3ζ or ITK deficiency increase NKT2 and NKT17 frequencies: in $CD247^{6F/6F}$ mice (C57BL/6 background), where TCR signal strength is reduced by roughly 60% due to a phenylalanine substitution in the ITAMs of the CD3ζ (TCR-ζ) chain, the NKT1 subset is reduced, while NKT2 and NKT17 frequencies are increased (Malhotra et al., 2018). In line with this model, Itk-deficient mice (required for a functional TCR signalling cascade) were shown to display low levels of Jarid2. Impaired Jarid2 expression affects NKT cell maturation by skewing the differentiation towards NKT2 and high levels of PLZF, again supporting the theory that lower TCR signalling directs a NKT2 phenotype (Pereira et al., 2014)

miR-181 play a role in the modulation of TCR signalling during positive selection. (Blume et al., 2016; Malhotra et al., 2018). Overexpression of miR-181 resulted in increased TCR signal strength mediated by increased levels of intracellular Ca^{2+} (Li et al., 2007a). As a consequence, deficiency in miR-181 decreases TCR signals and correlate with reduced frequencies of NKT1 cells and increased frequencies of NKT2 and NKT17 (Blume et al., 2016; Henao-Mejia et al., 2013). Moreover, a recent study identified the transcription factor

SOX4 as a regulator of miR-181 expression and therefore regulating TCR signalling and Ca^{2+} influx. Also in this model, NKT cells were skewed toward a NKT2 and NKT17 phenotype (Malhotra et al., 2018).

Overall, it emerges that the current literature does not allow the definition of a clear role of TCR signal strength in the cell fate decisions of NKT cells.

Microenvironmental factors

In addition to known and potentially unknown cell-intrinsic signals, the functional differentiation of NKT cell subsets also depends on microenvironmental stimuli.

NKT1 differentiation and maturation strongly depends on the upregulation of T-bet (Townsend et al., 2004). T-bet itself is upregulated in response to IL-15, which is trans presented by mTECs (Gordy et al., 2011; White et al., 2014).

NKT2 differentiation was shown to be influenced by IL-25 produced by a specialised subtype of mTECs, the so-called thymic tuft cells. In this scenario, tuft cells particularly supported the differentiation of steady-state IL-4-producing NKT2 cells (Miller et al., 2018). Moreover, a recent study demonstrated that the steady-state production of IL-4 depends on TCR signals which NKT2 cells receive in the medulla. By means of mice carrying tissue-specific deficiencies for CD1d, the authors found that among the different CD1d-antigen presenting cells, F4/80+ MerTK+ macrophages are essential for the steady-state IL-4 production of NKT cells and to some extent for the differentiation and survival of NKT2 cells (Wang et al., 2019).

The differentiation of NKT17 cells is under the control of TGF-ß- and IL-7-mediated signals. TGF-ß signalling was shown to impact the development, survival and functionality of NKT17 cells. In particular, both the peripheral IL-17 production and the expansion in response to inflammatory signals was highly dependent on TGF-ß signalling (Havenar-Daughton et al., 2012).

Additionally, both the survival and the homeostasis of NKT17 are strongly supported by IL-7 signalling (Webster et al., 2014).

Overall, these evidences support the hypothesis that microenvironmental factors define and modulate the diverse functional differentiation fates that

NKT cells experience both in thymus and in peripheral organs throughout their development.

1.4 NKT cells in disease and cancer immunotherapy

1.4.1 NKT cells in disease

As mentioned before, NKT cells can play opposite roles in a wide range of pathological conditions including infections, cancer and autoimmune disorders. Here, I present just a few examples and references (including relevant reviews), to provide a glimpse into this vast and fascinating topic to highlight the importance of NKT cell functional differentiation and their plasticity.

Over the years, a plethora of roles, which at times appear contradictory, have been suggested for NKT cells in the context of autoimmune and allergic disorders. This involved allergic and non-allergic asthma, type 1 diabetes, systemic lupus erythematosus and rheumatoid arthritis (Iwamura and Nakayama, 2018; Subleski et al., 2011; Wu and Van Kaer, 2009). NKT cells have also been shown to play a critical role in the pathogenesis of cardiovascular disorders, mainly through the secretion of pro-atherogenic factors (van Puijvelde and Kuiper, 2017). Moreover, in the last years, increasing knowledge has been gathered regarding the involvement of NKT cells in neurological diseases, including multiple sclerosis, ischemic stroke, brain tumours and neurodegenerative diseases (Cui and Wan, 2019). In many of these cases, the discrepancy between the results of various studies do not allow a clear consensus on the roles of NKT cells. Moreover, it is often still a matter of debate whether the perturbed NKT cell numbers and functions play causative roles in the pathogenesis of the respective disease or rather occur as a disease consequence.

In a few instances, NKT cells have been shown to play pathological roles in the development of the disease. One of these is non-alcoholic steatohepatitis (NASH) and liver cancer, where NKT cells actively induce NASH by secretion of LIGHT and cooperate with CD8+ T cells to induce liver damage (Wolf et al.,

2014). Interestingly and in striking contrast, a recent study demonstrated how gut microbiome can inhibit liver tumour growth by the activation and accumulation of hepatic NKT cells (Ma et al., 2018).

1.4.2 NKT cells in cancer immunotherapy

In the last few years, the interest into exploiting NKT cell as potential actors in immunotherapy has increased (Bae et al., 2019; Kitamura et al., 1999; Kriegsmann et al., 2018; Nair and Dhodapkar, 2017; Pyaram and Yadav, 2018; Wolf et al., 2018; Zhang et al., 2019).
NKT cells are well-known for their antitumor activity which they provide through direct or indirect mechanisms, including direct tumour lysis, recruitment and activation of other immune cells as well as modulation of immunosuppressive cells in the tumour microenvironment (Nair and Dhodapkar, 2017).
NKT cell cancer immunotherapies can be simplistically divided in 1) activation of NKT cells through α-GalCer injection or α-GalCer-loaded APCs and 2) NKT cell manipulation and generation of CAR-NKT cell therapy (Kriegsmann et al., 2018; Zhang et al., 2019).

In response to α-GalCer stimulation, NKT cells can release a diverse array of different cytokines (Giaccone et al., 2002; Ishikawa et al., 2005; Nieda et al., 2004). Interestingly, NKT cells were shown to play an important role in the counteraction of immune exhaustion. In this regard, NKT cells restored the function of both NK cells and exhausted CD8+ T cells mainly through cytokine release (IL-21, IL-2 and IL-12) (Bae et al., 2018; Seo et al., 2017; Seo et al., 2018).

The advantages of CAR-NKT over CAR-T cell immunotherapy are manifold: NKT cells seem to be less prone to generate GvHD, an occurring problem in CAR-T cell immunotherapies (Heczey et al., 2014). Moreover, CAR-NKT express a fully functional TCR which is capable of detecting cancer-mediated changes in lipid metabolism or endogenous lipids (Nair and Dhodapkar, 2017). Additionally, the direct tumour lysing effect carried out by NKT cells is highly

promoted by CD1d-TCR interaction. Therefore, CD1d-expressing tumours are more efficiently eradicated then the non-CD1d expressing ones (Bassiri et al., 2014; Haraguchi et al., 2006).

On the other side, the engineered CAR can directly engage the tumour cell and kill it. Within the tumour microenvironment NKT can inhibit the support provided by tumour associated macrophages (TAMs) (Song et al., 2009). In this regard, a study performed using a murine neuroblastoma model showed that CAR-NKT cells can colocalise with CD1d-expressing TAMs and kill them in a IL-15/CD1d-resctricted manner (Xu et al., 2019). These results led to the initiation of the first CAR-NKT clinical trial in man.

On-going clinical trials will reveal whether and to what extent NKT cell immunotherapy can become a powerful tool in our quest to combat cancer.

2. AIM OF THE STUDY

In the last decade, the general knowledge on NKT cell biology has significantly increased. Many outstanding studies unravelled some of the crucial molecular players and processes behind NKT cell differentiation.
However, the precise mechanisms driving the NKT cell development and the peculiar differentiation into subsets with distinct effector/memory properties and phenotypes remain unknown. In particular, the processes occurring during the early phases of NKT cell development are only incompletely understood.

To this end, in this project I aimed to establish and validate a novel genetic system allowing the kinetic analysis of a synchronous wave of NKT cell development from the initial point of positive selection to the generation of functional subsets. With this model I aimed to elucidate the early phases of development and validate some of the latest hypothesis proposed in the literature. In particular, I wanted to determine the impact of TCR signalling on subset fate decisions and to unravel the timing of subset differentiation and functional property acquisition.

My ultimate goal was to obtain a systems biological overview of the developmental acquisition of functional memory-like states by NKT cells.

3. MATERIALS AND METHODS

3.1 Materials

3.1.1 Laboratory equipment

Product	Description	Distributor
Agilent 2100 Bioanalyser	Bioanalyser	Agilent
AutoMACS pro	Cell Separator	Miltenyi Biotech
BD FACS Aria II™	Cell Sorter	Becton Dickinson
BD FACS Canto™	Flow Cytometer	Becton Dickinson
CytoFLEX LX	Flow Cytometer	Beckman Coulter
CytoFLEX S	Flow Cytometer	Beckman Coulter
FACS Aria III™	Cell Sorter	Becton Dickinson
FACS Fusion™	Cell Sorter	Becton Dickinson
LightCycler® 480 Instrument II	Quantitave PCR	Roche Life Science
NEBNext® Magnetic Separation Rack	Magnetic stand	BioLabs
NextSeq Illumina Sequencer	Sequencer	Illumina
QuantStudio 5 Real-Time PCR	Quantitave PCR	Thermo Fisher
Qubit 2.0 Fluorometer	DNA quantification device	Thermo Fisher
Sonorex RK 31 H	Sonicator	BANDELIN electronic

3.1.2 Consumables

Product	Cat. No	Distributor
2x TD buffer	FC-121-1030	Illumina
4-Hydroxytamoxifen	H6278-50MG	Sigma-Aldrich
5x RT-Buffer	EP0752	Thermo Fisher
Advantage 2 PCR Kit	639207	TaKaRa
Agencourt AMPure XP	A63880	Beckman Coulter
Agilent High Sensitivity DNA Kit	5067-4626	Agilent

α-Galactosylceramide	KRN7000	Funakoshi
Anti-APC MicroBeads	130-090-855	Miltenyi Biotec
Antistatic-spatula	17231B	LevGo
BD Pharmingen™ BrdU Flow Kits	559619	BD
Bromodeoxyuridine (BrdU)	423401	BioLegend
cDNA Synthesis Kit	634926	TaKaRa
Corn oil	C8267-500ML	Sigma-Aldrich
Deoxyribonuclease I from bovine pancreas	D4263-5VL	Sigma-Aldrich
Digitonin	G9441	Promega
DimerX I	557599	BD
Easycoll separating solution	L 6145	Biochrom
eBioscience™ Foxp3 / Transcription Factor Staining Buffer Set	00-5523-00	eBioscience™
Eppendorf Safe-Lock Tubes, 1.5 mL, amber	0030120191	Eppendorf
Exonuclease I	M0293	New England BioLabs
Fisherbrand™ Microscopic Slides	11562203	Fisher Scientific
Heparin	9041-08-1	Sigma-Aldrich
Illumina MiSeq v2 Reagent Kit	MS-102-2001	Illumina
Ionomycin	407953	Merck Millipore
Maxima RT	EP0752	Thermo Fisher
MinElute PCR Purification Kit	28004	Qiagen
Monensin 1000x	00-4505-51	eBioscience
NEBNext® High-Fidelity 2X PCR Master Mix	M0541	New England Labs
NexteraXT Kit	FC-131-1096	Illumina
Nuclease-Free Water	AM9937	Ambion
Percoll PLUS	17-5445-01	GE Healthcare
Phorbol 12-myristate 13-acetate	P8139-1MG	Sigma-Aldrich
Protein LoBind Tubes, 1.5 ml, PCR clean	0030108116	Eppendorf
Purified NA/LE Hamster Anti-mouse CD3ε	553057	BD
QIAquick Gel Extraction Kit	28704	Qiagen
Qubit™ dsDNA HS Assay Kit	Q32851	Thermo Fisher
RNeasy Plus Micro kit	74034	Qiagen
Roti®-Histofix 4 %	P087.4	Carl-Roth

SensiMixTM SYBR® 2x PCR Master Mix	QT650-02	Bioline
Sodium acetate	S2889-1KG	Sigma-Aldrich
Tn5 enzyme	FC-121-1030	Illumina
Zymoresearch DNA Clean & Concentrator™	D4004	Zymo Research

3.1.3 Antibodies and staining reagents

Name	Coupling	Clone	Dilution	Cat. No	Distributor
7-AAD	NA	NA	1:200-1:300	00-6993-50	Thermo Fisher
Anti-B220	Biotin	RA3-6B2	1.200	13-0452-82	eBioscience
Anti-BrdU	FITC	3D4	1:20	364104	BioLegend
Anti-CD3ε	PE/Cy7	145-2C11	1:200	1”319	BioLegend
Anti-CD3ε	Biotin	145-2C11	1:100	553059	BD
Anti-CD4	APC-Cy7	RM4-5	1:200	100525	BioLegend
Anti-CD4	BV605	GK1.5	1:400	100451	BioLegend
Anti-CD4	PE	RM4-5	1.500	12-0042-83	eBioscience
Anti-CD4	PE/Cy5	GK1.5	1:2000	100410	BioLegend
Anti-CD8a	APCeF780	53-6.7	1:200	47-0081-82	eBioscience
Anti-CD8a	BV605	53-6.7	1:100	100744	BioLegend
Anti-CD8a	FITC	53-6.7	1.800	11-0081-85	eBioscience
Anti-CD8a	PerCPeF710	53-6.7	1:1000	46-0081-82	eBioscience
Anti-CD11b	Biotin	M1/70	1:200	13-0112-82	eBioscience
Anti-CD11c	Biotin	N418	1:200	13-0114-82	eBioscience
Anti-CD16/ CD32	NA	NA	1:200	14-0161-86	eBioscience
Anti-CD19	Biotin	eBio103	1:200	13-0193-81	eBioscience
Anti-CD24	FITC	M1/69	1:1200	11-0242-82	eBioscience
Anti-CD24	PE/Cy7	M1/69	1:400	25-0242-82	eBioscience
Anti-CD27	APCeF780	LG.7F9	1.400	47-0271-82	eBioscience
Anti-CD44	Ax700	IM7	1:200	103026	BioLegend
Anti-CD44	PE/Cy7	IM7	1:2000	25-0441-82	eBioscience
Anti-CD69	PE/Cy7	H1-2F3	1:100	25-0691-82	eBioscience
Anti-CD103	BV510	2E7	1:50	121423	BioLegend
Anti-CD138	BV421	281-2	1:200	142508	BioLegend
Anti-CD197 (CCR7)	BV421	4B12	1:50	566291	BD
Anti-CD197 (CCR7)	PE	4B12	1:100	12-1971-82	eBioscience

Anti-CD278 (ICOS)	biotin	7E.17G9	1:100	13-9942-81	eBioscience
Anti-CD278 (ICOS)	BV421	C398.4A	1:1000	313523	BioLegend
Anti-CD279 (PD-1)	PE/Cy7	J43	1:500	25-9985-82	eBioscience
Anti-Egr2	PE	erongr2	1:400-800*	12-6691-82	eBioscience
Anti-Foxp3	PE	FJK-16s	1:30	12-5773-82	eBioscience
Anti-GATA3	PE	TWAJ	1:100	12-9966-42	eBioscience
Anti-GATA3	PE CF594	L50-823	1:50	563510	BD
Anti-GATA3	PerCPeF710	TWAJ	1:500-1000*	46-9966-42	eBioscience
Anti-IgG1	APC	X56	NA	550874	BD
Anti-IL-4	BV421	11B11	1:100	504119	BioLegend
Anti-IL-17A	BV605	TC11-18H10	1:50	564169	BD
Anti-IL-17RB	PE				
Anti-IL-23R	BV421	12B2B64	1:800	150907	BioLegend
Anti-IFN-γ	PE/Cy7	XMG1.2	1:200	25-7311-82	eBioscience
Anti-Ki67	PerCPeF710	SolA15	1:5000	46-5698-80	eBioscience
Anti-Neuropilin-1	BV421	3E12	1:100	145209	BioLegend
Anti-NK1.1	BV421	PK136	1:200	108741	BioLegend
Anti-NK1.1	BV650	PK136	1:50	108736	BioLegend
Anti-NK1.1	BUV395	PK136	1:50	564144	BD
Anti-NK1.1	BUV737	PK136	1:100	741715	BD
Anti-NK1.1	PE	PK136	1:100	12-5941-82	eBioscience
Anti-NK1.1	PE/Cy7	PK136	1:200	25-5941-81	eBioscience
Anti-PLZF	Ax488	Mags.21.F7	1:400-1:600*	53-9320-82	eBioscience
Anti-PLZF	PE	9E12	1:300	145803	BioLegend
Anti-PLZF	PE/Cy7	9E12	1:700-1:1400*	145806	BioLegend
Anti-RORγt	BV421	Q31-378	1:200-1:400*	562894	BD
Anti-RORγt	PEeF610	B2D	1:50-1:100*	61-6981-82	eBioscience
Anti-RORγt	PerCPeF710	B2D	1:200-1:400*	46-6981-82	eBioscience
Anti- $S1P_1$	NA	713412	1:12.5	MAB7089	R&D Systems
Anti-Streptavidin	PerCP-Cy5.5	NA	1:100	45-4317-82	eBioscience
Anti-Streptavidin	BV650	NA	1:100	405231	BioLegend
Anti-T-bet	BV605	4B10	1:50-100*	644817	BioLegend
Anti-T-bet	PE/Cy7	4B10	1:200-400*	25-5825-82	eBioscience
Anti-TCRß	BV510	H57-597	1:200	109234	BioLegend
Anti-TCRß	BV605	H57-597	1:100	562840	BD

Donkey Anti-Rat IgG (H+L)	FITC	NA	1:100	A18746	Thermo Fisher
LIVE/DEA™ Fixable Near-IR Dead Cell Stain Kit	NA	NA	1:2000	L10119	Invitrogen
mCD1d-PBS57	APC	NA	1:300	NA	NIH Tetramer Core facility
PromoFluor-840, NIR maleimide	NA	NA	1:1000	PK-PF840-3-01	BioConnect
Purified Mouse IgG1 λ	Isotype Control	A111-3	NA	553485	BD
Zombie UV™ Fixable Viability Kit	NA	NA	1:1000	423108	BioLegend

(* = dilutions used with eBioscience™ Foxp3 / Transcription Factor Staining Buffer Set)

3.1.4 Oligos

Name	Sequence
Ad1_noMX	AATGATACGGCGACCACCGAGATCTACACTCGTCGGCAGCGTCAGATGTG
Ad2.1_TAAGGCGA	CAAGCAGAAGACGGCATACGAGATTCGCCTTAGTCTCGTGGGCTCGGAGATGT
Ad2.2_CGTACTAG	CAAGCAGAAGACGGCATACGAGATCTAGTACGGTCTCGTGGGCTCGGAGATGT
Ad2.3_AGGCAGAA	CAAGCAGAAGACGGCATACGAGATTTCTGCCTGTCTCGTGGGCTCGGAGATGT
Ad2.4_TCCTGAGC	CAAGCAGAAGACGGCATACGAGATGCTCAGGAGTCTCGTGGGCTCGGAGATGT
Ad2.5_GGACTCCT	CAAGCAGAAGACGGCATACGAGATAGGAGTCCGTCTCGTGGGCTCGGAGATGT
Ad2.6_TAGGCATG	CAAGCAGAAGACGGCATACGAGATCATGCCTAGTCTCGTGGGCTCGGAGATGT
Ad2.7_CTCTCTAC	CAAGCAGAAGACGGCATACGAGATGTAGAGAGGTCTCGTGGGCTCGGAGATGT
Ad2.8_CAGAGAGG	CAAGCAGAAGACGGCATACGAGATCCTCTCTGGTCTCGTGGGCTCGGAGATGT
Ad2.10_CGAGGCTG	CAAGCAGAAGACGGCATACGAGATCAGCCTCGGTCTCGTGGGCTCGGAGATGT
Ad2.11_AAGAGGCA	CAAGCAGAAGACGGCATACGAGATTGCCTCTTGTCTCGTGGGCTCGGAGATGT

Ad2.12_GTAGAGGA	CAAGCAGAAGACGGCATACGAGATTCCTCTACGTCTCGT GGGCTCGGAGATGT
Ad2.13_GTCGTGAT	CAAGCAGAAGACGGCATACGAGATATCACGACGTCTCGT GGGCTCGGAGATGT
Ad2.14_ACCACTGT	CAAGCAGAAGACGGCATACGAGATACAGTGGTGTCTCGT GGGCTCGGAGATGT
Ad2.15_TGGATCTG	CAAGCAGAAGACGGCATACGAGATCAGATCCAGTCTCGT GGGCTCGGAGATGT
Ad2.16_CCGTTTGT	CAAGCAGAAGACGGCATACGAGATACAAACGGGTCTCG TGGGCTCGGAGATGT
E5V6NEXT	5'-iCiGiCACACTCTTTCCCTACACGACGCrGrGrG-3'
Illumina-adapter-1 (forward)	GTCTCGTGGGCTCGGAGATGTGTATAAGAGACAG
Illumina-adapter-2 (reverse)	TCGTCGGCAGCGTC AGATGTGTATAAGAGACAG
Mouse TCRα (reverse)	Illumina-adapter-2 GGTGAACAGGCAGAGGGTGCTGTC
P5-Nextera	AATGATACGGCGACCACCGAGATCTACACTCGTCGGCAG CGTC
P7-TrueSeqP5	CAAGCAGAAGACGGCATACGAGATACACTCTTTCCCTAC ACGACGCTCTTCCGATCT
SINGV6	5'-/5Biosg/ACACTCTTTCCCTACACGACGC-3'
Universal primer long, (short forward)	CTAATACGACTCACTATAGGGCAAGCAGTGGTATCAACG CAGAGT
Universal primer mix, (short forward)	Illumina-adapter-1 - CTAATACGACTCACTATAGGGC

3.1.5 Buffers

Name	Components	Cat. number	Distributor
CB Buffer	1x DPBS (500 ml)	14190-169	Thermo Fisher
	Fetal Bovine Serum (2%)	10270-106	Gibco
	EDTA 0.5 M (0.4%)	0000142515	Promega
FACS Buffer	1x DPBS (500 ml)	14190-169	Thermo Fisher
	BSA (0.5%)	0163.4	Carl-Roth
	Sodium azide (0.1%)	1.06688.0100	Merck
Lysis Buffer	2x TCL Buffer (50%)	1070498	Qiagen

	Nuclease-Free Water (49%)	AM9937	Ambion
	ß-mercaptoethanol (1%)	8.05740-0250	Merck
MACS Buffer	1x DPBS (500 ml)	14190-169	Thermo Fisher
	BSA (0.5%)	0163.4	Carl-Roth
	EDTA 0.5 M (0.4%)	0000142515	Promega
Stimulation medium	RPMI medium 1640 (500 ml)	21875-034	Gibco
	IL-2 (200 U/ml, 1:5000)	SRP3085	Sigma-Aldrich
	IL-7 (10 ng/ml)	577802	BioLegend
	LEAF™ Purified anti-mouse CD28 (10 µg/ml)	102111	BioLegend
T-cell medium	RPMI medium 1640 (500 ml)	21875-034	Gibco
	Fetal Bovine Serum (10%)	10270-106	Gibco
	L-Glutamine (1%)	25030-081	Gibco
	HEPES, 1M (1%)	15630-056	Gibco
	Sodium pyruvate (1%)	11360-039	Gibco
	Non-essential amino acids (1%)	L10119	Invitrogen
	Penicillin-Streptomycin (1%)	15140122	Gibco
	2-mercaptoethanol (0.1%)	31350-010	Gibco

3.2 Methods

3.2.1 Genetically modified mouse strains

All the mice used in this project have been housed in a specific pathogen-free (SPF) or specific and opportunistic pathogen free (SOPF) condition, according to the legislation of the European Union and the Region of Upper Bavaria. Mice were bred and housed in mouse facilities in Charles River Calco (Italy) and in the Centre for Preclinical Research of the MRI (Zentrum für Präklinisches Forschung, ZPF) in Munich.

All the mouse strains used in this project have been generated or later backcrossed to C57BL/6 background and have been previously published.

CD4-CreER^{t2}

CD4-CreER^{t2} mice express an inducible Cre-recombinase under the control of CD4. To generate the line, a targeting vector containing CreER^{t2} and a neomycin gene flanked by FRT sites was inserted in the Exon 2 of CD4 gene by homology recombination (Sledzinska et al., 2013).

Vα14i^{StopF}

Vα14i^{StopF} mice contains a conditional and productive NKT-TCR sequence which can be expressed upon Cre-recombinase expression. In detail, the knock-in allele is composed of four SV40-polyadenylation sites, a STOP-cassette flanked by loxP sites and a pre-rearranged Va14-Jα18 sequence. These elements were cloned into the endogenous TCRα locus downstream of Ja1 and upstream of the first Ca exon. The 4pA was inserted to abort any possible upstream recombination. The expression of the Vα14i^{StopF} transgene occurs upon deletion of the loxP-STOP-loxP cassette via Cre-recombinase (Vahl et al., 2013).

Traj18KO

Traj18KO mice bear a deletion of Jα18 segment in the TCRα locus, which prevents the generation of iNKT cells. The targeting vector contained a two loxP sites, one 5' and the other 3' of Traj18. Moreover, downstream of Traj18 an FRT-flanked Neomycin was inserted. Upon homologous recombination, Neomycin and Traj18 segment were removed by breeding the mice with CAG-FLP recombinase and CAG-Cre recombinase mice, respectively (Dashtsoodol et al., 2016).

Jα18-KO

Jα18-KO mice are deleted for the Jα18 segment in the TCRα locus and lack iNKT cells. The mice were generated by replacing the Jα18 fragment with a Neomycin gene by homologous recombination (Cui et al., 1997). The Neomycin cassette inserted in the TCRα locus was later found to disturb the TCR repertoire of conventional T cell (Bedel et al., 2012).

Nur77eGFP

Nur77eGFP mice were developed as a reporter of TCR and BCR signal strength. Nur77, encoded by the *Nr4a1* gene, is an orphan nuclear receptor which is located downstream of TCR which can be activated within few hours in response to TCR activation (Cunningham et al., 2006). The mice carry a modified BAC transgene, in which the eGFP was inserted at the start site of Nur77 (Zikherman et al., 2012).

PLZFeGFP

PLZFeGFP mice are reporters for the transcription factor promyelocytic leukemia zinc finger (PLZF). The mice carry a modified BAC transgene consisting of a complete PLZF locus where part of the start site was replaced with the eGFP coding part, followed by a stop codon (Zhu et al., 2013).

R26-tdTomato

R26-tdTomato mice are Cre-recombinase reporters which can express tdTomato fluorescent protein in the presence of Cre-recombinase. The targeting vector carried a CAG promoter followed by a floxed-STOP cassette and tdTomato fluorescent protein. The elements were inserted between Exon 1 and Exon 2 of Rosa-26 locus by homologous recombination. The STOP cassette can be excised upon Cre-recombinase activity (Madisen et al., 2010).

***Nr4a3*-Tocky**

Nr4a3-Tocky mice were design as a system to analyse the time and frequency domains of TCR signalling activation. The *Nr4a3* gene encodes for the Nor1 orphan receptor and it was found to be an immediate-early TCR gene. A BAC transgene carrying the *Nr4a3* gene was modified replacing the Exon 3 with a timer (Fast-FT) gene, followed by a poly-A tail and a floxed-Neomycin gene (Bending et al., 2018). A Timer (Fats-FT) gene encodes a mutated for of mCherry fluorescent protein. This protein was mutated in several position to generate an instable fluorescent protein which converts from a protonated blue GFP-like to an anionic red DsRed-like state (Subach et al., 2009).

To study the development and differentiation of NKT cells in vivo, I bred CD4-CreER^{t2} mice with Vα14i^{StopF} mice and generated an inducible Cre-recombinase system. I further bred the mice with either Traj18KO or Jα18-KO mice to abrogate the generation of endogenous NKT cells. For the purpose of this project, these two mouse models behave similarly and are therefore combined under the name Traj18KO.
To investigate NKT cell colonization of peripheral organs, I generated CD4-CreER^{t2} - Vα14i^{StopF}-tdTomato mice (with and without Traj18^{ko}). To dissect the TCR signal dynamics I bred the CD4-CreER^{t2} - Vα14i^{StopF} mice (with and without Traj18$^{ko/ko}$) with either Nur77eGFP mouse strain or *Nr4a3*-Tocky. CD4-CreER^{t2} - Vα14i^{StopF} - *Nr4a3*-Tocky mice were additionally bred with PLZFeGFP mice.

3.2.2 4-Hydroxytamoxifen preparation

4-Hydroxytamoxifen (4-OHT) was reconstituted and diluted at a final concentration of 3 mg/ml. To prepare 1 ml of solution, 3mg of 4-OHT were collected from the original vial with an antistatic spatula and weighted on a microscale directly in a 1.5 ml safe-lock light-protected tubes. Hundred microliters of 96% ethanol were added to the tube, followed by 900 µl of corn oil. The tube was then sealed and placed in a water bath sonicator for 30 min, or until it was completely dissolved. The tubes were then appropriately labelled and stored in a light-protected box in the freezer (-20° C). Each vial was sonicated for 10 min prior administration to the animals. During the whole preparation procedure, the appropriate Personal Protective Equipment (PPE) was used.

3.2.3 Mouse experiments

All the animals were analysed between 6 and 14 weeks of age. In order to induce the Cre-recombinase, one single dose of 100 µl of 4-OHT solution (corresponding to 0.3 mg of 4-OHT) was administered to the mice by oral gavage. All the experimental procedures were performed according to the

licence for animal experiments (TVA 55.2-1-54-2532-234-2015) granted by the Region of Upper Bavaria.

3.2.4 Organ collection and processing

Organ collection

Blood was aspirated with a syringe from the heart directly after euthanasia. The blood was then placed in a 50 ml tube containing 50 µl of heparin (20 U/ml), mixed and diluted with 20 ml of CB buffer. For each mouse, a total of 10 lymph nodes was collected and pooled: inguinal (2), branchial (2), axillary (2), and superficial cervical (4). Liver was perfused with cold PBS via the portal vein until the liver was opaque. Spleen and thymus were also collected. Every organ was placed in a tube containing CB buffer and kept on ice.

Organ processing

To lyse erythrocytes, 5 ml of Gey's solution was added to the blood samples. After 5 minutes, the solution was neutralized with 20 ml of CB Buffer, the samples were centrifuged and the procedure was repeated.

Lymph nodes, spleen and thymus were smashed between two microscopic glass slides. The single cell suspension was resuspended in CB buffer and filtered.

Liver was smashed through a 70 µm filter. The mononuclear cells were isolated with two methods: 1) the single cell suspension was washed in PBS and resuspended in 6ml of 40% isotonic Easycoll separating solution. 4ml of 80% isotonic Easycoll separating solution was placed in a 15 ml tube, and the single cell suspension solution was carefully overlayered. The samples were centrifuged at RT for 20 min at 900g (no brakes, no acceleration). The upper layer of hepatocytes was aspirated and the mononuclear cell were isolated from the 40/60% interface; 2) the single cell suspension was washed in MACS buffer and resuspended in 15 ml of 37% Percoll PLUS. The solution was thoroughly vortexed and centrifuged at RT for 20 min at 900g (no brakes, no acceleration). The supernatant was carefully aspirated and the cell suspension was washed with CB buffer. In both methods, RBC lysis was performed on the isolated cells to eliminate red blood cells.

For all the organs, living cells were counted using a Neubauer counting chamber and Trypan Blue.

3.2.5 Dimer preparation

Alpha-galactosylceramide (α-GalCer) was dissolved in DMSO at a concentration of 1 mg/ml and further diluted to 0.2 mg/ml with PBS containing 0.5% Tween20.

To prepare 50 µl of Dimer-APC staining, 11.2 µl of DimerX I–a recombinant CD1d:Ig fusion protein was mixed with 5.2 µl of diluted α-GalCer and incubated overnight at 37°C. The day after, the α-GalCer-loaded Dimer was labelled with 28 µl of APC Rat Anti-Mouse IgG1 and incubated 1 hour at RT. To stop the labelling reaction, 5.6 µl of Purified Mouse IgG1 λ Isotype Control was added to the mix. After 30 min of incubation at RT, the mixture was stored in the fridge. Dimer-APC was always prepared fresh on the day before the experiment.

3.2.6 Flow cytometry

Four to 8 million cells were stained in 96 well V-bottom plates for flow cytometry analyses. First, cells were washed with PBS and stained with fixable live-dead dye and anti-mouse CD16/CD32 monoclonal antibody, used for blocking the unspecific binding of antibodies to Fc receptors (25 min, 4°C). After washing with FACS buffer, the samples were stained with mCD1d-PBS57 tetramer for either 30 min at RT or 20 min at 4°C – depending on the quality of the NIH-tetramer batch. In the particular case of *Nr4a3*-Tocky analysis, cells were stained with mCD1d-PBS57 tetramer for 1h on ice (dilution 1:250). Cells were then washed and stained with extracellular markers antibodies (20 min, 4°C). In the case of biotinylated antibodies or chemokine receptor antibodies, a 2-step staining was performed. After mCD1d-PBS57 tetramer staining, the samples were incubated with biotinylated antibodies (30 min, 4°C) or chemokine receptor antibodies (40 min, 37°C). In case of S1PR1, cells were stained with anti-$S1P_1$ for 30 min at 4 °C, washed and stained with

secondary anti-rat FITC antibody (30 min, 4 °C). Following the incubation, the cells were washed and stained with the extracellular marker antibody mixture. Cells were then washed and fixed with either eBioscience™ Foxp3/Transcription Factor Staining Buffer Set (20 min, 4°C) or with a solution of 2% Roti®-Histofix 4 % (45min, 4°C). After the incubation time, cells were washed with Permeabilization Buffer, blocked with anti-CD16/CD32 monoclonal antibody and stained with the intracellular antibody mixture. Samples were intracellularly stained for 1h, 4°C, washed and stored in the fridge. In case of Roti®-Histofix 4 % fixation, the cells were stained overnight. Samples were acquired in BD FACS Canto™, CytoFLEX S or CytoFLEX LX flow cytometers.

3.2.7 In vivo Bromodeoxyuridine (BrdU) assay

Mice were injected i.p. with 200 µl of BrdU solution either 30 min or 4 hours before euthanasia. Thymus and spleen were collected and processed in order to obtain a single cell suspension. Ten million cells were transferred in a 96-well plate, washed and used for BrdU staining. Samples labelled with live-dead staining, blocked and stained with extracellular antibodies mixture as reported above. Samples were then fixed with 100µl of BD Cytofix/Cytoperm™ Buffer (BD Pharmingen™ BrdU Flow Kit) for 30 min on ice. After washing with diluted BD Perm/Wash™ Buffer (BD Pharmingen™ BrdU Flow Kit), cells were permeabilised with 100 µl of BD Cytoperm™ Permeabilization Buffer Plus (10 min, on ice) (BD Pharmingen™ BrdU Flow Kit), followed by a re-fixation of 5 min (on ice).

In order to render the incorporated BrdU available for labelling, cells were treated with Deoxyribonuclease I (DNase I). DNase I was solubilised with PBS to a final concentration of 1 mg/ml. The working solution consisted of 3 part of DNase solution and 7 part of FACS buffer. After washing, the supernatant was completely removed and each sample was resuspended in 35 µl of DNase working solution and incubated at 37°C for 1 hour. Following incubation, cells were washed wit BD Perm/Wash™ Buffer and stained with 50 µl of intracellular antibody mixture containing anti-BrdU antibody overnight at 4°C. The following day, cells were washed and resuspended in FACS buffer

containing the DNA-labelling dye 7-Aminoactinomycin D (7-AAD, dilution 1:200). Samples were acquired in CytoFLEX LX flow cytometer.

3.2.8 Ex vivo cytokine stimulation

Ten to 30 million thymocytes and splenocytes were used for ex vivo cytokine stimulation. For each sample, 2/3 of cells were stimulated and 1/3 were used as unstimulated control. Cells were resuspended at a concentration of 10 Mio/ml in T-cell medium. Phorbol-12-myristat-13-acetat (PMA, 100 ng/ml), ionomycin (1 µM), and monensin (2 µM) were added to the stimulated samples, while the unstimulated controls were only treated with monensin (2 µM). The samples were incubated for 4h in the incubator at 37° C. Cells were then washed with PBS and stained as described above.

3.2.9 iNKT cell enrichment

For diverse experiments which required sorted samples, NKT cell were enriched either by direct anti-TCR positive enrichment of by depletion of CD8+ cells.

NKT-TCR positive enrichment

Single cell suspension of thymocytes were stained with anti-CD16/CD32 monoclonal antibody (15 min, 4°C). After washing, cells were incubated with either mCD1d-PBS57 tetramer-APC or CD1d-Dimer-APC for 20 min at 4°C or 45min on ice, respectively. Samples were then washed, resuspended in MACS buffer (80 µl/10 Mio) and labelled with anti-APC MicroBeads (20 µl/10 Mio) for 15 min at 4°C. Cell were then washed and resuspended in 500µl of MACS buffer. Enrichment was performed with AutoMACS Pro using the program Possels.

CD8 depletion

Single cell suspension of thymocytes were stained with anti-CD16/CD32 monoclonal antibody (15 min, 4°C). Samples were then washed, resuspended

in 500 µl of MACS buffer and labelled with 70 µl of anti-CD8 MicroBeads for 15 min at 4°C. After washing, cells were resuspended in 2 ml of MACS buffer. Enrichment was performed through LS Columns with QuadroMACS.

3.2.10 In vitro TCR stimulation

One day before the experiment, tissue culture 96-well flat-bottom plates were coated with 100 µl of PBS containing anti-CD3ε antibody (2 µg/ml).
Thymocytes were enriched by CD8-depletion and consequently stained with 10 µl of CD1d-Dimer-APC for 1h on ice. Afterwards, cells were stained for the extracellular marker antibodies according to the sorting panel. The sorting was performed in a BD FACS Aria™ III or BD FACS Aria™ Fusion. The target populations were sorted in PBS and centrifuged at 300g for 5 min. The pre-coated 96-well plate was washed once with PBS. Cells were then resuspended in 200 µl of stimulation medium and plated in the pre-coated plate. Twenty-four hours later, samples were harvested, washed once with PBS and stained with fixable live-dead dye for 20 min. Samples were acquired with CytoFLEX LX flow cytometer with single tube loader mode.

3.2.11 TCR profiling

Sample preparation

Thymi and spleens were pre-enriched with AutoMACS Pro. Specifically, thymocytes were depleted with anti-CD24 antibody (FITC, 1:200) while spleens were depleted with anti-CD19, B220, CD11b and CD11c antibodies. The negative fraction was stained with extracellular marker antibodies according to the sorting panel. Cells were then resuspended in a solution of FACS Buffer and live-dead dye 7-AAD.
The sorting was performed in a BD FACS Aria™ III. For each sample, T cells and NKT cells were sorted in 1.5ml Protein low binding filled with 350 µl of RLT buffer. Tubes were centrifuged and stored at -80°C.

Library preparation

RNA extraction from sorted cells was performed using RNeasy Plus Micro kit. The cDNA was generated with reagents from cDNA Synthesis Kit according to an in-house modified protocol based on the manufacturer's protocol. One µl of 12 µM OligodT was mixed with 4,5 µl of RNA and incubated for 3 min at 72°C, followed by 2 min at 42°C and placed on ice immediately.
RACE-Mastermix was prepared as follow:

2.5 mM	DTT
1 mM	dNTP mix
0.6 µM	SMARTer IIA Oligonucleotide
10 U	RNase Inhibitor
50 U	SMARTScribe Reverse Transcriptase
1X	First-Strand-buffer

Directly after incubation, 4.5 µl RACE were added and the PCR program was continued for 90 min at 42°C and 10 min at 72°C. The DNA-amplicons for Illumina sequencing were generated by using Advantage 2 PCR employing a mTCRα reverse primer and a Universal primer mix (UPM). The full generated cDNA (10 µl) were processed. After agarose-electrophoresis, the DNA was purified using QIAquick Gel Extraction Kit. The purified product of each sample was indexed by an indexing-PCR with Nextera-Primers. Finally, a pool of the samples was sequenced employing Illumina MiSeq v2 Reagent Kit.

3.2.12 SCRB-sequencing

Sample preparation

Thymic NKT were pre-enriched with AutoMACS Pro. The positive (enriched) fraction was stained with extracellular marker antibodies according to the sorting panel. Cells were then resuspended in a solution of FACS Buffer and live-dead dye 7-AAD.
The sorting was performed in a BD FACS Aria™ II, BD FACS Aria™ III or BD FACS Aria™ Fusion. For each sample, 1000 cells were sorted in a well of a 96-

well PCR plate pre-filled with 5µl of lysis buffer. When possible, 3 wells were sorted for each population. Plates were sealed, centrifuged and stored at -80°C.

Library preparation

Frozen cell lysates were thawed and RNA was isolated using Agencourt AMPure XP magnetic beads. Purified RNA was resuspended in 5 µl of elution buffer and the template switching reverse transcription reaction was carried out as follows:

5 µl	RNA-containing eluate from sorted cells
1µl	10µM E3V6NEXT (barcoded oligodT)
2 µl	5x RT-Buffer
1 µl	10mM dNTPs
0.1 µl	100µM E5V6NEXT TSO (template switch oligo)
0.125 µl	Maxima RT
0.775 µl	ddH_2O

Samples were incubated for 90 min at 42 °C. Consequently, samples were pooled and cDNA was purified with Zymoresearch DNA Clean & Concentrator™ according to the manufacturer's protocol. DNA was eluted in 18 µl ddH_2O and residual primers were removed by adding 1 µl of Exonuclease I and 2 µl of buffer. Samples were incubated first for 30 min at 37°C and then 20 min at 80°C. cDNA was amplified with a single primer PCR as follows:

20 µl	cDNA (Exo I mix)
25 µl	Kapa Hifi Hot Start
1 µl	10µM SINGV6 primer
4 µl	H_20

PCR conditions:

98°C 3 min

98°C 15 sec
65°C 30 sec
68°C 6 min
} 15 cycles

72°C 10 min

Amplified cDNA was purified with Agencourt AMPure XP magnetic beads (0.6x) and the concentration was determined.
The full-length cDNA was then tagmented using the Nextera XT library preparation kit (Illumina). For each sample, two reactions were perfomed in parallel as follows:

5 µl	cDNA (0.8 ng)
10 µl	tagmentation buffer
5 µl	Tn5 enzyme

Samples were incubated for 10 min at 55 °C. The transposase reaction was stop by incubating the sample for 5 min at RT with 5 µl of stop-buffer. A second amplification step was performed as follow:

25 µl	transposed cDNA mix
5 µl	P7-TrueSeqP5 (5 µM)
2.5 µl	P5-Nextera (5 µM, Illumina)
2.5 µL	H_20
15 µl	MasterMix NPM

PCR conditions:

72°C 3 min	
95°C 30 sec	
95°C 15 sec	13 cycles
55°C 30 sec	
72°C 60 sec	
72°C 5 min	

For each sample, the two reactions were pooled, the cDNA was purified with Agencourt AMPure XP magnetic beads (0.6x) and the concentration was determined. The library quality was assessed with Bioanalyzer (Agilent High Sensitivity DNA Kit). Libraries were then sequenced on NextSeq Illumina Sequencer.

Analysis

After quality control of raw sequencing data, downstream processing of the UMI filtered count matrix was performed with R version 3.4.4.

For initial quality control and Principal Component analysis (PCA) genes having less than 20 reads in sum across all samples were removed from the data set. This is done to prevent the detection of high variation due to noisy measurements (e.g. genes with very few reads in unrelated samples) in the PCA. For visualization purposes data was variance stabilized with the rlog transformation implemented in the DESseq2 package. The 10% genes with the highest variation across all samples – computed on the basis of the rlog transformed data – were used as input for the PCA.

For detection of differential expression, the count matrix was filtered according to a less stringent criteria (sum of reads per gene across samples >= 1). Prior differential testing, dispersion of raw data was estimated with a parametric fit accounting for variation that arises from different timepoints in the dataset.

DEG analysis was performed with a likelihood-ratio test (LRT) and genes having an adjusted p-value less than 0.001 were considered to be significantly regulated across the time course. These genes were then used to perform cluster analysis. Eleven clusters with distinct expression profiles were determined and the spearman correlation of the contained genes to a manual curated set of transcription factors was calculated.

Pathway enrichment analysis was conducted with EnrichR within the Mouse Reactome database. A pathway was considered to be significantly regulated at an FDR level of 0.05.

3.2.13 ATAC-sequencing

Sample preparation

Thymic NKT were pre-enriched with AutoMACS Pro. The positive (enriched) fraction was stained with extracellular marker antibodies according to the sorting panel. Cells were then resuspended in a solution of FACS Buffer and live-dead dye 7-AAD.

The sorting was performed in a BD FACS Aria™ II, BD FACS Aria™ III or BD FACS Aria™ Fusion. For each sample, 50000 cells were sorted in 1.5ml Protein low binding tubes pre-coated with FCS and filled with 300 µl of FACS buffer. When 50000 cells were not available, a lower number of cells was sorted (up to a minimum of 16000). Samples were processed immediately after sorting.

Library preparation

The sorted populations were centrifuged at 600g for 5 min at 4 °C. The supernatant was carefully removed and the pellet was washed with 50 µl of cold PBS. The centrifugation and supernatant removal were repeated as before, and the pellet were kept on ice.

The transposase mixture was prepared as follows:

25 µl	2x TD buffer
2.5 µl	Tn5 enzyme
0.25ul	2% digitonin
22.25 µl	nuclease-free water

The mixture was added to the cell pellet (10 µl/10000 cells) and gently pipetted 2-3 times. The Transposase reaction was incubated in a ThermoMixer for 30 min at 37 °C with agitation at 300 rpm.

Immediately following the transposition, the DNA was purified using a MinElute PCR Purification Kit according to manufacturer's protocol. The DNA was eluted in 10 µl of elution buffer. The purified DNA was stored at -20 °C or immediately processed further.

A pre-amplification step of the transposed DNA fragments was performed as follows:

10 µl	Transposed DNA
10 µl	Nuclease-free water
2.5 µl	25 µM primer 1 (Ad1_noMX)
2.5 µl	25 µM barcoded primer 2 (*)
25 µl	NEBNext High-Fidelity 2x PCR Master Mix

*complete list of barcoded primer available in the material section (Ad1_2.1-Ad_2.16)

PCR conditions:	72°C 5 min	
	98°C 30 sec	
	98°C 10 sec	4 cycles
	63°C 30 sec	
	72°C 60 sec	
	8°C hold	

In order to define the amount of cycles required for an optimal amplification and stop the reaction before saturation, a qPCR of the PCR product was performed as follows:

5 µl	4 cycles PCR amplified DNA
2 µl	Nuclease-free water
0.25 µl	25 µM primer 1 (Ad1_noMX)
0.25 µl	25 µM barcoded primer 2
7.5 µl	SensiMix™ SYBR® 2x PCR Master Mix

qPCR conditions:	95°C 10 min	
	98°C 10 sec	19 cycles
	63°C 30 sec	
	72°C 60 sec	
	4°C hold	

The additional number of cycles needed for an optimal amplification of the 45 µl of transposed DNA was determined based on the amplification curve and the maximum fluorescence intensity. For each sample, the number of cycles which corresponded to ¼ of the maximum intensity was determined (Fig. 2).

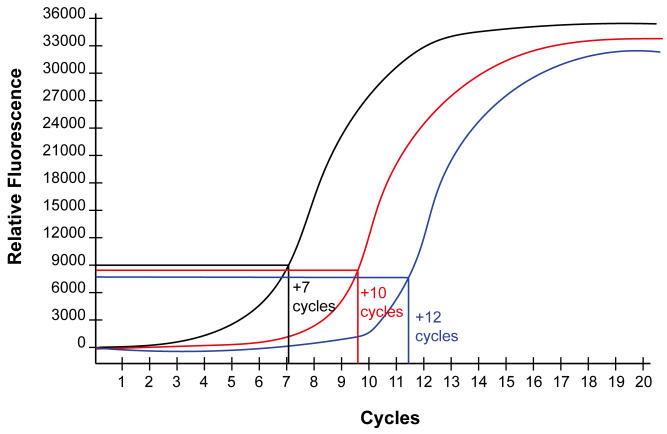

Fig. 2. Representative qPCR amplification plot.

The number of cycles to add to the transposed DNA for an optimal amplification is calculated for each single sample. The number of cycles which correspond to ¼ of the maximum fluorescence intensity is the number of PCR cycle to further amplify the library.

Each sample was then further amplified for the correct amount of cycles as follows:

PCR conditions:	98°C 30 sec	
	98°C 10 sec	X cycles
	63°C 30 sec	
	72°C 60 sec	
	8°C hold	

After the amplification, the library was purified using MinElute PCR Purification Kit according to manufacturer's protocol. To obtain an optimal absorption of the DNA into the membrane, the pH was reduced below 7.5 by adding 5 µl of NaAc (3M, pH5). The sample was eluted in 12 µl of elution buffer. The DNA concentration was measured with Qubit™ dsDNA HS Assay Kit and the library quality was evaluated with the bioanalyser using Agilent High Sensitivity DNA Kit.

To select for DNA fragments between 150bp and 600bp, SPRI size selection was performed. Elution buffer was added to the library up to a volume of 50 µl.

Thirty µl (0.6x) of AMPureXP magnetic beads were added to the library, mixed 10 times to achieve a homogeneous solution and incubated for 10 min at RT. After that, the tubes were placed in a magnetic. After 5 min, the clear supernatant was transferred to a clear tube, where 70 µl (2x) of beads were added and thoroughly mixed. After 10 min of incubation at RT, the tubes were moved to a magnetic stand for 5 min. With the tube in the magnetic stand, the supernatant was removed and the 200 µl of freshly prepared 80% ethanol was added. The magnetic stand was rotated of 90° and after 30 sec the ethanol was removed and the step was repeated one more time.

Afterwards, the pellet was dried for 3-5 min at RT and 17 µl of elution buffer was added to the pellet. The tube was then removed from the magnetic stand, thoroughly mixed and incubated at RT for 2 minutes to rehydrate. The samples were placed back in the magnet until the solution was completely clear. The supernatant was carefully removed and placed in a clear tube and stored at -20 °C. The DNA concentration was measured with Qubit™ dsDNA HS Assay Kit and the library size was evaluated with the bioanalyser using Agilent High Sensitivity DNA Kit.

Libraries were then sequenced on HiSeq1500 Illumina Sequencer.

Analysis

For the processing of the sequencing data, a customized in-house software pipeline was used. Illumina's bcl2fastq (v2.20.0.422) was used to convert the base calls in the per-cycle BCL files to the per-read FASTQ format from raw images. Along with base calling, demultiplexing of FASTQ files were performed using an in-house python (v 3.7.0) script. Sequencing adapters were trimmed using TrimGalore (v 0.6.0). Quality control of raw sequencing data was performed using FastQC (v 0.11.7) and MultiQC (v1.7). Reads were then mapped to the mouse genome (mm10) using bowtie2 (v 2.3.4.1) with very sensitive in-built pre-set option. Samtools (v 1.7) were used to process the output bam file and removing the duplicates. Peaks were called using MACS2 (v 2.1.2) with broad peaks parameter. Peaks for all the samples was merged with an in-house bash script and tab separated matrix of all peaks were generated using deeptools (v 3.1.3). Variance stabilized normalization was

performed using DESeq2 (v 1.24.0) and poor peaks were filtered out from the analysis.

3.2.14 Analyses and software

The flow cytometry data were analysed with FlowJo (version 10). The cytokine stimulation assay data were depicted using SPICE (version 6) software. The heatmaps were generated with R Studio (version 1.2.5001). All the other graphs were generated with GraphPad Prism (version 7. 0).

For the analysis of TCR sequencing data, samples were aligned to the international immunogenetics information system (IMGT) database from 22.05.2018 using MiXCR software (Bolotin et al., 2015). TCR rearrangement-analysis was performed employing VDJTools (Shugay et al., 2015).

4. RESULTS

4.1 A genetically induced synchronous wave of NKT cell development

To systematically investigate the earliest phases of NKT cell development and subsequent subset differentiation, we generated a genetic system to induce a timed wave of NKT cell generation. By combining CD4-CreER^{t2} (Sledzinska et al., 2013) with Vα14i^{StopF} (Vahl et al., 2013) knock-in transgenes, we generated mice that allow expression of a pre-rearranged Vα14-Jα18 (Vα14i) sequence inserted in the TCRα locus upon 4-hydroxytamoxifen (4-OHT) administration. The expression of this sequence is rendered conditional by the presence of an upstream loxP-flanked stop cassette (Fig. 3). The upstream rearrangements are abrogated by the insertion of 4 SV40 polyadenylation sites (4pA). Upon 4-hydroxytamoxifen (4-OHT) administration, in the cells expressing CD4 the CreER^{t2} can translocate into the nucleus and consequently excise the stop cassette, resulting in the expression of the pre-rearranged Vα14-Jα18 sequence. When this event occurs in a DP thymocyte containing a TCRß chain that together with the Vα14i-TCRα chain builds a glycolipid-recognizing TCR, it gives rise to a potential NKT cell precursor (Vα14i-DP). This cell can be positively selected by the interaction with another DP thymocyte presenting an endogenous glycolipid in a CD1d molecule. The CD1d-TCR interaction triggers strong TCR signals, which are followed by the induction of the key transcription factor PLZF (Seiler et al., 2012). PLZF expressing immature NKT cells can continue the development and differentiate into three functional subsets termed NKT1, NKT2 and NKT17. In this project, I induced the production of Vα14i-DP NKT cell precursor cells by administering a single dose of 4-OHT to mice with appropriate genotypes and analysed the fate of the induced NKT cell population at different time-points of their differentiation journey. From the remainder of this thesis, I will refer to the NKT cells generated by this genetic system as “induced NKT cells”.

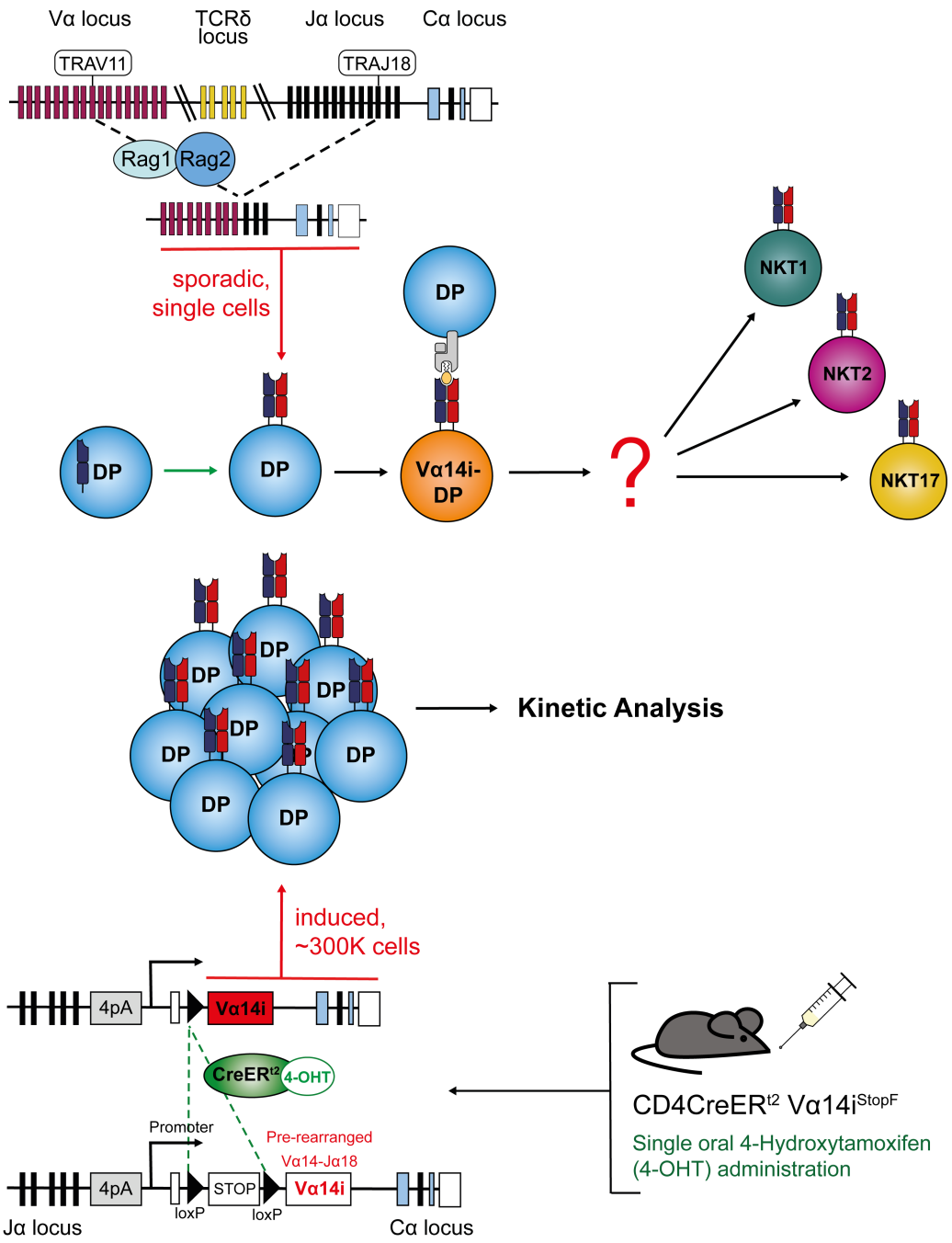

Fig. 3. Schematic representation of the endogenous Vα14-Jα18 rearrangement and the genetic system employed for the generation of a wave of NKT cell development.

Top part: somatic V(D)J recombination sporadically generates Vα14-Jα18 rearrangements. If this event occurs on a DP thymocyte expressing a correct TCRβ chain, this cell can become an NKT cell precursor (Vα14i-DP) and differentiate into NKT cell lineage. Bottom part: the knock-in allele is composed by a pre-rearranged Vα14-Jα18 (Vα14i) sequence inserted 3′ of Jα1 and 5′ of the first Cα exon into the endogenous TCRα locus. Upstream of the Vα14i, a STOP cassette (STOP) was inserted, flanked by loxP sites (loxP). The putative upstream rearrangements are abrogated by the insertion of 4 SV40 polyadenylation sites (4pA). Upon single 4-OHT administration by oral gavage,

Fig. 3 **(continued)** the Cre recombinase can excise the STOP cassette and lead to the expression of the Vα14i sequence on a significant fraction of DP thymocytes. If the DP thymocyte bears a TCRβ2, 7 or 8.2, the cell can be positively selected and differentiate into NKT cell lineage.
(blue receptor=TCRβ chain; red receptor=Invariant TCRα chain; grey receptor=CD1d; yellow ligand=glycolipid).

4.1.1 Leakiness of the Vα14i^{StopF} mouse line

The CD4-CreER^{t2} Vα14i^{StopF} mice bear only one Vα14i^{StopF} knock-in TCRα allele, and are therefore capable of producing T cells and NKT cells from the other wildtype TCRα allele. In order to eliminate endogenous pre-existing NKT cells and selectively analyse induced NKT cells, I further crossed CD4-CreER^{t2} Vα14i^{StopF} mice with Jα18-deficient mice, which should have resulted in a mouse fully competent on producing T cells (by the Jα18-deficient allele) but lacking NKT cells prior to 4-OHT administration. However, to my surprise, a minute fraction of NKT cells was present in CreER^{t2} Vα14i^{StopF} Traj18^{ko} mice also in absence of 4-OHT administration. In a wildtype mouse, most of the thymic NKT cells are mature and express either CD44 (Stage 2) or both CD44 and NK1.1 (Stage 3). Particularly small is the fraction of immature NKT cells, which is distributed between Stage 0 (CD24+ CD44− NK1.1−) and Stage 1 (CD24− CD44− NK1.1−) (Fig. 4A).
In CD4-CreER^{t2} Vα14i^{StopF} Traj18^{ko} mice, 12 hours after 4-OHT administration over 90% of the cells were Stage 0 CD24− CD44− NK1.1−, and therefore should represent the induced population. However, the remaining 8% were mostly CD44+ NK1.1+ CD24−, strongly resembling mature NKT cells (Fig. 4A). Similar to the thymus, pre-existing mature NKT cells were also detected in the spleens of mice 12h after 4-OHT (Fig. 4B). At this time-point, no immature induced NKT cells can be detected in the spleen of mice. Although the fraction of these “leaky” mature NKT cells was lower in the spleen compared to the thymus, their stage distribution in CD4-CreER^{t2} Vα14i^{StopF} Traj18^{ko} mice was very similar to the control. This underscores the notion that the minute fraction of mature NKT cells detectable in CD4-CreER^{t2} Vα14i^{StopF} Traj18^{ko} mice did not derive from the induced wave but was rather generated before 4-OHT administration.

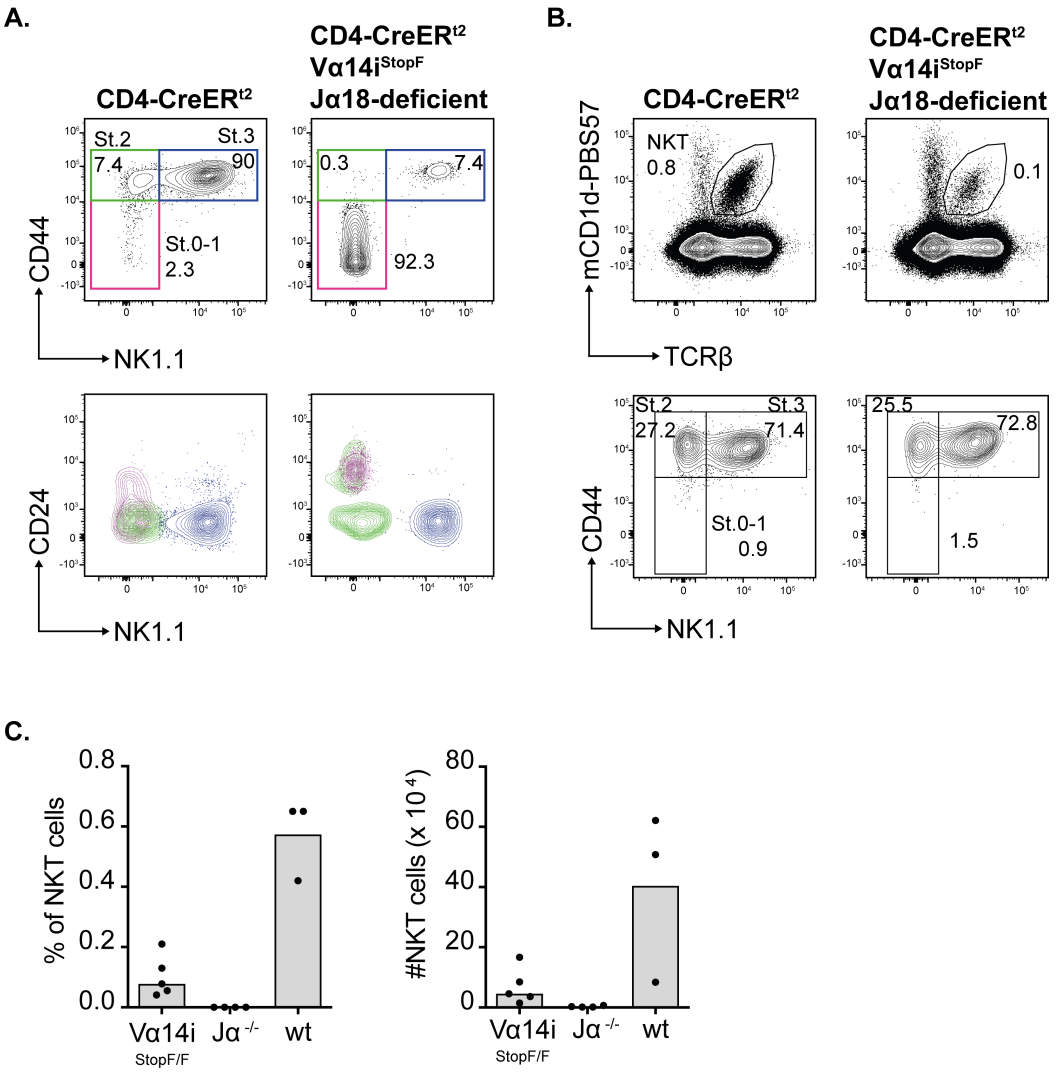

Fig. 4. Endogenous NKT cells generated independently from 4-OHT administration.
Ex vivo analysis of NKT cells in thymus (A and C) and spleen (B) using flow cytometry. **A.** Representative flow cytometry plots of thymic NKT cells from mice fed with 4-OHT 12h before euthanasia. The samples are pregated on mCD1d-PBS57+ cells. The percentages are indicative for the displayed samples. **B.** Representative flow cytometry plots of splenic NKT cells from mice fed with 4-OHT 12h before euthanasia. The first row is pregated on lymphocytes while the second row is pregated on mCD1d-PBS57+ cells (namely NKT cells). The percentages are indicative for the displayed samples. **C.** Bar chart of percentage (of lymphocytes) and absolute number of NKT cells in the thymus of homozygous Vα14i^{StopF} (Vα14i $^{StopF/F}$), homozygous Traj18KO and Jα18-KO (Jα $^{-/-}$) and wildtype (wt) mice. The percentages report the mean of two experiments.

To verify the source of these "leaky" mature NKT cells, I analysed NKT cell populations in homozygous Vα14i$^{StopF/StopF}$ and homozygous Jα18-deficient

mice. My experiments determined that these NKT cells were exclusively generated by the Vα14i^{StopF} knock-in allele (Fig. 4C).

4.1.2 Aberrant NKT cell generation: Vα replacement?

Despite the insertion of four SV40 polyadenylation sites 3' of the Jα1 and the presence of a STOP cassette upstream of the pre-rearranged Vα14-Jα18 sequence, the Vα14i^{StopF} allele is capable of generating a minute amount of T cells (not shown) and NKT cells in absence of 4-OHT administration. This occurs also in absence of the CD4-CreER^{t2} knock-in allele, demonstrating that NKT cell generation is not due to Cre-ER^{t2} activity in absence of 4-OHT.

Literature research revealed a study conducted by Golub et al. who showed that Vα-gene replacement can occur in VαJα rearranged sequences in the TCRα locus due to the presence of a Vα-embedded heptamer. These heptamers are present at the 3' location of most of the V gene segments. The sequence is composed of a highly conserved GTG motif (required for V(D)J recombination) and at least two more nucleotides from the consensus heptamer (CACTGTG). Rag enzymes can recognise and cut at both the RSS of the germline Vα and at the embedded heptamer in a knock-in VαJα sequence, exposing two coding ends – 3' of the germline Vα and 5' of the knock-in Jα – which can be joined, resulting in the replacement of the Vα knock-in gene segment with another Vα gene segment (Golub et al., 2001).

I therefore searched for the presence of an embedded heptamer in the 3' area of the Vα sequence within the Vα14-Jα18 knock-in sequence and found two possible embedded heptamers in the last 15 nucleotides of the Vα14 sequence (Suppl. Fig. 1).

To test whether the embedded heptamer is the cause of the aberrant T and NKT cell production, I FACS-sorted NKT cells and T cells (pooled CD4+ and CD8+) from thymi and spleens of four homozygous Vα14i$^{StopF/StopF}$ mice and gave the samples to a collaborator for TCR repertoire sequencing using 5' RACE-PCR (Suppl. Table 1). If Vα replacement occurs, T cell TCRs should be composed of Jα18 gene segment combined with diverse germline Vα gene segments. In the case of NKT cells, the putative Vα replacement would not be detected in most cases since the generation of NKT cells is restricted to the

presence of Vα14-Jα18. A replacement of Vα14 by a germline Vα14 could only be detected if a silent mutation or tolerable non-silent mutation would be present.

As expected, the sequencing results revealed that the NKT cells generated in the Vα14i$^{StopF/StopF}$ mice uniformly expressed a Vα14-Jα18 TCR (encoded by TRAV11 and TRAV18, respectively) (Fig. 5 and Suppl. Fig. 2). A small number of diverging rearrangements detected might be due to contamination with T cells during the sorting.

The analysis of the TCR repertoire of T cells revealed a more complex scenario. Control wildtype T cells showed a highly diverse TCR repertoire both in thymus and in spleen (Fig. 6). In the thymus, roughly half of the TCR repertoire of Vα14i$^{StopF/StopF}$ T cells were composed of sequences containing Jα18 (TRAJ18) rearranged to diverse Vα gene segments, supporting the hypothesis of Vα gene replacement. However, the other half of the TCR repertoire was composed by different V-J rearrangements which did not include TRAJ18.

In the spleen, the TCR repertoire of Vα14i$^{StopF/StopF}$ T cells show a certain degree of variability between different animals (Fig.6 and Suppl. Fig. 2). In mouse #2, almost 75% of all rearrangement included TRAJ18, further supporting the hypothesis of Vα rearrangement. The TCR repertoire of mouse #3 was almost restricted to two TRAJs, namely TRAJ18 (40%) and TRAJ24 (35%). Interestingly, over 50% of the rearrangements bearing TRAJ18 were combined with TRAV11. Moreover, mouse #1 and 4 had a TCR repertoire more similar to the thymus, with a preponderant Jα18 usage but with additional rearrangements.

Overall, the TCR repertoire analysis confirmed that Vα gene replacement contributes to the aberrant generation of NKT and T cells in homozygous Vα14i$^{StopF/StopF}$ mice. However, it is clear that other processes are involved in the generation of these cells.

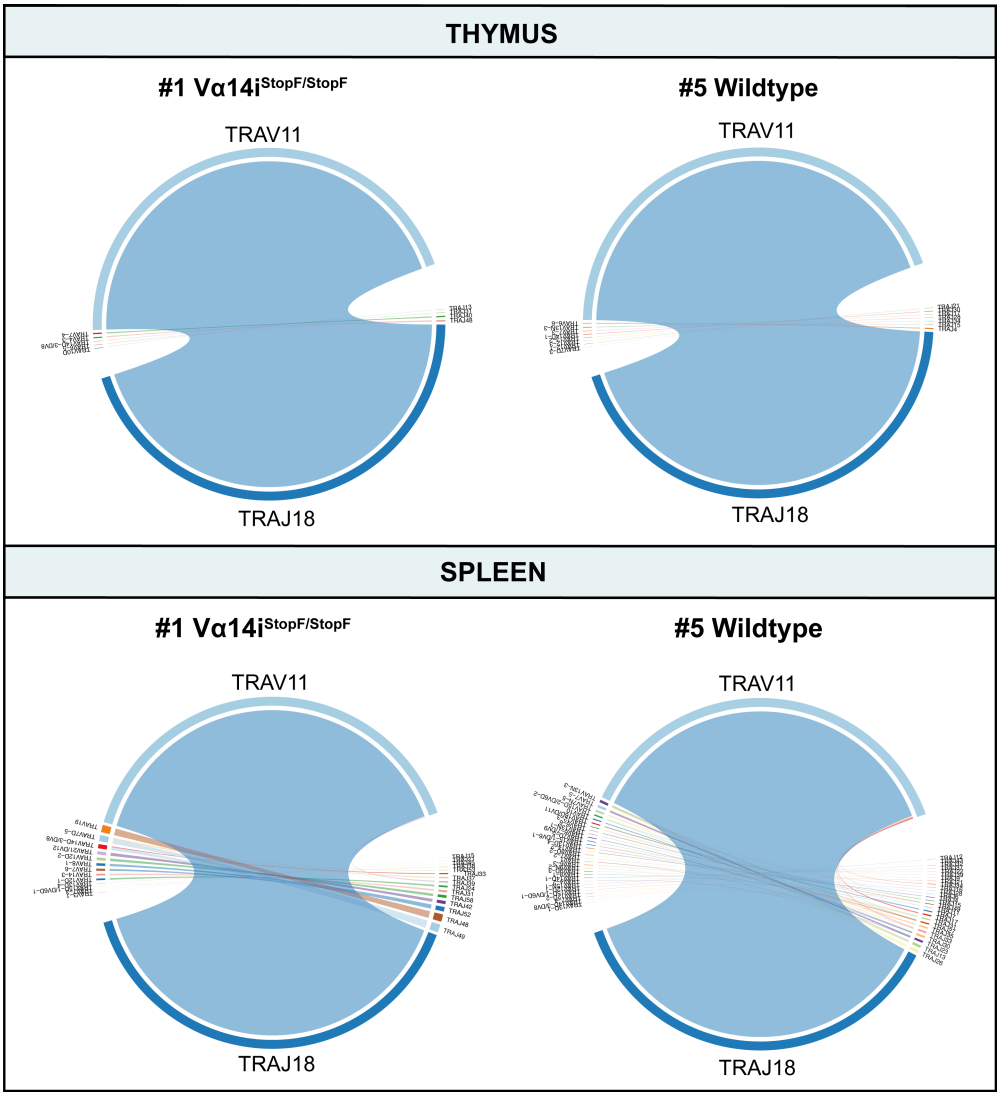

Fig.5. TCR repertoire of NKT cells.

Thymic and splenic NKT cells from Vα14i$^{StopF/StopF}$ and wildtype mice were sorted and the TCR repertoire was defined by 5' RACE PCR. The plots show all the TCR rearrangements detected by sequencing. TRAJ18 (Jα18 gene segment) and TRAV11 (Vα14 gene segment) are highlighted. The TCR rearrangement analysis was performed with VDJTools.

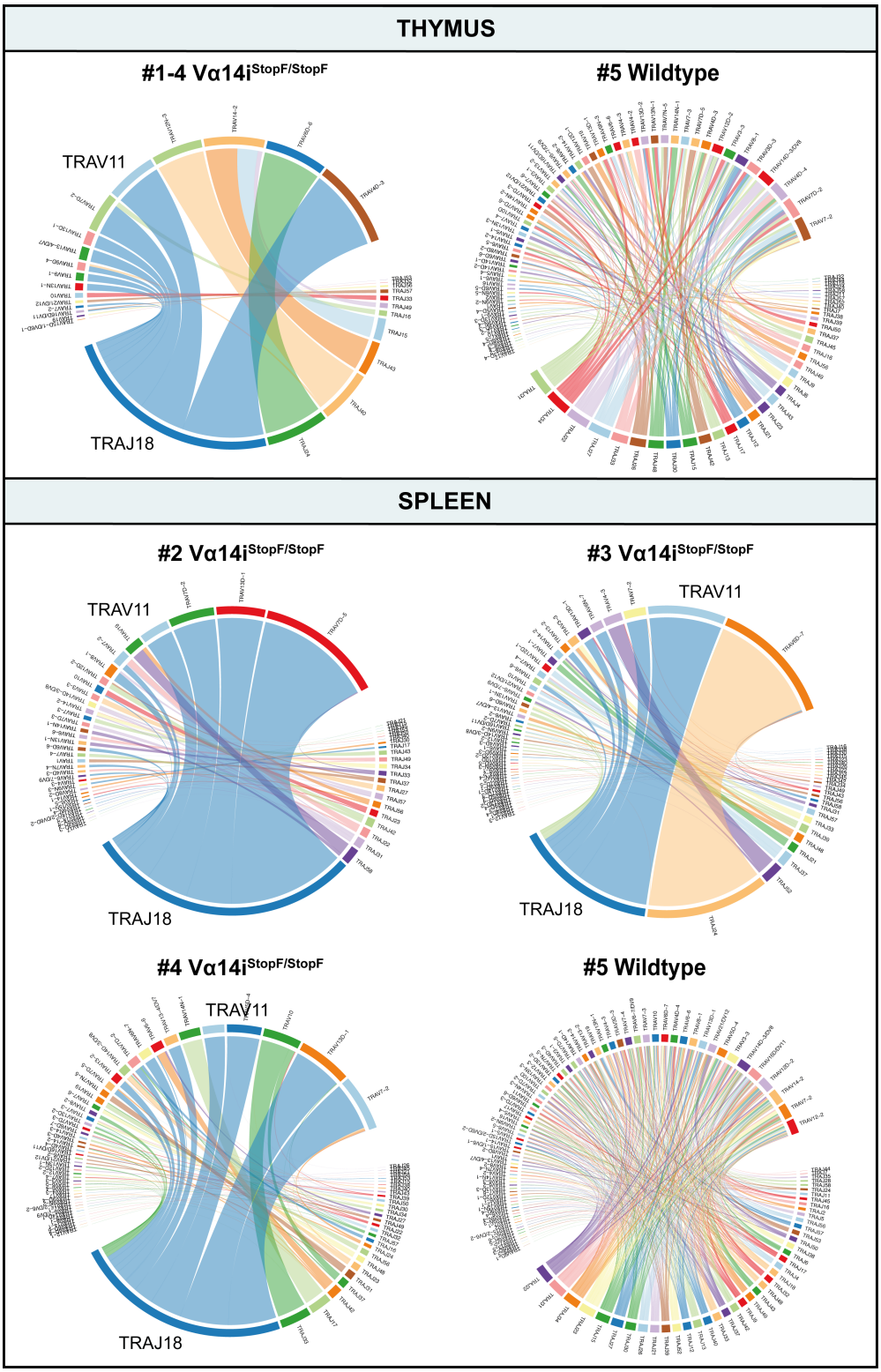

Fig. 6. TCR repertoire of T cells.

Thymic and splenic T cells from Vα14i$^{StopF/StopF}$ and wildtype mice were sorted and the TCR repertoire was defined by 5' RACE PCR. The plots show all the TCR rearrangements detected by sequencing. TRAJ18 (Jα18 gene segment) and TRAV11 (Vα14 gene segment) are highlighted. The TCR rearrangement analysis was performed with VDJTools.

4.1.3 Size of induced NKT cell wave

To thoroughly dissect changes occurring during NKT cell differentiation, I analysed mice at different timepoints between 6 hours and 28 days after 4-OHT administration. To distinguish pre-existing NKT from the induced NKT cells, I made use of gating strategies based on differential surface protein expression between induced and pre-existing NKT cells as well as a fluorescent tdTomato Cre activity reporter. For the early timepoints (between 6h and 5d), I gated on CD44$^{low/-}$ NK1.1− NKT cells. Considering the gradual upregulation of CD44 observed over time, from 6d to 28d I made use of a reporter knock-in allele expressing tdTomato upon Cre-mediated excision of a loxP-flanked stop cassette. This allowed to selectively label the NKT cells which underwent Cre-mediated recombination. A significant population of induced tetramer-reacting NKT cell precursors was detected already 6h after 4-OHT administration (Fig. 7A, 7B).

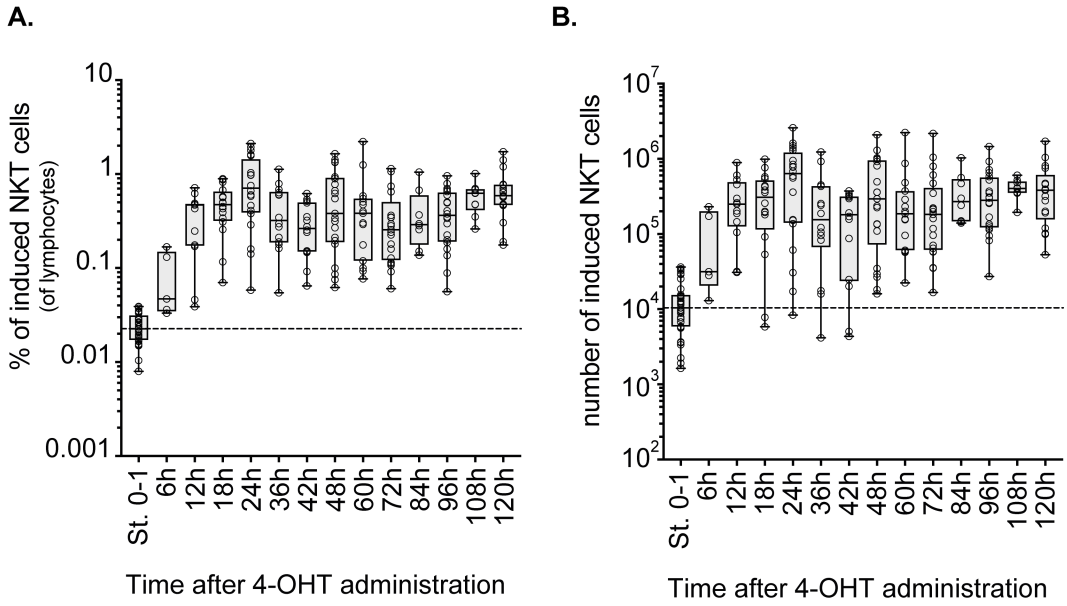

Fig. 7. Size of the induced wave of NKT cell development.

Ex vivo analysis of thymic NKT cells from induced mice between 12h and 120h (5d) after 4-OHT administration. Box plots shows the percentage (calculated out of lymphocytes) **(A)** and the absolute numbers **(B)** of induced NKT cells. The boxes extend from the 25th to 75th percentiles, while the whiskers go from the smallest to the largest value. Both percentages and absolute numbers are

Fig. 7 **(continued)** displayed in logarithmic scale. Data are representative of at least 4 experiments. "St. 0-1" represents Stage 0-1 immature NKT cells ($CD44^{low}$ NK1.1−) from wildtype mice.

Despite some differences between individual mice, I could generate up to 2.5 million of early NKT cells (Fig. 7A) corresponding to roughly 2% of the whole thymic lymphocytes (Fig. 7B).
Overall, the system allows the generation of a substantial wave of NKT cell development which can be employed to monitor the dynamic changes occurring during the development and differentiation of NKT cells in vivo.

4.2 Monitoring NKT cell maturation

Throughout the functional differentiation process, NKT cells undergo profound phenotypic changes (Gapin, 2016). CD24, CD44 and NK1.1 represent the extracellular markers which have been initially employed to distinguish different maturational steps (Bennstein, 2017). Although it is now clear that the NKT cells do not follow a linear maturation model but rather a lineage differentiation model, these markers remain important for the distinction between early (CD24+) and mature (CD44+) cells. Moreover, NK1.1 is mainly expressed on NKT1 subset, and it is therefore helpful to identify these cells (Lee et al., 2013).
The transcription factors PLZF and RORγt are most commonly used to define NKT cell subsets. In fact, these subsets are characterized by differential expression of these two transcription factors. PLZF was shown to be a key transcription factor for NKT cell differentiation (Kovalovsky et al., 2008; Savage et al., 2008), while RORγt plays an important role regulating the lifespan of DP thymocytes and consequently TCR rearrangements (Guo et al., 2002; Sun et al., 2000). Regarding the NKT cell functional subsets, NKT17 is the only RORγt positive subset and it contains intermediate PLZF expression, while the NKT1 and NKT2 subsets are characterized by low and high PLZF expression, respectively (Lee et al., 2013).

Lastly, mature NKT cells subsets are all CD8− and have a diverse expression of CD4. NKT17 cells are mainly DN, NKT1 cells are roughly half CD4+ and half DN while NKT2 cells are mostly CD4+ (Lee et al., 2013).
In this section, I sought to dynamically monitor the NKT cell maturation starting from the positive selection upon TCR expression throughout the differentiation. With this analysis, I aim to validate the generation of bona fide NKT cells and discover unknown dynamics of crucial factors for NKT cell development and differentiation.

4.2.1 RORγt and PLZF dynamics

Considering the importance of PLZF and RORγt for NKT cell identity and functionality, I sought to define their dynamic changes during differentiation. Twelve hours after 4-OHT administration, induced NKT cells resemble the DP precursors by expressing RORγt (Fig. 8A, 8B). Upon positive selection, NKT cells first downregulate RORγt followed by upregulation of PLZF starting at 36h toward a PLZF^{high} state. At 5d after induction, where most of the induced NKT cells express high levels of PLZF, a first clear fate divergence occurs; a fraction of PLZF^{high} cells re-upregulates RORγt and subsequently acquires a PLZF^{int} state, resembling the NKT17 subset. Furthermore, between 8 and 10d after induction, a fraction of PLZF^{high} RORγt− cells gradually decreases PLZF expression, while a fraction of cells maintains a high expression of PLZF throughout the development. At 28d most of the NKT cells express low levels of PLZF while small fractions are either PLZF^{high} or RORγt+ PLZF^{int}, highly resembling the steady state distribution observed in wildtype thymi.
Overall, these data show that the induced NKT cells homogeneously develop up to a PLZF^{high} state, which represents a key turning point for the divergence into distinct further specifications. Interestingly, although DP thymocytes already express RORγt, all the immature NKT cells first downregulate RORγt, followed by a second re-upregulation which only occurs in some of the cells expressing levels of PLZF. Due to the differential expression of these transcription factors in mature NKT cell subsets, the following analyses will be performed by subgating the induced NKT cells into subsets based on the RORγt and PLZF expression.

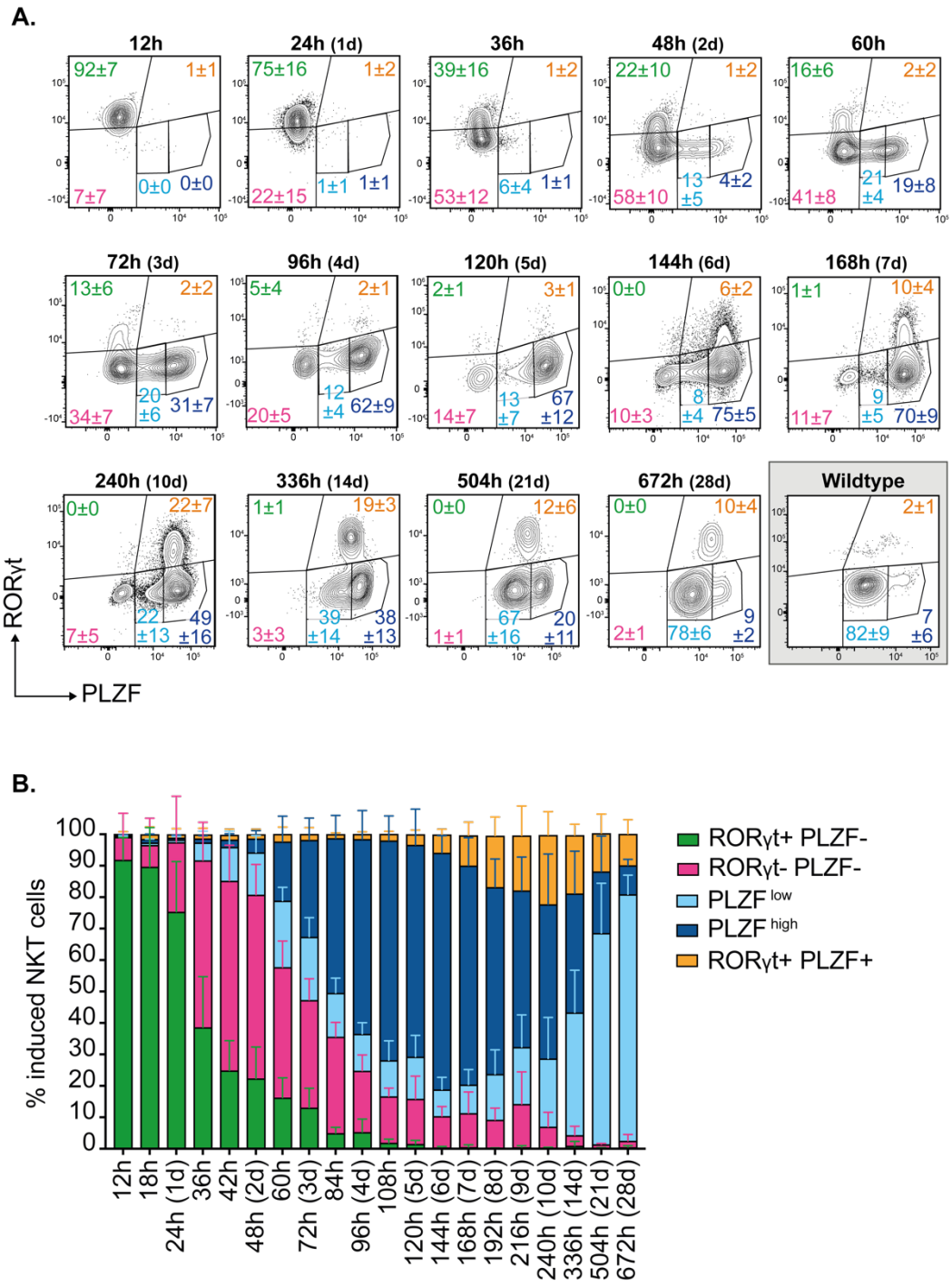

Fig. 8. RORγt and PLZF dynamics during NKT cell development

Ex vivo flow cytometric analyses of thymi from inducible mice at different timepoints after 4-OHT administration. **A.** Representative facs plot of RORγt and PLZF expression in thymic induced NKT cells at different timepoints. The percentages represent mean and SD of at least four mice. Data is representative of at least 2 experiments. **B.** The bar graph depicts the mean and SD of each RORγt/PLZF subset for each timepoint. Data is representative of at least 4 mice and at least 2 experiments.

4.2.2 Maturation markers: CD24, CD44 and NK1.1

CD24 is highly express on DP thymocytes (Wilson et al., 1988). Therefore, newly selected immature NKT cell should initially retain its expression. These cells (classified as Stage 0) are known to lose the expression of CD24 (Stage 1) and in the following acquire the memory marker CD44 (Stage 2/3). However, the exact timing of these dynamic changes remains unclear.

The kinetic analysis of the CD24 and CD44 markers through development showed a gradual downregulation of CD24 followed by the upregulation of CD44 (Fig. 9A and Suppl. Fig. 3A). Interestingly, although for the first 3 days after Vα14i-TCR induction over 94% of NKT cells are positive for CD24 (Suppl. Fig. 3A), the intensity of CD24 gradually decreases starting from 1 day after induction (Fig. 9A). Oppositely, from 3d after induction CD44 expression gradually increases reaching over 93% of CD44 positivity from 14d (Fig. 9A, 9B). Moreover, starting from 8d after induction, a fraction of CD44+ cells start to express NK1.1, resulting in almost 80% of NK1.1+ NKT cells at day 28. (Fig. 9B).

I further analysed the CD44 and NK1.1 expression on the different induced NKT cells subsets (Fig. 10). Prior to PLZF expression, the induced NKT cells are largely CD44− (Fig. 10A, 10B). $PLZF^{low}$ NKT cells upregulate CD44 starting from around 5d after induction, followed by the acquisition of a NK1.1 phenotype (Fig. 10C). At 21d after induction, the $PLZF^{low}$ subset highly resembles wildtype NKT1 cells.

The $PLZF^{high}$ fraction acquires a CD44+ phenotype from 4-5 days and largely remais NK1.1− throught the 4 weeks of development I analysed (Fig. 10D). From 14d after induction, the CD44/NK1.1 distribution resembles the NKT2 wildtype subset, for the exception of the CD44− fraction which is observed in wiltype NKT2 but is lacking in the induced $PLZF^{high}$ subset.

Lastly, at 5d the few RORγt+ PLZF+ cell detected display a largely CD44− phenotype (80%) (Fig. 10E); a rapid upregulation of CD44 is observed from 6d after induction, and at 14d all the RORγt+ PLZF+ cells express CD44. Interestingly, a fraction of the cells acquire NK1.1 starting from 10d after induction, resulting in approximately 50% of NK1.1+ cells at 28d (compared to 25% in wiltype NKT17).

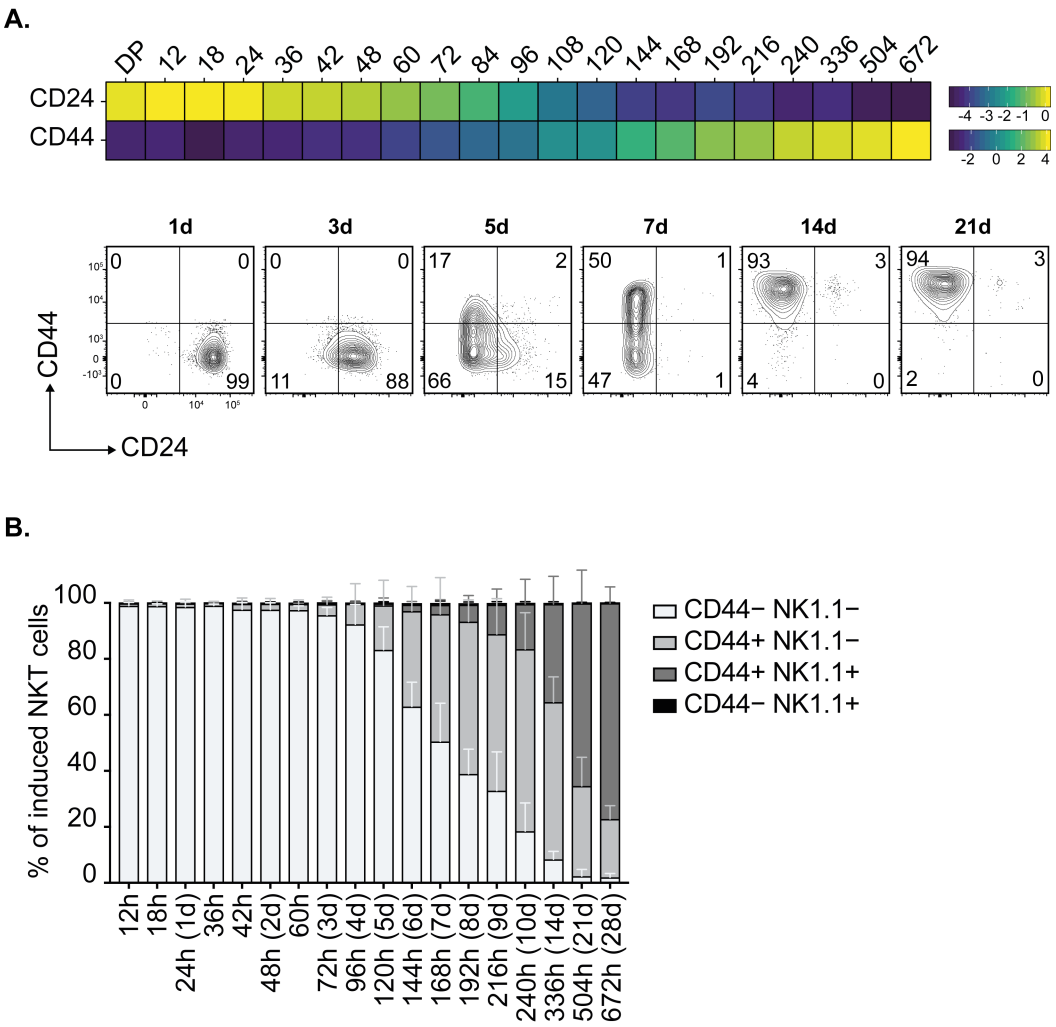

Fig. 9. Maturation markers dynamics during NKT cells development.

Ex vivo flow cytometric analyses of thymi from inducible mice at different timepoints after 4-OHT administration. **A.** The graphs depict CD24 and CD44 expression across the development of NKT cells. Top graph: median fluorescence intensity of CD24 and CD44 calculated from induced NKT cells at different timepoints. The values were normalised to the values of DP thymocytes (for CD24) and CD4+ T cells (for CD44). For each timepoint, a mean of the values was calculated. The log2 of the mean values was calculated and displayed in the heatmap. Lower graph: representative facs plot of CD24 and CD44 expression in thymic induced NKT cells at different timepoints. The percentages refer to the displayed samples. **B.** The bar graph depicts the mean and SD of each of four subsets calculated based on CD44 and NK1.1 espression for each timepoint. Data is representative of at least 4 mice and at least 2 experiments.

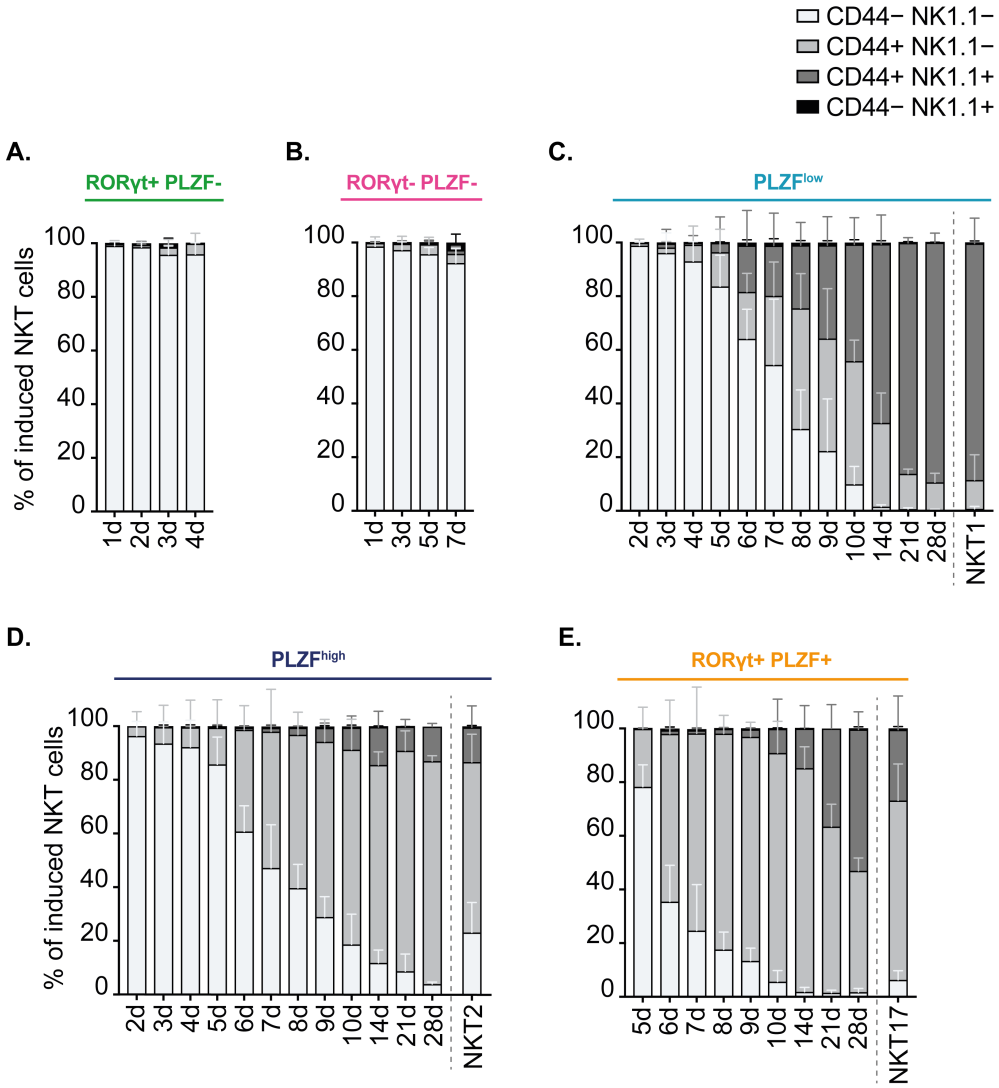

Fig. 10. CD44 and NK1.1 dynamic during NKT cells development.

Ex vivo flow cytometric analyses of thymi from inducible mice at different timepoints after 4-OHT administration. The bar graphs depicts the mean and SD of the percentage of four CD44/NK1.1 subsets calculated at different timepoint for 5 subsets: RORγt+ PLZF− **(A)**, RORγt+ PLZF− **(B)**, PLZF^{low} **(C)**, PLZF^{high} **(D)** and RORγt+ PLZF+ **(E)**. Subsets with less than 150 events were excluded. Data is representative of at least 3 mice and at least 2 independent experiments, with the exception of sample "672h (28d)" (graph D) were two mice from one experiment are displayed.

Overall, these data precisely clarify the timing of NKT cell maturation juged by the acquisition of surface markers and transcription factors. By means of these analyses I could confirm that the NKT cells generated through this inducible system succesfully mature and display a high degree of similarity

with the corresponding mature NKT cell subsets in wild-type mice. By comparing these data with the linear maturation classification, I could estimate the length of each maturation stage: Stage 0 (CD24+ CD44–) corresponds to the first 3 days after TCR expression, followed by Stage 1 (CD24– CD44–) between 3d and 4-5d; Stage 2 (CD44+ CD24–) initiates around 5d while Stage 3 (CD44+ NK1.1+) appears at 8-10d after induction.

4.2.3 Dynamic changes of CD4 and CD8 expression

DP thymocytes – the precursors of most NKT cells – express both CD4 and CD8 co-receptors on their surface. However, murine mature NKT cells lack the expression of CD8 and are either CD4+ or DN (Bendelac et al., 1997). A putative dynamic of these two markers has been proposed based on the observation of early NKT cells in young mice (Benlagha et al., 2005). Stage 0 CD24+ showed a major CD4+ phenotype, but a DP^{low} population was also observed. Considering that immature CD4+ NKT could give rise to DN NKT, a DP → CD4+ → DN sequence of events was proposed.
I theferore evaluated the dynamic changes of CD4 and CD8 throughout the development. At 12h after induction, all NKT cells express both CD4 and CD8; these cells rapidly initiate the downregulation of both markers towards a DN state (36h) (Fig. 11A, 11B). At 60h, induced NKT cells re-upregulate CD4, reaching over 85% of CD4+ cells at 6d. These results are in line with the observation that NKT cell precursors display a preponderant CD4+ phenotype (Wang and Hogquist, 2018). From 6d after induction, a fraction of NKT cells downregulate again CD4 toward a DN state. From day 14, roughly 30% of NKT cells are DN cells.

The analysis of the expression of CD4 and CD8 on the induced RORγt/PLZF subsets showed that the rapid CD4/CD8 downregulation initiates already in the RORγt+ PLZF– fraction (Fig. 12A) and is accelerated once RORγt is downregulated (Fig. 12B). PLZF is upregulated only in DN cells which gradually re-acquire CD4 (Fig. 12C, 12E). However, the re-upregulation of CD4 is independent from the expression of PLZF, since also the RORγt– PLZF– cells re-upregulate CD4 (Fig. 12B). From 6d after induction onwards, the $PLZF^{high}$

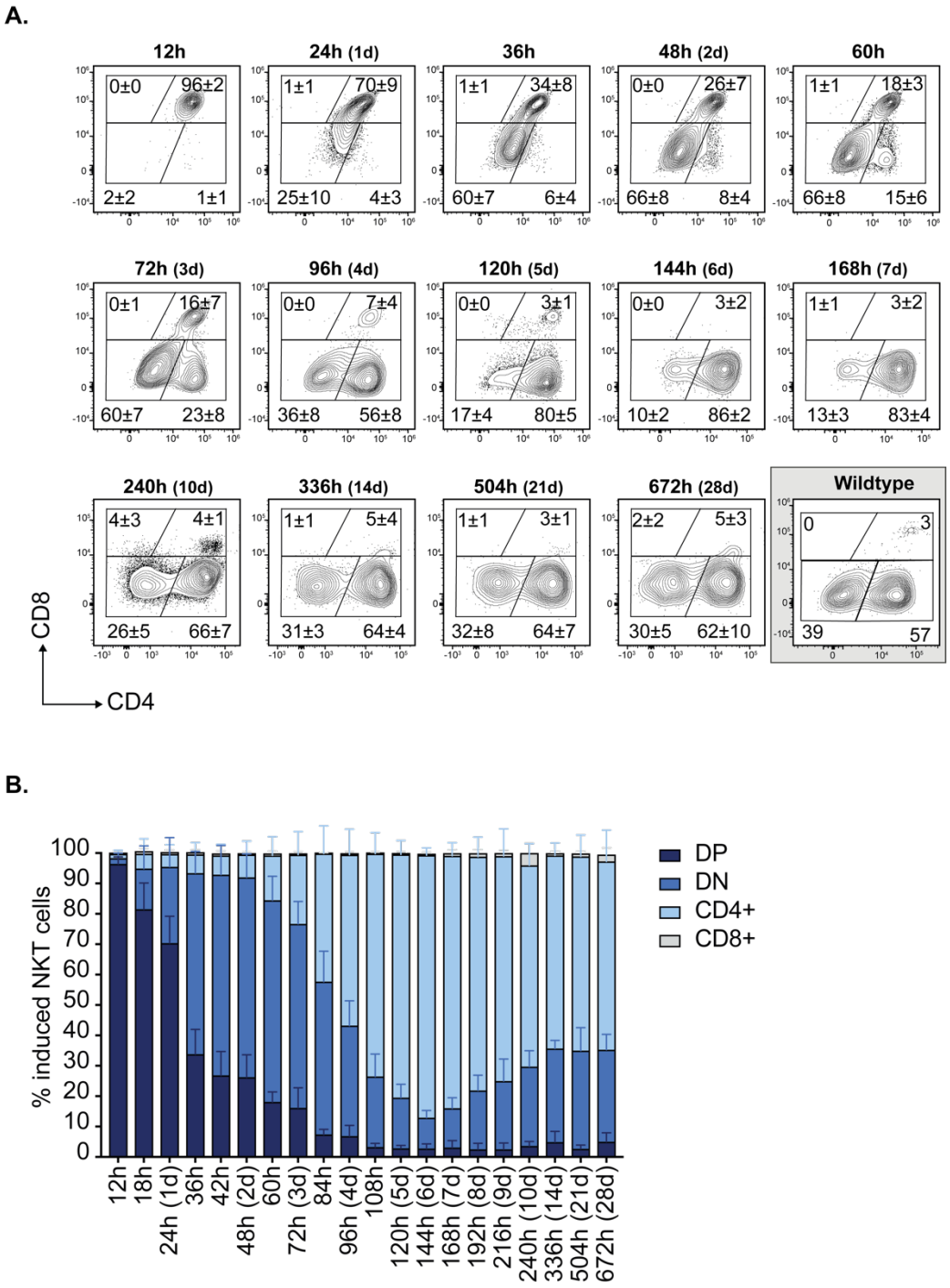

Fig. 11. Dynamic changes of CD4 and CD8 markers during NKT cell development.

A. Representative facs plot of CD4 and CD8 expression in thymic induced NKT cells at different timepoints. The percentages represent mean and SD of at least four mice. Data is representative of at least 2 experiments. **B.** The bar graph depicts the mean and SD of each CD4/CD8 subgroup at different timepoints. Data is representative of at least 4 mice and at least 2 experiments.

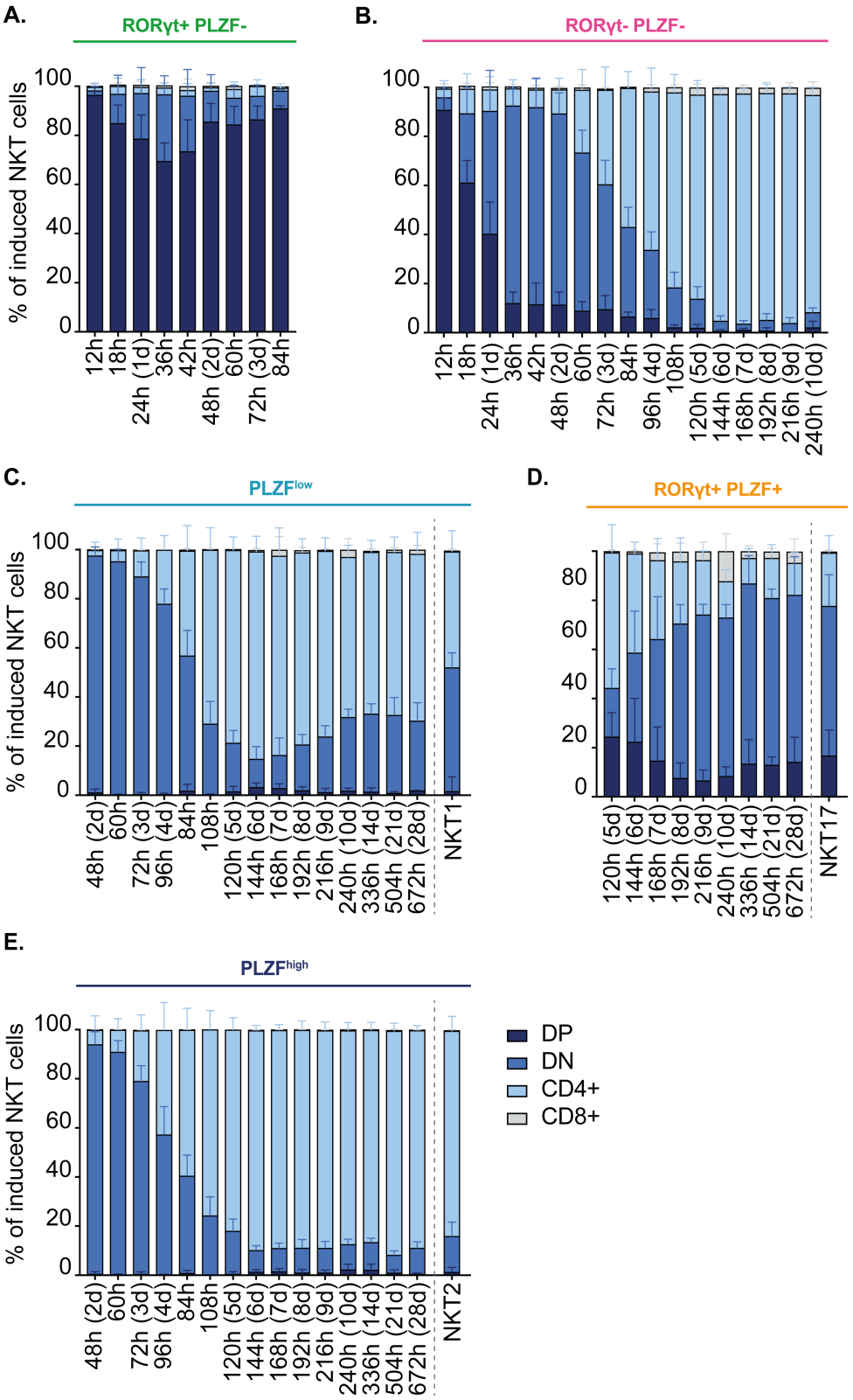

Fig. 12. CD4 and CD8 expression of induced NKT cells subsets.

Ex vivo flow cytometric analyses of thymi from inducible mice at different timepoints after 4-OHT administration. The bar graphs depict the mean and SD of the percentage of four CD4/CD8

Fig. 12 **(continued)** subgroups at different timepoint calculated for 5 subsets: RORγt+ PLZF− **(A)**, RORγt+ PLZF− **(B)**, PLZF^{low} **(C)**, PLZF^{high} **(E)** and RORγt+ PLZF+ **(D)**. Subsets with less than 150 events were excluded. Data is representative of at least 3 mice and at least 2 independent experiments, with the exception of sample "672h (28d)" (graph E) were two mice from one experiment are displayed.

fraction maintains stable CD4 expression, while the fraction that downregulates PLZF (PLZF^{low}) undergoes a partial downregulation of CD4. Moreover, the cells that re-upregulate RORγt display a prominent DN phenotype. Interestingly, eventually all the induced subsets reach a CD4/CD8 distribution which resemble the corresponding mature NKT1, NKT2 and NKT17 subsets (Fig. 12C-E).

These results elucidate the timing of CD4 and CD8 expression upon positive selection. The data indicate that early NKT cells undergo the follow dynamics: DP→ DN→ CD4+→ DN. Moreover, a differential expression is detected between the subsets defined by differential RORγt/PLZF expression and it recapitulates the distribution found in mature wildtype NKT cells subsets.

Overall, monitoring these dynamic changes confirmed that the NKT cells induced by my genetic system faithfully recapitulate the maturation and differentiation of endogenous NKT cells. Moreover, the system allows a timed analysis of the earliest step of differentiation, which to date remained largely enigmatic due to the rarity of these cells.

4.2.4 Transcriptome analysis of early NKT cells

To further investigate the changes occurring during early NKT cell development, I performed bulk RNA sequencing using the single-cell RNA barcoding and sequencing (SCRB-seq or 3'seq) method. For this purpose, I FACS-sorted 1000 cells from the induced developing NKT cells at different time-point (between 12h and 5d after induction) as well as from the NKT1, NKT2 and NKT17 mature wildtype subsets. Additionally, I also purified 1000

DP thymocytes (from the 12h induced mice) and wildtype Stage 0 (CD24+) NKT cells. For each condition, four biological replicates were sequenced.
The principal component analysis (PCA) indicates close transcriptional proximity of each developmental timepoint with their preceding and following timepoints (Fig. 13). Moreover, while DP thymocyte transcriptomes are found very close to those of the 12h timepoint NKT cells, the mature NKT1, NKT2 and NKT17 transcriptomes are located at the opposite edge and spatialy separated from those of the timepoints of the induced wave. This suggests that even the latest timepoint of the NKT cell developmental wave (5d) is still transcriptomically different from all mature NKT cell subsets. Therefore, it seem that the principal component 1 describes the development and maturation of NKT cells. Strikingly, Stage 0 NKT cell transcriptomes map very close to those of the 36-48h timepoint NKT cells.

To define the extent of significant changes occurring during the first 5d of development, the sequencing data were analysed in collaboration with Thomas Engleitner. For this analysis, we focused on the induced NKT cells wave and therefore excluded CD24+ NKT cells as well as NKT1, NKT2 and NKT17 cells. The analysis showed 3111 significantly regulated genes (p-value <0.001), whose expression was depicted in a heatmap where the significantly regulated genes were sorted according to their peak expression at the different timepoints (Fig. 14A). The majority of the changes occurred in the earliest phase of the development (transition from DP to 12h) and in the later timepoints (especially at 5d after induction).

We further performed a likelihood-ratio test (LRT) and clustered the significantly regulated genes in 11 unbiased clusters (Fig. 14B). Each cluster of gene was then corrrelated to the expression levels of the transcription factors PLZF, RORγt, Nur77/*Nr4a1* and NFATc1 (Fig. 15A). This analysis revealed a reverse correlation of PLZF and RORγt with every cluster. Moreover, cluster 10 had a high correlation with PLZF, while cluster 4 has a modest correlation with the TCR signalling-induced transcription factors Nr4a1 and NFATc.

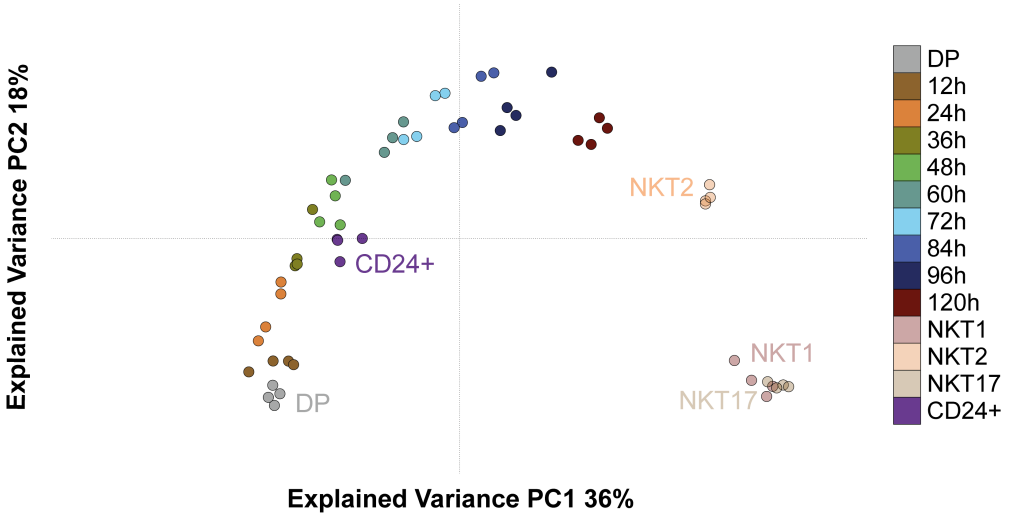

Fig. 13. Principal component analysis of SCRB-seq data.
The pricipal component analysis was generated on the 10% most variable genes (~1500 genes). Control samples are highlighted in the plot. Samples were sorted as follows: DP=DP thymocytes (TCRβ−, CD1d-PBS57-Tetramer−, CD69−); CD24+=early wildtype NKT cells (CD1d-PBS57-Tetramer+, CD44−, CD24+); NKT1 (CD1d-PBS57-Tetramer+, CD44+, NK1.1+, CD27+, CD138−); NKT2 (CD1d-PBS57-Tetramer+, NK1.1−, PLZFeGFP+, ICOS+, IL17RB+, CD138−); NKT17 (CD1d-PBS57-Tetramer+, CD19−, ICOS+, CD138+).

I therefore performed pathway enrichment analysis to determine the functionality of the genes contained in both cluster 10 and cluster 4. The analysis of cluster 10 (PLZF-correlated) revealed an enrichment for genes involved in translational regulation. Fittingly, cluster 4 (Nur77/NFATc-correlated) contained genes involved in TCR signalling as well as chromatine modification.

Overall, the transcriptome analysis revealed remarkable and distinct changes occurring during the very early phases of the development as well as before the subset differentiation initiation.

The monitoring of the dynamic changes at the protein level confirmed that the NKT cells generated through this genetic system faithfully recapitulate the maturation and differentiation of endogenous NKT cells. Moreover, the system

allowed a timed analysis of the earliest fate decision and differentiation steps, which to date remain largely enigmatic due to the rarity of these cells.

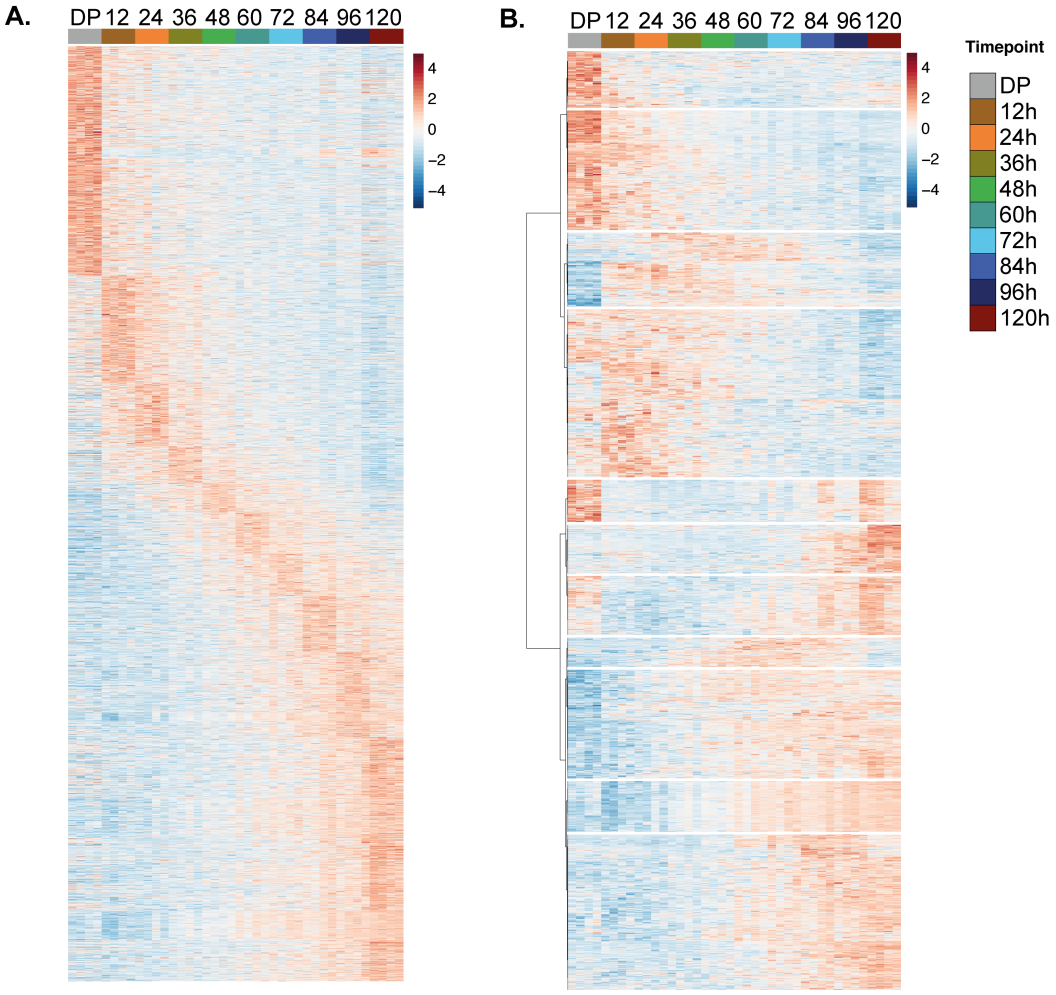

Fig. 14. Heatmaps of significantly regulated genes.

The RNA-seq data were analysed using DESeq2 and plotted in two heatmaps. **A.** The heatmap reports the significantly regulated genes sorted according to their maximum expression at each timepoint. **B.** To cluster the data, an LRT test was applied. The heatmap shows the 11 clusters generated (arranged from 1 to 11 from top to bottom).

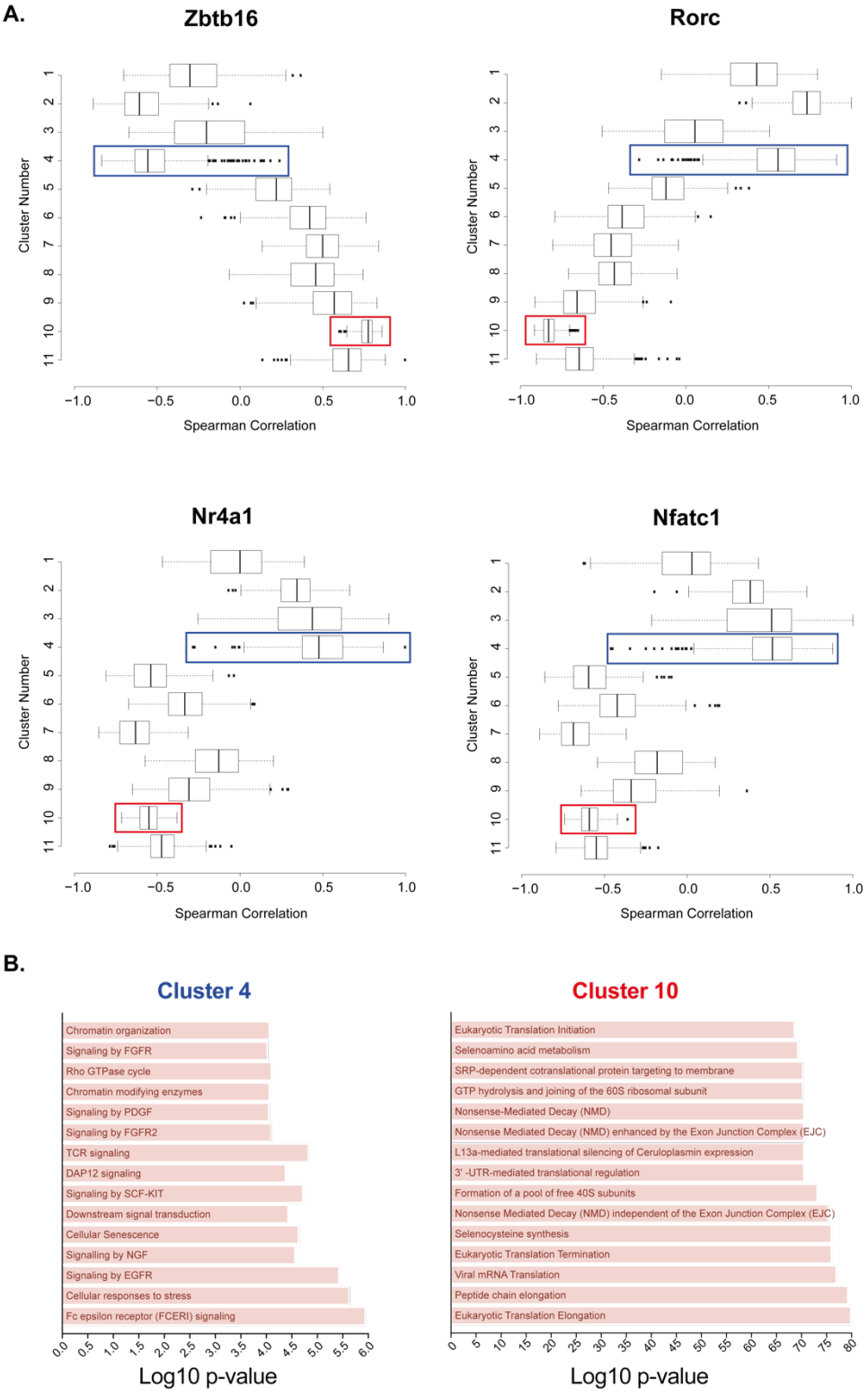

Fig. 15. Correlation analysis of gene clusters to defined transcription factors.

A. Spearman correlation analysis of all the 11 clusters generated to PLZF (Zbtb16), RORγt (Rorc), Nur77 (Nr4a1) and Nfatc1. Cluster 4 and cluster 10 were used for further pathway enrichment analysis are highlighted in blue and red, respectively. **B.** Pathway enrichment analysis was performed on the genes included in cluster 4 and cluster 10 using the EnrichR platform. The list of enriched

Fig. 15 **(continued)** pathways was obtained from Reactome Pathway Database and filtered for adjusted p-value<0.05. Pathways with less then 10 genes enriched were excluded. The list was then ranked according to the adjusted p-value and the first 15 most significanlty enriched pathways were selected. The plot report the selected pathways ranked accoriding to the log10 p-values.

4.3 Timing of thymic egress

NKT cells arise in the thymus, from where they emigrate to different organs of the body (Berzins et al., 2011; Hammond et al., 2001; Matsuda et al., 2000; Slauenwhite and Johnston, 2015; Wingender et al., 2012). By means of in situ labelling and intrathymic injection studies, it was shown that NKT cells migrate to the peripheral organs in an immature $CD44^{high}$ NK1.1− state and acquire NK1.1 expression in loco (Benlagha et al., 2002; Pellicci et al., 2002). Moreover, parabiosis studies showed that mature NKT cells are largely resident cells, suggesting that migration occurs prior to final maturation (Wang and Hogquist, 2018).

NKT cells migrate in response to microenvironmental signals. It was shown that CCR7, S1PR1 and CD69 are crucial factors required for the migration to peripheral organs (Allende et al., 2008; Kimura et al., 2018; Wang and Hogquist, 2018). In this section, I aim to precisely define the timing of thymic egress and the phenotype of recent thymic emigrant (RTE) NKT cells.

4.3.1 Regulation of NKT cell migration

Thymic CCR7+ NKT cell precursors were shown to possess the potential to migrate to peripheral sites where they further differentiate into mature NKT cell subsets (Wang and Hogquist, 2018). I therefore evaluated the expression of CCR7 on induced NKT cells in the thymus. CCR7 levels gradually increase from 42h to 6d — where 95% of the cells express CCR7 — and consequently decrease up to 21d (Fig. 16A).

S1PR1 represents an essential factor for thymic egress (Allende et al., 2008), and is in turn regulated by CD69. Thymic NKT cells showed a rapid increase

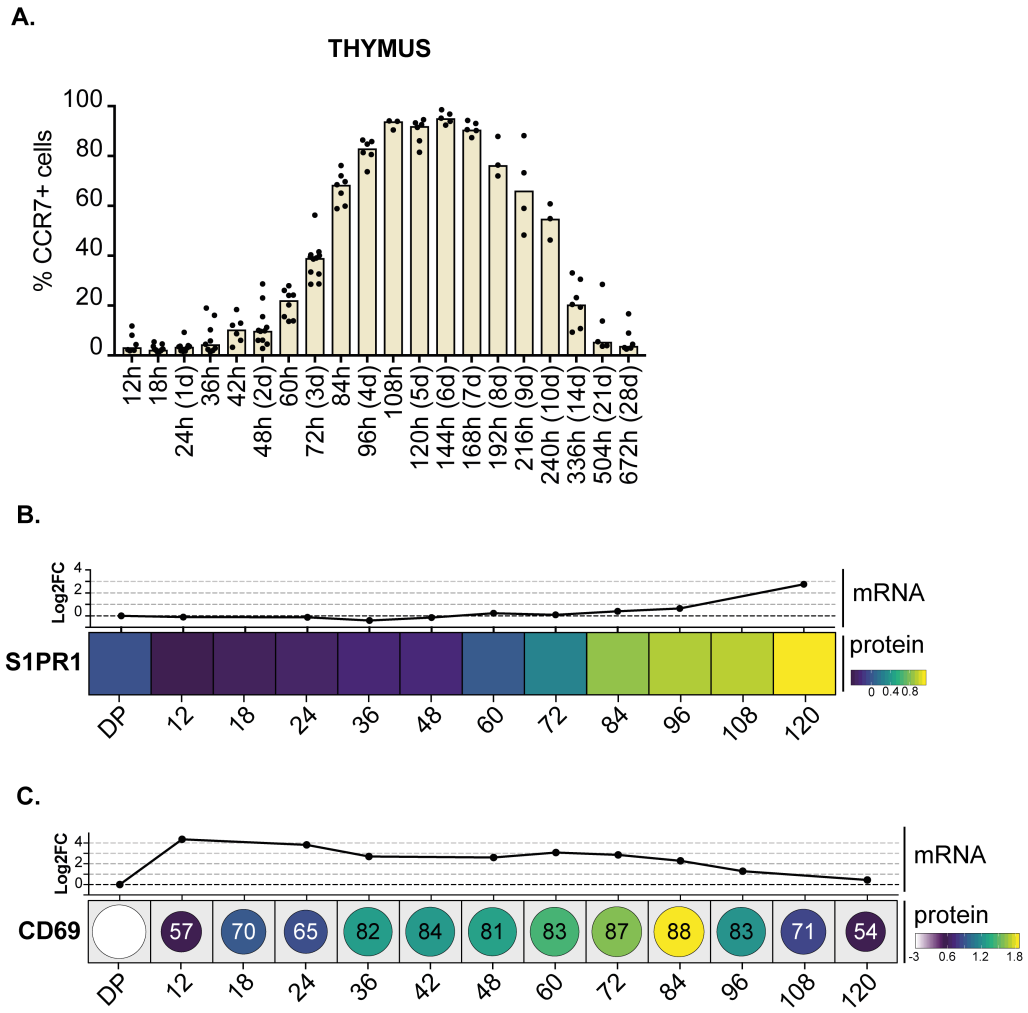

Fig. 16. Expression of migratory markers.

Ex vivo flow cytometric and transcriptomic analyses of thymi from inducible mice at different timepoints after 4-OHT administration. **A.** The bar graph indicate the median of the percentage of thymic CCR7+ induced NKT cells at different timepoints. **B.** The heatmap reports S1PR1 expression across NKT cell development. Median fluorescence intensity (MFI) of S1PR1 was calculated for induced NKT cells at different timepoints. The values were normalised to the MFI of TCRβ− CD1d-PBS57 Tetramer− cells. For each timepoint, a mean of the normalised values was calculated. The heatmap reports the the log2 of the mean values. **C.** The heatmap reports CD69 expression across NKT cell deelopment. For each timepoint, induced NKT cells were gated on CD69+ and MFI of CD69 was calculated. The size of the circles and the number reported inside the circles indicate the percentage of CD69+ induced NKT cells. The MFI values were normalised to the MFI of Stage 3 (NK1.1+ CD44+) NKT cells. For each timepoint, a mean of the normalised values was calculated. The heatmap reports the the log2 of the mean values. (B-C. The protein control sample “DP” is gated on TCRβ− CD1d-PBS57 Tetramer− RORγt^{high} cells. The mRNA levels were calculated from the SCRB-seq. The values reported indicate the log2 fold-change to DP thymocytes (gated as TCRβ− CD1d-PBS57 Tetramer− CD4+ CD8+ CD69−)).

of both S1PR1 protein and mRNA levels between 3d and 5d of development (Fig. 16B). Interestingly, the expression of CD69 showed a mirrored pattern, with decreasing levels of mRNA from 3d and protein from 4d after induction (Fig. 16C). Overall, these data show that thymic induced NKT cells acquire a migratory potential starting at day 4 of their development.

4.3.2 Timing of thymic egress

To further investigate the timing of peripheral colonisation, I crossed a tdTomato-based Cre activity reporter into the inducible system (CD4-CreER^{t2} Va14i^{StopF} mice) and monitored the appearance of tdTomato+ NKT cells in blood, spleen and liver over time. To control for the small fraction of endogenous CD4+ NKT cells which also expresses tdTomato upon 4-OHT administration, we included control CD4-CreER^{t2} tdTomato+ mice.
Starting 6d after 4-OHT administration, we detected significant populations of tdTomato+ recent thymic emigrant (RTE) NKT cells in the blood and spleen (Fig. 17A, 17B). In line with these results, at 6d after induction 85% of splenic tdTomato+ NKT cells expressed CCR7 (Fig. 17D). Interestingly, the liver colonisation with NKT cells occurred 2 days later compared to the spleen (Fig. 17C).
To reduce the number of endogenous tdTomato+ NKT cells and improve the detection of early RTE NKT cells, we also employed CD4-CreER^{t2} Va14i^{StopF} Traj18^{ko} tdTomato mice for these studies.

In this setup, I was able to detect some splenic tdTomato+ NKT cells already at 5d after induction (Fig. 17E). Similar to the previous results, the liver colonisation was delayed of 1-2 days compared to the spleen (Fig. 17F).
Overall, I identified a window of thymic egress for developing NKT cells which opens at 5d after initial Vα14i-TCR expression. However, my system does not allow us to exclude that a minor fraction of cells egresses the thymus earlier than 5d.

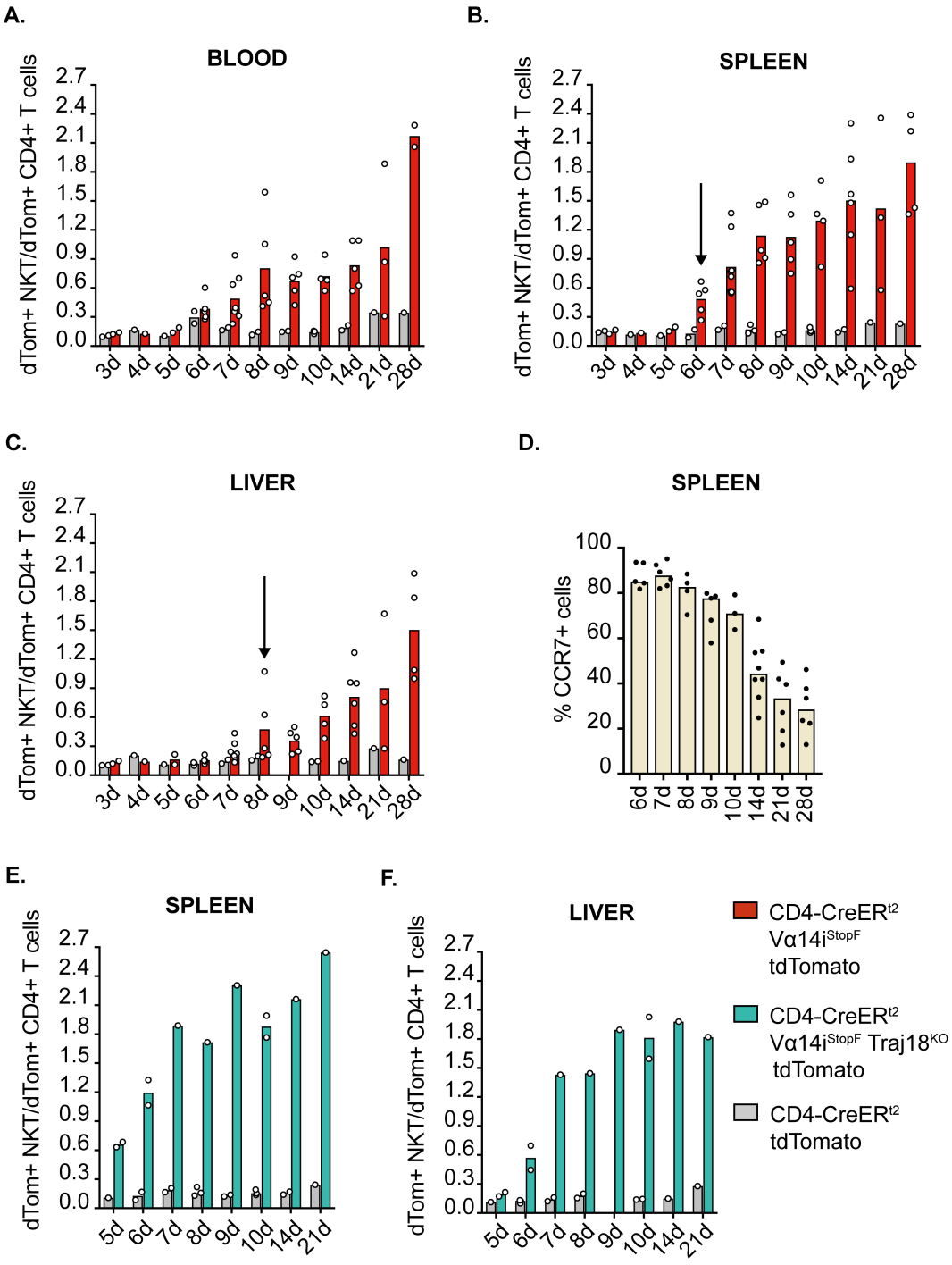

Fig. 17. Timing of thymic egress

Ex vivo flow cytometric analyses of blood, spleen and liver from inducible mice at different timepoints after 4-OHT administration. **A-C, E, F.** The bar graphs report the normalised fraction of tdTomato NKT cells. For each sample, the percentage of tdTomato+ NKT cells was normalised to the percentage of tdTomato+ CD4+ T cells. Each dot represents the ratio for each sample. The bars report the mean of the ratios for each timepoint. **D.** The bar graph indicates the median of the percentage of splenic CCR7+ induced NKT cells at different timepoints.

4.3.3 Phenotype of recent thymic emigrant NKT cells

After having identified the timing of thymic egress, I analysed the phenotype of RTE NKT cells. The splenic tdTomato+ NKT cells detected 6d after induction had a prominent PLZF^{high}, CD44+/− and NK1.1− phenotype (Fig. 18A). Although with a slight delay and to a less extent compared to the thymus, from 7d after induction a fraction of PLZF^{high} NKT cells starts to re-upregulate RORγt, displaying a CD44+, CD4+/− phenotype (Fig. 18A, 18D and 18G).

Interestingly, similarly to the thymus, the splenic RORγt+ PLZF+ subset acquire NK1.1 expression, resulting in over 50% of NK1.1+ cells at 28d after induction.
Additionally, part of the PLZF^{high} NKT cells diminish their PLZF levels, acquire NK1.1 and display a CD4+ phenotype (Fig. 18A, 18B and 18E). Lastly, a fraction of cells remains PLZF^{high} with a largely CD44+ CD4+ phenotype.

Overall, the maturation processes in the spleen highly mirrors that in the thymus. From 5d after induction, a fraction of cells egress the thymus, while the remaining cells lose the expression of CCR7 and are retained in the thymus, where they further mature. The RTE NKT cells colonise the spleen in a PLZF^{high} NK1.1− state and further differentiate in situ, giving rise to all the three NKT cells subsets.

4.4 TCR signalling during early NKT cell development

4.4.1 Timing and strength of TCR signalling

Positive selection represents the crucial step for the initiation of NKT cell differentiation (Das et al., 2010). I therefore investigated strength and timing of TCR signalling during early NKT cell development by means of the Nur77eGFP system (Zikherman et al., 2012). Nur77 (*Nr4a1*) is an orphan

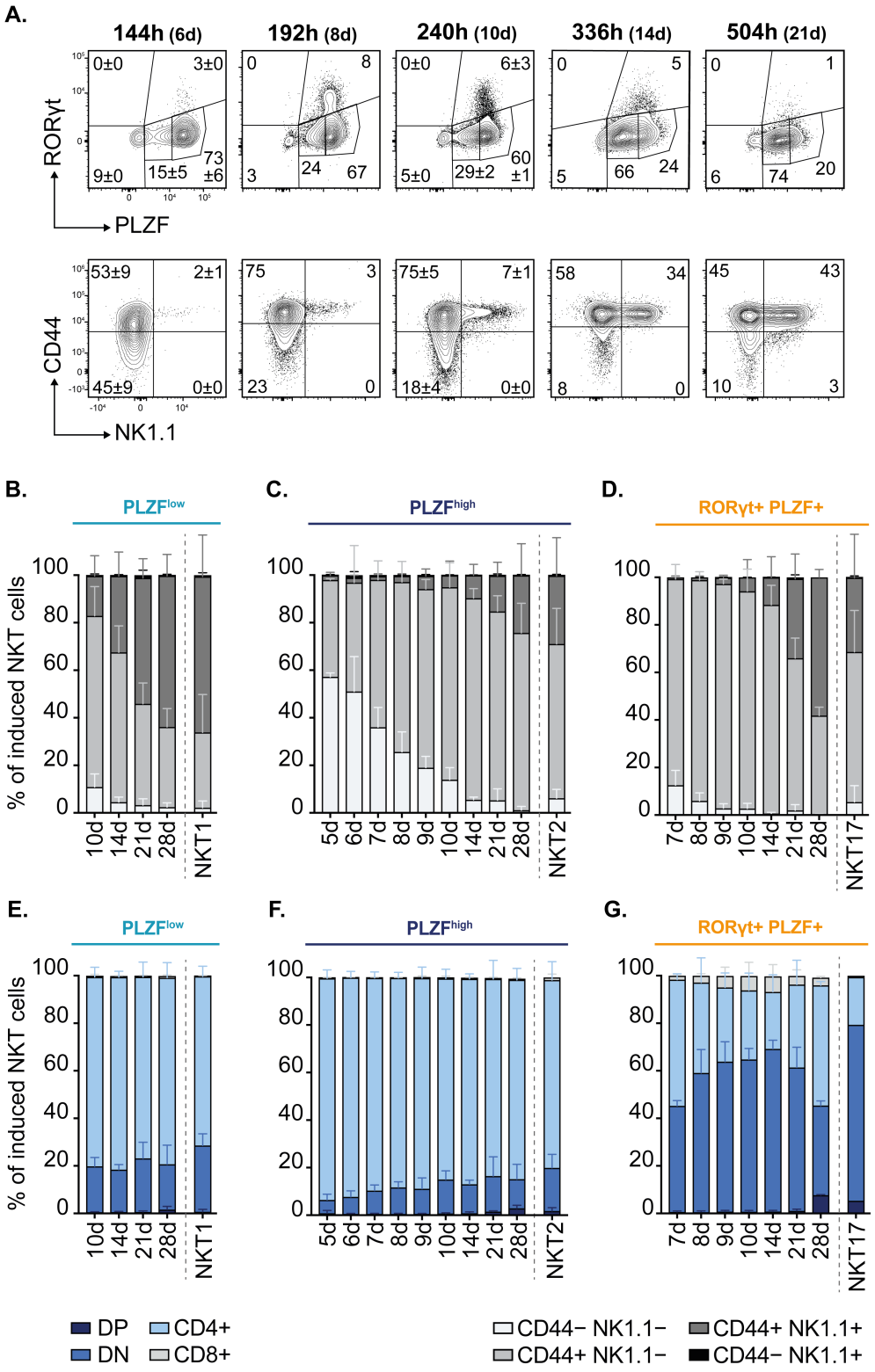

Fig. 18. Phenotype of splenic recent thymic emigrant NKT cells.

Ex vivo flow cytometric analyses of spleens from inducible tdTomato mice at different timepoints after 4-OHT administration. **A.** Representative facs plot of RORγt, PLZF, CD44 and NK1.1 expression in splenic induced NKT cells of CD4-CreER^{t2} Vα14i^{StopF} Traj18^{KO} tdTomato mice at different timepoints.

Fig.18 **(continued)**. The percentages represent mean and SD of at least two mice, except for timepoint 8d, 14d and 21d where one mouse is displayed. **B-G**. The bar graphs depict the mean and SD of the percentage of four CD44/NK1.1 (B-D) and four CD4/CD8 (E-G) subgroups at different timepoint calculated on 3 subsets: $PLZF^{low}$ (B,E), $PLZF^{high}$ (C, F) and RORγt+ PLZF+ (D,G). Subsets with less than 150 events were excluded. Data is representative of at least 2 mice and at least 2 independent experiments.

nuclear receptor whose expression closely correlates with TCR signal strength. Nur77eGFP BAC-transgenic mice were shown to report antigen receptor signal strength in various lymphocyte populations through eGFP expression. Already at 6h after Vα14i-TCR induction, roughly 35% of the thymic induced NKT cells received a TCR signal judging by intermediate levels of Nur77eGFP expression (Fig. 19A, 19B). Upon RORγt downregulation, over 95% of the cells express high levels of Nur77eGFP (Fig. 19B). Following PLZF expression, the TCR signal strength reporter intensity gradually declines. Although the developmental wave of induced NKT cells is, at least initially, highly synchronous and confined to a small window of time, a certain time lag between the first and the last induced NKT cell is inevitable. In this regard, the induced dynamic changes in RORγt and PLZF expression can be used to further fine-tune developmental timing, discriminating "younger" RORγt+ from "older" $PLZF^{high}$ NKT cells. Therefore, the reduction in Nur77eGFP signal we detect upon PLZF induction indicates that the first cells that start to express PLZF must be the first cells to express TCR and receive TCR signals and are now experiencing a downregulation TCR signalling-induced gene expression programs.

Interestingly, while the fraction of RORγt+ PLZF− Nur77eGFP+ NKT cells never exceeds 70%, a major increase in both percentage and signal intensity occurs upon RORγt downregulation, suggesting that the loss of RORγt faithfully marks the positively-selected induced NKT cells (Fig. 19B). As a consequence of the positive selection, the expression of diverse early factors was induced. Egr2, CD69 and GATA3 proteins were upregulated on over 50% of the induced NKT cells already 12h after 4-OHT administration (Fig. 19C and Fig.16C). Slightly slower was the expression kinetic of ICOS and PD-1,

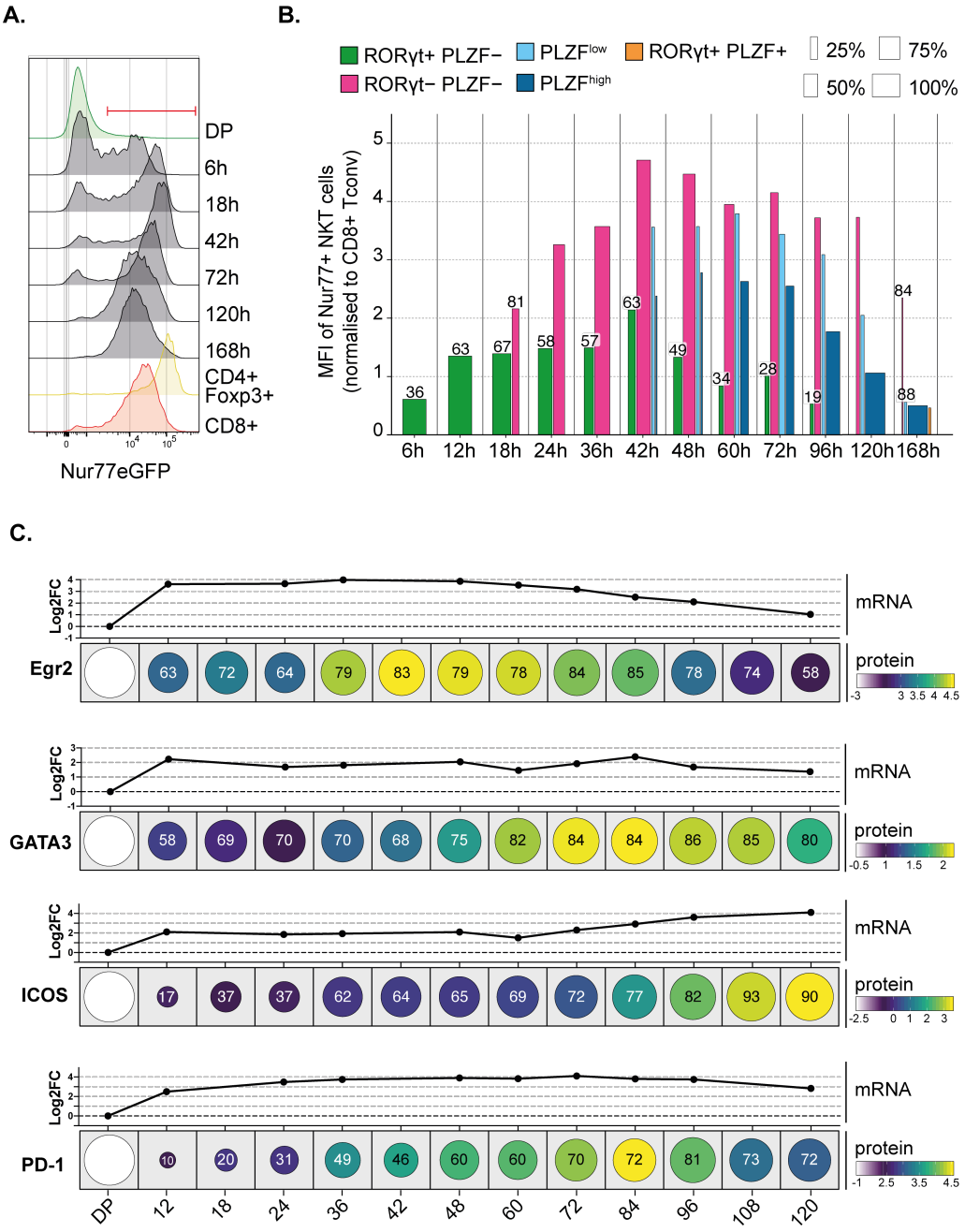

Fig.19. Analysis of TCR signalling kinetics during early NKT cell development.

Ex vivo flow cytometric and trasncriptomic analyses of thymi from inducible mice at different timepoints after 4-OHT administration. **A.** Representative histograms of Nur77eGFP dynamics in thymic induced NKT cells at different timepoints and additional immune cell populations. For the analyses, induced NKT cells and CD4+ Foxp3+ cells were gated on Nur77eGFP+ as depicted (red gate). **B.** The bar graphs report the Intensity and fraction of Nur77eGFP+ induced NKT cells. For each sample, the Nur77eGFP median fluorescence intensity of Nur77eGFP+ induced NKT cell subsets was normalised to the median fluorescence intensity of CD8+ T cells. The bars report the mean of the ratios for each timepoint. The numbers reported on top of the columns indicate the percentage of Nur77eGFP+ cells for each subset. When omitted, the percentage is >95%. The width of the column represents the percentage of each RORγt/PLZF subset. **C.** The heatmaps reports the

Fig.19 **(continued)** expression of different markers (Egr2, GATA3, ICOS and PD-1) across NKT cell development. For each timepoint, induced NKT cells were gated on the marker+ fraction and the median fluorescence intensity was calculated. The size of the circles and the number reported inside the circles indicate the percentage of marker+ induced NKT cells. The median fluorescence intensity values were normalised to the median fluorescence intensity of Stage 3 (NK1.1+ CD44+) NKT cells. For each timepoint, a mean of the normalised values was calculated. The heatmap reports the the log2 of the mean values. The protein control sample "DP" is gated on TCRβ− CD1d-PBS57 Tetramer− RORγt^{high} cells. The mRNA levels were calculated from the SCRB-seq. The values reported indicate the log2 fold-change to DP thymocytes (gated as TCRβ− CD1d-PBS57 Tetramer− CD4+ CD8+ CD69−).

which reached 50% of positive cells at around 36h. The protein levels were mirrored by RNA expression (Fig. 19C).

Although the Nur77eGFP system reports the strength of the TCR signal, the long half-life of eGFP impedes an accurate estimation of the TCR signal duration. In fact, at 12h after induction the *Nr4a1* mRNA is over 5 log2 fold higher than DP thymocytes, but it immediately declines. A very similar pattern is seen in Nor1/*Nr4a3* mRNA levels (Suppl. Fig. 4). While the eGFP decay initiates at 42h (Fig. 19B), at 60h the mRNA levels of both *Nr4a1* and *Nr4a3* genes are comparable to the DP precursors, confirming that the real TCR signalling is in fact much shorter than what is reported by the Nur77eGFP reporter mouse.

To more precisely define the length of the TCR signal, we made use of the recently published *Nr4a3*-Tocky mice (Bending et al., 2018). These mice carry a BAC transgene encoding a fluorescent Timer protein (Tocky) under the *Nr4a3* gene locus expression control. The Timer protein spontaneously converts from an unstable blue form to a stable red form with a conversion half-life of 8h, allowing a precise calculation of the timing and frequency domain of activation of TCR signal.

To bypass the loss of *Nr4a3*-Tocky signal occurring upon fixation, we employed PLZFeGFP mice (Zhu et al., 2013), substituted RORγt staining with extracellular CD8 staining and analysed mice at 24h, 48h and 72h (Fig. 20A).

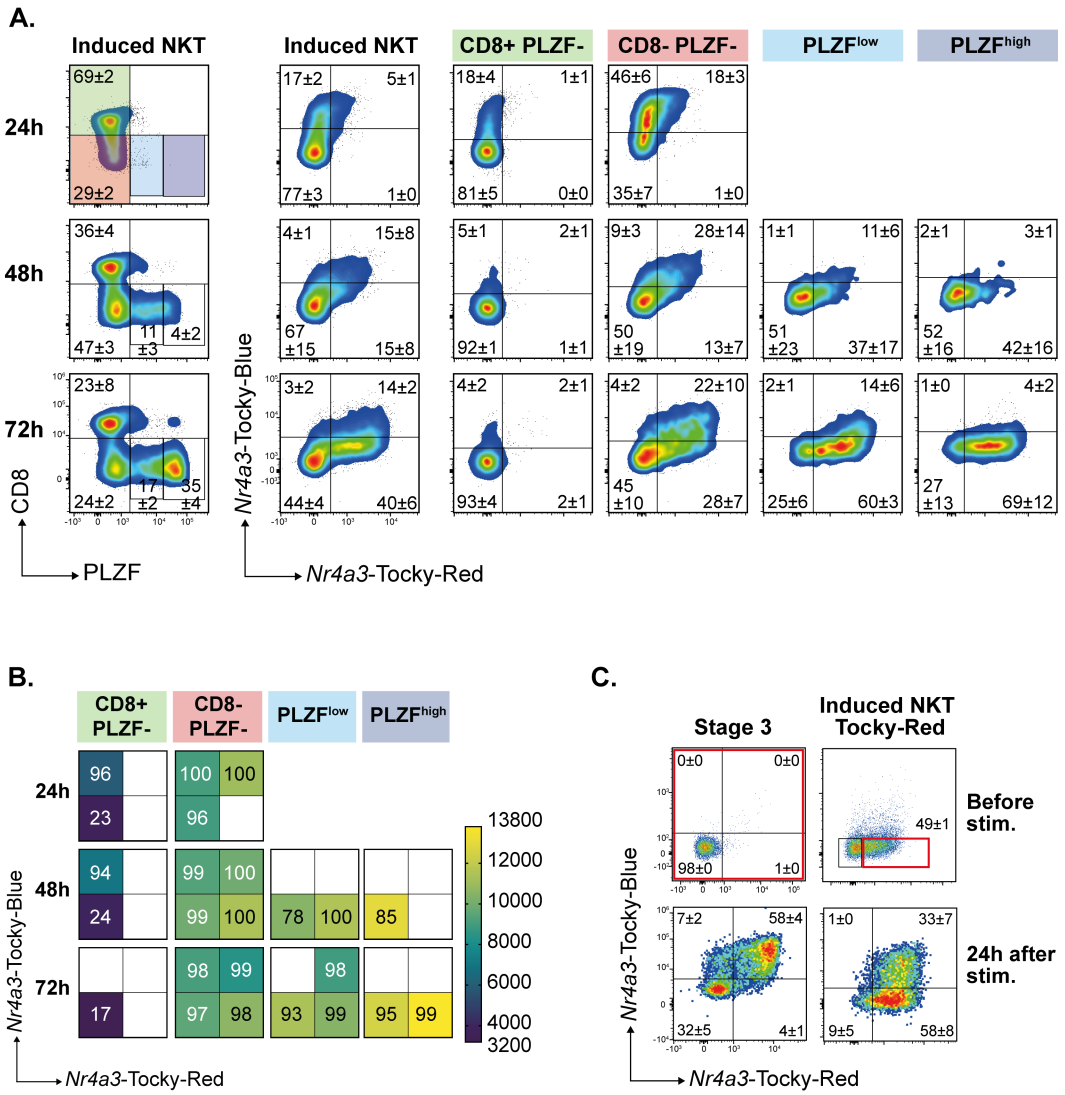

Fig. 20. Analysis of TCR signalling by means of *Nr4a3*-Tocky mice.

A. Ex vivo flow cytometric analyses of thymi from inducible *Nr4a3*-Tocky mice at 24, 48 and 72 hours after 4-OHT administration. The facs plots report the blue-to-red conversion of the *Nr4a3*-Timer protein in the whole induced wave of NKT cells and in the different subsets. The percentages indicate mean and SD of at least three mice. Data is representative of at least 4 experiments. **B.** The heatmap reports the intensity and percentage of CD69+ induced NKT cells for each subgroup (as reported in A.). For each quadrant, the percentage and median fluorescence intensity (MFI) of CD69+ cells was determined. The heatmap colour indicate the absolute MFI, while the number in the quadrants indicate the percentage of CD69+ NKT cells. **C.** Sorted thymic *Nr4a3*-Tocky-red induced NKT cells and Stage 3 NKT were stimulated in vitro with α-CD3 and α-CD28 antibodies for 24h. The *Nr4a3*-Tocky re-activation was determined by flow cytometry. The percentages indicate mean and SD of four mice and three independent experiments.In one experiment, two mice were pooled into one sample.

In the early CD8+ PLZF− cells, all the *Nr4a3*-Tocky-expressing NKT cells are blue and located in the "New locus", representing cells which recently received a TCR signal. Upon downregulation of CD8, the blue protein spontaneously converts into red and the cells move clockwise from a blue state to a blue-red state, entering the so-called "Persistent locus". If the TCR signal is suspended, the cells lose the blue colour and enter the red "Arrested locus". In the PLZF^{high} fraction, all the *Nr4a3*-Tocky-positive NKT cells are red, thus devoid of TCR signals for at least 8h. These data demonstrate that NKT cells receive TCR signals for not longer than 2 days after Vα14i-TCR induction.

Although all positively selected induced NKT cells expressed Nur77eGFP, *Nr4a3*-Tocky mice displayed a considerable fraction of *Nr4a3*-Tocky-negative NKT cells (Fig. 20A). This suggested the possibility that developing NKT cells receive different TCR signals. However, the analysis of CD69 expression showed that upon CD8 downregulation, all the NKT cells homogenously express high levels of CD69, and no considerable difference was detected in the percentage and level of CD69 between *Nr4a3*-Tocky-negative and *Nr4a3*-Tocky-positive NKT cells (Fig. 20B). Therefore, in my opinion it is unlikely that a strong difference in TCR signal strength distinguishes *Nr4a3*-Tocky-negative and *Nr4a3*-Tocky-positive developing NKT cells.
Overall, the analysis of Nur77eGFP and *Nr4a3*-Tocky mice confirmed that early NKT cells receive a strong TCR signal upon positive selection with a limited duration of approximately 2 days.

4.4.2 The cessation of TCR signalling in NKT cells is not cell-intrinsic

At steady-state, mature NKT cells are known to lack TCR signal activation (Moran et al., 2011). Considering that the TCR signalling observed using the *Nr4a3*-Tocky reporter during the early NKT cell development is limited to 2 days, I wanted to evaluate whether the TCR signal cessation is due to cell-intrinsic or extrinsic mechanisms. In this regard, the *Nr4a3*-Tocky system allows the determination of the frequency of transcriptional activation by the detection of new blue protein transcribed upon re-activation of TCR signalling.

Therefore, I FACS-sorted thymic *Nr4a3*-Tocky-red NKT cells at 72h after induction as well as Stage 3 NKT (as positive control), stimulated them in vitro with α-CD3 and α-CD28 antibodies for 24h and evaluated the TCR signalling re-activation by flow cytometric analysis (Fig. 20D). Almost 30% of stimulated *Nr4a3*-Tocky-red NKT restarted the production of blue protein and therefore moved back to the blue-red Persistent locus.
These data suggest that after positive selection, TCR signalling is not inhibited by cell intrinsic mechanisms.

4.4.3 Early NKT cells display largely homogenous TCR signal strength

Recent studies proposed a role for TCR signal strength in functional NKT cells subset differentiation (Tuttle et al., 2018; Zhao et al., 2018). However, whether and to which extent TCR signal strength affects the fate decision of NKT cells remains controversial (Blume et al., 2016; Chen et al., 2017; Henao-Mejia et al., 2013; Lu et al., 2019; Malhotra et al., 2018; Pereira et al., 2014). I therefore evaluated the homogeneity of TCR signal strength during NKT cell development. I calculated the percentage of robust coefficient of variation (%rCV) of Nur77eGFP in positively-selected early NKT cells and compared it to that of CD8+ conventional T cells and regulatory T cells (Tregs). Considering that the highly variable CD8+ T cell TCR repertoire allows the recognition of numerous types of antigens with different affinity, it is expected that CD8+ T cells population display a rather heterogeneous TCR signal strength. Oppositely, Treg cells are considered to differentiate upon high affinity antigen encounter, which would translate in a more homogeneous TCR signal strength within the Treg population. The comparison between CD8+ T cells and Treg cells showed that the %rCV of Nur77eGFP in Treg is only 65% of that of CD8+ T cells (Fig. 21A, 21B). This indicates that indeed the Treg cell population has a more homogeneous Nur77eGFP intensity compared to CD8+ T cells. The analysis of the induced NKT cell subsets did not show considerable differences in %rCV between 36h, 48h and 72h. However, for all subsets the coefficient of variation of induced NKT cells was roughly half of that of CD8+ T cells and slightly lower of that of Treg cells.

These results indicate that early developing NKT cell receive a homogeneous TCR signal, arguing against a critical role of TCR signal strength in NKT cell subset differentiation.

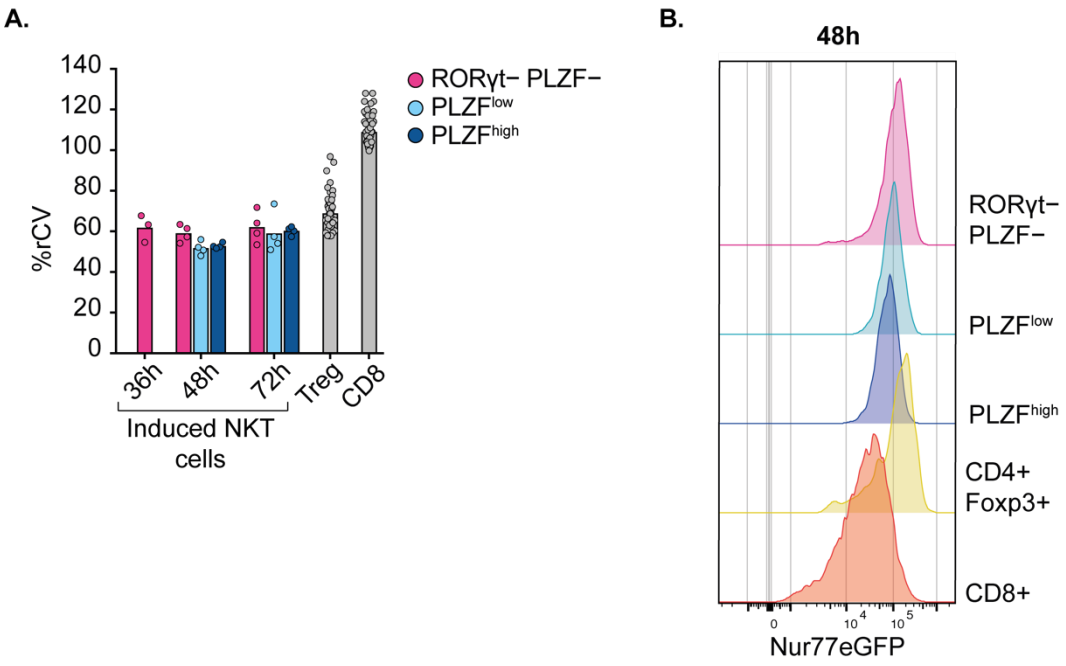

Fig. 21. Analysis of TCR signalling by evaluating the distribution of Nur77eGFP intensity. Ex vivo flow cytometric analyses of thymi from inducible Nur77eGFP mice at 36, 48 and 72 hours after 4-OHT administration. **A.** Representative histograms of Nur77eGFP expression in thymic induced NKT cell subsets at 48h after induction and in additional immune cell populations. **B.** The bar graph reports the percentage robust coefficient of variation (%rCV) of different induced NKT cell subsets, regulatory T (Treg) cells and CD8+ T cells (CD8). For the induced NKT cells and Treg cells (CD4+ Foxp3+), the %rCV was calculated on the fraction of Nur77eFP+ cells, while for CD8+ T cells it was calculated on the whole population. The %rCV was determined using FlowJo software.

4.5 Evaluation of NKT cell proliferation

Immature NKT cells are known to undergo a proliferative burst in response to positive selection, which diminishes during the maturation process (Das et al., 2010). Although diverse studies have evaluated NKT cell proliferation, there is no clear consensus on the amount and timing of the proliferation. In this

regard, several studies suggested that the proliferation of developing NKT cells initiates only upon CD24 downregulation (Stage 1). This notion is supported by low Ki67 expression and the small cell size of CD24+ Stage 0 NKT cells. (Benlagha et al., 2002; Benlagha et al., 2005; Wang and Hogquist, 2018). Moreover, deficiency of c-Myc – a critical factor for cellular proliferation – was shown to drastically reduce NKT cell numbers in Stage 1, 2 and 3 but not Stage 0, suggesting that the proliferative burst occurs from Stage 1 onwards (Dose et al., 2009).

On the other side, various studies show high BrdU incorporation and Ki67 expression already at Stage 0, therefore supporting the idea that proliferation occurs immediately after positive selection (Prevot et al., 2015; Pyaram et al., 2019; Salio et al., 2014).

In this section, I aim to define the timing and amount of proliferation during NKT cell development.

4.5.1 NKT cells proliferation is temporally-distant from the positive selection

To unravel the controversies regarding the timing of cellular proliferation during NKT cell development, I analysed the proliferation of induced NKT cells at different time points after induced TCR expression by DNA staining and BrdU incorporation in vivo.

Over 28d of development, the thymic NKT cell proliferation is confined to a window of time between 3d and 14d after induced TCR expression, with maximal proliferation at 6d (Fig. 22A). Splenic RTE NKT cells show moderate proliferation which diminishes over time (Fig. 22B).

The analysis of thymic induced NKT cells subsets revealed that the proliferation is initially restricted to PLZF+ NKT cells, but during the peak of proliferation an increase in PLZF− proliferation is also observed. Interestingly, at later timepoints, minimal proliferation of $PLZF^{low}$ cells is observed, while $PLZF^{high}$ cells maintain a moderate proliferation (Suppl. Fig. 5A). Although to a lesser extent, a similar proliferation pattern is also detected in splenic RTE NKT cells (Suppl. Fig. 5C). Notably, the timepoint of the highest proliferation of thymic developing NKT cells (6d) correlates with the time of thymic egress,

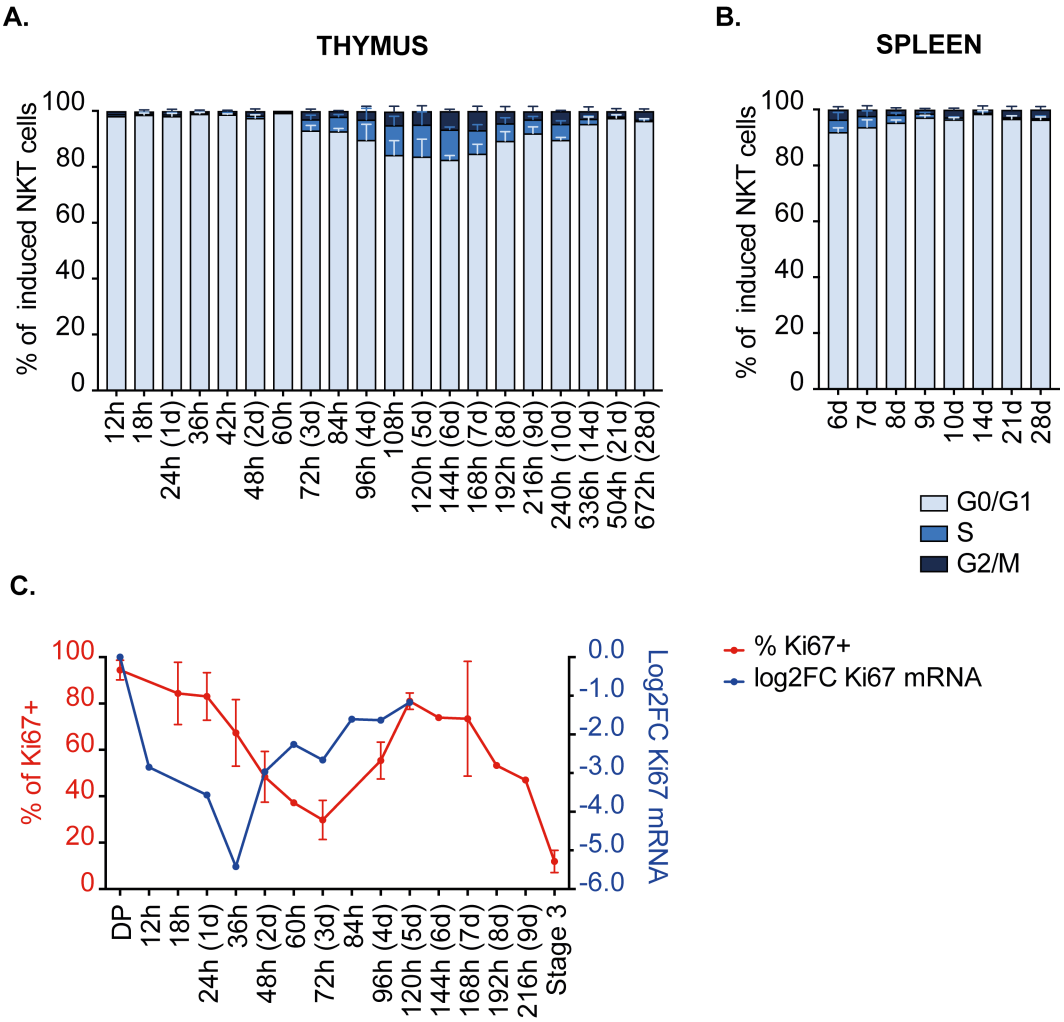

Fig. 22. Kinetic assessment of NKT cell proliferation.

Ex vivo flow cytometric analyses of thymi and spleen from inducible mice at different timepoints. **A-B.** The bar graphs report the proliferation of thymic and splenic induced NKT cells at different timepoints. Proliferation was assessed using the DNA binding dye DAPI. The analysis of G0/G1, S and G2/M phases was performed with the Cell cycle algorithm function of FlowJo (Watson Pragmatic Model, constrain: G2 Peak = G1 CV). **C.** The graph indicates the levels of Ki67 protein and mRNA levels on induced NKT cells at different timepoints. The protein control sample "DP" is gated on TCRβ− CD1d-PBS57 Tetramer− RORγt^{high} cells. The mRNA levels were calculated from the SCRB-seq. The values reported indicate the log2 fold-change to DP thymocytes (gated as TCRβ− CD1d-PBS57 Tetramer− CD4+ CD8+ CD69−).

supporting the idea of robust NKT cell proliferation prior thymic egress (Benlagha et al., 2002).

As mentioned above, c-Myc plays an important role in the proliferation of early NKT cells (Dose et al., 2009). The analysis of the induced NKT cell transcriptome revealed that MYC mRNA levels gradually increase from 1d to 2d after induction and further remain high until 5d (Suppl. Fig. 5B). This is in line with the proliferation initiation at 3d after induction of TCR expression reported above.

Although thymic NKT cells do not significantly proliferate prior 3d after induction, at 1d after induction over 80% of induced NKT cells express Ki67. The percentage of positive cells gradually decreases up to 25% at 3d (Fig. 22C and Suppl. Fig. 6). Concomitant to the initiation of the proliferation, Ki67 is re-upregulated and follows the cell cycle pattern.

Overall, these data show a considerable delay of one to two days between the start of TCR signalling and proliferation of early NKT cells. Considering that Stage 0 corresponds to the first 3d after induction, this indicates that proliferation initiates in the late Stage 0 but is mainly confined to Stage 1 and Stage 2.
The high expression of Ki67 on DP thymocytes would suggest that recently-selected NKT cells might originate from non-quiescent precursors and that, in response to positive selection, NKT cells are triggered to temporally enter a quiescent state (defined by the rapid downregulation of Ki67). This would be in line with the detection of low levels of Ki67 in cells which recently exited the cell cycle (Sobecki et al., 2017). However, the signals which govern Ki67 downregulation and its consequent re-upregulation and initiation of the proliferation remains to be elucidated.

4.5.2 Distribution and cell cycle speed of proliferative immature NKT cells

To confirm these findings with a different method and to further define the identity of cycling NKT cells, I analysed mice (between 1d and 5d after induction) injected with BrdU either 30 minutes or 4 hours before euthanasia (Fig. 23A and Suppl. Fig. 7). The measurement of incorporated BrdU confirms

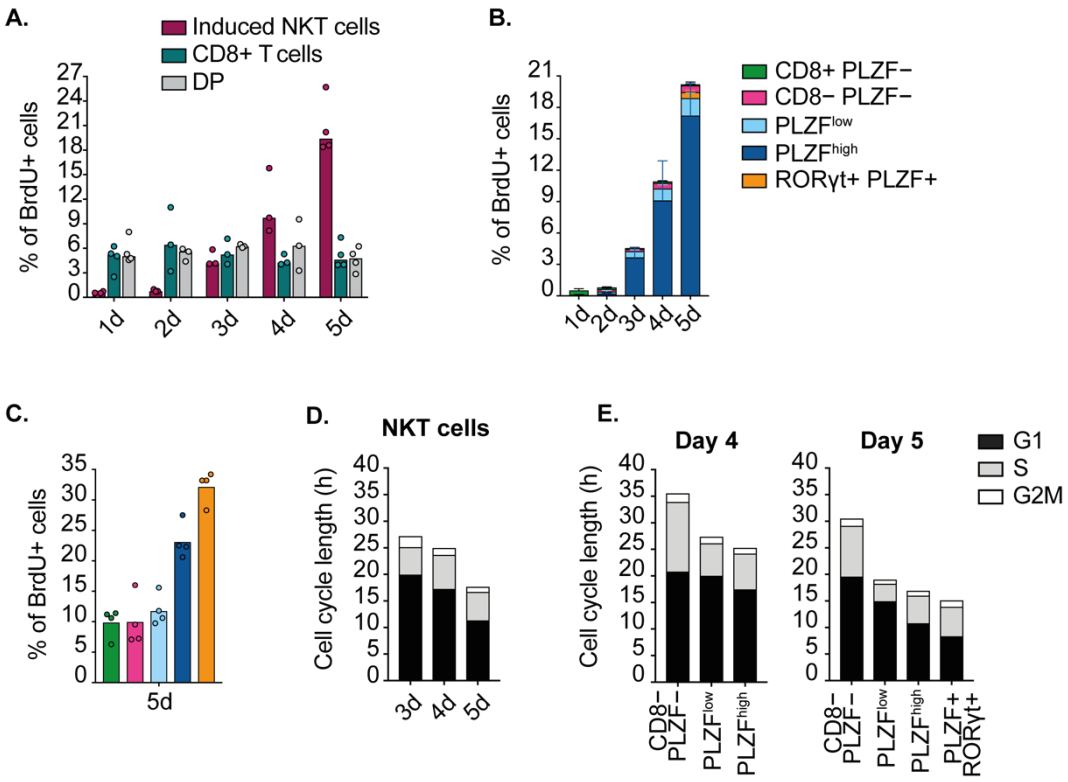

Fig. 23. Distribution and cell cycle speed of proliferative immature NKT cells.

Ex vivo flow cytometric analyses of thymi and spleen from inducible mice between 1d and 5d after induction. **A.** The bar graphs report the percentage of BrdU+ thymic induced NKT cells, CD8+ T cells and DP thymocytes at different timepoints. **B.** The graph indicates the RORγt/PLZF subset distribution of the BrdU+ induced NKT cells. The percentages refer to the induced NKT cells. For the PLZF− fraction, RORγt staining was substituted by CD8 staining. **C.** The plot indicates the percentage of BrdU+ induced NKT cells for each subset at 5d after induction. **D-E** Cell cycle length was computationally calculated using the BrdU incorporation and the Ki67 protein level information measured by flow cytometry. The graphs report the average cell cycle length (in hours) of whole induced NKT cells at 3d, 4d and 5d after induction (D) and of induced NKT cells subsets at 4d and 5d after induction (E).

the above-mentioned result, with the proliferation starting at 3 days and increasing up to 5d (Fig. 23A). I further defined the RORγt/PLZF distribution of the BrdU+ induced NKT cells, and found that the majority of the proliferative NKT cells express high levels of PLZF (Fig. 23B). Interestingly, the few RORγt+ PLZF+ NKT cells detected at 5d after induction display over 30% of BrdU incorporation (Fig. 23C).

In order to quantify the cell cycle speed throughout NKT cell development, I made use of an algorithm developped by a collaborator to calculate the cell cycle length of induced NKT cells at different time points based on the BrdU incorporation data and the Ki67 expression levels (Kretschmer et al., in press) (Suppl. Fig. 7). For this analysis, I focused on the proliferative phase, meaning between 3d and 5d after induction.
The algorithm predicted that at both 3d and 4d after induction, the division time of the induced NKT cells is around 25-27 hours (Fig. 23D). A slight increase in cell cycle speed is seen at 5d (18h). The analysis of the RORγt/PLZF-defined subsets showed that PLZF− NKT cells undergo the slowest cell division both at 4d and at 5d (Fig. 23E). A moderate progressive decrease in division time was observed in relation to the increasing levels of PLZF.

Overall these result show that mainly NKT cells expressing high levels of PLZF proliferate. The BrdU incorporation data suggest that PLZF+ RORγt+ NKT cells derive from the fraction of highly proliferative PLZFhigh cells.

4.6 Timing of functional differentiation

As a result of the NKT cell differentiation process, three functionally distinct subsets are generated in thymus and periphery: NKT1, NKT2 and NKT17. These subsets can be separated based on the expression of transcription factors (such as RORγt, PLZF and T-bet) but most importantly based on their cytokine producing potential (Das et al., 2010).
Although a distinct NKT1, NKT2 and NKT17 cytokine pattern can be detected (secreting mainly Th-1, Th-2 and Th-17 cytokines, respectively), some NKT1 and NKT2 cells bear the unique feature of producing both IL-4 and IFN-γ, while a fraction of NKT17 is capable of releasing both IL-4 and IL-17 (Georgiev et al., 2016; Stetson et al., 2003).

The NKT1 subset is considered to be the last one to differentiate, as several studies showed that NK1.1+ NKT cells appear only in the late phases of the

development (Benlagha et al., 2002; Pellicci et al., 2002). However, the timing of the different subset differentiation remains elusive.

In this section, I aim to define the timing of subset differentiation and their acquisition of the ability to produce cytokines.

4.6.1 Timing of the acquisition of cytokine production capabilities

The NKT1, NKT2 and NKT17 functional subsets highly differ in terms of cytokine profiles (Georgiev et al., 2016). I therefore investigated the acquisition of cytokine production capabilities and the changes in cytokine repertoire during NKT cell development and differentiation.

To this end, thymocytes were isolated at various time-points after Vα14i-TCR induction and stimulated with PMA/Ionomycin for 4h in the presence of monensin followed by flow cytometric analysis of intracellular cytokines. Prior to PLZF expression, NKT cells are not capable of producing any cytokine (Fig. 24A and Suppl. Fig. 8). Two days after Vα14i-TCR induction, we detected IL-4 production abilities in $PLZF^{low}$ cells, followed by double IL-4/IFN-γ producers within $PLZF^{high}$ cells (60h). From day 3 to day 6 of their development, induced NKT cells display a largely constant cytokine production repertoire, with $PLZF^{high}$ cells containing higher cytokine production potentials compared to $PLZF^{low}$ NKT cells.

From 7 days onwards, the NKT cells which re-upregulated RORγt acutely display a drastically different cytokine profile repertoire compared to the rest of the induced NKT cells (Fig. 24B). At 7d, over 65% of the RORγt+ $PLZF^{high}$ cells are capable of producing either only IL-17 (32%) or both IL-4 and IL-17 (34%). Over time, the fraction of IL-4/IL-17 double producers is largely replaced by the IL-17 single producers.

The difference between the cytokine production profiles in $PLZF^{high}$ and $PLZF^{low}$ developing NKT cells is less pronounced. Over time, the $PLZF^{high}$

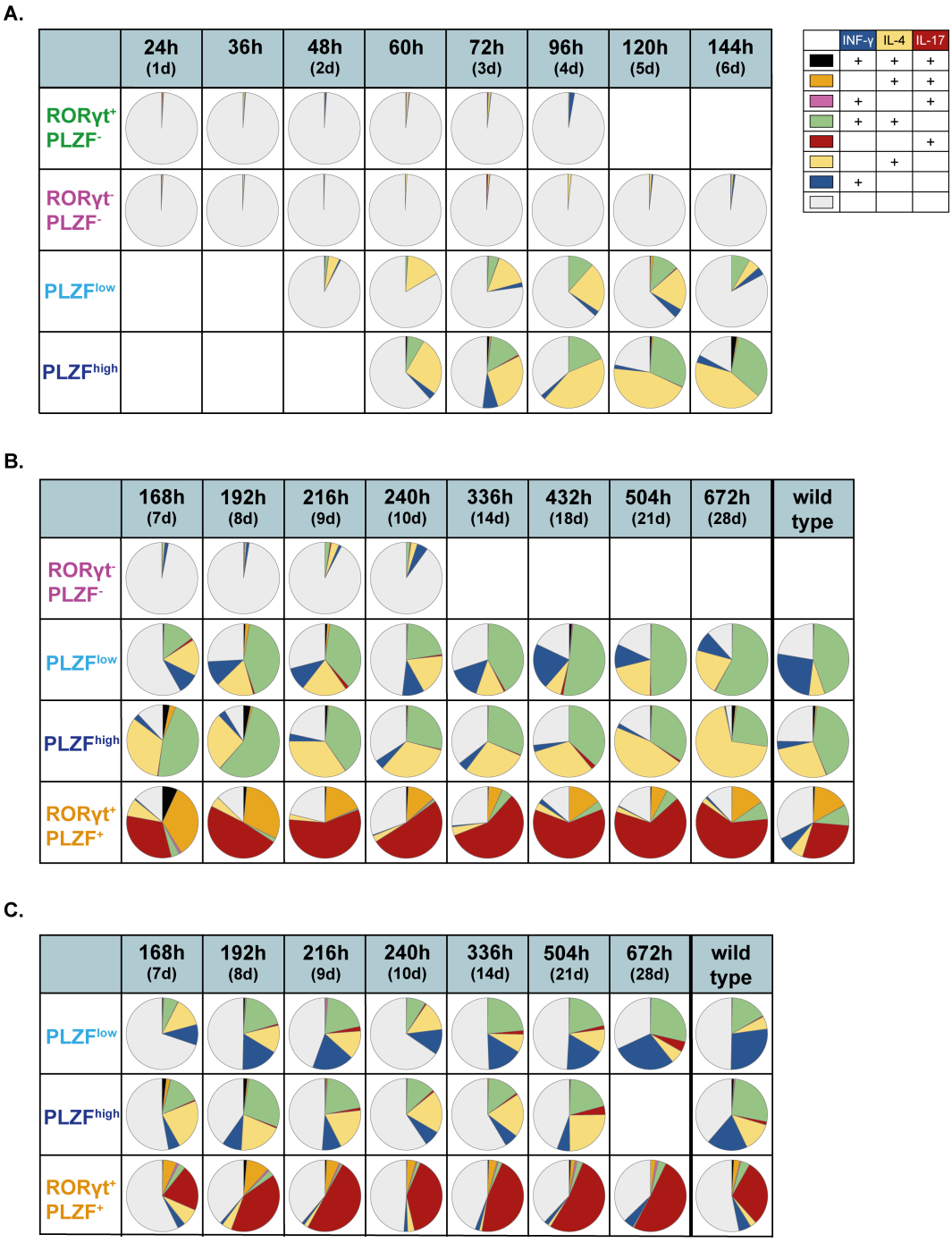

Fig. 24. Repertoire of cytokine production capabilities during NKT cell differentiation.
Ex vivo flow cytometric analyses of thymi and spleen from inducible mice at different timepoints. Cells were stimulated ex vivo with PMA and ionomycin, and the intracellular levels of cytokines were evaluated by flow cytometry. Single, double and triple producers of IL-4, IFN-γ and IL-17 were determined by the Boolean tool "Create combinational gates" from FlowJo. The pie charts report the percentages of thymic **(A-B)** and splenic **(C)** induced NKT cell expressing the reported combination of cytokines at different timepoints. Graphs were generated with SPICE v6.

fraction is mainly composed of single IL-4 and to a less extent double IL-4/IFN-γ producers. In contrast, the majority of the stimulated PLZF^{low} cells produce both IL-4 and IFN-γ, but a fraction of them produces only IFN-γ. However, at 28d there is still a substantial fraction of cells producing only IL-4.

The analysis of the splenic induced NKT cells shows an overall minor fraction of cells capable of producing cytokines compared to the thymus (Fig. 24C). The RORγt+ PLZF+ developing NKT cell fraction largely lacked the ability to produce both IL-4 and IL-17 and mainly produced only IL-17. Moreover, PLZF^{low} and PLZF^{high} NKT cells did not display major differences in their cytokine production repertoire, although the PLZF^{low} fraction had a higher potential to produce only IFN-γ.

To further investigate the timing of acquisition of cytokine production capabilities, I evaluated the chromatin accessibility at the cytokine loci by means of ATAC-sequencing. To this end, I FACS sorted 16000-50000 cells from the induced NKT cell populations between 12h and 120h after induction. Moreover, I purified DP thymocytes as well as NKT1 cells as controls. On these samples, ATAC-sequencing was performed in collaboration with Gunnar Schotta and the analysis was conducted in collaboration with Gaurav Jain.
The analysis of a selected group of cytokine loci revealed that several cytokine loci open toward the late timepoints (from around 96h after induction) (Fig. 25 and Suppl. Fig. 9A). In this regard, an increasing chromatin opening of both IL-4 and IFN-γ is observed from 84h after induction. These results show a moderate delay compared to the functional experiment I performed. This could be attributed to the fact that in the ATAC-sequencing the analysis was performed on the bulk induced population while the cytokine stimulation analysis was sub grouped in RORγt and PLZF subsets. Therefore, considering that in the cytokine stimulation experiment only a fraction of PLZF+ NKT cells initially produces cytokines, it is possible that the bulk ATAC-seq data is not sufficiently sensitive to detect these changes.

Interestingly, in addition to IL-4 and IFN-γ, other cytokine loci undergo a progressive opening; these include IL-6, IL-21 and IL-22, whose loci open

A.

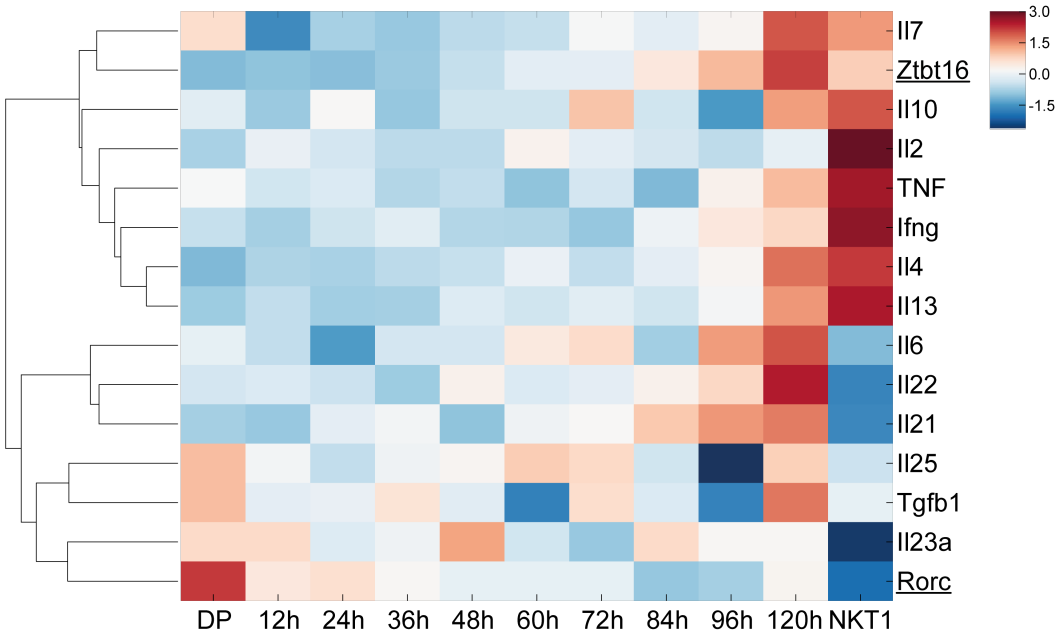

Fig. 25. Chromatin accessibility at diverse cytokine loci.

The heatmap reports the chromatin accessibility of diverse cytokines at different timepoint calculated from the ATAC-seq data. Mean of the peaks were calculated for the cytokine regions and plotted in the heat maps for each time point using seaborn (v 0.9.0) clustermap. The colour bar represents the openness of the region with blue representing less open region while red representing more open regions. PLZF (Zbtb16) and RORγt (Rorc) genes were included as control (underlined). Each column represents the mean of 2-5 biological samples.

between 84h and 120h but interestingly undergo further closing again in NKT1 cells. Differently, IL-13, TNF and IL-7 loci open at a similar time compared to the other cytokine loci but are found similarly open in NKT1 cells. Lastly, the IL-2 gene locus remains mainly closed up to 120h but it is found open in NKT1 control cells, suggesting that this chromatin change might occur later in the differentiation process.

Although a change in chromatin accessibility was observed for diverse cytokines, the transcriptome data analysis revealed that the mRNA levels were not always significantly increased (Suppl. Fig. 9B).

Overall, the data show that the timing of the functional differentiation dramatically differs between subsets. The cells which re-upregulate RORγt present a drastically different repertoire immediately when they emerge, both

in the thymus and in the spleen, suggesting that the NKT17 differentiation is very fast and homogenous upon RORγt upregulation. Differently, in case of NKT1 the acquisition of distinct functional properties is surprisingly slow. Moreover, the ATAC-seq data show a modest increase in accessibility at diverse cytokine gene loci toward the end of the first 5d of development, while the mRNA levels remained unchanged for many cytokines. This suggests that during the differentiation process, the immature NKT cells undergo chromatin remodelling at functional loci in preparation for subsequent functional differentiation.

4.6.2 Rapid and distinct NKT17 differentiation program

Given the extremely rapid acquisition of a specific cytokine production repertoire displayed by RORγt+ PLZF+ NKT cells, I sought to further investigate the timing of NKT17 subset-specific markers expression. I therefore measured the expression of CD138 (Dai et al., 2015), IL-23R (Rachitskaya et al., 2008), CD103 (Drees et al., 2017), ICOS (Engel et al., 2016), Neuropilin-1 (Nrp-1) (Milpied et al., 2011) and GATA3 (Lee et al., 2013) on thymic and splenic induced NKT cells. Overall, I detected a remarkably different phenotype of RORγt+ PLZF+ NKT cells compared to the RORγt− counterpart. CD138 and IL-23R were nearly exclusively expressed on RORγt+ NKT cells both in the thymus and in the spleen (Fig. 26A, 26B). A similar expression pattern was detected for CD103 on splenic induced NKT cells, while the thymic subsets displayed a differential expression of CD103 with a strong enrichment on the RORγt+ fraction (Fig. 26C).

ICOS, Nrp-1 and GATA3 are expressed on both NKT17 and NKT2 cells. Along this line, the analysis revealed a preponderant expression of ICOS, Nrp-1 and GATA3 on PLZF^{high} and PLZF+ RORγt+ cells in both thymus and spleen, with minimal expression on PLZF^{low} cells, especially towards the later timepoints (Fig. 27A-27C).

Overall, our analysis confirms that also the surface phenotype of the induced RORγt+ PLZF+ NKT cells strongly resemble bona fide NKT17 cells right from the beginning of their differentiation. Moreover, the rapid acquisition of their specialized phenotype and distinct cytokine production profile implies that the

NKT17 subsets differentiation is driven by a highly specific and divergent program.

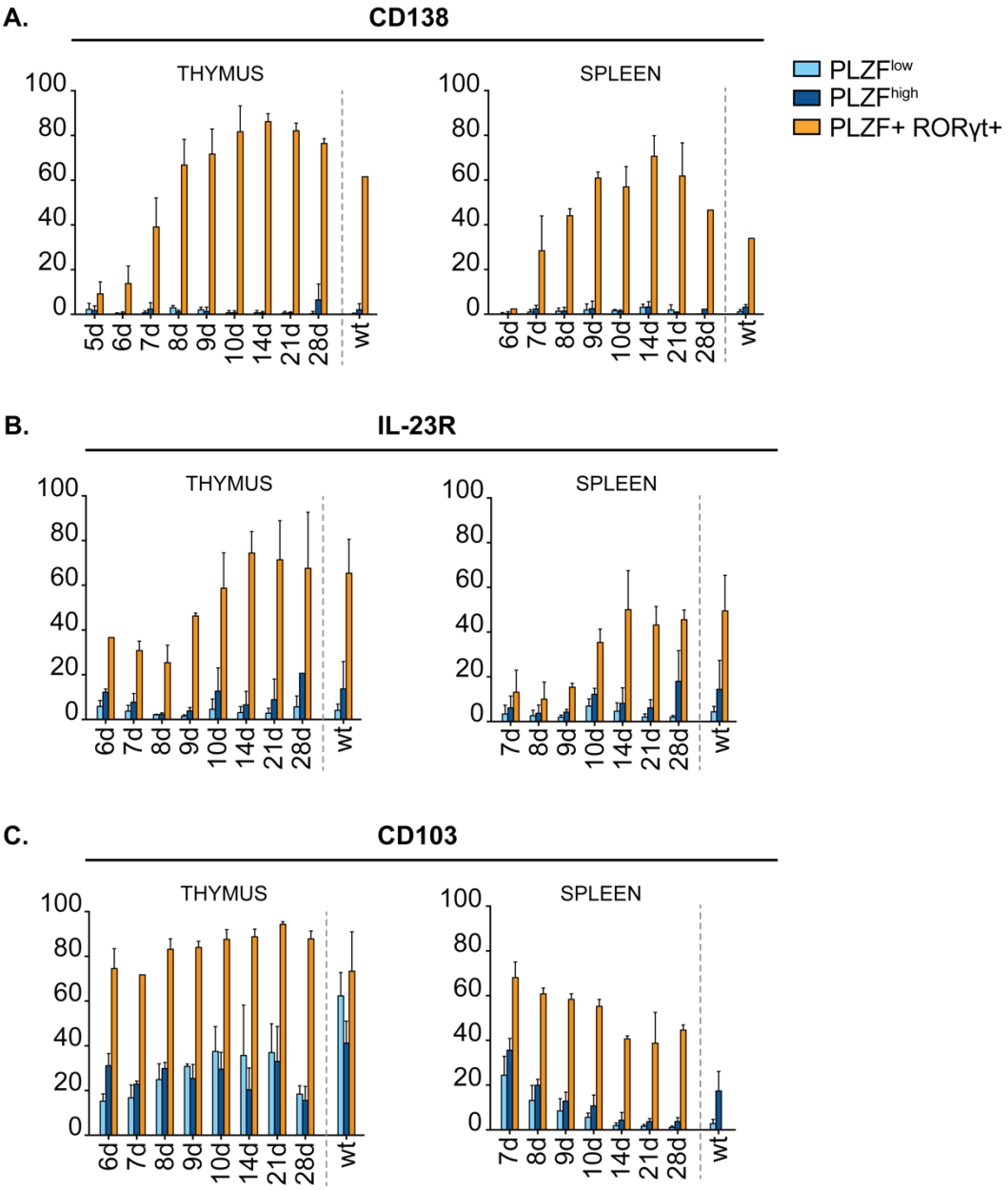

Fig. 26. Expression pattern of NKT17-specific markers.

Ex vivo flow cytometric analyses of thymi and spleen from tdTomato+ inducible mice at different timepoints. The bar graphs indicate the percentage of CD138 **(A)**, IL-23R **(B)** and CD103 **(C)** positive cells for each induced NKT cell subset.

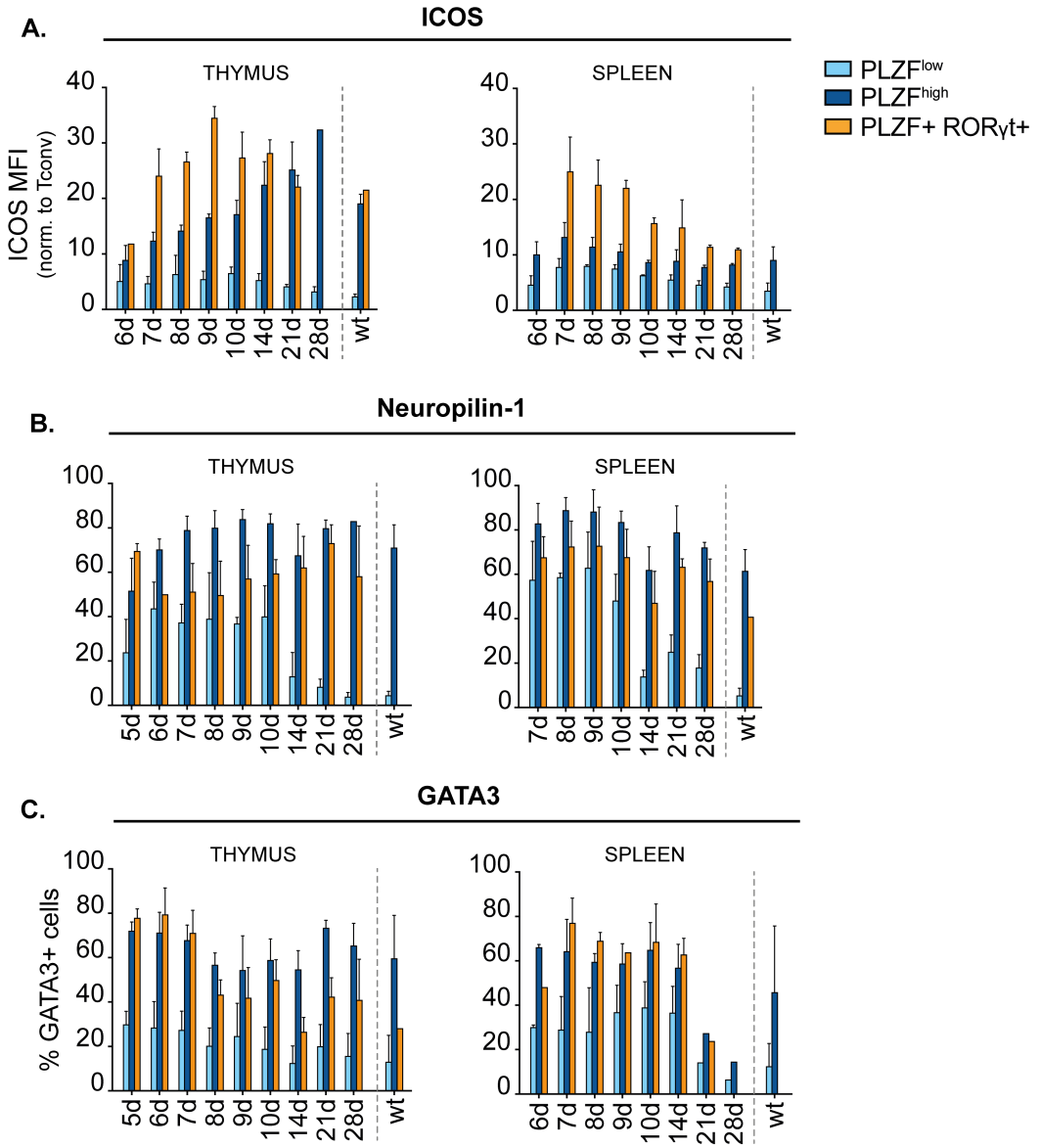

Fig. 27. Expression pattern of NKT17-specific markers.

Ex vivo flow cytometric analyses of thymi and spleen from tdTomato+ inducible mice at different timepoints. **A.** The plot indicates the intensity of ICOS expression for each induced NKT cell subset. The median fluorescence intensity (MFI) of induced NKT cells was normalised to the MFI of conventional T cells (gated as TCRβ+ CD1d-PBS57 Tetramer−). **B-C.** The bar graphs indicate the percentage of Neuropilin-1 (B) and GATA3 (C) positive cells for each induced NKT cell subset.

4.6.3 Slow NKT1 identity acquisition

According to the linear differentiation model, CD44^{high} NK1.1− NKT cells (Stage 2) give rise to CD44^{high} NK1.1+ (Stage 3), mostly composed by NKT1 cells (Bennstein, 2017). However, evidence was presented that only the IL17RB− CD44^{high} fraction of NKT cells, which correspond to IL-4 non-producers, can give rise to NKT1 (Lee et al., 2013; Watarai et al., 2012). Moreover, PLZF^{high} CCR7+ NKT cells were shown to possess the ability to differentiate into all the three functional NKT cells subsets, including NKT1 (Wang and Hogquist, 2018).

We therefore investigated the timing of NKT1 subset differentiation through the monitoring of the dynamic changes in NKT1-subsets specific markers, including T-bet, NK1.1 and CD69 (Kimura et al., 2018; Townsend et al., 2004). At 6d after induction, a fraction of PLZF^{high} NKT cells initiates to express T-bet (Fig. 28A). Between 8d and 10d, the T-bet+ PLZF^{high} fraction initiates a gradual downregulation of PLZF towards a PLZF^{low} state, associated with the upregulation of NK1.1. At 28d, the majority of T-bet+ cells express low levels of PLZF and are NK1.1+ (Fig. 28A, 28B). These data support my previous statement that PLZF^{high} cells decrease their PLZF intensity to a PLZF^{low} state and slowly acquire a NKT1-like phenotype. Moreover, the gradual acquisition of NKT1-specific markers correlates with the acquisition of IFN-γ only production which I detected from 7d in PLZF^{low} cells (Fig. 28B).

In addition to T-bet and NK1.1, I also analysed the expression of CD69 (Fig. 28C). In the thymus, CD69 undergoes two waves of expression; the first (from 12h to 7d) in response to TCR signals (Fig.16C) and the second (from 14d to 28d) upon NKT cell subset specification. In fact, at 5d after TCR induction 50% of the induced NKT cells still express CD69 regardless of the subset (Fig. 28C). The levels decrease up to 10d, when CD69 is barely detected. From 14d onwards, CD69 is re-upregulated on both PLZF^{low} and PLZF+ RORγt+ cells, while PLZF^{high} cells express minimal levels. In the spleen, CD69 is preferentially expressed on PLZF^{low} cells.

Overall, the data show that NKT1 identity acquisition initiates at a similar time as the differentiation of RORγt+ PLZF+ cells (around 6d after induction)

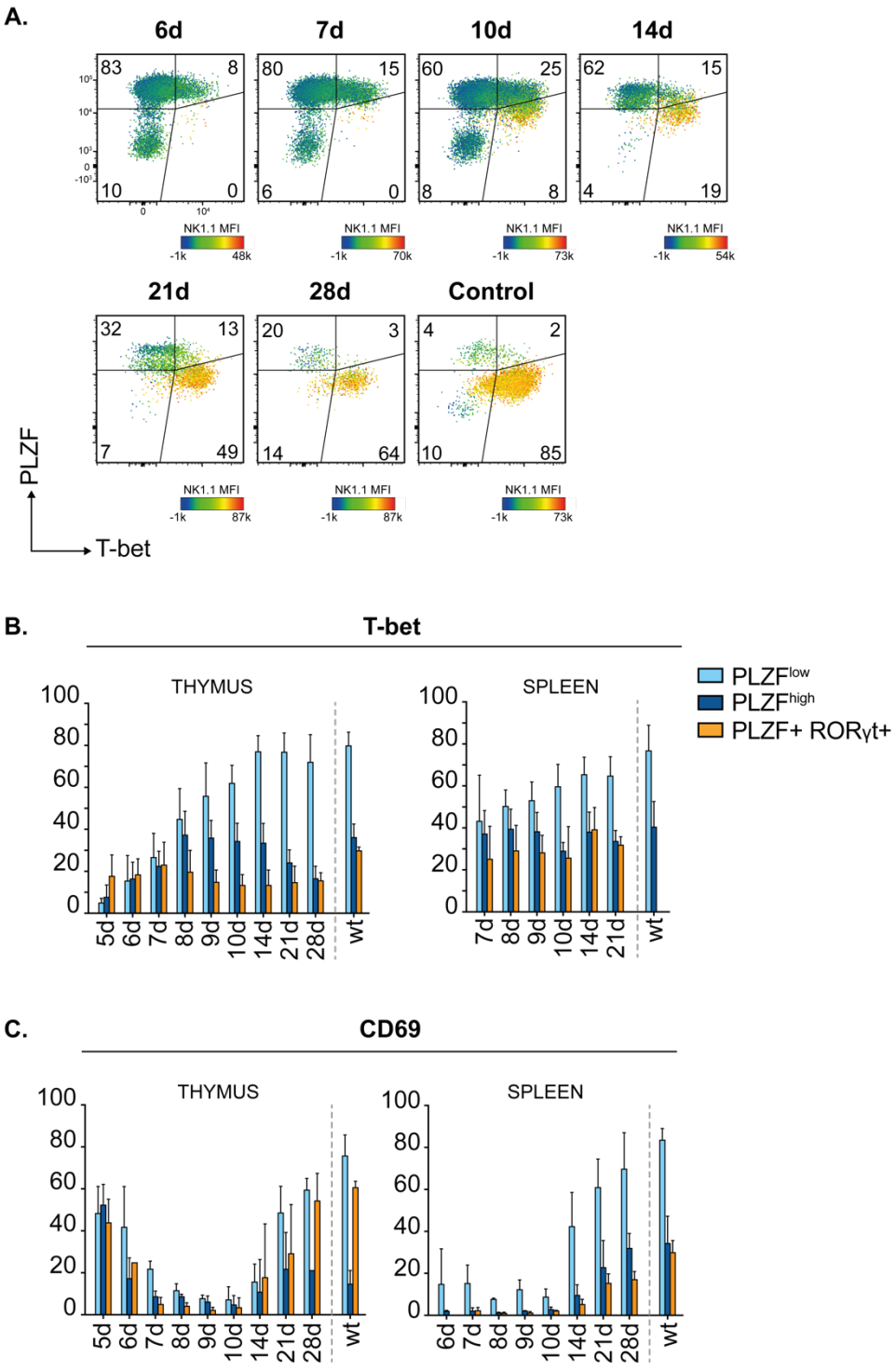

Fig. 28. Expression pattern of NKT1-specific markers.

Ex vivo flow cytometric analyses of thymi and spleen from tdTomato+ inducible mice at different timepoints. **A.** Representative facs plot of T-bet and PLZF expression in thymic induced NKT cells at different timepoints. The percentages are representative of the displayed plots. The heatmap colour map reports the intensity NK1.1 intensity, and was generated with FlowJo. **B-C.** The bar graphs indicate the percentage T-bet (B) and CD69 (C) positive cells for each induced NKT cell subset.

with T-bet upregulation at the PLZF^{high} state. However, the subset specification is suprisingly slow compared to NKT17, as a significant population of T-bet+ PLZF^{low} NK1.1+ cells is only detected at 14d. These results are in line with the slow Th-1 cytokine production repertoire acquisition.

5. DISCUSSION

5.1 Establishment of a novel genetic system to investigate early NKT cell differentation through a synchronous developmental wave

During the last decade, many studies have investigated the processes underlying the development and the unique functional effector differentation of NKT cells (Bennstein, 2017). The analysis of diverse knock-out mice has been extremely informative to unravel the importance of defined factors for the proper development and fucntional differentiation of NKT cells. However, to date there is still not a clear consensus of the precise mechanisms which drive the functional differentiation of NKT cells. Recent studies propose that the subset fate decision is determined during the positive selection process (Tuttle et al., 2018; Zhao et al., 2018); therefore, it is necessary to investigate the early phases of development in order to identify crucial mechanisms.

A major problem limiting the analysis of early NKT cell development is the rarety of early NKT cells. In fact, the thymus of adult mice is populated by almost exclusively mature NKT cells, and only a minute fraction of immature cells (Lee et al., 2013).

Notable pioneering work has been performed through the monitoring of NKT cell development in very young mice. However, also in this case, the number of early NKT cells is very small and a substancial animal usage is thus required (Benlagha et al., 2002; Benlagha et al., 2005; Pellicci et al., 2002). Alternatively, important insight were obtained through fetal thymic organ culture (FTOC) (Pellicci et al., 2002). However, all these methods do not allow a precise temporal monitoring of the changes occuring during the early phases of NKT cell development. This is also partly due to the continuous selection of new immature NKT cells, which in turn contributes to the generation of a pool of early NKT cells which are not synchronically developing.

More recently, the continuous improvement in transcriptional profiling allowed the transcriptomic analysis of rare early NKT cells (Engel et al., 2016; Lee et al., 2016). Nevertheless, these analyses are partly biased by the markers employed to define early NKT cells, and might in turn neglect additional intermediate developmental steps. Overall, it is evident that a genetic system to investigate the early phases of NKT cell development is required to fully understand this important process.

In this project, I succesfully established and validated a new system which combines the usage of an inducible Cre-recombinase with a Vα14i knock-in allele (Vα14i^{StopF}) (Vahl et al., 2013). Compared to the above mentioned methods, this system allows the generation of a substantial, initially synchronous wave of NKT cell development, thus permitting to monitor the diverse dynamic changes that govern NKT cell differentiation in a precise temporal manner.

5.1.1 Generation of bona fide NKT cells

Some of the observation I made using the inducible NKT system are comparable to the results obtained by the study of very young wildtype mice (Benlagha et al., 2002; Benlagha et al., 2005; Pellicci et al., 2002).

The earliest NKT cells detected in newborn mice express high levels of CD24, which are gradually downregulated in a timeframe of approximately 5d. Moreover, NKT cells undergo a gradual upregulation of CD44 followed by the acquisition of NK1.1 (Benlagha et al., 2002; Benlagha et al., 2005; Pellicci et al., 2002). These results are very similar to the dynamic changes in CD24, CD44 and NK1.1 I observe in the induced NKT cells at different timepoints.
RTE NKT cells detected in spleen and liver from 8d after birth show a substantial NK1.1− phenotype (Benlagha et al., 2002; Pellicci et al., 2002). Similarly, my data show a major NK1.1− phenotype of RTEs followed by acquisition of NK1.1 in peripheral organs.
Although NKT cells are known to develop before birth, there is no clear evidence on the exact timepoint when development starts. Morevoer, the rate

of NKT cells generation at different moments of the mouse life is not determined. For these reasons, it is not possible to fully compare our system to the published data in a timed manner.

In addition to the maturation markers, I analysed the cytokine production capabilities as well as subsets-specific markers at different timepoints. The results show that from 6d after induction, the wave of NKT cell development differentiate into functional subsets which highly resemble the wildtype NKT1, NKT2 and NKT17 subsets.

The extensive phenotypic and functional characterisation I performed indicate that the maturation and differentiation of the induced NKT cells into functional subsets is comparable to the physiological scenario. Therefore, the NKT cells generated by this system can be considered bona fide NKT cells.

5.1.2 Immediate post-selection NKT cells are possibly not detected in wiltype

Stage 0 NKT cells are normally defined as the earliest post-selection NKT cells. These cells are characterised as $CD24^{high}$ $CD44^{low}$ NK1.1− (Das et al., 2010). My data show that, upon TCR induction, the expression of CD24 on NKT cells remains high for around 2 days, and then slowly decreases. In the first 2 days after induction, I could detect diverse changes occurring; these include the downregulation of CD4 and CD8 to DN state and partial upregulation of CD4, the downregulation of RORγt and the partial upregulation of PLZF on the first developping cells as well as the initial aquisition of cytokine production capabilities.
Therefore, the Stage 0 NKT cells which are commonly defined as the post-selection phase might in reality be a mixture of cells which encompass the first two days of development after positive selection.

Some studies report that the most precise way to define post-selection NKT cells is the use of CD69 (Bennstein, 2017; Wang and Hogquist, 2018). However, I showed that CD69 is upregulated very quickly after positive selection but its

expression remains high for a few days after TCR signalling has ceased. A similar delay was also shown in human T cells (Ashouri and Weiss, 2017). Moreover, my data show a conspicuous delay in CD69 protein decay compared to the mRNA degradation. In this regard, Stage 0 NKT cells (gated as $CD24^{high}$ $CD69^{high}$) were shown to express low levels of PLZF mRNA (Savage et al., 2008). Compared to my data, this could possibly correspond to 2 days after TCR induction on DP thymocytes.
Therefore, the usage of CD69 as additional marker to define post-selection NKT cells does not stringently allow a more precise definition of the cells which have been very recently selected.

A different study showed that only 0.5-2% of the $CD24^{high}$ Tetramer+ cells express RORγt. Considering that my data show that all the post-selection NKT cells express RORγt for a period of at least 12h, it is clear that only a minor fraction of wildtype $CD24^{high}$ NKT cells comprises the immediate post-selection phase (Klibi et al., 2019).
Along this line, the RNA-seq data I generated in this project show that the transcriptome of FACS-sorted wildtype CD24+ CD44− NK1.1− cells (Stage 0) is most similar to those of the induced NKT cell wave between 36h and 48h after induction.

Overall, these data show that the Stage 0 NKT cells, commonly attributed as newly selected NKT cells, are mostly composed by cells which are 1-2 days apart from the beginning of positive selection. Moreover, considering that the estimated length of the TCR signalling is no longer than two days, it is reasonable to propose that the Stage 0 cells do not represent immediate post-selection NKT.
However, this does not fully explain the high proliferation rate of Stage 0 NKT cells reported by some studies (Prevot et al., 2015; Pyaram et al., 2019; Salio et al., 2014). In fact, in my data induced NKT cells display major proliferation at around 5-6d after induction.

To summarise, my analysis revealed that the Stage 0 NKT cells detected in wildtype mice do not faithfully represent early positively selected NKT cells.

On the other hand, my inducible system allows the precise monitoring of the very early development and therefore could be extremely useful for the analysis of the immediate post-selection phase of NKT cell development.

5.1.3 PLZF^{high} NKT cells constitute a mixture of immature and mature cells

The NKT2 subset is normally defined based on the high expression of PLZF and the production of IL-4, and it is considered to be composed by an heterogeneous CD44+/− population (Lee et al., 2013). However, the Hogquist group has proposed that this subsets of cells constitute an heterogeneous population of immature NKT cells and mature NKT2 cells (Lee et al., 2016). In this regard, they made use of IL-17RB staining and an IL-4 reporter allele to separate PLZF^{high} cells in NKT2 (IL-17RB+ IL-4+) and NKT cell precursors (NKTp) (IL-17RB− IL-4−). The RNA sequencing analyses they performed on these subsets revealed a distinct transcriptome of NKTp which differs from all the mature subsets, including the phenotypically similar NKT2 mature subset (Lee et al., 2016). Moreover, a following study highlighted the existence of a PLZF^{high} NKT cell precursor population which can be identified by the expression of CCR7. These cells present a CD44$^{-/low}$, CD4+, CD24−, CD69−, T-bet−, RORγt−, IL-4− phenotype, expressed high levels of Ki67 and low levels of Nur77^{GFP} reporter. These NKT cell precursors were shown to be capable of generating all the NKT cell subsets upon intrathymic injection (Wang and Hogquist, 2018).

My data show that immature NKT cells undergo an initial downregulation of RORγt followed by PLZF upregulation; at 5-6d after induction, most of the cells express high levels of PLZF. At that time, the cells uniformly express CCR7, are mostly CD4+, CD24−, CD44$^{-/low}$, T-bet− and RORγt−. Both the Ki67 and the Nur77eGFP expression correlate with the published data, but 50% of the cells still express low levels of CD69. One clear difference with regards to my data relates to PD-1. The Hogquist group showed that CCR7 and PD-1 are mutually exclusively expressed by NKTp and NKT2, respectively. However, my data show that the induced NKT cells express high levels of PD-1.

Therefore, my data confirm the presence of an immature PLZF^{high} population with overall a highly similar phenotype to the published study, which is capable of differentiating into all of the mature subsets. The reasons underlying the few discrepancies between my study and the Hogquist NKTp characterization need to be investigated, but might relate to a heterogenous nature of NKTp.

To further support this statement, my data show that 4 weeks after induction, nearly all the PLZF^{high} cells present a CD44+ phenotype, while roughly 20% of the control NKT2 cells (gated as PLZF^{high} cells) are CD44−. However, most precisely NKT2 cells are defined as IL-4 producers. Published data show that roughly 25% of PLZF^{high} IL-4 producers are CD44− (Wang and Hogquist, 2018). Differently from wildtype mice – where a constant but minute input of newly differentiating NKT cells continuously occur – the inducible system generates one single wave of NKT cell development. Therefore, after a certain period of time all the positively selected NKT cells mature and differentiate into functional subsets. Therefore, the final PLZF^{high} fraction truly corresponds to fully differentiated NKT2 cells. Considering that at 4 weeks after induction my data show that all PLZF^{high} cells are CD44+, this suggests that the CD44− NKT2 fraction indeed corresponds to a more immature NKT fraction. In this case, high PLZF expression and IL-4 production might not be sufficient to define fully mature NKT2 cells. To test whether the CD44− PLZF^{high} fraction with IL-4 producing ability retains a differentiation potential, it could be interesting to purify that fraction of cells and perform intrathymic injection experiment.

Due to the highly overlapping phenotypes of immature NKT cells and the NKT2 subset, our analyses of the inducible system to date do not allow to precisely determine the timing of NKT2 differentiation. Moreover, C57BL/6 mice are not the optimal system for the investigation of NKT2 cell differentiation, due to their low presence. In this regard, the BALB/c genetic background would be more suitable to study NKT2 differentiation. Interestingly, the C57BL/6-BALB/c F1 genetic background recapitulates many aspects of the Th2 and NKT2 skewing found in pure BALB/c mice (S. Jameson, personal communication). Therefore, I could cross the inducible system to

BALB/c mice and analyse the differentiation of NKT2 cells in C57BL/6-BALB/c F1 mice. To define the boundary between immature potential and fully differentiation, I could purify PLZF^{high} NKT cells at different timepoints and evaluate their differentiation potential by intrathymic injection experiments. Moreover, further subgrouping of the PLZF^{high} fraction could be achieved based on the expression of diverse markers including CD44, CCR7 and IL-17RB.

Overall, my data confirm that throughout their development, immature NKT cells uniformly go through a PLZF^{high} CCR7+ CD4+ CD44+/− state which precedes the initiation of the differentiation of NKT1 and NKT17. However, the timing of the NKT2 differentiation could not be defined due to the high similarity between NKT2 and immature NKT cells. In this regard, I could perform single cell RNA sequencing on induced NKT cells at different timepoints. This would allow a precise separation of immature NKT cells and NKT2 cells on a single cell level and the determination of the timing of NKT2 differentiation.

5.1.4 Possible improvement of the inducible system and potential advantages

The genetic system I established and validated turned out to be invaluable for the investigation of diverse aspects of NKT cell development and differentiation. However, the “leaky” generation of small amounts of NKT cells in absence of 4-OHT administration challenged some of my analyses. The TCR repertoire analysis of T cells showed a clear bias toward the usage of TRAJ18, supporting the hypothesis that Vα gene replacement is the main process which leads to the unwanted NKT cell production. However, other TRAJ are also used in the T cells generated in Vα14i homozygous mice, implying the occurrence of diverse processes. In the Vα14i knock-in, two sequences abort transcription downstream of all the endogenous Vα and Jα gene segments (an SV40 polyadenylation site and a STOP cassette) and thereby prevent the transcription of the exons encoding the constant regions of the TCRα chain. The presence of TCRs with diverse TRAJ segments implicates the excision of these stop signals.

One possible explanation could be a recently published RAG-mediated cutting mechanism termed "Cut-and-Run" (Kirkham et al., 2019). During V(D)J recombination, the excised DNA (excised signal circle, ESC) can associate with the RAG enzymes, allowing single RSS cuts in multiple genomic regions. In the case of the Vα14i knock-in, the ESC-RAG complex could cut at the cryptic embedded heptamer within the Vα14i knock-in leading to homologous recombination with the upstream endogenous TRAJ18, resulting in the knock-in excision and allowing the locus to recombine. In this case, the Jα locus would lack all TRAJs which are located 3' of the TRAJ18. In fact, the vast majority of the non-TRAJ18 TRAJs detected by the sequencing are located 5' of TRAJ18. The few rearrangements containing TRAJs lower than TRAJ18 could occur by ESC-RAG complex-mediated cut at the cryptic heptamer within the knock-in and another cut inside the 3' region of the Jα locus followed by non-homologous end joining. This would lead to the excision of the knock-in and only a minor part of the Jα locus and allowing the recombination of other TRAJs.

In all these hypothesised processes, the embedded heptamer is the common element responsible for "leaky" T and NKT cell generation. By the employment of CRISPR-Cas, I could try to solve this issue by replacing the nucleotides located 3' of the knock-in Vα14 region and eliminate any possible embedded heptamer. This procedure would allow the generation of mice which do not produce NKT cells in absence of 4-OHT administration.

In this model, the use the of tdTomato Cre activity reporter would be unnecessary; considering that tdTomato is expressed at a very variable ratio and marks only a fraction of the induced NKT cells, the elimination of endogenous NKT cells would results in an increased amount of peripheral NKT cells for analysis. One of the main advantages of the improved model would be the possibility to better investigate the peripheral maturation and subsets differentiation. This would allow me to more precisely monitor the timing and amount of thymic egress. Moreover, I could compare the phenotype of RTE in different organs including lymph nodes, intestine, lungs and skin. Additionally, I could monitor more efficiently and unambiguously whether the peripheral NKT cell subsets distribution which is observed in different organs

derives through organ-specific microenvironment adaptation or it is already instructed from the thymus.

A recent publication reported that, in the medulla, NKT2 cells receive a second pulse of TCR signalling mediated by the interaction with macrophages (Wang et al., 2019). In the current setup it is not possible to utilise the *Nr4a3*-Tocky reporter at later timepoints to analyse TCR signalling precisely in developing NKT2 cells or to isolate the signalling cells for downstream analyses, since the fluorescence from the timer protein would interfere with the tdTomato reporter needed to identify developing NKT cells.

By means of the improved system in combination with *Nr4a3*-Tocky I could unambiguously monitor potential TCR signals in the late phases of differentiation. Although my data gathered with the Nur77eGFP reported do not show TCR signal re-activation until 7d after induction, it cannot be excluded that this could occur at later timepoints. Moreover, I could evaluate potential TCR signals upon the colonization of peripheral sites.

5.2 New insights into the functional differentiation of NKT cells

Differentiation, maturation and survival of functional NKT cell subsets have been shown to specifically depend on a various molecules and transcription factors (Kovalovsky et al., 2008; Michel et al., 2008; Savage et al., 2008; Townsend et al., 2004).

Although the knowledge in this regard has significantly increased in the last years, the timing and mechanism behind the subset fate decision is still largely unknown. Some studies proposed that NKT cell precursors receive TCR signals with diverse strengths which in turn define their fate (Tuttle et al., 2018; Zhao et al., 2018). Alternatively, other evidence demonstrate that NKT cell subset identity and survival depend on the presence of defined microenvironmental stimuli (Gordy et al., 2011; Havenar-Daughton et al., 2012; Miller et al., 2018; Webster et al., 2014; White et al., 2014). However, it has not been yet shown whether these factors play a role in shaping the subset identity of NKT cells during development.

5.2.1 Similar initiation time but different duration for NKT1 and NKT17 subset differentiation

The currently available methods to study the timing of differentiation and maturation rely on the analysis of very young mice or the use fetal thymic organ culture (FTOC) (Benlagha et al., 2002; Benlagha et al., 2005; Pellicci et al., 2002). However, these methods were mostly used to evaluate the maturation of NKT cells at a time when the linear maturation model was the accepted model and there was no knowledge about the existence of functional subsets. Therefore, the timing of NKT1, NKT2 and NKT17 differentiation has not been addressed to date.

Based on the aforementioned studies, the current concept assumes that NKT2 and NKT17 differentiate first while NKT1 is the last subset to differentiate. This statement is mainly based on phenotypic analysis of young mice and intrathymic injection experiments which report the detection of CD44^{high} NK1.1− NKT cells (Stage 2, including NKT2 and NKT17) before the detection of NK1.1+ (Stage 3, mainly NKT1) (Benlagha et al., 2002; Benlagha et al., 2005; Pellicci et al., 2002).

My data provide a very precise analysis of the timing of differentiation. Although the current setup does not allow a definitive statement of the differentiation of NKT2 cells, I could very well define the differentiation times of NKT1 and NKT17 cells. The analysis of the signature transcription factors T-bet (for NKT1) and RORγt (for NKT17) revealed that the differentiation of both subsets initiates at 5-6d after the start of development from a DP thymocyte from a PLZF^{high} state.

In 2008, Michel et al. proposed that NKT17 cells follow a separate differentiation program compared to NKT1 and NKT17 which implies the retention of RORγt expression from the DP thymocyte precursors (Michel et al., 2008). However, although the Hogquist group showed that CCR7+ PLZF^{high} RORγt− NKT cell precursors can give rise to both RORγt+ and T-bet+ NKT cells, it has never been determined whether NKT17 cells follow a distinct differentiation pathway or not. My data neatly show that NKT17 cells follow a common NKT differentiation pathway up to a PLZF^{high} stage, from which they

derive through yet unknown mechanisms mostly likely linked to the re-upregulation of RORγt.

The cytokine production potential analysis revealed that, upon RORγt upregulation, the profile of NKT17 is highly specific. In fact, no IL-17 production potential is detected in RORγt− NKT cells. Moreover, the newly differentiated NKT17 cells immediately have a great potential to produce both IL-4 and IL-17, and the ability to produce both cytokines simultaneously decreases throughout the differentiation process. In line with this observation, Georgiev et al. showed that a fraction of NKT17 are capable of producing both cytokines (Georgiev et al., 2016). The authors suggested that these double producer are in turn a developmental precursors of IL-17 single producers and could arise from IL-4 producing NKT2 cells.
My data highly supports the hypothesis that IL-4/IL-17 double producers represent an early state of NKT17 differentiation. Moreover, considering that most of the PLZF^{high} developing NKT cells are capable of producting IL-4 prior to RORγt re-upregulaion, it is likely that, as suggested by the authors, the IL-4/IL-17 double producers derive from IL-4 producers. However, my data does not allow to strictly define whether and if yes to what extent the IL-4 single producer NKT cells I see at 5d as PLZF^{high} constitute fully mature NKT2 cells. I favor the notion that the NKT cell subsets derive from a common PLZF^{high} progenitor cell population, that might already be heterogenous with respect to its differentiation potential.
In addition to the cytokine production, the monitoring of NKT17-specific markers delineate an incredibly quick acquisition of the complete NKT17-phenotype after RORγt upregulation.

In the case of NKT1, although T-bet is starting to be upregulated at a similar time point as RORγt, the differentation of these cells requires a much longer process compared to NKT17. In fact, a significant PLZF^{low} NK1.1+ population is identified only at 14d after induction of NKT cell generation. The current interpretation of the late NKT1 differentiation mainly derives from the delayed detection of NK1.1+ NKT cells. However, my data show that NK1.1 (as well as

CD69) is expressed relatively late compared to the initiation of the NKT1 differentiation (defined by T-bet upregulation).
Therefore, my data reveal a more precise timing of differentiation for both NKT1 and NKT17. Although both signature transcription factor are upregulated at the same time, the NKT1 identity acquisition is significantly slower (14 to 20 days) compared to NKT17 (2 to 3 days).

5.2.2 Differences in TCR signal strength are likely not the driving force for NKT cell functional differentiation

An existing debate regards the role of TCR signalling in NKT cell lineage choice and subset differentiation. Various studies have shown an impaired NKT cell subset distribution in different experimental setups where TCR signalling was genetically altered (Blume et al., 2016; Chen et al., 2017; Henao-Mejia et al., 2013; Lu et al., 2019; Malhotra et al., 2018; Pereira et al., 2014; Tuttle et al., 2018; Zhao et al., 2018). However, the results are partially incongruent and therefore do not allow a precise definition of the impact of differing TCR signal strength on NKT cell fate decisions.
The most recent publications point towards the hypothesis that high TCR signal strength is required for NKT2 and NKT17 differentiation, while NKT1 cells differentiate in the presence of hypomorphic TCR signalling (Joseph et al., 2019; Tuttle et al., 2018; Zhao et al., 2018). In essence, the authors hypothesize that during the positive selection, developing NKT cells receive TCR signals of varying strength, which in turn define the differentiation trajectory which they will take.
Considering that the inducible system is highly synchronous and has an optimal resolution on the extremely early phases of development, I tested the putative presence of differential TCR signal strength within the immature NKT cells. However, my data show very homogeneous TCR signal strength within early developing NKT cells, strongly suggesting that all the positively-selected immature NKT cells receive highly similar TCR signals and therefore arguing against an essential role for TCR signalling in the NKT cell fate decision.

The Nur77eGFP signal I measured in the induced NKT cell population is very homogeneous and comparable to Treg cells, but there is no available information regarding how the mouse models hyporesponsive to TCR stimulation utilised in the previous studies would translate in term of Nur77eGFP signal intensity on developing NKT cells. Therefore, it is difficult to compare and reconcile the different experimental results.

To test the hypothesis of varying TCR signal strengths received during positive selection, I would first need to unbiasedly determine a range of Nur77eGFP intensity for low and high TCR signal strengths. In this regard, I could define the Nur77eGFP levels of low TCR signal strength by using one of the published mouse models hyporesponsive to TCR stimulation, such as SKG or YYAA mice (Tuttle et al., 2018). One possible approach would consist in breeding one of these genetic models with impaired TCR signals with my inducible NKT cell generation system bearing the Nur77eGFP reporter.
I could monitor the range of Nur77eGFP intensity that immature NKT cells express during their development in an impaired TCR signalling context. I could compare these levels of Nur77eGFP to the levels I measured in the induced wave and determine their similarity. If the Nur77eGFP range of the hypomorphic model would be very close or even overlapping with the signal I measured in the induced NKT cells, I could not exclude that some immature NKT cells receive a lower TCR signal. Oppositely, if the Nur77eGFP intensity of the hyporesponsive TCR signalling model would be significantly lower than the signal I measured in all the induced NKT cells, I could prove that early NKT cells receive a homogeneously high TCR signalling during development.

The different subsets distribution detected in the impaired-TCR signalling mice suggested a differential TCR signal requirements for the diverse subset. In fact, recent studies showed that NKT2 and NKT17 subsets require high TCR signal to differentiate, while NKT1 cells were capable of differentiating even in a low-TCR signal context (Tuttle et al., 2018; Zhao et al., 2018). Similarly, two studies showed that in a persistent/increased TCR signalling context resulting from SFRs knock-out, the NKT1 fraction is partially decreased, while NKT2 and NKT17 are increased (Chen et al., 2017; Lu et al., 2019).

However, several studies point toward the opposite direction, showing that low TCR signalling result in a decrease of NKT1 cells an increase of NKT2 and NKT17 cells (Blume et al., 2016; Henao-Mejia et al., 2013; Malhotra et al., 2018). Due to the partially incongruent results, it is not clear whether NKT cells receive different TCR signal strength during development. In this regard, my data suggest that the signal received is very homogeneous arguing against TCR signal strength as main instructing principle of NKT cell subset differentiation.

To directly test if low-TCR strength and high-TCR strength immature NKT cells have diverse differentiation potential, I could purify *Nr4a3*-Tocky low and *Nr4a3*-Tocky high cells (or Nur77eGFP low and Nur77eGFP high NKT cells), culture them in vitro ad determine their differentiation potential by the measurement of subsets-specific transcription factors (RORγt, PLZF and T-bet) and cytokine production capabilities. Additionally, the sorted cells could be intrathymically injected in Traj18KO mice and the same aspects could be evaluated.

5.2.3 Beyond TCR signalling: location and microenvironmental stimuli

Considering that my data point toward an independence of NKT cell differentiation from TCR signal strengths differences, additional processes might play critical roles.
As previously described, the differentiation and homeostasis of NKT cell subsets depends on the presence of determinate environmental stimuli (Gordy et al., 2011; Havenar-Daughton et al., 2012; Miller et al., 2018; Webster et al., 2014; White et al., 2014).
It is therefore possible that the subset differentiation is driven by stimuli which are differentially distributed within the thymus.

In this regard, NKT cells were shown to be differentially distributed throughout the areas of the organs (Lee et al., 2015). Moreover, although developing NKT cells are positively selected in the thymic cortex, immature

CCR7+ NKT cells were shown to mainly locate in the medulla, demonstrating that NKT cells move within different compartments during their differentiation.

Based on these evidences, it is reasonable to hypothesize that during their development, NKT cells move to different locations in the thymus where they receive specific instructive signals which drive the different differentiation routs.

Therefore, it would be extremely informative to monitor the localisation of the cells during the early phase of development and after the subset diversion.

To test this, I could visualise immature NKT cells on tissue slides. However, the lack of NKT cell-specific antibodies and the difficulty to stain NKT cells with α-GalCer loaded tetramers in tissues renders such analyses particularly difficult. To overcome this issue, I could employ RNAscope, a technique which utilises RNA probes to specifically label cells. Especially thanks to the RNA sequencing data I generated and the available databases, I could determine target genes which are specific for NKT cells and highly transcribed during the first 5 days after induction. These, in combination with an existing Vα14-Jα18 probe and perhaps *Nr4a1*/*Nr4a3* probes, would allow me to define developing NKT cells within the organ. Since this technique allows the cleavage of the probe and consequent re-staining of the slides up to 3 times, I could additionally define the appearance of signature transcription factors and consequently determine the putative existence of environmental niches, which drive the subset-specific differentiation.

An interesting aspect which I observed with my system consists in the proportion of NKT17 cells generated. In fact, although wildtype B6 NKT17 cell represent roughly 2-4% of all NKT cells, at 10d after induction NKT17 represent over 20% of all induced NKT cells, and decreases to 10% at 28d after induction. A Similar percentage of RORγt+ NKT cells was observed 5 days after intrathymic injection of CCR7+ NKT cells (Wang and Hogquist, 2018). One explanation could be the highest apoptosis rate observed in NKT17 cells compared to NKT2 and NKT1 subset cells (Klibi et al., 2019). Alternatively, homeostatic processes could take place depending on the location where NKT17 move. Moreover, since NKT17 are prevalent in the lymph nodes, the

decrease observed in the thymus could also be the result of the migration. To test this, I could purify RORγt+ NKT cells at 10d after induction, adoptively transfer them into Traj18$^{ko/ko}$ mice and evaluate the organ distribution few days later.

In summary, I succesfully established a novel genetic system to investigate the earliest developmental phases and functional differentiation of NKT cell subsets.

Through extensive phenotypic and functional analyses I could precisely determine the diverse timing of NKT1 and NKT17 differentiation as well as the exact timing and extent of cellular proliferation.

By means of Nur77eGFP and *Nr4a3*-Tocky mouse models I monitored the TCR signal strength during the early developmental phases. My data show highly homogeneous TCR signal strength and therefore argue against a central role of TCR signal strength in instructing NKT cell subset differentiation.

Lastly, the transcriptomic and epigenomic data I generated will be used to further investigate and uncover crucial processes involved in the NKT cell development and acquisition of their unique functional phenotypes.

SUPPLEMENTAL MATERIAL

Supplementary Figures

A.

GGGTGGCTGGCAAGACCCAAGTGGAGCAGAGTCCTCAGTCCCTGGTTGTCC
GTCAGGGAGAGAACTGCGTCCTTCAATGTAATTACAGTGTGACCCCCGACAA
CCACTTAAGGTGGTTCAAACAGGACACAGGCAAAGGTCTTGTGTCCCTGACA
GTCCTGGTTGACCAAAAAGACAAAACGTCAAATGGGAGATACTCAGCAACTC
TGGATAAAGATGCTAAGCACAGCACGCTGCACATCACAGCCACCCTGCTGGA
TGACACTGCCACCTACATCTGTGTGGTGGGGGATAGAGGTTCAGCCTTAGGG
AGGCTGCATTTTGGAGCTGGGACTCAGCTGATTGTCATACCTG

B.

1. AT**CTGTGTG**GTGGGG
2. **ATCTGTG**TGGTGGGG

Suppl. Fig. 1. Sequence of part of the Vα14i^{StopF} knock-in.

A. The sequence reports the Vα14-Jα18 pre-rearranged sequence which is present in the Vα14i^{StopF} mice. The blue sequence represents the Vα14 gene segment, while the green sequence is the Jα18 gene segment. The 15 bp highlighted in yellow mark the region which contains the putative embedded heptamers. **B.** Two putative embedded heptamer (marked in red) which were identified in the 3' area of the Vα14 sequence (highlighted in yellow in A).

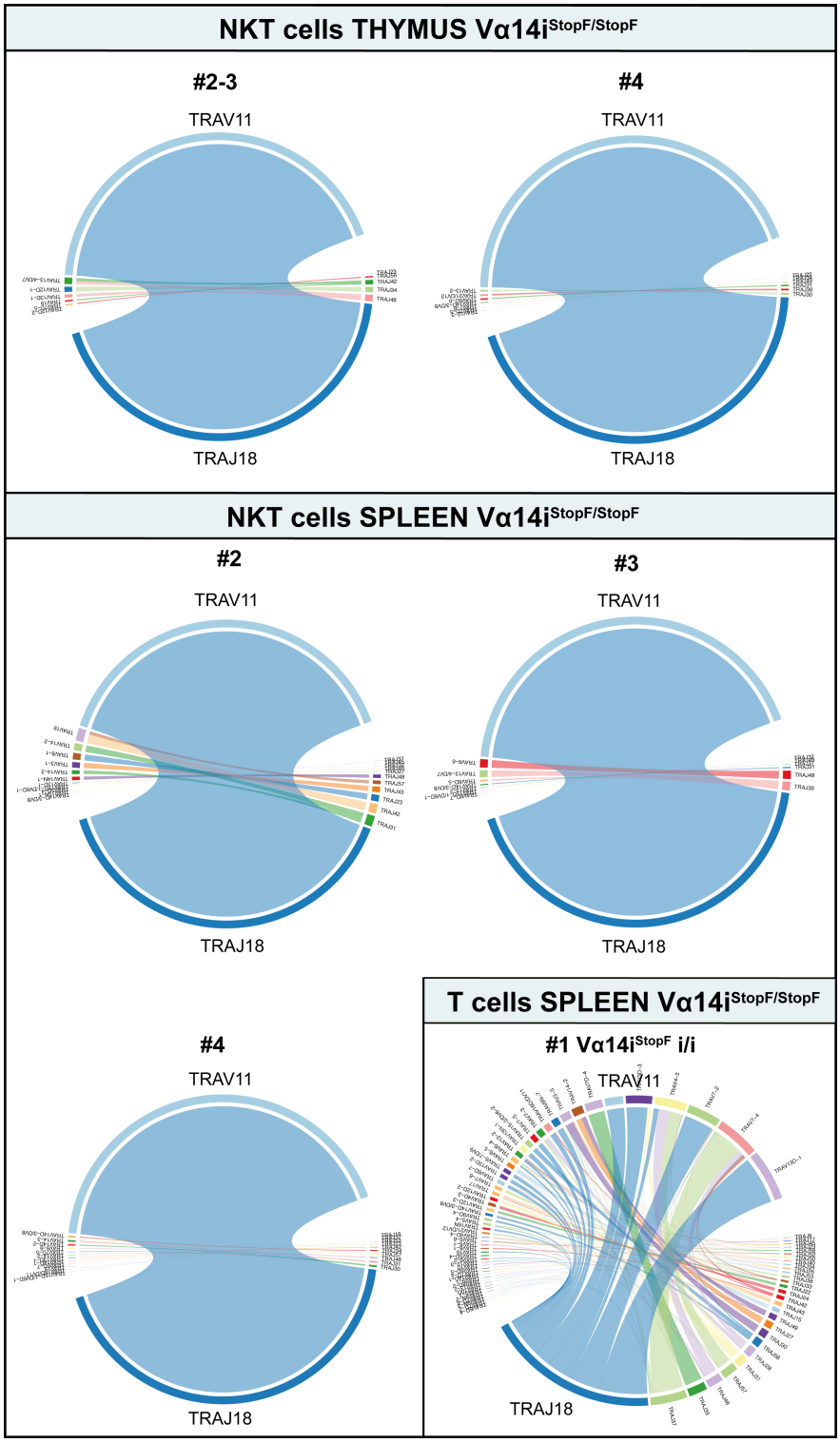

Suppl. Fig. 2. TCR repertoire of T cells and NKT cells.

Thymic and splenic T cells from Vα14i$^{StopF/StopF}$ and wildtype mice were sorted and the TCR repertoire was defined by 5' RACE PCR. The plots show all the TCR rearrangements detected by sequencing. TRAJ18 (Jα18 gene segment) and TRAV11 (Vα14 gene segment) are highlighted. The TCR rearrangement analysis was performed with VDJTools.

A.

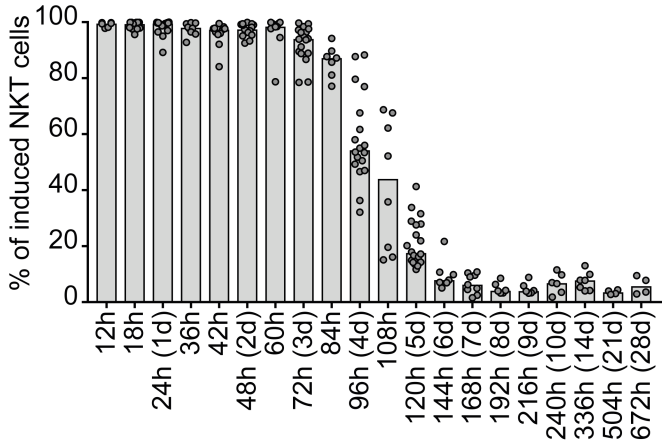

Suppl. Fig. 3. Percentage of CD24+ induced NKT cells throughout the development.

Ex vivo flow cytometric analyses of thymi from inducible mice at different timepoints. The graph reports the median percentages of CD24+ induced NKT cells.

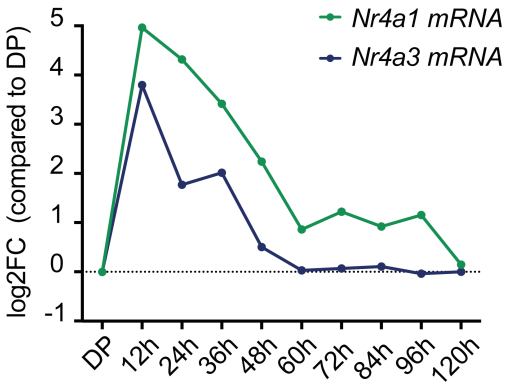

Suppl. Fig. 4. mRNA levels of immediate-early response genes induced by TCR engagement. The plot reports the mRNA levels of *Nr4a1* and *Nr4a3* genes at different timepoints. The mRNA levels were calculated from the SCRB-seq. The values reported indicate the log2 fold-change to DP thymocytes (gated as TCRβ− CD1d-PBS57 Tetramer− CD4+ CD8+ CD69−).

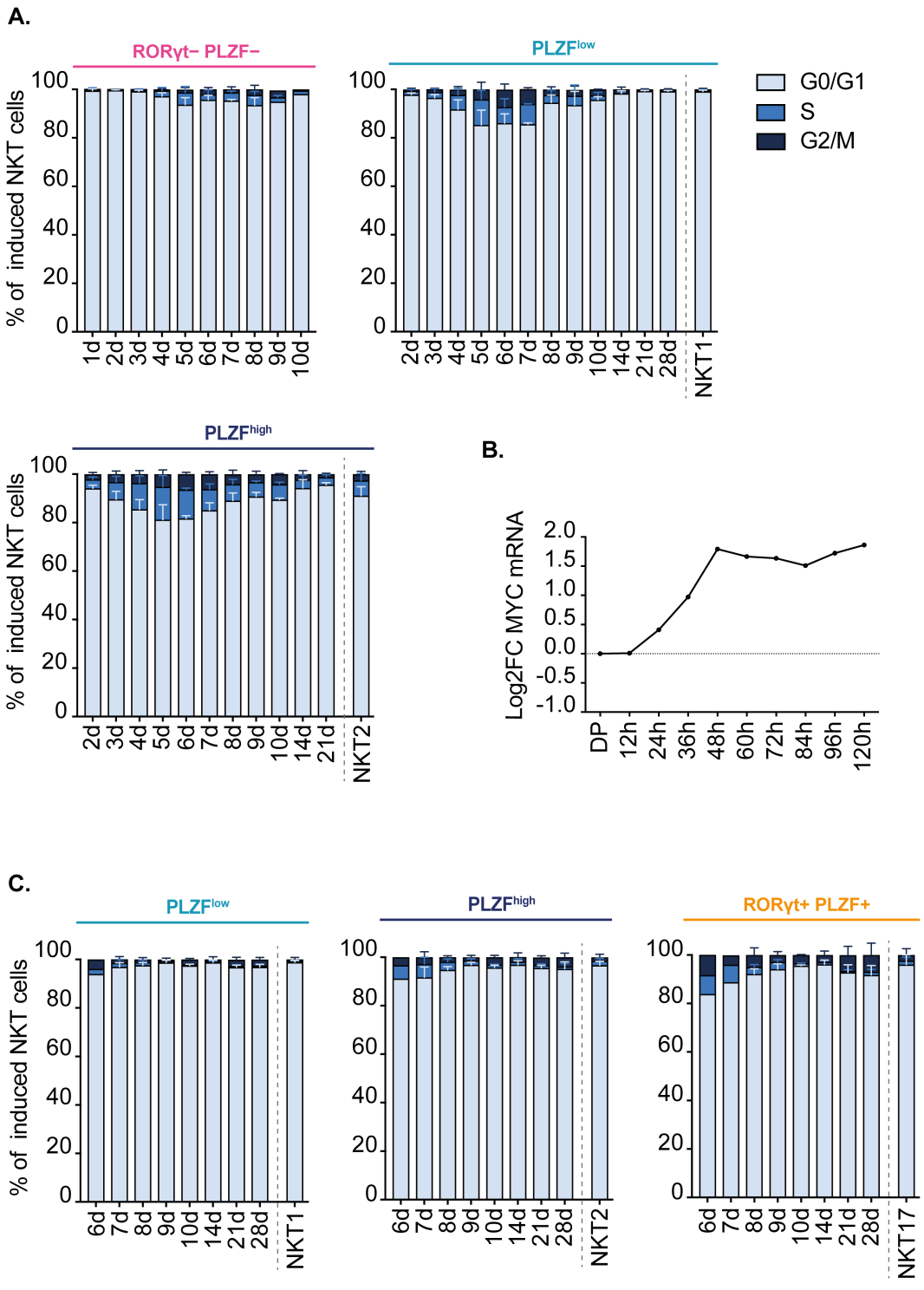

Suppl. Fig. 5. Assessment of induced NKT cells subsets proliferation.

Ex vivo flow cytometric analyses of thymi from inducible mice at different timepoints. **A, C.** The bar graphs report the percentage of G0/G1, S and G2/M cells in thymi (A) and splenic (C) induced NKT cells subsets. **B.** The plot indicates the mRNA expression levels of c-Myc in induced NKT cells at different timepoints. The values were calculated from the SCRB-seq and indicate the log2 fold-change to DP thymocytes (gated as TCRβ− CD1d-PBS57 Tetramer− CD4+ CD8+ CD69−).

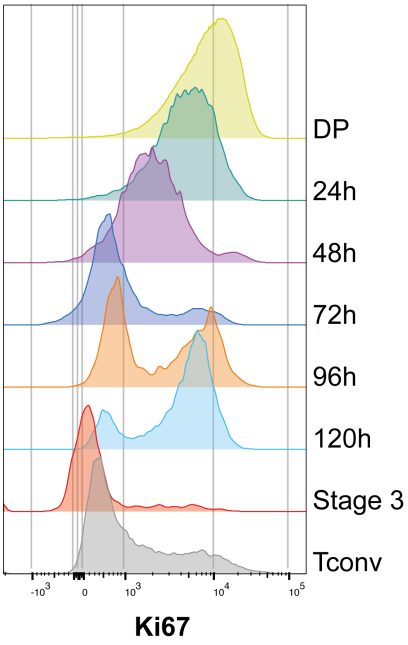

Suppl. Fig. 6. Expression of Ki67.

Representative histogram of Ki67 expression measured by flow cytometry across populations. (DP=DP thymocytes gated as TCRβ−,CD1d-PBS57 Tetramer−, RORγt^{high}; Stage 3= CD1d-PBS57 Tetramer+, NK1.1+, CD4.4+ mature NKT cells; Tconv= TCRβ+, CD1d-PBS57 Tetramer− conventional T cells; timepoint between 12h and 120h=induced NKT cells).

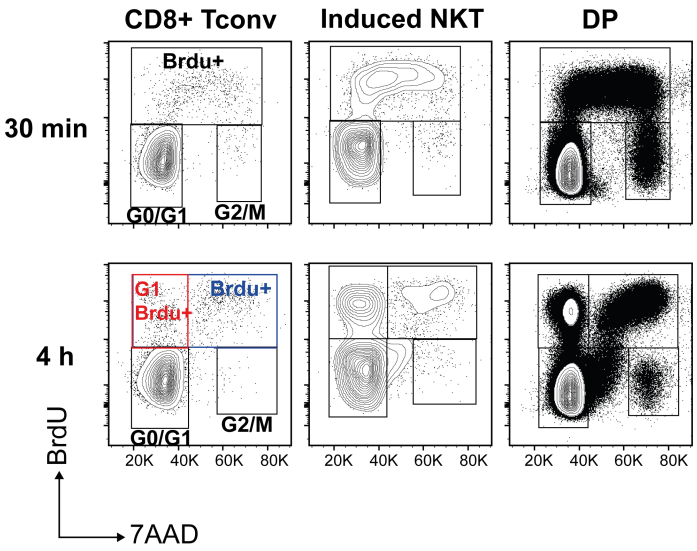

Suppl. Fig. 7. Measurement of BrdU incorporation.

Representative facs plots indicating the extent of BrdU incorporation in CD8+ T cells, induced NKT cells and DP thymocytes at 5d after induction. The mice were injected either 30 min (first row) or 4h (last row) before euthanasia. The populations were gates as G0/G1, BrdU+ and G2/M. In the 4h samples, an additional G1 BrdU+ gate was made. The percentages for each gate were calculated and used for the computational cell cycle length calculation.

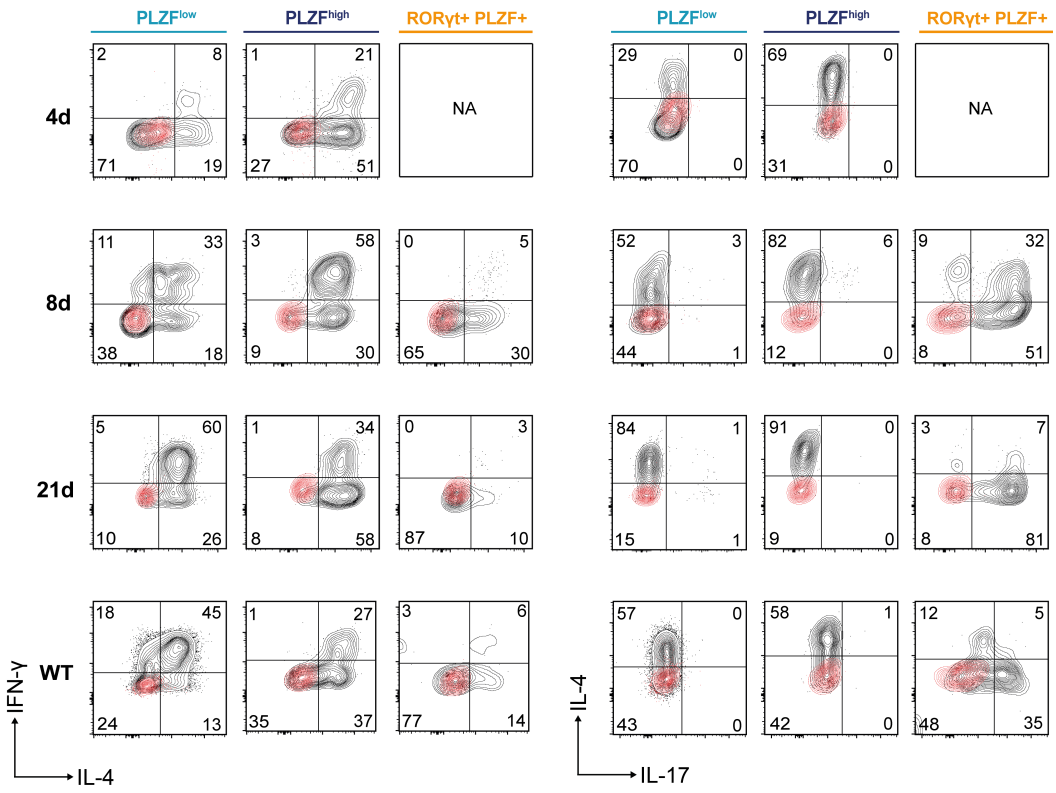

Suppl. Fig. 8. NKT cells cytokine profile.

Representative facs plots indicating the cytokine repertoire of thymic induced NKT cells upon PMA and Ionomycin stimulation (plus monensin). The first three rows are pre-gated on induced NKT cells at 4d, 8d and 21d after induction, while the last row reports wildtype NKT cells. Samples were subgated in subsets according to PLZF and RORγt. Each cytokine gate was made according to the corresponding unstimulated sample (only treated with monensin, red overlapped population). The percentages are representative of the displayed samples.

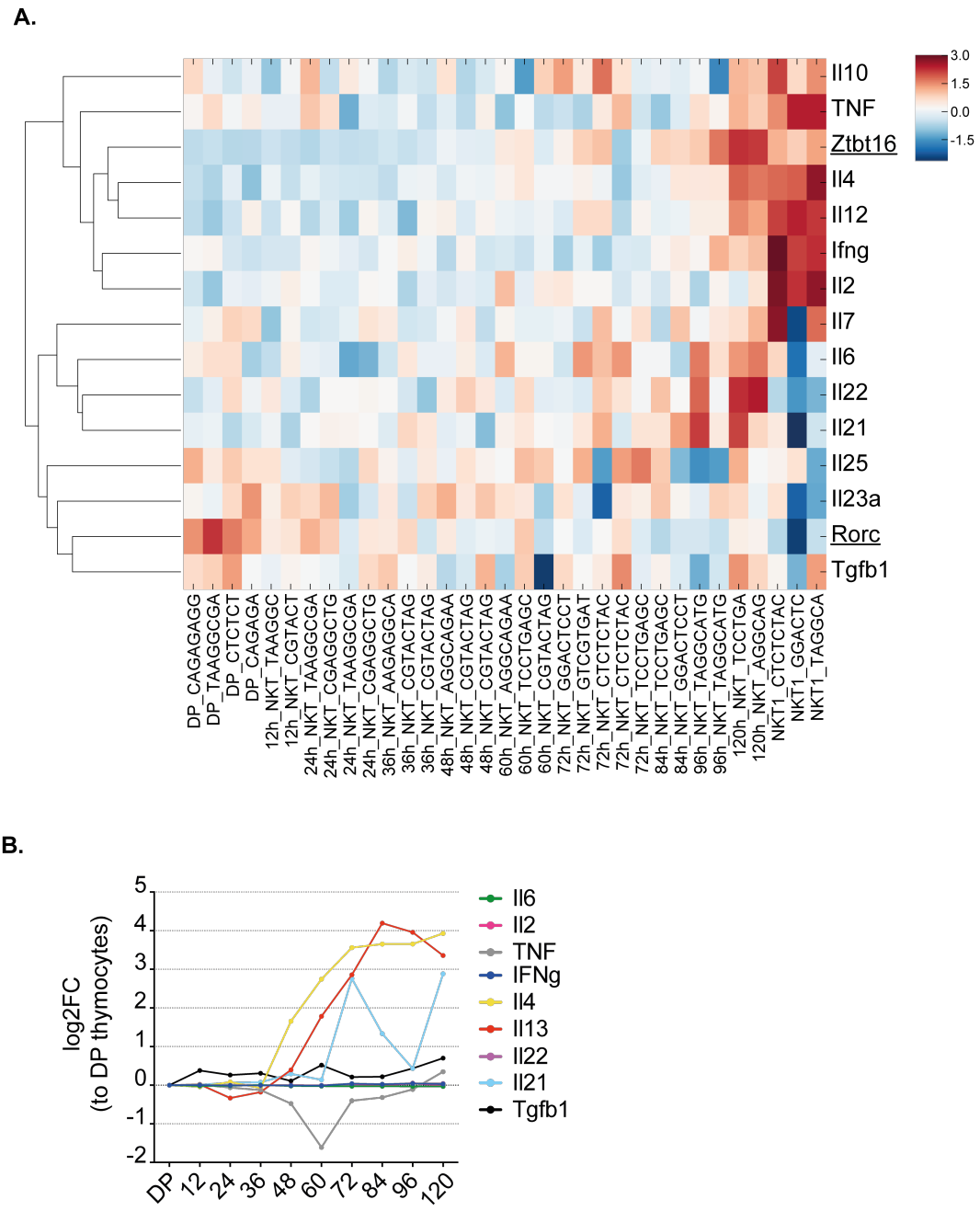

Suppl. Fig. 9. Chromatin accessibility and mRNA levels of cytokines.

A. The heatmap reports the chromatin accessibility of diverse cytokines at different timepoint calculated from the ATAC-seq data. Mean of the peaks were calculated for the cytokine regions and plotted in the heat maps for each time point using seaborn (v 0.9.0) clustermap. The colour bar represents the openness of the region with blue representing less open region while red representing more open regions. PLZF (Zbtb16) and RORγt (Rorc) genes were included as control (underlined). Each column represents a separate biological sample. The corresponding timepoints are reported below the map. **B.** mRNA levels of cytokines accross the NKT cell development The values were calculated from the SCRB-seq and indicate the log2 fold-change to DP thymocytes (gated as TCRβ− CD1d-PBS57 Tetramer− CD4+ CD8+ CD69−).

Supplementary Tables

ORGAN	CELL TYPE	#1 Vα14i i/i	#2 Vα14i i/i	#3 Vα14i i/i	#4 Vα14i i/i	#5 Wildtype
THYMUS	NKT cells	9175	1887	1533	5873	10000
	T cells	307	255	210	818	5000
SPLEEN	NKT cells	10000	7932	10000	8083	10000
	T cells	25000	25058	25000	25000	25000

Suppl. Fig. 1. Summary of population sorted for TCR sequencing.

The table reports the number of cells sorted for each population from each mouse. Due to low cell number, the samples marked in red and the samples in blue were pooled, respectively.

REFERENCES

Abarrategui, I., and M.S. Krangel. 2006. Regulation of T cell receptor-alpha gene recombination by transcription. *Nat Immunol* 7:1109-1115.

Abarrategui, I., and M.S. Krangel. 2007. Noncoding transcription controls downstream promoters to regulate T-cell receptor alpha recombination. *EMBO J* 26:4380-4390.

Adachi, Y., H. Koseki, M. Zijlstra, and M. Taniguchi. 1995. Positive selection of invariant V alpha 14+ T cells by non-major histocompatibility complex-encoded class I-like molecules expressed on bone marrow-derived cells. *Proc Natl Acad Sci U S A* 92:1200-1204.

Adolfsson, J., O.J. Borge, D. Bryder, K. Theilgaard-Monch, I. Astrand-Grundstrom, E. Sitnicka, Y. Sasaki, and S.E. Jacobsen. 2001. Upregulation of Flt3 expression within the bone marrow Lin(-)Sca1(+)c-kit(+) stem cell compartment is accompanied by loss of self-renewal capacity. *Immunity* 15:659-669.

Adolfsson, J., R. Mansson, N. Buza-Vidas, A. Hultquist, K. Liuba, C.T. Jensen, D. Bryder, L. Yang, O.J. Borge, L.A. Thoren, K. Anderson, E. Sitnicka, Y. Sasaki, M. Sigvardsson, and S.E. Jacobsen. 2005. Identification of Flt3+ lympho-myeloid stem cells lacking erythro-megakaryocytic potential a revised road map for adult blood lineage commitment. *Cell* 121:295-306.

Akira, S., K. Okazaki, and H. Sakano. 1987. Two pairs of recombination signals are sufficient to cause immunoglobulin V-(D)-J joining. *Science* 238:1134-1138.

Allende, M.L., D. Zhou, D.N. Kalkofen, S. Benhamed, G. Tuymetova, C. Borowski, A. Bendelac, and R.L. Proia. 2008. S1P1 receptor expression regulates emergence of NKT cells in peripheral tissues. *FASEB J* 22:307-315.

Allman, D., A. Sambandam, S. Kim, J.P. Miller, A. Pagan, D. Well, A. Meraz, and A. Bhandoola. 2003. Thymopoiesis independent of common lymphoid progenitors. *Nat Immunol* 4:168-174.

Anderson, C.K., A.I. Salter, L.E. Toussaint, E.C. Reilly, C. Fugere, N. Srivastava, W.G. Kerr, and L. Brossay. 2015. Role of SHIP1 in Invariant NKT Cell Development and Functions. *J Immunol* 195:2149-2156.

Arase, H., N. Arase, K. Nakagawa, R.A. Good, and K. Onoe. 1993. NK1.1+ CD4+ CD8- thymocytes with specific lymphokine secretion. *Eur J Immunol* 23:307-310.

Arase, H., N. Arase, K. Ogasawara, R.A. Good, and K. Onoe. 1992. An NK1.1+ CD4+8- single-positive thymocyte subpopulation that expresses a highly skewed T-cell antigen receptor V beta family. *Proc Natl Acad Sci U S A* 89:6506-6510.

Ardouin, L., J. Ismaili, B. Malissen, and M. Malissen. 1998. The CD3-gammadeltaepsilon and CD3-zeta/eta modules are each essential for allelic exclusion at the T cell receptor beta locus but are both dispensable

for the initiation of V to (D)J recombination at the T cell receptor-beta, -gamma, and -delta loci. *J Exp Med* 187:105-116.

Ashouri, J.F., and A. Weiss. 2017. Endogenous Nur77 Is a Specific Indicator of Antigen Receptor Signaling in Human T and B Cells. *J Immunol* 198:657-668.

Bae, E.A., H. Seo, B.S. Kim, J. Choi, I. Jeon, K.S. Shin, C.H. Koh, B. Song, I.K. Kim, B.S. Min, Y.D. Han, S.J. Shin, and C.Y. Kang. 2018. Activation of NKT Cells in an Anti-PD-1-Resistant Tumor Model Enhances Antitumor Immunity by Reinvigorating Exhausted CD8 T Cells. *Cancer Res* 78:5315-5326.

Bae, E.A., H. Seo, I.K. Kim, I. Jeon, and C.Y. Kang. 2019. Roles of NKT cells in cancer immunotherapy. *Arch Pharm Res* 42:543-548.

Baev, D.V., X.H. Peng, L. Song, J.R. Barnhart, G.M. Crooks, K.I. Weinberg, and L.S. Metelitsa. 2004. Distinct homeostatic requirements of CD4+ and CD4- subsets of Valpha24-invariant natural killer T cells in humans. *Blood* 104:4150-4156.

Balciunaite, G., R. Ceredig, S. Massa, and A.G. Rolink. 2005. A B220+ CD117+ CD19- hematopoietic progenitor with potent lymphoid and myeloid developmental potential. *Eur J Immunol* 35:2019-2030.

Barral, P., P. Polzella, A. Bruckbauer, N. van Rooijen, G.S. Besra, V. Cerundolo, and F.D. Batista. 2010. CD169(+) macrophages present lipid antigens to mediate early activation of iNKT cells in lymph nodes. *Nat Immunol* 11:303-312.

Bassiri, H., R. Das, P. Guan, D.M. Barrett, P.J. Brennan, P.P. Banerjee, S.J. Wiener, J.S. Orange, M.B. Brenner, S.A. Grupp, and K.E. Nichols. 2014. iNKT cell cytotoxic responses control T-lymphoma growth in vitro and in vivo. *Cancer Immunol Res* 2:59-69.

Beckman, E.M., S.A. Porcelli, C.T. Morita, S.M. Behar, S.T. Furlong, and M.B. Brenner. 1994. Recognition of a lipid antigen by CD1-restricted alpha beta+ T cells. *Nature* 372:691-694.

Bedel, R., J.L. Matsuda, M. Brigl, J. White, J. Kappler, P. Marrack, and L. Gapin. 2012. Lower TCR repertoire diversity in Traj18-deficient mice. *Nat Immunol* 13:705-706.

Bendelac, A. 1995. Positive selection of mouse NK1+ T cells by CD1-expressing cortical thymocytes. *J Exp Med* 182:2091-2096.

Bendelac, A., O. Lantz, M.E. Quimby, J.W. Yewdell, J.R. Bennink, and R.R. Brutkiewicz. 1995. CD1 recognition by mouse NK1+ T lymphocytes. *Science* 268:863-865.

Bendelac, A., M.N. Rivera, S.H. Park, and J.H. Roark. 1997. Mouse CD1-specific NK1 T cells: development, specificity, and function. *Annu Rev Immunol* 15:535-562.

Bendelac, A., and R.H. Schwartz. 1991. Th0 cells in the thymus: the question of T-helper lineages. *Immunol Rev* 123:169-188.

Bending, D., P.P. Martin, A. Paduraru, C. Ducker, E. Marzaganov, M. Laviron, S. Kitano, H. Miyachi, T. Crompton, and M. Ono. 2018. A timer for analyzing temporally dynamic changes in transcription during differentiation in vivo. *J Cell Biol* 217:2931-2950.

Benlagha, K., T. Kyin, A. Beavis, L. Teyton, and A. Bendelac. 2002. A thymic precursor to the NK T cell lineage. *Science* 296:553-555.

Benlagha, K., D.G. Wei, J. Veiga, L. Teyton, and A. Bendelac. 2005. Characterization of the early stages of thymic NKT cell development. *J Exp Med* 202:485-492.

Benlagha, K., A. Weiss, A. Beavis, L. Teyton, and A. Bendelac. 2000. In vivo identification of glycolipid antigen-specific T cells using fluorescent CD1d tetramers. *J Exp Med* 191:1895-1903.

Bennstein, S.B. 2017. Unraveling Natural Killer T-Cells Development. *Front Immunol* 8:1950.

Berzins, S.P., A.D. Cochrane, D.G. Pellicci, M.J. Smyth, and D.I. Godfrey. 2005. Limited correlation between human thymus and blood NKT cell content revealed by an ontogeny study of paired tissue samples. *Eur J Immunol* 35:1399-1407.

Berzins, S.P., M.J. Smyth, and A.G. Baxter. 2011. Presumed guilty: natural killer T cell defects and human disease. *Nat Rev Immunol* 11:131-142.

Blume, J., S. Zur Lage, K. Witzlau, H. Georgiev, S. Weiss, M. Lyszkiewicz, N. Zietara, and A. Krueger. 2016. Overexpression of Valpha14Jalpha18 TCR promotes development of iNKT cells in the absence of miR-181a/b-1. *Immunol Cell Biol* 94:741-746.

Bolotin, D.A., S. Poslavsky, I. Mitrophanov, M. Shugay, I.Z. Mamedov, E.V. Putintseva, and D.M. Chudakov. 2015. MiXCR: software for comprehensive adaptive immunity profiling. *Nat Methods* 12:380-381.

Borgulya, P., H. Kishi, Y. Uematsu, and H. von Boehmer. 1992. Exclusion and inclusion of alpha and beta T cell receptor alleles. *Cell* 69:529-537.

Born, W., J. Yague, E. Palmer, J. Kappler, and P. Marrack. 1985. Rearrangement of T-cell receptor beta-chain genes during T-cell development. *Proc Natl Acad Sci U S A* 82:2925-2929.

Borowski, C., and A. Bendelac. 2005. Signaling for NKT cell development: the SAP-FynT connection. *J Exp Med* 201:833-836.

Bosc, N., and M.P. Lefranc. 2003. The mouse (Mus musculus) T cell receptor alpha (TRA) and delta (TRD) variable genes. *Dev Comp Immunol* 27:465-497.

Brigl, M., L. Bry, S.C. Kent, J.E. Gumperz, and M.B. Brenner. 2003. Mechanism of CD1d-restricted natural killer T cell activation during microbial infection. *Nat Immunol* 4:1230-1237.

Brigl, M., R.V. Tatituri, G.F. Watts, V. Bhowruth, E.A. Leadbetter, N. Barton, N.R. Cohen, F.F. Hsu, G.S. Besra, and M.B. Brenner. 2011. Innate and cytokine-driven signals, rather than microbial antigens, dominate in natural killer T cell activation during microbial infection. *J Exp Med* 208:1163-1177.

Brutkiewicz, R.R., J.R. Bennink, J.W. Yewdell, and A. Bendelac. 1995. TAP-independent, beta 2-microglobulin-dependent surface expression of functional mouse CD1.1. *J Exp Med* 182:1913-1919.

Budd, R.C., G.C. Miescher, R.C. Howe, R.K. Lees, C. Bron, and H.R. MacDonald. 1987. Developmentally regulated expression of T cell receptor beta chain variable domains in immature thymocytes. *J Exp Med* 166:577-582.

Buechel, H.M., M.H. Stradner, and L.M. D'Cruz. 2015. Stages versus subsets: Invariant Natural Killer T cell lineage differentiation. *Cytokine* 72:204-209.

Cannons, J.L., S.G. Tangye, and P.L. Schwartzberg. 2011. SLAM family receptors and SAP adaptors in immunity. *Annu Rev Immunol* 29:665-705.

Carlson, C.M., B.T. Endrizzi, J. Wu, X. Ding, M.A. Weinreich, E.R. Walsh, M.A. Wani, J.B. Lingrel, K.A. Hogquist, and S.C. Jameson. 2006. Kruppel-like factor 2 regulates thymocyte and T-cell migration. *Nature* 442:299-302.

Carnaud, C., D. Lee, O. Donnars, S.H. Park, A. Beavis, Y. Koezuka, and A. Bendelac. 1999. Cutting edge: Cross-talk between cells of the innate immune system: NKT cells rapidly activate NK cells. *J Immunol* 163:4647-4650.

Ceredig, R., F. Lynch, and P. Newman. 1987. Phenotypic properties, interleukin 2 production, and developmental origin of a "mature" subpopulation of Lyt-2- L3T4- mouse thymocytes. *Proc Natl Acad Sci U S A* 84:8578-8582.

Chan, A.C., E. Leeansyah, A. Cochrane, Y. d'Udekem d'Acoz, D. Mittag, L.C. Harrison, D.I. Godfrey, and S.P. Berzins. 2013. Ex-vivo analysis of human natural killer T cells demonstrates heterogeneity between tissues and within established CD4(+) and CD4(-) subsets. *Clin Exp Immunol* 172:129-137.

Chan, A.C., P. Neeson, E. Leeansyah, K. Tainton, H. Quach, H.M. Prince, D.I. Godfrey, D. Ritchie, and S.P. Berzins. 2010. Testing the NKT cell hypothesis in lenalidomide-treated myelodysplastic syndrome patients. *Leukemia* 24:592-600.

Chan, A.C., L. Serwecinska, A. Cochrane, L.C. Harrison, D.I. Godfrey, and S.P. Berzins. 2009. Immune characterization of an individual with an exceptionally high natural killer T cell frequency and her immediate family. *Clin Exp Immunol* 156:238-245.

Chang, P.P., P. Barral, J. Fitch, A. Pratama, C.S. Ma, A. Kallies, J.J. Hogan, V. Cerundolo, S.G. Tangye, R. Bittman, S.L. Nutt, R. Brink, D.I. Godfrey, F.D. Batista, and C.G. Vinuesa. 2011a. Identification of Bcl-6-dependent follicular helper NKT cells that provide cognate help for B cell responses. *Nat Immunol* 13:35-43.

Chang, Y.J., H.Y. Kim, L.A. Albacker, H.H. Lee, N. Baumgarth, S. Akira, P.B. Savage, S. Endo, T. Yamamura, J. Maaskant, N. Kitano, A. Singh, A. Bhatt, G.S. Besra, P. van den Elzen, B. Appelmelk, R.W. Franck, G. Chen, R.H. DeKruyff, M. Shimamura, P. Illarionov, and D.T. Umetsu. 2011b. Influenza infection in suckling mice expands an NKT cell subset that protects against airway hyperreactivity. *J Clin Invest* 121:57-69.

Chaplin, D.D. 2010. Overview of the immune response. *J Allergy Clin Immunol* 125:S3-23.

Chen, S., C. Cai, Z. Li, G. Liu, Y. Wang, M. Blonska, D. Li, J. Du, X. Lin, M. Yang, and Z. Dong. 2017. Dissection of SAP-dependent and SAP-independent SLAM family signaling in NKT cell development and humoral immunity. *J Exp Med* 214:475-489.

Coquet, J.M., S. Chakravarti, K. Kyparissoudis, F.W. McNab, L.A. Pitt, B.S. McKenzie, S.P. Berzins, M.J. Smyth, and D.I. Godfrey. 2008. Diverse cytokine production by NKT cell subsets and identification of an IL-17-

producing CD4-NK1.1- NKT cell population. *Proc Natl Acad Sci U S A* 105:11287-11292.

Cruz Tleugabulova, M., M. Zhao, I. Lau, M. Kuypers, C. Wirianto, J.M. Umana, Q. Lin, M. Kronenberg, and T. Mallevaey. 2019. The Protein Phosphatase Shp1 Regulates Invariant NKT Cell Effector Differentiation Independently of TCR and Slam Signaling. *J Immunol* 202:2276-2286.

Cui, J., T. Shin, T. Kawano, H. Sato, E. Kondo, I. Toura, Y. Kaneko, H. Koseki, M. Kanno, and M. Taniguchi. 1997. Requirement for Valpha14 NKT cells in IL-12-mediated rejection of tumors. *Science* 278:1623-1626.

Cui, Y., and Q. Wan. 2019. NKT Cells in Neurological Diseases. *Front Cell Neurosci* 13:245.

Cunningham, N.R., S.C. Artim, C.M. Fornadel, M.C. Sellars, S.G. Edmonson, G. Scott, F. Albino, A. Mathur, and J.A. Punt. 2006. Immature CD4+CD8+ thymocytes and mature T cells regulate Nur77 distinctly in response to TCR stimulation. *J Immunol* 177:6660-6666.

Curry, J.D., J.K. Geier, and M.S. Schlissel. 2005. Single-strand recombination signal sequence nicks in vivo: evidence for a capture model of synapsis. *Nat Immunol* 6:1272-1279.

D'Cruz, L.M., J. Knell, J.K. Fujimoto, and A.W. Goldrath. 2010. An essential role for the transcription factor HEB in thymocyte survival, Tcra rearrangement and the development of natural killer T cells. *Nat Immunol* 11:240-249.

D'Cruz, L.M., M.H. Stradner, C.Y. Yang, and A.W. Goldrath. 2014. E and Id proteins influence invariant NKT cell sublineage differentiation and proliferation. *J Immunol* 192:2227-2236.

Dai, H., A. Rahman, A. Saxena, A.K. Jaiswal, A. Mohamood, L. Ramirez, S. Noel, H. Rabb, C. Jie, and A.R. Hamad. 2015. Syndecan-1 identifies and controls the frequency of IL-17-producing naive natural killer T (NKT17) cells in mice. *Eur J Immunol* 45:3045-3051.

Das, R., D.B. Sant'Angelo, and K.E. Nichols. 2010. Transcriptional control of invariant NKT cell development. *Immunol Rev* 238:195-215.

Dashtsoodol, N., T. Shigeura, M. Aihara, R. Ozawa, S. Kojo, M. Harada, T.A. Endo, T. Watanabe, O. Ohara, and M. Taniguchi. 2017. Alternative pathway for the development of Valpha14(+) NKT cells directly from CD4(-)CD8(-) thymocytes that bypasses the CD4(+)CD8(+) stage. *Nat Immunol* 18:274-282.

Dashtsoodol, N., T. Shigeura, R. Ozawa, M. Harada, S. Kojo, T. Watanabe, H. Koseki, M. Nakayama, O. Ohara, and M. Taniguchi. 2016. Generation of Novel Traj18-Deficient Mice Lacking Valpha14 Natural Killer T Cells with an Undisturbed T Cell Receptor alpha-Chain Repertoire. *PLoS One* 11:e0153347.

Dashtsoodol, N., H. Watarai, S. Sakata, and M. Taniguchi. 2008. Identification of CD4(-)CD8(-) double-negative natural killer T cell precursors in the thymus. *PLoS One* 3:e3688.

Davis, M.M., and P.J. Bjorkman. 1988. T-cell antigen receptor genes and T-cell recognition. *Nature* 334:395-402.

De Santo, C., R. Arscott, S. Booth, I. Karydis, M. Jones, R. Asher, M. Salio, M. Middleton, and V. Cerundolo. 2010. Invariant NKT cells modulate the suppressive activity of IL-10-secreting neutrophils differentiated with serum amyloid A. *Nat Immunol* 11:1039-1046.

Desanti, G.E., W.E. Jenkinson, S.M. Parnell, A. Boudil, L. Gautreau-Rolland, B. Eksteen, S. Ezine, P.J. Lane, E.J. Jenkinson, and G. Anderson. 2011. Clonal analysis reveals uniformity in the molecular profile and lineage potential of CCR9(+) and CCR9(-) thymus-settling progenitors. *J Immunol* 186:5227-5235.

Diana, J., V. Brezar, L. Beaudoin, M. Dalod, A. Mellor, A. Tafuri, M. von Herrath, C. Boitard, R. Mallone, and A. Lehuen. 2011. Viral infection prevents diabetes by inducing regulatory T cells through NKT cell-plasmacytoid dendritic cell interplay. *J Exp Med* 208:729-745.

Dobenecker, M.W., J.K. Kim, J. Marcello, T.C. Fang, R. Prinjha, R. Bosselut, and A. Tarakhovsky. 2015. Coupling of T cell receptor specificity to natural killer T cell development by bivalent histone H3 methylation. *J Exp Med* 212:297-306.

Doherty, D.G., A.M. Melo, A. Moreno-Olivera, and A.C. Solomos. 2018. Activation and Regulation of B Cell Responses by Invariant Natural Killer T Cells. *Front Immunol* 9:1360.

Dose, M., B.P. Sleckman, J. Han, A.L. Bredemeyer, A. Bendelac, and F. Gounari. 2009. Intrathymic proliferation wave essential for Valpha14+ natural killer T cell development depends on c-Myc. *Proc Natl Acad Sci U S A* 106:8641-8646.

Drees, C., J.C. Vahl, S. Bortoluzzi, K.D. Heger, J.C. Fischer, F.T. Wunderlich, C. Peschel, and M. Schmidt-Supprian. 2017. Roquin Paralogs Differentially Regulate Functional NKT Cell Subsets. *J Immunol* 198:2747-2759.

Dutta, M., Z.J. Kraus, J. Gomez-Rodriguez, S.H. Hwang, J.L. Cannons, J. Cheng, S.Y. Lee, D.L. Wiest, E.K. Wakeland, and P.L. Schwartzberg. 2013. A role for Ly108 in the induction of promyelocytic zinc finger transcription factor in developing thymocytes. *J Immunol* 190:2121-2128.

Early, P., H. Huang, M. Davis, K. Calame, and L. Hood. 1980. An immunoglobulin heavy chain variable region gene is generated from three segments of DNA: VH, D and JH. *Cell* 19:981-992.

Eberl, G., and H.R. MacDonald. 2000. Selective induction of NK cell proliferation and cytotoxicity by activated NKT cells. *Eur J Immunol* 30:985-992.

Egawa, T., G. Eberl, I. Taniuchi, K. Benlagha, F. Geissmann, L. Hennighausen, A. Bendelac, and D.R. Littman. 2005. Genetic evidence supporting selection of the Valpha14i NKT cell lineage from double-positive thymocyte precursors. *Immunity* 22:705-716.

Engel, I., G. Seumois, L. Chavez, D. Samaniego-Castruita, B. White, A. Chawla, D. Mock, P. Vijayanand, and M. Kronenberg. 2016. Innate-like functions of natural killer T cell subsets result from highly divergent gene programs. *Nat Immunol* 17:728-739.

Falk, I., G. Nerz, I. Haidl, A. Krotkova, and K. Eichmann. 2001. Immature thymocytes that fail to express TCRbeta and/or TCRgamma delta proteins

die by apoptotic cell death in the CD44(-)CD25(-) (DN4) subset. *Eur J Immunol* 31:3308-3317.

Fehling, H.J., A. Krotkova, C. Saint-Ruf, and H. von Boehmer. 1995. Crucial role of the pre-T-cell receptor alpha gene in development of alpha beta but not gamma delta T cells. *Nature* 375:795-798.

Fischer, K., E. Scotet, M. Niemeyer, H. Koebernick, J. Zerrahn, S. Maillet, R. Hurwitz, M. Kursar, M. Bonneville, S.H. Kaufmann, and U.E. Schaible. 2004. Mycobacterial phosphatidylinositol mannoside is a natural antigen for CD1d-restricted T cells. *Proc Natl Acad Sci U S A* 101:10685-10690.

Forestier, C., S.H. Park, D. Wei, K. Benlagha, L. Teyton, and A. Bendelac. 2003. T cell development in mice expressing CD1d directed by a classical MHC class II promoter. *J Immunol* 171:4096-4104.

Fowlkes, B.J., A.M. Kruisbeek, H. Ton-That, M.A. Weston, J.E. Coligan, R.H. Schwartz, and D.M. Pardoll. 1987. A novel population of T-cell receptor alpha beta-bearing thymocytes which predominantly expresses a single V beta gene family. *Nature* 329:251-254.

Fujii, S., K. Liu, C. Smith, A.J. Bonito, and R.M. Steinman. 2004. The linkage of innate to adaptive immunity via maturing dendritic cells in vivo requires CD40 ligation in addition to antigen presentation and CD80/86 costimulation. *J Exp Med* 199:1607-1618.

Fujii, S., K. Shimizu, M. Kronenberg, and R.M. Steinman. 2002. Prolonged IFN-gamma-producing NKT response induced with alpha-galactosylceramide-loaded DCs. *Nat Immunol* 3:867-874.

Fujii, S., K. Shimizu, C. Smith, L. Bonifaz, and R.M. Steinman. 2003. Activation of natural killer T cells by alpha-galactosylceramide rapidly induces the full maturation of dendritic cells in vivo and thereby acts as an adjuvant for combined CD4 and CD8 T cell immunity to a coadministered protein. *J Exp Med* 198:267-279.

Gadola, S.D., M. Koch, J. Marles-Wright, N.M. Lissin, D. Shepherd, G. Matulis, K. Harlos, P.M. Villiger, D.I. Stuart, B.K. Jakobsen, V. Cerundolo, and E.Y. Jones. 2006. Structure and binding kinetics of three different human CD1d-alpha-galactosylceramide-specific T cell receptors. *J Exp Med* 203:699-710.

Gadue, P., and P.L. Stein. 2002. NK T cell precursors exhibit differential cytokine regulation and require Itk for efficient maturation. *J Immunol* 169:2397-2406.

Gapin, L. 2016. Development of invariant natural killer T cells. *Curr Opin Immunol* 39:68-74.

Gaud, G., R. Lesourne, and P.E. Love. 2018. Regulatory mechanisms in T cell receptor signalling. *Nat Rev Immunol* 18:485-497.

Gegonne, A., Q.R. Chen, A. Dey, R. Etzensperger, X. Tai, A. Singer, D. Meerzaman, K. Ozato, and D.S. Singer. 2018. Immature CD8 Single-Positive Thymocytes Are a Molecularly Distinct Subpopulation, Selectively Dependent on BRD4 for Their Differentiation. *Cell Rep* 24:117-129.

Georgiev, H., I. Ravens, C. Benarafa, R. Forster, and G. Bernhardt. 2016. Distinct gene expression patterns correlate with developmental and functional traits of iNKT subsets. *Nat Commun* 7:13116.

Gerber, D.J., V. Azuara, J.P. Levraud, S.Y. Huang, M.P. Lembezat, and P. Pereira. 1999. IL-4-producing gamma delta T cells that express a very restricted TCR repertoire are preferentially localized in liver and spleen. *J Immunol* 163:3076-3082.

Giaccone, G., C.J. Punt, Y. Ando, R. Ruijter, N. Nishi, M. Peters, B.M. von Blomberg, R.J. Scheper, H.J. van der Vliet, A.J. van den Eertwegh, M. Roelvink, J. Beijnen, H. Zwierzina, and H.M. Pinedo. 2002. A phase I study of the natural killer T-cell ligand alpha-galactosylceramide (KRN7000) in patients with solid tumors. *Clin Cancer Res* 8:3702-3709.

Girard, J.P., C. Moussion, and R. Forster. 2012. HEVs, lymphatics and homeostatic immune cell trafficking in lymph nodes. *Nat Rev Immunol* 12:762-773.

Gleimer, M., H. von Boehmer, and T. Kreslavsky. 2012. PLZF Controls the Expression of a Limited Number of Genes Essential for NKT Cell Function. *Front Immunol* 3:374.

Glusman, G., L. Rowen, I. Lee, C. Boysen, J.C. Roach, A.F. Smit, K. Wang, B.F. Koop, and L. Hood. 2001. Comparative genomics of the human and mouse T cell receptor loci. *Immunity* 15:337-349.

Godfrey, D.I., J. Kennedy, P. Mombaerts, S. Tonegawa, and A. Zlotnik. 1994. Onset of TCR-beta gene rearrangement and role of TCR-beta expression during CD3-CD4-CD8- thymocyte differentiation. *J Immunol* 152:4783-4792.

Godfrey, D.I., H.R. MacDonald, M. Kronenberg, M.J. Smyth, and L. Van Kaer. 2004. NKT cells: what's in a name? *Nat Rev Immunol* 4:231-237.

Godfrey, D.I., A.P. Uldrich, J. McCluskey, J. Rossjohn, and D.B. Moody. 2015. The burgeoning family of unconventional T cells. *Nat Immunol* 16:1114-1123.

Golub, R., C.Y. Huang, O. Kanagawa, and G.E. Wu. 2001. Valpha gene replacement in a TCRalpha knock-in mouse. *Eur J Immunol* 31:2919-2925.

Gordy, L.E., J.S. Bezbradica, A.I. Flyak, C.T. Spencer, A. Dunkle, J. Sun, A.K. Stanic, M.R. Boothby, Y.W. He, Z. Zhao, L. Van Kaer, and S. Joyce. 2011. IL-15 regulates homeostasis and terminal maturation of NKT cells. *J Immunol* 187:6335-6345.

Griewank, K., C. Borowski, S. Rietdijk, N. Wang, A. Julien, D.G. Wei, A.A. Mamchak, C. Terhorst, and A. Bendelac. 2007. Homotypic interactions mediated by Slamf1 and Slamf6 receptors control NKT cell lineage development. *Immunity* 27:751-762.

Gumperz, J.E., C. Roy, A. Makowska, D. Lum, M. Sugita, T. Podrebarac, Y. Koezuka, S.A. Porcelli, S. Cardell, M.B. Brenner, and S.M. Behar. 2000. Murine CD1d-restricted T cell recognition of cellular lipids. *Immunity* 12:211-221.

Guo, J., A. Hawwari, H. Li, Z. Sun, S.K. Mahanta, D.R. Littman, M.S. Krangel, and Y.W. He. 2002. Regulation of the TCRalpha repertoire by the survival window of CD4(+)CD8(+) thymocytes. *Nat Immunol* 3:469-476.

Haks, M.C., P. Krimpenfort, J. Borst, and A.M. Kruisbeek. 1998. The CD3gamma chain is essential for development of both the TCRalphabeta and TCRgammadelta lineages. *EMBO J* 17:1871-1882.

Hammond, K.J., D.G. Pellicci, L.D. Poulton, O.V. Naidenko, A.A. Scalzo, A.G. Baxter, and D.I. Godfrey. 2001. CD1d-restricted NKT cells: an interstrain comparison. *J Immunol* 167:1164-1173.

Haraguchi, K., T. Takahashi, F. Nakahara, A. Matsumoto, M. Kurokawa, S. Ogawa, H. Oda, H. Hirai, and S. Chiba. 2006. CD1d expression level in tumor cells is an important determinant for anti-tumor immunity by natural killer T cells. *Leuk Lymphoma* 47:2218-2223.

Havenar-Daughton, C., S. Li, K. Benlagha, and J.C. Marie. 2012. Development and function of murine RORgammat+ iNKT cells are under TGF-beta signaling control. *Blood* 119:3486-3494.

Hawwari, A., C. Bock, and M.S. Krangel. 2005. Regulation of T cell receptor alpha gene assembly by a complex hierarchy of germline Jalpha promoters. *Nat Immunol* 6:481-489.

Hawwari, A., and M.S. Krangel. 2005. Regulation of TCR delta and alpha repertoires by local and long-distance control of variable gene segment chromatin structure. *J Exp Med* 202:467-472.

Hawwari, A., and M.S. Krangel. 2007. Role for rearranged variable gene segments in directing secondary T cell receptor alpha recombination. *Proc Natl Acad Sci U S A* 104:903-907.

Hayakawa, K., B.T. Lin, and R.R. Hardy. 1992. Murine thymic CD4+ T cell subsets: a subset (Thy0) that secretes diverse cytokines and overexpresses the V beta 8 T cell receptor gene family. *J Exp Med* 176:269-274.

Heczey, A., D. Liu, G. Tian, A.N. Courtney, J. Wei, E. Marinova, X. Gao, L. Guo, E. Yvon, J. Hicks, H. Liu, G. Dotti, and L.S. Metelitsa. 2014. Invariant NKT cells with chimeric antigen receptor provide a novel platform for safe and effective cancer immunotherapy. *Blood* 124:2824-2833.

Henao-Mejia, J., A. Williams, L.A. Goff, M. Staron, P. Licona-Limon, S.M. Kaech, M. Nakayama, J.L. Rinn, and R.A. Flavell. 2013. The microRNA miR-181 is a critical cellular metabolic rheostat essential for NKT cell ontogenesis and lymphocyte development and homeostasis. *Immunity* 38:984-997.

Hermans, I.F., J.D. Silk, U. Gileadi, M. Salio, B. Mathew, G. Ritter, R. Schmidt, A.L. Harris, L. Old, and V. Cerundolo. 2003. NKT cells enhance CD4+ and CD8+ T cell responses to soluble antigen in vivo through direct interaction with dendritic cells. *J Immunol* 171:5140-5147.

Hozumi, N., and S. Tonegawa. 1976. Evidence for somatic rearrangement of immunoglobulin genes coding for variable and constant regions. *Proc Natl Acad Sci U S A* 73:3628-3632.

Hsu, L.Y., Y.X. Tan, Z. Xiao, M. Malissen, and A. Weiss. 2009. A hypomorphic allele of ZAP-70 reveals a distinct thymic threshold for autoimmune disease versus autoimmune reactivity. *J Exp Med* 206:2527-2541.

Hu, T., A. Simmons, J. Yuan, T.P. Bender, and J. Alberola-Ila. 2010. The transcription factor c-Myb primes CD4+CD8+ immature thymocytes for selection into the iNKT lineage. *Nat Immunol* 11:435-441.

Huang, B., J. Gomez-Rodriguez, S. Preite, L.J. Garrett, U.L. Harper, and P.L. Schwartzberg. 2016. CRISPR-Mediated Triple Knockout of SLAMF1, SLAMF5 and SLAMF6 Supports Positive Signaling Roles in NKT Cell Development. *PLoS One* 11:e0156072.

Huang, C., and O. Kanagawa. 2001. Ordered and coordinated rearrangement of the TCR alpha locus: role of secondary rearrangement in thymic selection. *J Immunol* 166:2597-2601.

Igarashi, H., S.C. Gregory, T. Yokota, N. Sakaguchi, and P.W. Kincade. 2002. Transcription from the RAG1 locus marks the earliest lymphocyte progenitors in bone marrow. *Immunity* 17:117-130.

Imai, K., M. Kanno, H. Kimoto, K. Shigemoto, S. Yamamoto, and M. Taniguchi. 1986. Sequence and expression of transcripts of the T-cell antigen receptor alpha-chain gene in a functional, antigen-specific suppressor-T-cell hybridoma. *Proc Natl Acad Sci U S A* 83:8708-8712.

Ishikawa, A., S. Motohashi, E. Ishikawa, H. Fuchida, K. Higashino, M. Otsuji, T. Iizasa, T. Nakayama, M. Taniguchi, and T. Fujisawa. 2005. A phase I study of alpha-galactosylceramide (KRN7000)-pulsed dendritic cells in patients with advanced and recurrent non-small cell lung cancer. *Clin Cancer Res* 11:1910-1917.

Itohara, S., A.G. Farr, J.J. Lafaille, M. Bonneville, Y. Takagaki, W. Haas, and S. Tonegawa. 1990. Homing of a gamma delta thymocyte subset with homogeneous T-cell receptors to mucosal epithelia. *Nature* 343:754-757.

Iwamura, C., and T. Nakayama. 2018. Role of CD1d- and MR1-Restricted T Cells in Asthma. *Front Immunol* 9:1942.

Jameson, S.C., K.A. Hogquist, and M.J. Bevan. 1995. Positive selection of thymocytes. *Annu Rev Immunol* 13:93-126.

Johnston, B., C.H. Kim, D. Soler, M. Emoto, and E.C. Butcher. 2003. Differential chemokine responses and homing patterns of murine TCR alpha beta NKT cell subsets. *J Immunol* 171:2960-2969.

Jones, J.M., and M. Gellert. 2002. Ordered assembly of the V(D)J synaptic complex ensures accurate recombination. *EMBO J* 21:4162-4171.

Jordan, M.A., J.M. Fletcher, R. Jose, S. Chowdhury, N. Gerlach, J. Allison, and A.G. Baxter. 2011. Role of SLAM in NKT cell development revealed by transgenic complementation in NOD mice. *J Immunol* 186:3953-3965.

Joseph, C., J. Klibi, L. Amable, L. Comba, A. Cascioferro, M. Delord, V. Parietti, C. Lenoir, S. Latour, B. Lucas, C. Viret, A. Toubert, and K. Benlagha. 2019. TCR density in early iNKT cell precursors regulates agonist selection and subset differentiation in mice. *Eur J Immunol* 49:894-910.

Juno, J.A., Y. Keynan, and K.R. Fowke. 2012. Invariant NKT cells: regulation and function during viral infection. *PLoS Pathog* 8:e1002838.

Kageyama, R., J.L. Cannons, F. Zhao, I. Yusuf, C. Lao, M. Locci, P.L. Schwartzberg, and S. Crotty. 2012. The receptor Ly108 functions as a SAP adaptor-dependent on-off switch for T cell help to B cells and NKT cell development. *Immunity* 36:986-1002.

Kain, L., B. Webb, B.L. Anderson, S. Deng, M. Holt, A. Costanzo, M. Zhao, K. Self, A. Teyton, C. Everett, M. Kronenberg, D.M. Zajonc, A. Bendelac, P.B.

Savage, and L. Teyton. 2014. The identification of the endogenous ligands of natural killer T cells reveals the presence of mammalian alpha-linked glycosylceramides. *Immunity* 41:543-554.

Kasler, H.G., I.S. Lee, H.W. Lim, and E. Verdin. 2018. Histone Deacetylase 7 mediates tissue-specific autoimmunity via control of innate effector function in invariant Natural Killer T Cells. *Elife* 7:

Kasler, H.G., B.D. Young, D. Mottet, H.W. Lim, A.M. Collins, E.N. Olson, and E. Verdin. 2011. Histone deacetylase 7 regulates cell survival and TCR signaling in CD4/CD8 double-positive thymocytes. *J Immunol* 186:4782-4793.

Katayama, C.D., F.J. Eidelman, A. Duncan, F. Hooshmand, and S.M. Hedrick. 1995. Predicted complementarity determining regions of the T cell antigen receptor determine antigen specificity. *EMBO J* 14:927-938.

Kawakami, K., Y. Kinjo, S. Yara, K. Uezu, Y. Koguchi, M. Tohyama, M. Azuma, K. Takeda, S. Akira, and A. Saito. 2001. Enhanced gamma interferon production through activation of Valpha14(+) natural killer T cells by alpha-galactosylceramide in interleukin-18-deficient mice with systemic cryptococcosis. *Infect Immun* 69:6643-6650.

Kawakami, K., N. Yamamoto, Y. Kinjo, K. Miyagi, C. Nakasone, K. Uezu, T. Kinjo, T. Nakayama, M. Taniguchi, and A. Saito. 2003. Critical role of Valpha14+ natural killer T cells in the innate phase of host protection against Streptococcus pneumoniae infection. *Eur J Immunol* 33:3322-3330.

Kawano, T., J. Cui, Y. Koezuka, I. Toura, Y. Kaneko, K. Motoki, H. Ueno, R. Nakagawa, H. Sato, E. Kondo, H. Koseki, and M. Taniguchi. 1997. CD1d-restricted and TCR-mediated activation of valpha14 NKT cells by glycosylceramides. *Science* 278:1626-1629.

Kenna, T., L. Golden-Mason, S.A. Porcelli, Y. Koezuka, J.E. Hegarty, C. O'Farrelly, and D.G. Doherty. 2003. NKT cells from normal and tumor-bearing human livers are phenotypically and functionally distinct from murine NKT cells. *J Immunol* 171:1775-1779.

Kim, E.Y., J.T. Battaile, A.C. Patel, Y. You, E. Agapov, M.H. Grayson, L.A. Benoit, D.E. Byers, Y. Alevy, J. Tucker, S. Swanson, R. Tidwell, J.W. Tyner, J.D. Morton, M. Castro, D. Polineni, G.A. Patterson, R.A. Schwendener, J.D. Allard, G. Peltz, and M.J. Holtzman. 2008. Persistent activation of an innate immune response translates respiratory viral infection into chronic lung disease. *Nat Med* 14:633-640.

Kimura, M.Y., A. Igi, K. Hayashizaki, Y. Mita, M. Shinzawa, T. Kadakia, Y. Endo, S. Ogawa, R. Yagi, S. Motohashi, A. Singer, and T. Nakayama. 2018. CD69 prevents PLZF(hi) innate precursors from prematurely exiting the thymus and aborting NKT2 cell differentiation. *Nat Commun* 9:3749.

King, I.L., A. Fortier, M. Tighe, J. Dibble, G.F. Watts, N. Veerapen, A.M. Haberman, G.S. Besra, M. Mohrs, M.B. Brenner, and E.A. Leadbetter. 2011. Invariant natural killer T cells direct B cell responses to cognate lipid antigen in an IL-21-dependent manner. *Nat Immunol* 13:44-50.

Kinjo, Y., P. Illarionov, J.L. Vela, B. Pei, E. Girardi, X. Li, Y. Li, M. Imamura, Y. Kaneko, A. Okawara, Y. Miyazaki, A. Gomez-Velasco, P. Rogers, S. Dahesh,

S. Uchiyama, A. Khurana, K. Kawahara, H. Yesilkaya, P.W. Andrew, C.H. Wong, K. Kawakami, V. Nizet, G.S. Besra, M. Tsuji, D.M. Zajonc, and M. Kronenberg. 2011. Invariant natural killer T cells recognize glycolipids from pathogenic Gram-positive bacteria. *Nat Immunol* 12:966-974.

Kinjo, Y., E. Tupin, D. Wu, M. Fujio, R. Garcia-Navarro, M.R. Benhnia, D.M. Zajonc, G. Ben-Menachem, G.D. Ainge, G.F. Painter, A. Khurana, K. Hoebe, S.M. Behar, B. Beutler, I.A. Wilson, M. Tsuji, T.J. Sellati, C.H. Wong, and M. Kronenberg. 2006. Natural killer T cells recognize diacylglycerol antigens from pathogenic bacteria. *Nat Immunol* 7:978-986.

Kinjo, Y., D. Wu, G. Kim, G.W. Xing, M.A. Poles, D.D. Ho, M. Tsuji, K. Kawahara, C.H. Wong, and M. Kronenberg. 2005. Recognition of bacterial glycosphingolipids by natural killer T cells. *Nature* 434:520-525.

Kirkham, C.M., J.N.F. Scott, X. Wang, A.L. Smith, A.P. Kupinski, A.M. Ford, D.R. Westhead, P.G. Stockley, R. Tuma, and J. Boyes. 2019. Cut-and-Run: A Distinct Mechanism by which V(D)J Recombination Causes Genome Instability. *Mol Cell* 74:584-597 e589.

Kitamura, H., K. Iwakabe, T. Yahata, S. Nishimura, A. Ohta, Y. Ohmi, M. Sato, K. Takeda, K. Okumura, L. Van Kaer, T. Kawano, M. Taniguchi, and T. Nishimura. 1999. The natural killer T (NKT) cell ligand alpha-galactosylceramide demonstrates its immunopotentiating effect by inducing interleukin (IL)-12 production by dendritic cells and IL-12 receptor expression on NKT cells. *J Exp Med* 189:1121-1128.

Kjer-Nielsen, L., O. Patel, A.J. Corbett, J. Le Nours, B. Meehan, L. Liu, M. Bhati, Z. Chen, L. Kostenko, R. Reantragoon, N.A. Williamson, A.W. Purcell, N.L. Dudek, M.J. McConville, R.A. O'Hair, G.N. Khairallah, D.I. Godfrey, D.P. Fairlie, J. Rossjohn, and J. McCluskey. 2012. MR1 presents microbial vitamin B metabolites to MAIT cells. *Nature* 491:717-723.

Klein, L., B. Kyewski, P.M. Allen, and K.A. Hogquist. 2014. Positive and negative selection of the T cell repertoire: what thymocytes see (and don't see). *Nat Rev Immunol* 14:377-391.

Klibi, J., S. Li, L. Amable, C. Joseph, S. Brunet, M. Delord, V. Parietti, J. Jaubert, J. Marie, S. Karray, G. Eberl, B. Lucas, A. Toubert, and K. Benlagha. 2019. Characterization of the developmental landscape of murine RORgammat+ iNKT cells. *Int Immunol*

Koay, H.F., N.A. Gherardin, A. Enders, L. Loh, L.K. Mackay, C.F. Almeida, B.E. Russ, C.A. Nold-Petry, M.F. Nold, S. Bedoui, Z. Chen, A.J. Corbett, S.B. Eckle, B. Meehan, Y. d'Udekem, I.E. Konstantinov, M. Lappas, L. Liu, C.C. Goodnow, D.P. Fairlie, J. Rossjohn, M.M. Chong, K. Kedzierska, S.P. Berzins, G.T. Belz, J. McCluskey, A.P. Uldrich, D.I. Godfrey, and D.G. Pellicci. 2016. A three-stage intrathymic development pathway for the mucosal-associated invariant T cell lineage. *Nat Immunol* 17:1300-1311.

Kondo, M., I.L. Weissman, and K. Akashi. 1997. Identification of clonogenic common lymphoid progenitors in mouse bone marrow. *Cell* 91:661-672.

Koseki, H., K. Imai, F. Nakayama, T. Sado, K. Moriwaki, and M. Taniguchi. 1990. Homogenous junctional sequence of the V14+ T-cell antigen receptor

alpha chain expanded in unprimed mice. *Proc Natl Acad Sci U S A* 87:5248-5252.

Kovalovsky, D., E.S. Alonzo, O.U. Uche, M. Eidson, K.E. Nichols, and D.B. Sant'Angelo. 2010. PLZF induces the spontaneous acquisition of memory/effector functions in T cells independently of NKT cell-related signals. *J Immunol* 184:6746-6755.

Kovalovsky, D., O.U. Uche, S. Eladad, R.M. Hobbs, W. Yi, E. Alonzo, K. Chua, M. Eidson, H.J. Kim, J.S. Im, P.P. Pandolfi, and D.B. Sant'Angelo. 2008. The BTB-zinc finger transcriptional regulator PLZF controls the development of invariant natural killer T cell effector functions. *Nat Immunol* 9:1055-1064.

Krangel, M.S., J. Carabana, I. Abbarategui, R. Schlimgen, and A. Hawwari. 2004. Enforcing order within a complex locus: current perspectives on the control of V(D)J recombination at the murine T-cell receptor alpha/delta locus. *Immunol Rev* 200:224-232.

Kreslavsky, T., A.K. Savage, R. Hobbs, F. Gounari, R. Bronson, P. Pereira, P.P. Pandolfi, A. Bendelac, and H. von Boehmer. 2009. TCR-inducible PLZF transcription factor required for innate phenotype of a subset of gammadelta T cells with restricted TCR diversity. *Proc Natl Acad Sci U S A* 106:12453-12458.

Kriegsmann, K., M. Kriegsmann, M. von Bergwelt-Baildon, M. Cremer, and M. Witzens-Harig. 2018. NKT cells - New players in CAR cell immunotherapy? *Eur J Haematol* 101:750-757.

Kuylenstierna, C., N.K. Bjorkstrom, S.K. Andersson, P. Sahlstrom, L. Bosnjak, D. Paquin-Proulx, K.J. Malmberg, H.G. Ljunggren, M. Moll, and J.K. Sandberg. 2011. NKG2D performs two functions in invariant NKT cells: direct TCR-independent activation of NK-like cytolysis and co-stimulation of activation by CD1d. *Eur J Immunol* 41:1913-1923.

Kwon, D.I., and Y.J. Lee. 2017. Lineage Differentiation Program of Invariant Natural Killer T Cells. *Immune Netw* 17:365-377.

Lang, G.A., M.A. Exley, and M.L. Lang. 2006. The CD1d-binding glycolipid alpha-galactosylceramide enhances humoral immunity to T-dependent and T-independent antigen in a CD1d-dependent manner. *Immunology* 119:116-125.

Lantz, O., and A. Bendelac. 1994. An invariant T cell receptor alpha chain is used by a unique subset of major histocompatibility complex class I-specific CD4+ and CD4-8- T cells in mice and humans. *J Exp Med* 180:1097-1106.

Lazarevic, V., A.J. Zullo, M.N. Schweitzer, T.L. Staton, E.M. Gallo, G.R. Crabtree, and L.H. Glimcher. 2009. The gene encoding early growth response 2, a target of the transcription factor NFAT, is required for the development and maturation of natural killer T cells. *Nat Immunol* 10:306-313.

Lee, P.T., K. Benlagha, L. Teyton, and A. Bendelac. 2002. Distinct functional lineages of human V(alpha)24 natural killer T cells. *J Exp Med* 195:637-641.

Lee, W.Y., T.J. Moriarty, C.H. Wong, H. Zhou, R.M. Strieter, N. van Rooijen, G. Chaconas, and P. Kubes. 2010a. An intravascular immune response to

Borrelia burgdorferi involves Kupffer cells and iNKT cells. *Nat Immunol* 11:295-302.

Lee, Y.J., K.L. Holzapfel, J. Zhu, S.C. Jameson, and K.A. Hogquist. 2013. Steady-state production of IL-4 modulates immunity in mouse strains and is determined by lineage diversity of iNKT cells. *Nat Immunol* 14:1146-1154.

Lee, Y.J., Y.K. Jeon, B.H. Kang, D.H. Chung, C.G. Park, H.Y. Shin, K.C. Jung, and S.H. Park. 2010b. Generation of PLZF+ CD4+ T cells via MHC class II-dependent thymocyte-thymocyte interaction is a physiological process in humans. *J Exp Med* 207:237-246.

Lee, Y.J., G.J. Starrett, S.T. Lee, R. Yang, C.M. Henzler, S.C. Jameson, and K.A. Hogquist. 2016. Lineage-Specific Effector Signatures of Invariant NKT Cells Are Shared amongst gammadelta T, Innate Lymphoid, and Th Cells. *J Immunol* 197:1460-1470.

Lee, Y.J., H. Wang, G.J. Starrett, V. Phuong, S.C. Jameson, and K.A. Hogquist. 2015. Tissue-Specific Distribution of iNKT Cells Impacts Their Cytokine Response. *Immunity* 43:566-578.

Leishman, A.J., L. Gapin, M. Capone, E. Palmer, H.R. MacDonald, M. Kronenberg, and H. Cheroutre. 2002. Precursors of functional MHC class I- or class II-restricted CD8alphaalpha(+) T cells are positively selected in the thymus by agonist self-peptides. *Immunity* 16:355-364.

Levitsky, H.I., P.T. Golumbek, and D.M. Pardoll. 1991. The fate of CD4-8- T cell receptor-alpha beta+ thymocytes. *J Immunol* 146:1113-1117.

Lewis, S., A. Gifford, and D. Baltimore. 1985. DNA elements are asymmetrically joined during the site-specific recombination of kappa immunoglobulin genes. *Science* 228:677-685.

Li, Q.J., J. Chau, P.J. Ebert, G. Sylvester, H. Min, G. Liu, R. Braich, M. Manoharan, J. Soutschek, P. Skare, L.O. Klein, M.M. Davis, and C.Z. Chen. 2007a. miR-181a is an intrinsic modulator of T cell sensitivity and selection. *Cell* 129:147-161.

Li, W., M.G. Kim, T.S. Gourley, B.P. McCarthy, D.B. Sant'Angelo, and C.H. Chang. 2005. An alternate pathway for CD4 T cell development: thymocyte-expressed MHC class II selects a distinct T cell population. *Immunity* 23:375-386.

Li, W., M.H. Sofi, S. Rietdijk, N. Wang, C. Terhorst, and C.H. Chang. 2007b. The SLAM-associated protein signaling pathway is required for development of CD4+ T cells selected by homotypic thymocyte interaction. *Immunity* 27:763-774.

Li, W., M.H. Sofi, N. Yeh, S. Sehra, B.P. McCarthy, D.R. Patel, R.R. Brutkiewicz, M.H. Kaplan, and C.H. Chang. 2007c. Thymic selection pathway regulates the effector function of CD4 T cells. *J Exp Med* 204:2145-2157.

Lind, E.F., S.E. Prockop, H.E. Porritt, and H.T. Petrie. 2001. Mapping precursor movement through the postnatal thymus reveals specific microenvironments supporting defined stages of early lymphoid development. *J Exp Med* 194:127-134.

Livak, F., M. Tourigny, D.G. Schatz, and H.T. Petrie. 1999. Characterization of TCR gene rearrangements during adult murine T cell development. *J Immunol* 162:2575-2580.

Lu, Y., M.C. Zhong, J. Qian, V. Calderon, M. Cruz Tleugabulova, T. Mallevaey, and A. Veillette. 2019. SLAM receptors foster iNKT cell development by reducing TCR signal strength after positive selection. *Nat Immunol* 20:447-457.

Luoma, A.M., C.D. Castro, T. Mayassi, L.A. Bembinster, L. Bai, D. Picard, B. Anderson, L. Scharf, J.E. Kung, L.V. Sibener, P.B. Savage, B. Jabri, A. Bendelac, and E.J. Adams. 2013. Crystal structure of Vdelta1 T cell receptor in complex with CD1d-sulfatide shows MHC-like recognition of a self-lipid by human gammadelta T cells. *Immunity* 39:1032-1042.

Lynch, L., X. Michelet, S. Zhang, P.J. Brennan, A. Moseman, C. Lester, G. Besra, E.E. Vomhof-Dekrey, M. Tighe, H.F. Koay, D.I. Godfrey, E.A. Leadbetter, D.B. Sant'Angelo, U. von Andrian, and M.B. Brenner. 2015. Regulatory iNKT cells lack expression of the transcription factor PLZF and control the homeostasis of T(reg) cells and macrophages in adipose tissue. *Nat Immunol* 16:85-95.

Ma, C., M. Han, B. Heinrich, Q. Fu, Q. Zhang, M. Sandhu, D. Agdashian, M. Terabe, J.A. Berzofsky, V. Fako, T. Ritz, T. Longerich, C.M. Theriot, J.A. McCulloch, S. Roy, W. Yuan, V. Thovarai, S.K. Sen, M. Ruchirawat, F. Korangy, X.W. Wang, G. Trinchieri, and T.F. Greten. 2018. Gut microbiome-mediated bile acid metabolism regulates liver cancer via NKT cells. *Science* 360:

MacDonald, H.R., R.C. Budd, and R.C. Howe. 1988. A CD3- subset of CD4-8+ thymocytes: a rapidly cycling intermediate in the generation of CD4+8+ cells. *Eur J Immunol* 18:519-523.

Madisen, L., T.A. Zwingman, S.M. Sunkin, S.W. Oh, H.A. Zariwala, H. Gu, L.L. Ng, R.D. Palmiter, M.J. Hawrylycz, A.R. Jones, E.S. Lein, and H. Zeng. 2010. A robust and high-throughput Cre reporting and characterization system for the whole mouse brain. *Nat Neurosci* 13:133-140.

Maeda, M., S. Lohwasser, T. Yamamura, and F. Takei. 2001. Regulation of NKT cells by Ly49: analysis of primary NKT cells and generation of NKT cell line. *J Immunol* 167:4180-4186.

Malhotra, N., Y. Qi, N.A. Spidale, M. Frascoli, B. Miu, O. Cho, K. Sylvia, and J. Kang. 2018. SOX4 controls invariant NKT cell differentiation by tuning TCR signaling. *J Exp Med* 215:2887-2900.

Malu, S., V. Malshetty, D. Francis, and P. Cortes. 2012. Role of non-homologous end joining in V(D)J recombination. *Immunol Res* 54:233-246.

Mao, A.P., M.G. Constantinides, R. Mathew, Z. Zuo, X. Chen, M.T. Weirauch, and A. Bendelac. 2016. Multiple layers of transcriptional regulation by PLZF in NKT-cell development. *Proc Natl Acad Sci U S A* 113:7602-7607.

Matsuda, J.L., O.V. Naidenko, L. Gapin, T. Nakayama, M. Taniguchi, C.R. Wang, Y. Koezuka, and M. Kronenberg. 2000. Tracking the response of natural killer T cells to a glycolipid antigen using CD1d tetramers. *J Exp Med* 192:741-754.

Mattner, J., K.L. Debord, N. Ismail, R.D. Goff, C. Cantu, 3rd, D. Zhou, P. Saint-Mezard, V. Wang, Y. Gao, N. Yin, K. Hoebe, O. Schneewind, D. Walker, B. Beutler, L. Teyton, P.B. Savage, and A. Bendelac. 2005. Exogenous and endogenous glycolipid antigens activate NKT cells during microbial infections. *Nature* 434:525-529.

Max, E.E., J.G. Seidman, and P. Leder. 1979. Sequences of five potential recombination sites encoded close to an immunoglobulin kappa constant region gene. *Proc Natl Acad Sci U S A* 76:3450-3454.

Mayans, S., D. Stepniak, S. Palida, A. Larange, J. Dreux, B. Arlian, R. Shinnakasu, M. Kronenberg, H. Cheroutre, and F. Lambolez. 2014. alphabetaT cell receptors expressed by CD4(-)CD8alphabeta(-) intraepithelial T cells drive their fate into a unique lineage with unusual MHC reactivities. *Immunity* 41:207-218.

McBlane, J.F., D.C. van Gent, D.A. Ramsden, C. Romeo, C.A. Cuomo, M. Gellert, and M.A. Oettinger. 1995. Cleavage at a V(D)J recombination signal requires only RAG1 and RAG2 proteins and occurs in two steps. *Cell* 83:387-395.

McDonald, B.D., J.J. Bunker, I.E. Ishizuka, B. Jabri, and A. Bendelac. 2014. Elevated T cell receptor signaling identifies a thymic precursor to the TCRalphabeta(+)CD4(-)CD8beta(-) intraepithelial lymphocyte lineage. *Immunity* 41:219-229.

Mendiratta, S.K., W.D. Martin, S. Hong, A. Boesteanu, S. Joyce, and L. Van Kaer. 1997. CD1d1 mutant mice are deficient in natural T cells that promptly produce IL-4. *Immunity* 6:469-477.

Michel, M.L., A.C. Keller, C. Paget, M. Fujio, F. Trottein, P.B. Savage, C.H. Wong, E. Schneider, M. Dy, and M.C. Leite-de-Moraes. 2007. Identification of an IL-17-producing NK1.1(neg) iNKT cell population involved in airway neutrophilia. *J Exp Med* 204:995-1001.

Michel, M.L., D. Mendes-da-Cruz, A.C. Keller, M. Lochner, E. Schneider, M. Dy, G. Eberl, and M.C. Leite-de-Moraes. 2008. Critical role of ROR-gammat in a new thymic pathway leading to IL-17-producing invariant NKT cell differentiation. *Proc Natl Acad Sci U S A* 105:19845-19850.

Miller, C.N., I. Proekt, J. von Moltke, K.L. Wells, A.R. Rajpurkar, H. Wang, K. Rattay, I.S. Khan, T.C. Metzger, J.L. Pollack, A.C. Fries, W.W. Lwin, E.J. Wigton, A.V. Parent, B. Kyewski, D.J. Erle, K.A. Hogquist, L.M. Steinmetz, R.M. Locksley, and M.S. Anderson. 2018. Thymic tuft cells promote an IL-4-enriched medulla and shape thymocyte development. *Nature* 559:627-631.

Milpied, P., B. Massot, A. Renand, S. Diem, A. Herbelin, M. Leite-de-Moraes, M.T. Rubio, and O. Hermine. 2011. IL-17-producing invariant NKT cells in lymphoid organs are recent thymic emigrants identified by neuropilin-1 expression. *Blood* 118:2993-3002.

Monteiro, M., C.F. Almeida, M. Caridade, J.C. Ribot, J. Duarte, A. Agua-Doce, I. Wollenberg, B. Silva-Santos, and L. Graca. 2010. Identification of regulatory Foxp3+ invariant NKT cells induced by TGF-beta. *J Immunol* 185:2157-2163.

Moran, A.E., and K.A. Hogquist. 2012. T-cell receptor affinity in thymic development. *Immunology* 135:261-267.

Moran, A.E., K.L. Holzapfel, Y. Xing, N.R. Cunningham, J.S. Maltzman, J. Punt, and K.A. Hogquist. 2011. T cell receptor signal strength in Treg and iNKT cell development demonstrated by a novel fluorescent reporter mouse. *J Exp Med* 208:1279-1289.

Nagarajan, N.A., and M. Kronenberg. 2007. Invariant NKT cells amplify the innate immune response to lipopolysaccharide. *J Immunol* 178:2706-2713.

Nair, S., and M.V. Dhodapkar. 2017. Natural Killer T Cells in Cancer Immunotherapy. *Front Immunol* 8:1178.

Nichols, K.E., J. Hom, S.Y. Gong, A. Ganguly, C.S. Ma, J.L. Cannons, S.G. Tangye, P.L. Schwartzberg, G.A. Koretzky, and P.L. Stein. 2005. Regulation of NKT cell development by SAP, the protein defective in XLP. *Nat Med* 11:340-345.

Nieda, M., M. Okai, A. Tazbirkova, H. Lin, A. Yamaura, K. Ide, R. Abraham, T. Juji, D.J. Macfarlane, and A.J. Nicol. 2004. Therapeutic activation of Valpha24+Vbeta11+ NKT cells in human subjects results in highly coordinated secondary activation of acquired and innate immunity. *Blood* 103:383-389.

Nieuwenhuis, E.E., T. Matsumoto, M. Exley, R.A. Schleipman, J. Glickman, D.T. Bailey, N. Corazza, S.P. Colgan, A.B. Onderdonk, and R.S. Blumberg. 2002. CD1d-dependent macrophage-mediated clearance of Pseudomonas aeruginosa from lung. *Nat Med* 8:588-593.

Novotny, J., S. Tonegawa, H. Saito, D.M. Kranz, and H.N. Eisen. 1986. Secondary, tertiary, and quaternary structure of T-cell-specific immunoglobulin-like polypeptide chains. *Proc Natl Acad Sci U S A* 83:742-746.

Nunez-Cruz, S., W.C. Yeo, J. Rothman, P. Ojha, H. Bassiri, M. Juntilla, D. Davidson, A. Veillette, G.A. Koretzky, and K.E. Nichols. 2008. Differential requirement for the SAP-Fyn interaction during NK T cell development and function. *J Immunol* 181:2311-2320.

O'Hagan, K.L., J. Zhao, O. Pryshchep, C.R. Wang, and H. Phee. 2015. Pak2 Controls Acquisition of NKT Cell Fate by Regulating Expression of the Transcription Factors PLZF and Egr2. *J Immunol* 195:5272-5284.

Oettinger, M.A., D.G. Schatz, C. Gorka, and D. Baltimore. 1990. RAG-1 and RAG-2, adjacent genes that synergistically activate V(D)J recombination. *Science* 248:1517-1523.

Ou, X., J. Huo, Y. Huang, Y.F. Li, S. Xu, and K.P. Lam. 2019. Transcription factor YY1 is essential for iNKT cell development. *Cell Mol Immunol* 16:547-556.

Paget, C., T. Mallevaey, A.O. Speak, D. Torres, J. Fontaine, K.C. Sheehan, M. Capron, B. Ryffel, C. Faveeuw, M. Leite de Moraes, F. Platt, and F. Trottein. 2007. Activation of invariant NKT cells by toll-like receptor 9-stimulated dendritic cells requires type I interferon and charged glycosphingolipids. *Immunity* 27:597-609.

Park, J.Y., D.T. DiPalma, J. Kwon, J. Fink, and J.H. Park. 2019. Quantitative Difference in PLZF Protein Expression Determines iNKT Lineage Fate and Controls Innate CD8 T Cell Generation. *Cell Rep* 27:2548-2557 e2544.

Pasquier, B., L. Yin, M.C. Fondaneche, F. Relouzat, C. Bloch-Queyrat, N. Lambert, A. Fischer, G. de Saint-Basile, and S. Latour. 2005. Defective NKT cell development in mice and humans lacking the adapter SAP, the X-linked lymphoproliferative syndrome gene product. *J Exp Med* 201:695-701.

Paterson, D.J., and A.F. Williams. 1987. An intermediate cell in thymocyte differentiation that expresses CD8 but not CD4 antigen. *J Exp Med* 166:1603-1608.

Pei, B., A.O. Speak, D. Shepherd, T. Butters, V. Cerundolo, F.M. Platt, and M. Kronenberg. 2011. Diverse endogenous antigens for mouse NKT cells: self-antigens that are not glycosphingolipids. *J Immunol* 186:1348-1360.

Pellicci, D.G., K.J. Hammond, A.P. Uldrich, A.G. Baxter, M.J. Smyth, and D.I. Godfrey. 2002. A natural killer T (NKT) cell developmental pathway iInvolving a thymus-dependent NK1.1(-)CD4(+) CD1d-dependent precursor stage. *J Exp Med* 195:835-844.

Pereira, R.M., G.J. Martinez, I. Engel, F. Cruz-Guilloty, B.A. Barboza, A. Tsagaratou, C.W. Lio, L.J. Berg, Y. Lee, M. Kronenberg, H.S. Bandukwala, and A. Rao. 2014. Jarid2 is induced by TCR signalling and controls iNKT cell maturation. *Nat Commun* 5:4540.

Petrie, H.T., F. Livak, D.G. Schatz, A. Strasser, I.N. Crispe, and K. Shortman. 1993. Multiple rearrangements in T cell receptor alpha chain genes maximize the production of useful thymocytes. *J Exp Med* 178:615-622.

Petrie, H.T., and J.C. Zuniga-Pflucker. 2007. Zoned out: functional mapping of stromal signaling microenvironments in the thymus. *Annu Rev Immunol* 25:649-679.

Pobezinsky, L.A., R. Etzensperger, S. Jeurling, A. Alag, T. Kadakia, T.M. McCaughtry, M.Y. Kimura, S.O. Sharrow, T.I. Guinter, L. Feigenbaum, and A. Singer. 2015. Let-7 microRNAs target the lineage-specific transcription factor PLZF to regulate terminal NKT cell differentiation and effector function. *Nat Immunol* 16:517-524.

Porcelli, S., C.T. Morita, and M.B. Brenner. 1992. CD1b restricts the response of human CD4-8- T lymphocytes to a microbial antigen. *Nature* 360:593-597.

Porritt, H.E., K. Gordon, and H.T. Petrie. 2003. Kinetics of steady-state differentiation and mapping of intrathymic-signaling environments by stem cell transplantation in nonirradiated mice. *J Exp Med* 198:957-962.

Porritt, H.E., L.L. Rumfelt, S. Tabrizifard, T.M. Schmitt, J.C. Zuniga-Pflucker, and H.T. Petrie. 2004. Heterogeneity among DN1 prothymocytes reveals multiple progenitors with different capacities to generate T cell and non-T cell lineages. *Immunity* 20:735-745.

Porubsky, S., A.O. Speak, B. Luckow, V. Cerundolo, F.M. Platt, and H.J. Grone. 2007. Normal development and function of invariant natural killer T cells in mice with isoglobotrihexosylceramide (iGb3) deficiency. *Proc Natl Acad Sci U S A* 104:5977-5982.

Prevot, N., K. Pyaram, E. Bischoff, J.M. Sen, J.D. Powell, and C.H. Chang. 2015. Mammalian target of rapamycin complex 2 regulates invariant NKT cell development and function independent of promyelocytic leukemia zinc-finger. *J Immunol* 194:223-230.

Pyaram, K., A. Kumar, Y.H. Kim, S. Noel, S.P. Reddy, H. Rabb, and C.H. Chang. 2019. Keap1-Nrf2 System Plays an Important Role in Invariant Natural Killer T Cell Development and Homeostasis. *Cell Rep* 27:699-707 e694.

Pyaram, K., and V.N. Yadav. 2018. Advances in NKT cell Immunotherapy for Glioblastoma. *J Cancer Sci Ther* 10:

Raberger, J., A. Schebesta, S. Sakaguchi, N. Boucheron, K.E. Blomberg, A. Berglof, T. Kolbe, C.I. Smith, T. Rulicke, and W. Ellmeier. 2008. The transcriptional regulator PLZF induces the development of CD44 high memory phenotype T cells. *Proc Natl Acad Sci U S A* 105:17919-17924.

Rachitskaya, A.V., A.M. Hansen, R. Horai, Z. Li, R. Villasmil, D. Luger, R.B. Nussenblatt, and R.R. Caspi. 2008. Cutting edge: NKT cells constitutively express IL-23 receptor and RORgammat and rapidly produce IL-17 upon receptor ligation in an IL-6-independent fashion. *J Immunol* 180:5167-5171.

Reilly, E.C., J.R. Wands, and L. Brossay. 2010. Cytokine dependent and independent iNKT cell activation. *Cytokine* 51:227-231.

Roelofs-Haarhuis, K., X. Wu, and E. Gleichmann. 2004. Oral tolerance to nickel requires CD4+ invariant NKT cells for the infectious spread of tolerance and the induction of specific regulatory T cells. *J Immunol* 173:1043-1050.

Rowen, L., B.F. Koop, and L. Hood. 1996. The complete 685-kilobase DNA sequence of the human beta T cell receptor locus. *Science* 272:1755-1762.

Rumfelt, L.L., Y. Zhou, B.M. Rowley, S.A. Shinton, and R.R. Hardy. 2006. Lineage specification and plasticity in CD19- early B cell precursors. *J Exp Med* 203:675-687.

Sada-Ovalle, I., A. Chiba, A. Gonzales, M.B. Brenner, and S.M. Behar. 2008. Innate invariant NKT cells recognize Mycobacterium tuberculosis-infected macrophages, produce interferon-gamma, and kill intracellular bacteria. *PLoS Pathog* 4:e1000239.

Sag, D., P. Krause, C.C. Hedrick, M. Kronenberg, and G. Wingender. 2014. IL-10-producing NKT10 cells are a distinct regulatory invariant NKT cell subset. *J Clin Invest* 124:3725-3740.

Sakaguchi, N., T. Takahashi, H. Hata, T. Nomura, T. Tagami, S. Yamazaki, T. Sakihama, T. Matsutani, I. Negishi, S. Nakatsuru, and S. Sakaguchi. 2003. Altered thymic T-cell selection due to a mutation of the ZAP-70 gene causes autoimmune arthritis in mice. *Nature* 426:454-460.

Sakano, H., K. Huppi, G. Heinrich, and S. Tonegawa. 1979. Sequences at the somatic recombination sites of immunoglobulin light-chain genes. *Nature* 280:288-294.

Salio, M., D.J. Puleston, T.S. Mathan, D. Shepherd, A.J. Stranks, E. Adamopoulou, N. Veerapen, G.S. Besra, G.A. Hollander, A.K. Simon, and V. Cerundolo. 2014. Essential role for autophagy during invariant NKT cell development. *Proc Natl Acad Sci U S A* 111:E5678-5687.

Salio, M., A.O. Speak, D. Shepherd, P. Polzella, P.A. Illarionov, N. Veerapen, G.S. Besra, F.M. Platt, and V. Cerundolo. 2007. Modulation of human natural

killer T cell ligands on TLR-mediated antigen-presenting cell activation. *Proc Natl Acad Sci U S A* 104:20490-20495.

Salou, M., F. Legoux, J. Gilet, A. Darbois, A. du Halgouet, R. Alonso, W. Richer, A.G. Goubet, C. Daviaud, L. Menger, E. Procopio, V. Premel, and O. Lantz. 2019. A common transcriptomic program acquired in the thymus defines tissue residency of MAIT and NKT subsets. *J Exp Med* 216:133-151.

Sambandam, A., J.J. Bell, B.A. Schwarz, V.P. Zediak, A.W. Chi, D.A. Zlotoff, S.L. Krishnamoorthy, J.M. Burg, and A. Bhandoola. 2008. Progenitor migration to the thymus and T cell lineage commitment. *Immunol Res* 42:65-74.

Savage, A.K., M.G. Constantinides, and A. Bendelac. 2011. Promyelocytic leukemia zinc finger turns on the effector T cell program without requirement for agonist TCR signaling. *J Immunol* 186:5801-5806.

Savage, A.K., M.G. Constantinides, J. Han, D. Picard, E. Martin, B. Li, O. Lantz, and A. Bendelac. 2008. The transcription factor PLZF directs the effector program of the NKT cell lineage. *Immunity* 29:391-403.

Schmieg, J., G. Yang, R.W. Franck, N. Van Rooijen, and M. Tsuji. 2005. Glycolipid presentation to natural killer T cells differs in an organ-dependent fashion. *Proc Natl Acad Sci U S A* 102:1127-1132.

Schulz, C., U.H. von Andrian, and S. Massberg. 2009. Hematopoietic stem and progenitor cells: their mobilization and homing to bone marrow and peripheral tissue. *Immunol Res* 44:160-168.

Seach, N., L. Guerri, L. Le Bourhis, Y. Mburu, Y. Cui, S. Bessoles, C. Soudais, and O. Lantz. 2013. Double-positive thymocytes select mucosal-associated invariant T cells. *J Immunol* 191:6002-6009.

Seiler, M.P., R. Mathew, M.K. Liszewski, C.J. Spooner, K. Barr, F. Meng, H. Singh, and A. Bendelac. 2012. Elevated and sustained expression of the transcription factors Egr1 and Egr2 controls NKT lineage differentiation in response to TCR signaling. *Nat Immunol* 13:264-271.

Seo, H., I. Jeon, B.S. Kim, M. Park, E.A. Bae, B. Song, C.H. Koh, K.S. Shin, I.K. Kim, K. Choi, T. Oh, J. Min, B.S. Min, Y.D. Han, S.J. Kang, S.J. Shin, Y. Chung, and C.Y. Kang. 2017. IL-21-mediated reversal of NK cell exhaustion facilitates anti-tumour immunity in MHC class I-deficient tumours. *Nat Commun* 8:15776.

Seo, H., B.S. Kim, E.A. Bae, B.S. Min, Y.D. Han, S.J. Shin, and C.Y. Kang. 2018. IL21 Therapy Combined with PD-1 and Tim-3 Blockade Provides Enhanced NK Cell Antitumor Activity against MHC Class I-Deficient Tumors. *Cancer Immunol Res* 6:685-695.

Shah, H.B., S.K. Joshi, P. Rampuria, T.S. Devera, G.A. Lang, W. Stohl, and M.L. Lang. 2013. BAFF- and APRIL-dependent maintenance of antibody titers after immunization with T-dependent antigen and CD1d-binding ligand. *J Immunol* 191:1154-1163.

Sharma, A., R. Berga-Bolanos, and J.M. Sen. 2014. T cell factor-1 controls the lifetime of CD4+ CD8+ thymocytes in vivo and distal T cell receptor alpha-chain rearrangement required for NKT cell development. *PLoS One* 9:e115803.

Sheng, H., I. Marrero, I. Maricic, S.S. Fanchiang, S. Zhang, D.B. Sant'Angelo, and V. Kumar. 2019. Distinct PLZF(+)CD8alphaalpha(+) Unconventional T Cells Enriched in Liver Use a Cytotoxic Mechanism to Limit Autoimmunity. *J Immunol* 203:2150-2162.

Shugay, M., D.V. Bagaev, M.A. Turchaninova, D.A. Bolotin, O.V. Britanova, E.V. Putintseva, M.V. Pogorelyy, V.I. Nazarov, I.V. Zvyagin, V.I. Kirgizova, K.I. Kirgizov, E.V. Skorobogatova, and D.M. Chudakov. 2015. VDJtools: Unifying Post-analysis of T Cell Receptor Repertoires. *PLoS Comput Biol* 11:e1004503.

Singh, A.K., P. Tripathi, and S.L. Cardell. 2018. Type II NKT Cells: An Elusive Population With Immunoregulatory Properties. *Front Immunol* 9:1969.

Slauenwhite, D., and B. Johnston. 2015. Regulation of NKT Cell Localization in Homeostasis and Infection. *Front Immunol* 6:255.

Sleckman, B.P., C.G. Bardon, R. Ferrini, L. Davidson, and F.W. Alt. 1997. Function of the TCR alpha enhancer in alphabeta and gammadelta T cells. *Immunity* 7:505-515.

Sledzinska, A., S. Hemmers, F. Mair, O. Gorka, J. Ruland, L. Fairbairn, A. Nissler, W. Muller, A. Waisman, B. Becher, and T. Buch. 2013. TGF-beta signalling is required for CD4(+) T cell homeostasis but dispensable for regulatory T cell function. *PLoS Biol* 11:e1001674.

Sobecki, M., K. Mrouj, J. Colinge, F. Gerbe, P. Jay, L. Krasinska, V. Dulic, and D. Fisher. 2017. Cell-Cycle Regulation Accounts for Variability in Ki-67 Expression Levels. *Cancer Res* 77:2722-2734.

Song, L., S. Asgharzadeh, J. Salo, K. Engell, H.W. Wu, R. Sposto, T. Ara, A.M. Silverman, Y.A. DeClerck, R.C. Seeger, and L.S. Metelitsa. 2009. Valpha24-invariant NKT cells mediate antitumor activity via killing of tumor-associated macrophages. *J Clin Invest* 119:1524-1536.

Spangrude, G.J., S. Heimfeld, and I.L. Weissman. 1988. Purification and characterization of mouse hematopoietic stem cells. *Science* 241:58-62.

Steen, S.B., L. Gomelsky, and D.B. Roth. 1996. The 12/23 rule is enforced at the cleavage step of V(D)J recombination in vivo. *Genes Cells* 1:543-553.

Stetson, D.B., M. Mohrs, R.L. Reinhardt, J.L. Baron, Z.E. Wang, L. Gapin, M. Kronenberg, and R.M. Locksley. 2003. Constitutive cytokine mRNAs mark natural killer (NK) and NK T cells poised for rapid effector function. *J Exp Med* 198:1069-1076.

Subach, F.V., O.M. Subach, I.S. Gundorov, K.S. Morozova, K.D. Piatkevich, A.M. Cuervo, and V.V. Verkhusha. 2009. Monomeric fluorescent timers that change color from blue to red report on cellular trafficking. *Nat Chem Biol* 5:118-126.

Subleski, J.J., Q. Jiang, J.M. Weiss, and R.H. Wiltrout. 2011. The split personality of NKT cells in malignancy, autoimmune and allergic disorders. *Immunotherapy* 3:1167-1184.

Sun, Z., D. Unutmaz, Y.R. Zou, M.J. Sunshine, A. Pierani, S. Brenner-Morton, R.E. Mebius, and D.R. Littman. 2000. Requirement for RORgamma in thymocyte survival and lymphoid organ development. *Science* 288:2369-2373.

Sykes, M. 1990. Unusual T cell populations in adult murine bone marrow. Prevalence of CD3+CD4-CD8- and alpha beta TCR+NK1.1+ cells. *J Immunol* 145:3209-3215.

Taghon, T., M.A. Yui, R. Pant, R.A. Diamond, and E.V. Rothenberg. 2006. Developmental and molecular characterization of emerging beta- and gammadelta-selected pre-T cells in the adult mouse thymus. *Immunity* 24:53-64.

Takagaki, Y., A. DeCloux, M. Bonneville, and S. Tonegawa. 1989. Diversity of gamma delta T-cell receptors on murine intestinal intra-epithelial lymphocytes. *Nature* 339:712-714.

Thuderoz, F., M.A. Simonet, O. Hansen, N. Pasqual, A. Dariz, T.P. Baum, V. Hierle, J. Demongeot, P.N. Marche, and E. Jouvin-Marche. 2010. Numerical modelling of the V-J combinations of the T cell receptor TRA/TRD locus. *PLoS Comput Biol* 6:e1000682.

Tourigny, M.R., S. Mazel, D.B. Burtrum, and H.T. Petrie. 1997. T cell receptor (TCR)-beta gene recombination: dissociation from cell cycle regulation and developmental progression during T cell ontogeny. *J Exp Med* 185:1549-1556.

Townsend, M.J., A.S. Weinmann, J.L. Matsuda, R. Salomon, P.J. Farnham, C.A. Biron, L. Gapin, and L.H. Glimcher. 2004. T-bet regulates the terminal maturation and homeostasis of NK and Valpha14i NKT cells. *Immunity* 20:477-494.

Tuttle, K.D., S.H. Krovi, J. Zhang, R. Bedel, L. Harmacek, L.K. Peterson, L.L. Dragone, A. Lefferts, C. Halluszczak, K. Riemondy, J.R. Hesselberth, A. Rao, B.P. O'Connor, P. Marrack, J. Scott-Browne, and L. Gapin. 2018. TCR signal strength controls thymic differentiation of iNKT cell subsets. *Nat Commun* 9:2650.

Tyznik, A.J., E. Tupin, N.A. Nagarajan, M.J. Her, C.A. Benedict, and M. Kronenberg. 2008. Cutting edge: the mechanism of invariant NKT cell responses to viral danger signals. *J Immunol* 181:4452-4456.

Vahl, J.C., K. Heger, N. Knies, M.Y. Hein, L. Boon, H. Yagita, B. Polic, and M. Schmidt-Supprian. 2013. NKT cell-TCR expression activates conventional T cells in vivo, but is largely dispensable for mature NKT cell biology. *PLoS Biol* 11:e1001589.

van Gent, D.C., K. Hiom, T.T. Paull, and M. Gellert. 1997. Stimulation of V(D)J cleavage by high mobility group proteins. *EMBO J* 16:2665-2670.

van Oers, N.S., H. von Boehmer, and A. Weiss. 1995. The pre-T cell receptor (TCR) complex is functionally coupled to the TCR-zeta subunit. *J Exp Med* 182:1585-1590.

van Puijvelde, G.H.M., and J. Kuiper. 2017. NKT cells in cardiovascular diseases. *Eur J Pharmacol* 816:47-57.

Villey, I., D. Caillol, F. Selz, P. Ferrier, and J.P. de Villartay. 1996. Defect in rearrangement of the most 5' TCR-J alpha following targeted deletion of T early alpha (TEA): implications for TCR alpha locus accessibility. *Immunity* 5:331-342.

Waldmann, H. 2016. Mechanisms of immunological tolerance. *Clin Biochem* 49:324-328.

Wang, H., E.R. Breed, Y.J. Lee, L.J. Qian, S.C. Jameson, and K.A. Hogquist. 2019. Myeloid cells activate iNKT cells to produce IL-4 in the thymic medulla. *Proc Natl Acad Sci U S A* 116:22262-22268.

Wang, H., and K.A. Hogquist. 2018. CCR7 defines a precursor for murine iNKT cells in thymus and periphery. *Elife* 7:

Watarai, H., E. Sekine-Kondo, T. Shigeura, Y. Motomura, T. Yasuda, R. Satoh, H. Yoshida, M. Kubo, H. Kawamoto, H. Koseki, and M. Taniguchi. 2012. Development and function of invariant natural killer T cells producing T(h)2- and T(h)17-cytokines. *PLoS Biol* 10:e1001255.

Webster, K.E., H.O. Kim, K. Kyparissoudis, T.M. Corpuz, G.V. Pinget, A.P. Uldrich, R. Brink, G.T. Belz, J.H. Cho, D.I. Godfrey, and J. Sprent. 2014. IL-17-producing NKT cells depend exclusively on IL-7 for homeostasis and survival. *Mucosal Immunol* 7:1058-1067.

Wesley, J.D., M.S. Tessmer, D. Chaukos, and L. Brossay. 2008. NK cell-like behavior of Valpha14i NK T cells during MCMV infection. *PLoS Pathog* 4:e1000106.

White, A.J., W.E. Jenkinson, J.E. Cowan, S.M. Parnell, A. Bacon, N.D. Jones, E.J. Jenkinson, and G. Anderson. 2014. An essential role for medullary thymic epithelial cells during the intrathymic development of invariant NKT cells. *J Immunol* 192:2659-2666.

Wilson, A., L.M. Day, R. Scollay, and K. Shortman. 1988. Subpopulations of mature murine thymocytes: properties of CD4-CD8+ and CD4+CD8- thymocytes lacking the heat-stable antigen. *Cell Immunol* 117:312-326.

Wilson, A., W. Held, and H.R. MacDonald. 1994. Two waves of recombinase gene expression in developing thymocytes. *J Exp Med* 179:1355-1360.

Wingender, G., P. Rogers, G. Batzer, M.S. Lee, D. Bai, B. Pei, A. Khurana, M. Kronenberg, and A.A. Horner. 2011. Invariant NKT cells are required for airway inflammation induced by environmental antigens. *J Exp Med* 208:1151-1162.

Wingender, G., D. Stepniak, P. Krebs, L. Lin, S. McBride, B. Wei, J. Braun, S.K. Mazmanian, and M. Kronenberg. 2012. Intestinal microbes affect phenotypes and functions of invariant natural killer T cells in mice. *Gastroenterology* 143:418-428.

Wolf, B.J., J.E. Choi, and M.A. Exley. 2018. Novel Approaches to Exploiting Invariant NKT Cells in Cancer Immunotherapy. *Front Immunol* 9:384.

Wolf, M.J., A. Adili, K. Piotrowitz, Z. Abdullah, Y. Boege, K. Stemmer, M. Ringelhan, N. Simonavicius, M. Egger, D. Wohlleber, A. Lorentzen, C. Einer, S. Schulz, T. Clavel, U. Protzer, C. Thiele, H. Zischka, H. Moch, M. Tschop, A.V. Tumanov, D. Haller, K. Unger, M. Karin, M. Kopf, P. Knolle, A. Weber, and M. Heikenwalder. 2014. Metabolic activation of intrahepatic CD8+ T cells and NKT cells causes nonalcoholic steatohepatitis and liver cancer via cross-talk with hepatocytes. *Cancer Cell* 26:549-564.

Wu, L., and L. Van Kaer. 2009. Natural killer T cells and autoimmune disease. *Curr Mol Med* 9:4-14.

Xu, X., W. Huang, A. Heczey, D. Liu, L. Guo, M.S. Wood, J. Jin, A.N. Courtney, B. Liu, E.J. Di Pierro, J. Hicks, G.A. Barragan, H. Ngai, Y. Chen, B. Savoldo, G. Dotti, and L.S. Metelitsa. 2019. NKT cells co-expressing a GD2-specific chimeric antigen receptor and IL-15 show enhanced in vivo persistence and antitumor activity against neuroblastoma. *Clin Cancer Res*

Yoshimoto, T., and W.E. Paul. 1994. CD4pos, NK1.1pos T cells promptly produce interleukin 4 in response to in vivo challenge with anti-CD3. *J Exp Med* 179:1285-1295.

Zhang, S., A. Laouar, L.K. Denzin, and D.B. Sant'Angelo. 2015. Zbtb16 (PLZF) is stably suppressed and not inducible in non-innate T cells via T cell receptor-mediated signaling. *Sci Rep* 5:12113.

Zhang, Y., R. Springfield, S. Chen, X. Li, X. Feng, R. Moshirian, R. Yang, and W. Yuan. 2019. alpha-GalCer and iNKT Cell-Based Cancer Immunotherapy: Realizing the Therapeutic Potentials. *Front Immunol* 10:1126.

Zhao, M., M.N.D. Svensson, K. Venken, A. Chawla, S. Liang, I. Engel, P. Mydel, J. Day, D. Elewaut, N. Bottini, and M. Kronenberg. 2018. Altered thymic differentiation and modulation of arthritis by invariant NKT cells expressing mutant ZAP70. *Nat Commun* 9:2627.

Zhou, D., J. Mattner, C. Cantu, 3rd, N. Schrantz, N. Yin, Y. Gao, Y. Sagiv, K. Hudspeth, Y.P. Wu, T. Yamashita, S. Teneberg, D. Wang, R.L. Proia, S.B. Levery, P.B. Savage, L. Teyton, and A. Bendelac. 2004. Lysosomal glycosphingolipid recognition by NKT cells. *Science* 306:1786-1789.

Zhu, L., Y. Qiao, E.S. Choi, J. Das, D.B. Sant'angelo, and C.H. Chang. 2013. A transgenic TCR directs the development of IL-4+ and PLZF+ innate CD4 T cells. *J Immunol* 191:737-744.

Zikherman, J., R. Parameswaran, and A. Weiss. 2012. Endogenous antigen tunes the responsiveness of naive B cells but not T cells. *Nature* 489:160-164.

Zlotnik, A., D.I. Godfrey, M. Fischer, and T. Suda. 1992. Cytokine production by mature and immature CD4-CD8- T cells. Alpha beta-T cell receptor+ CD4-CD8- T cells produce IL-4. *J Immunol* 149:1211-1215.

Zlotoff, D.A., and A. Bhandoola. 2011. Hematopoietic progenitor migration to the adult thymus. *Ann N Y Acad Sci* 1217:122-138.

ACKNOWLEDGMENTS

First of all, I would like to express my sincere gratitude and my special appreciation to my advisor Prof. Marc Schmidt-Supprian for the continuous guidance and constant support and encouragement he provided throughout these years. His genuine interest in research and enthusiasm for the project were a source of inspiration. His supervision was fundamental for the completion of this work and I am truly grateful for this unique opportunity.

Particular thanks go to the members of my thesis advisory committee Prof. Ludger Klein and Prof. Thomas Korn for their constant encouragement and the precious inputs they provided me during these years.

I would like to truly thank my collaborators Thomas Engleitner, Rupert Öllinger, Gaurav Jain, Jonas Mir and Christoph Binz for the important contribution to this project and the kindness they have always showed me.

I wish to express my deepest gratitude to all the member of the Schmidt-Supprian group for the wonderful working atmosphere and the constant support. I absolutely enjoyed the time we spent together, both at work and beyond. A special thank goes to Christoph Drees, who truly transmitted me the deep passion he had for research and for this project and deeply believed in my abilities. His presence and support were fundamental for the starting of my Ph.D studies.

I would like to thank Carina Diehl and Tim Ammon, who have been incredibly supportive and helpful throughout this entire journey. Thanks for the great inputs and the pleasant scientific (and non-) discussion.

I am very thankful for the opportunity I had to work with Nyambayar Dashtsoodol, an exceptionally competent person in the NKT cell field with whom I shared part of this project. The scientific discussions, the inputs for this work and the experimental support have been extremely important for me.

I would like to thank Julia Knogler for her significant contribution and experimental support during these years. Thank to Claudia Mugler for her constant positive attitude and kindness.

I would like to thank Sabine Helmrath, Seren Baygün, Francisco Osorio Barrios, Daniel Kovacs, Hyunju Oh-Strauß and Valeria Soberon for the fruitful scientific discussions and the entertaining funny chats.

Thanks to the previous Schmidt-Supprian group members Maike Kober, David Rieß, Barbara Habermehl and Mayur Bakshi for the constructive comments. I would like to thank the master student Liya Zaygerman for the sincere interest she showed for the project and the significant help she provided.

I wish to thank all the people whose assistance was important during these years. I would like to thank Markus Utz for the technical support with the FACS sorting experiments. Moreover, I would like to thank the animal caretakers from the "Zentrum für Präklinische Forschung" at the Klinikum rechts der Isar for their assistance and especially Christian Herrler for the positive spirit and the precious help. I would like to thank the Medical Life Science and Technology PhD program and particularly the Collaborative Research Centre 1054 for their financial and organisational support.

Beyond work, I would like to profoundly thank my parents for the immense support they have always given me throughout all the steps of my life. They constantly believed in my abilities and for this I am really grateful.
Last but not least, I would like to thank Alessandro, my strength and my support during these years. You have been a fundamental part of this journey. Thank you for being you.